2015

Studies of TBM rock cutting and frictional ignition control in underground coal mines

Gaofeng Wang
University of Wollongong

UNIVERSITY OF WOLLONGONG

School of Civil, Mining and Environmental Engineering

Faculty of Engineering and Information Sciences

STUDIES OF TBM ROCK CUTTING AND FRICTIONAL IGNITION CONTROL IN UNDERGROUND COAL MINES

Gaofeng WANG

B.Sc. Mining Engineering

This thesis is presented in fulfilment of the requirements for the

award of the degree of

DOCTOR OF PHILOSOPHY

of the

University of Wollongong

December 2015

CERTIFICATION

I, Gaofeng WANG, declare that this thesis, submitted in fulfilment of the requirements for the award of Doctor of Philosophy, in the School of Civil, Mining and Environmental Engineering, University of Wollongong, is wholly my own work except where specific references or acknowledgement are made. The document has not been submitted for qualifications at any other academic institution.

Gaofeng WANG

12/2015

ABSTRACT

Great consumption of coal has transformed the underground coal mining industry with new features. The first is the increasing depth of cover of coal mining operations due to shallow resources being exhausted. Some operations overseas have been operated at an overburden of more than 1300 meters. The second feature is the intensified production concentration associated with the greatly improved advancing rate of longwall faces； a single face output has reached more than 10 million tonnes per annum.

Deep operations are exposed to a high ground stress regime, high gas content, and coal and gas outburst risk. These issues cause changes in mine design, including but not limited to high demand for stone roadways， which are more stable than coal ones under high ground stress conditions. Stone gate roads are needed to accommodate cross measure drilling to protect coal gate drivage from the risk of high gas emissions and outburst hazards.

Increasing longwall face advancing rate shortens the lifespan of panels. Further, it necessitates short longwall development time to achieve smooth panel succession. Improved coal gate development and stone gate development are essential to fulfil this requirement.

A Tunnel Boring Machine (TBM) is a kind of tunnel construction machinery which integrates the functions of excavation, ground support, mucking, lining， and surveying. It can achieve much higher heading rates than conventional drill and blast and roadheader methods, consequently, it has been proposed to be employed in underground coal mines to accommodate the requirement of high development rate.

Application of TBMs in underground coal mines can date back to 1960’s. The early successful cases were in Britain and Germany. During 1971-1981, more than 40 km of German coal mine roadways were bored by TBMs. With the increase of mining depth and operational cost, the European underground coal mining industry experienced significant shrinkage in the past decades, and no new large scale projects

were developed, and as a result, research on the application of TBMs in underground coal mines ceased.

The majority of the historical applications of TBMs were successful from the perspective of advance rates, and some of them were both faster and more economical than conventional methods; although a few ones turned out to fail. All the constructions using TBMs were access drift and stone main development, which had large cross section areas with diameter larger than 5 meters. However, there were no applications for small cross section degassing stone drivage.

Prediction of advance rate and construction cost is an integral part of the feasibility study whilst the prediction of cutting forces is the basis of the advance rate and construction cost predictions. Tunnelling in deep underground coal mines is exposed to high ground pressures, which imposes substantial influence on cutting forces. The existing cutting force prediction models have not considered the influence of the confining pressure.

A series of experimental studies were conducted to study confining pressure's influence on cutting forces. Indentation test methodology was adopted to conduct the study. V shape and Constant Cross Section (CCS) disc cutter rings with 450 mm diameter and 30 mm thickness were designed for the tests, and the included edge angle for the V shape cutter ring was 80°. Rectangular sandstone samples with dimensions of $400\ \text{mm} \times 260\ \text{mm} \times 120\ \text{mm}$ were used in the tests. Confining pressures of 0, 3, 6, and 9 MPa were adopted.

Experimental results show that, for the CCS disc cutter, the cutting force disparities among different confining pressures were of marginal extent and irregular with shallow penetration. The disparities increased and became notable with penetration deepening. Positive correlation existed between confining pressure and the maximum load force with confinement less than 6 MPa. The maximum load began to flatten or even decrease from some point between 6 and 9 MPa confinement. For the V shape disc cutter, the cutting force disparities among different confining pressures were irregular but generally increased with mounting confinement. Compared with the

CCS disc cutter, the confining pressure's influence on maximum load was more marginal and irregular.

Understanding the working mechanism of disc cutting is the prerequisite for establishing an accurate mechanical model for cutting force prediction, and furthermore, the TBM performance prediction models. The subsurface cracks and crushed zone are indicators of disc cutting mechanisms. Deep underground roadways are exposed to high ground pressures. However the confining pressure's influence on development of crack systems and crushed zones have not been adequately explored. These issues were studied by laboratory tests.

Test results demonstrate that both confining pressure and penetration depth impose influence on crack development under the CCS disc cutter. Firstly, confining pressure influences the crack number and orientation. Radial and lateral crack numbers increase with mounting confinement; although the vertical crack numbers did not change. Radial crack orientation turned increasingly lateral with confinement pressure increment. Secondly, crack system was influenced by penetration. When it was 6 mm deep, most cracks initiated from the contact corner of the disc cutter radially and laterally. More specifically, for confinement pressures of 0, 3 and 6 MPa, all the cracks initiated from the contact corners; while one radial crack initiated beneath away from that under 9 MPa confinement. When the penetration increased to 9 mm deep, aside from the propagation of readily existed cracks, median vertical cracks initiated and propagated.

V shape disc cutter indentation induced less cracks than the CCS one. Its cracks were more vertical. In addition, the V shape disc cutter indentation was less sensitive to confinement pressure than the CCS one, which was reflected on both crack numbers and crack orientation.

The study on crushed zones revealed that they were in wedge shape under CCS disc cutter. The crushed zones had the same width with cutter thickness. However, the wedge height varied with changes of confinement pressure and penetration. Deepening of penetration increased the height of crushed zones, while mounting

confinement decreased that. More specifically, under 6 mm penetration, the crushed zone height was 30, 25, 25, and 23 mm for confinement pressures of 0, 3, 6, and 9 MPa, respectively. Under 9 mm penetration, the crushed zone height was 42, 37, 40, and 33 mm for confinement pressures of 0, 3, 6, and 9 MPa, respectively. In addition, the crushed zone boundaries were enclosed by shear failure cracks.

For the V shape disc cutter, the crushed zones were of little significance from both shape and size perspectives. However, their enlargement with increasing of penetration and confining pressure was appreciable.

Aside from the traditional circular shape TBM, unconventional rectangular TBM's have also been proposed for application in underground coal mines. Their application for coal drivage can be exposed to the risk of cutting frictional ignition, which is a frequent and fearful hazard for the underground coal mining industry. The occurrence of cutting frictional ignitions is closely related to cutting picks' failure patterns.

Laboratory tests were designed and conducted to study cutting pick failure patterns and related mechanical characteristics to provide guidelines for cutting pick selection and design to minimize the risk of frictional ignition. Five types of cutting picks commonly used in the underground coal mining industry were tested. Their tool range length ranges from 100 to 140 mm, with three tip attachment patterns of slotted, slug and laid-on. Experimental results identified three kinds of failure patterns: at tip (detipping), at shank, and at tip and shank simultaneously. Detipping is the most incendive failure pattern. Cutting pick mechanical performances were also recorded and analysed.

Test results show that tip attachment pattern and tool range length impose notable influences on the failure pattern. With the same tool range, slug tipped picks have the lowest detipping risk, followed by slotted and then laid-on ones. Increasing tool range length can change failure patterns from detipping to shank failure, which in turn reduces the frictional ignition risk; the threshold value to eliminate the detipping chance is 140 mm for the tested picks.

In addition, detipped picks showed distinctive features of high stiffness and low pick resilience. The load-displacement characteristics demonstrate that detipped picks had the average displacement at peak load of 11.4 mm, while that was 21.0 and 26.3 mm for the other two failure patterns. The average pick resilience for detipped picks was 2894 Nm, whereas that of the other two failure patterns were 5222 and 7640 Nm.

ACKNOWLEDGEMENTS

The study presented in this thesis is funded by the University of Wollongong and the China Scholarship Council. I would like to express my sincere gratitude to a number of individuals who have assisted me in doing this study.

First of all, I wish to express my sincere gratitude to my supervisor Associate Prof. Ting X. Ren, for his supervision, generous support, encouragement, and guidance during the research.

I would also like to express my sincere thanks to my co-supervisor Prof. Chris Cook, and associate-supervisor Prof. Yu-sheng Jiang from China University of Mining and Technology Beijing, for their helpful advice, guidance and support to conduct my research work.

I am grateful to Dr. Chen Cao, Dr. Jan Nemcik and Prof. Naj Aziz for their support on laboratory test design, test preparation, thesis correction and warm encouragement.

I would also like to thank the technical officers, including but not limited to:

- Alan Grant for teaching me laboratory skills, helping me set up the test platform and offering constructive suggestions.
- Cameron Neilson for his assistance on experiment design, tool fabricating, and laboratory testing.
- Duncan Best, Col Devenish, Ritchie Mclean and Richard Gasser for their support in laboratory testing.

Acknowledgement with sincere appreciation extends to Xu-wei Li, Wei-guo Zeng and Li-bin Gong for their support in carrying out the laboratory experiments.

Finally, I would like to thank my father, my mother, and my brother for their enduring support. Special thanks to my beloved wife, Chun-yan for her patience, understanding, love, encouragement, and especially looking after our lovely baby back in China.

TABLE OF CONTENTS

LIST OF FIGURES

LIST OF TABLES

1 CHAPTER ONE – INTRODUCTION

1.1 Challenges to underground coal mine development

Coal is one of the major energy sources in the world. High demand of coal has made the coal operations be located deeper and more intensified. The deepest underground coal mining operation has an overburden of more than 1300 m (Liu, 2012). Annual production from a single underground coal mine has reached up to 20 Million metric tons (Mmt), and that of one single longwall face has surpassed 10 Mmt in some highly productive mines (Xu, 2010). Underground coal mine development, including stone and coal drivage, has become the bottle neck for improving productivity and reducing cost. The specific challenges faced by development are discussed as follows.

Firstly, deep underground coal mining operations require a large amount of stone roadways, whereas the conventional methods, such as drill and blasting and roadheader methods, can hardly accommodate the required development rate. In deep mines, coal seams are exposed to a high ground stress regime and high methane content (Liu, 2013). High ground stresses deteriorate the stability of underground openings, which causes support difficulties for roadways, especially for coal mains. In this situation, stone mains have to be constructed to accommodate high ground stresses. In addition, high gas content, combined with high ground stress, also increases the possibility of coal and gas outbursts (Lama and Bodziony, 1998). The most practical way to control the outburst risk is to de-stress and de-gas the coal in working areas in advance by cross measure drilling from stone roadways (Hao et al., 2014). Therefore, stone drivage is in high demand by the industry.

Secondly, the conventional methods of coal gateroad development pose increasing constraints to smooth longwall panel succession, i.e., the next panel in the mining sequence must be ready for the longwall equipment to be relocated before the end of producing panel. By using highly mechanized longwall face machinery, the longwall face advance rate has been greatly increased, whilst the improvement in longwall development rate was less than that at the longwall face (Trackemas and Peng, 2013).

It causes a development lag and further adversely influences longwall panel succession (Misra 1996, Kizil et al. 2011).

It can be concluded that, underground coal mine development is now facing new challenges due to the deepening of mines and improvement in longwall face productivity. Extensive stone roadways are needed to accommodate the stress and gas problems resulting from mining operations at greater depths. A higher coal drivage rate is required to maintain smooth longwall panel succession.

1.2 Tunnel Boring Machines (TBM)

Tunnel Boring Machines (TBM) are a kind of tunnel construction machine that integrates the functions of excavation, ground support, mucking, lining and surveying. They adopt advanced mechanical, electrical, hydraulic, optics and geotechnical technologies and have been applied in construction of subways, sewerage tunnels, hydraulic tunnels, railway tunnels, highway tunnels and mining tunnels (Brox, 2013, Willis, 2012, Donnelly et al., 2014). Traditional TBMs, which are circular in shape, mainly include three categories: open-type TBM, single shield TBM and double shield TBM, as shown in Figure 1-1. Among them, the open-type has been used in underground coal mines (Cigla et al., 2001, Brox, 2013, Hunt, 1978). Compared with the conventional drill and blast and roadheader methods, TBM drivage has the merits of higher advancing rate, shorter project duration, and cleaner working environment (Aston et al., 1988).

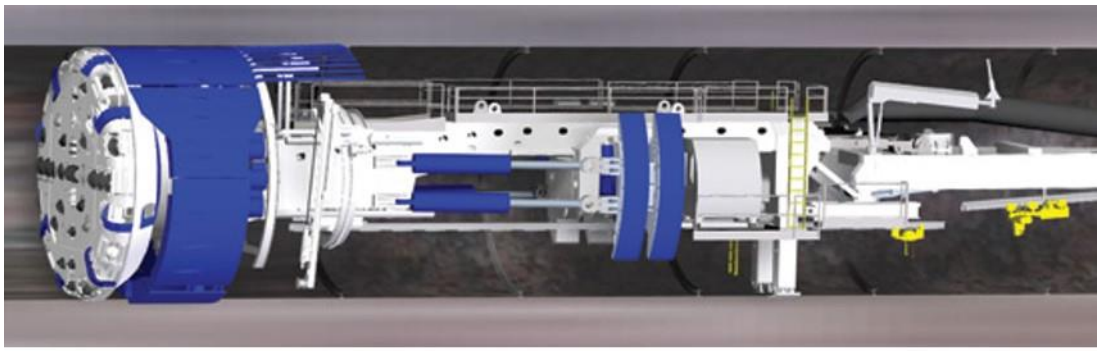

（a）Open-type TBM

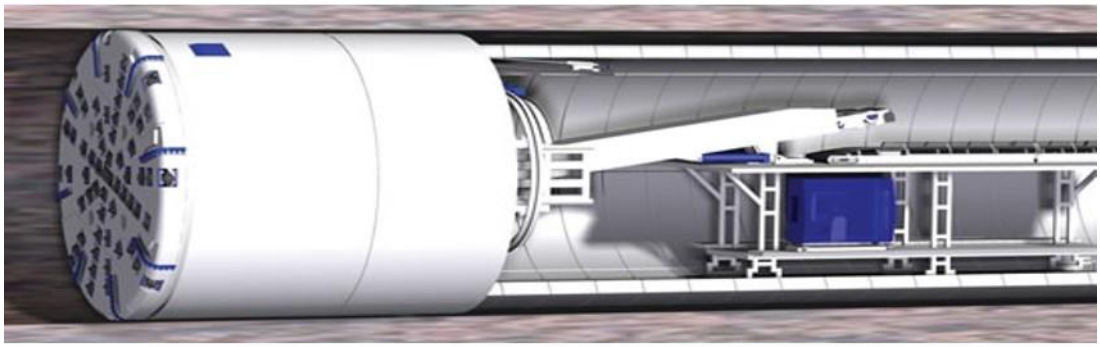

（b）Single shield TBM

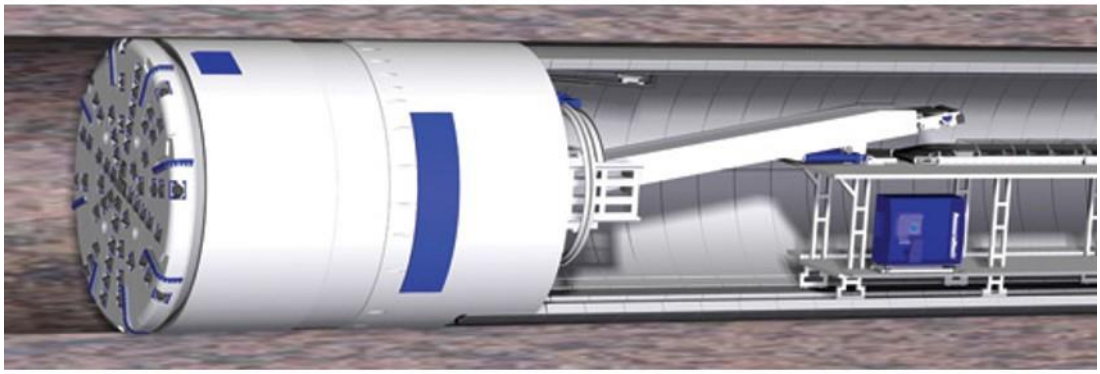

（c）Double shield TBM

Figure 1-1 Schematics of different categories of traditional TBMs (The Robbins company, 2013).

TBM's can achieve higher heading rate than conventional drill and blast and roadheader methods (Cigla et al., 2001, Donnelly et al., 2014). Tunnel construction procedures mainly include rock breaking, mucking and ground support. Compared to conventional excavation methods, TBM drivage has two advantages: (1) it is full face mechanized rock cutting that is proven to be more efficient; (2) it conducts rock cutting, mucking and ground support, concurrently (Tarkoy, 1995). By contrast,

conventional drill and blast rock breaking involves sequential procedures including drilling, explosive charging, shot-firing, and smoke exhausting. This rock breaking is time consuming. In addition, mucking and ground support cannot be implemented at the same time as rock breaking. Roadheader methods adopt partial face cutting, which is less efficient than full face cutting. In addition, most roadheaders do not have the function of ground support.

The field data substantiate TBM's superiority on advancing rate. TBM projects have achieved advancing rates of over 1000 m per month, and records of over 100 m per day have also been reported (Ramamurthy, 2008, Liu et al., 2012). By contrast, the comparable figures for conventional methods are still low; drill and blast method's advancing rate is roughly 150 m per month; and that for roadheaders is around 300 m per month.

Aside from traditional TBMs, unconventional ones with irregular faces also have been developed, as shown in Figure 1-2. It shows a multiple-axis tunnel boring machine, which is designed for box-shaped large-section tunnels. Like traditional TBMs, unconventional ones also provide an integrated continuous full face cutting, bolting and mucking system, which can achieve high advancing rate.

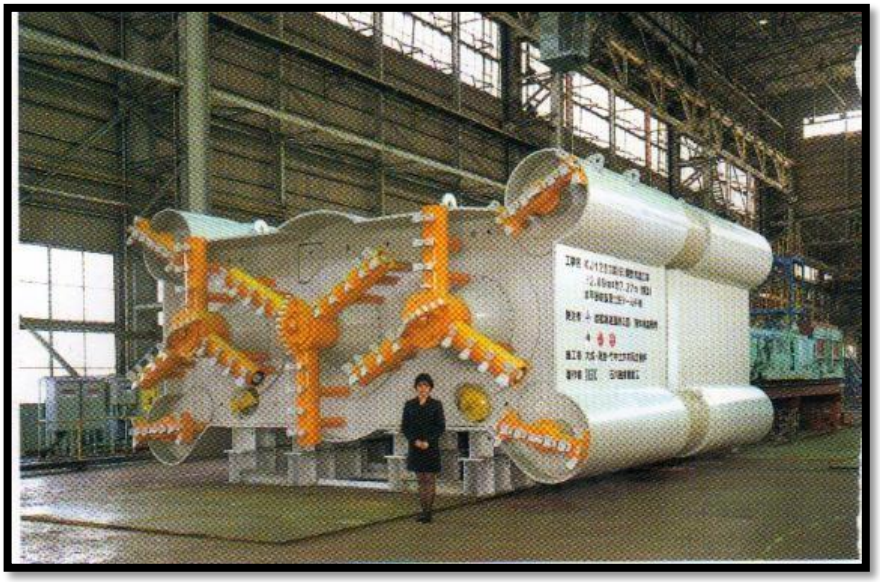

Figure 1-2 IHI proposed irregular face TBM (IHI and coal, 2012).

1.3 Applying TBM technology to accommodate underground coal mine development challenges

Traditional TBMs have been employed to drive stone roadways in underground coal mines due to the aforementioned merits. The early successful cases were in Britain and Germany. During 1971-1981, more than 40 km of German coal mine roadways were bored by TBMs. Such constructions are all access drifts and stone mains, which have large cross section areas with diameter over 5 m (Harding, 1981, Stack, 1982, Farmer and Glossop, 1983, Handewith, 1983, Palmer et al., 1985, Hunt, 1978). Applications for small cross section degassing stone drivages have not been reported so far. The European underground coal mining industry underwent shrinkage in the past decades, and no new large scale projects were developed. So research on application of TBMs in underground coal mines ceased.

Unconventional TBM's have also been proposed for application in underground coal mines. By 2005, both IHI and Pacific Tunnelling had developed concepts and detailed engineering designs for coal development TBMs, (Gibson, 2005). In 2014, a coal driving TBM was launched in Shenhua mining group, as shown in Figure 1-3.

Figure 1-3 Unconventional rectangular shape TBM proposed for longwall gateroad development (NHI, 2014).

1.4 Objectives and methodology

Application of TBMs in underground coal mines needs a comprehensive feasibility study. Lessons and experience of the precedent cases are important parts of the study, which assist performance prediction and avoiding the previously encountered problems. So, the first objective of this thesis is to provide a critical review of the precedent underground coal mine TBM projects

Advance rate and construction cost are the two criteria for application of TBMs in underground coal mines. Prediction of advance rate and construction cost is an integral part of the feasibility study. Prediction of cutting forces is the basis of the advance rate and construction cost predictions (Innaurato et al., 2007, Lindqvist, 1982, Rostami and Ozdemir, 1993, Roxborough and Phillips, 1975, Sanio, 1985, Snowdon et al., 1982). Tunnelling in deep underground coal mines is exposed to high ground stresses, which impose a substantial influence on cutting forces. However, the existing cutting force prediction models have not taken the influence of confining pressure into consideration. So, the second objective of this thesis is to design a laboratory testing method to study confining pressure's influence on cutting forces.

Understanding disc cutting mechanisms is a prerequisite to establishing the accurate mechanical models for cutting force prediction, and furtherly the TBM performance prediction models (Roxborough and Phillips, 1975, Ozdemir et al., 1977, Cook et al., 1984, Lindqvist, 1984, Howarth and Bridge, 1988, Rostami and Ozdemir, 1993, Innaurato and Oreste, 2011, Rostami, 2013). The subsurface crack system and crushed zone are indicators of disc cutting mechanisms. The influence of confining pressure on development of cracks and crushed zones has not been adequately explored. Hence, the third objective is to evaluate the influence of confining pressure on crack and crushed zone development using an experimental study.

Application of TBMs for coal drivage faces the risk of cutting frictional ignition. It refers to ignition of firedamp with the igniting sources generated by the cutting picks' striking on incendive rocks. Cutting frictional ignition is a frequent and fearful

hazard for the underground coal mining industry, especially for longwall gateroad development operations (Krog and Schatzel, 2009). The cause of cutting frictional ignitions is closely related to cutting picks' failure patterns. So, the fourth objective is design a testing method to study cutting picks' failure patterns and related mechanical characteristics to provide guidelines for cutting pick selection and design to minimize the risk of frictional ignition.

1.5 Thesis structure

This thesis includes three major parts: The first part is a critical review of historical cases of TBM applications in underground coal mines; The second part mainly focuses on the study of cutting force and cutting mechanisms with reference to the application in stone drivage; The third part relates to the application in coal drivage, which is an experimental study on cutting pick selection to prevent cutting frictional ignitions.

Based on the contents, this thesis is organized into eight chapters. A flowchart of the thesis layout is shown in Figure 1-4.

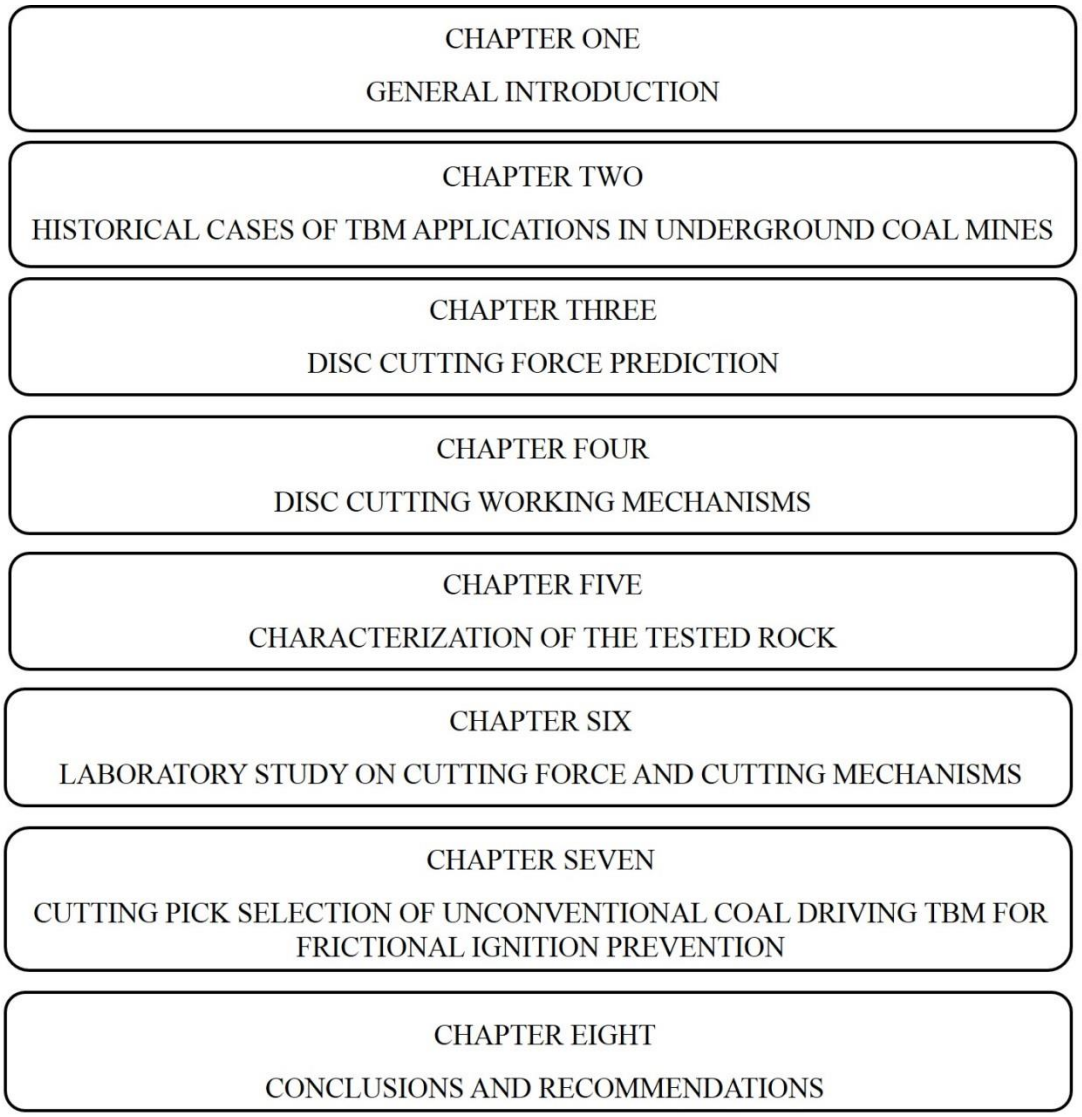

Figure 1-4 Structure of chapters in the thesis.

Chapter 1 presents the general introduction of the research and objectives of the thesis work.

Chapter 2 reviews historical cases of the application of TBMs in underground coal mines. Firstly, seven representative cases were introduced in detail. Then a critical analysis is provided from the perspectives of advancing rate, construction cost, and project risks.

Chapter 3 presents a critical literature review on disc cutter and disc cutting force prediction. Firstly, the development history of the disc cutter is described. Then,

classical disc cutter cutting force prediction models is critically reviewed. Finally, drawbacks of the established cutting force prediction models are analysed, and absence of confinement's influence in the established cutting force prediction models is targeted for further study.

Chapter 4 presents a critical literature review on disc cutter cutting mechanisms. Analytical, experimental and numerical studies on disc cutting mechanisms are critically reviewed respectively, and the limitations of these studies are summarized.

Chapter 5 presents a characterization study of the tested rock, which is a sandstone. Characterization techniques for physical and mechanical properties are described in detail. The Uniaxial Compressive Strength (UCS), tensile strength, shear strength, cohesion, internal friction angle, Young's modulus, and Poison's ratio are determined.

Chapter 6 presents the laboratory study on cutting force and cutting mechanism. Firstly, the design of the experiment is elaborated, including disc cutter design, rock preparation, and test platform set up. Secondly, testing procedures are described. Subsequently, the test results are summarized and analysed. Finally, the significance of the findings on the improvement of cutting force prediction models, cutterhead layout design, and disc cutter selection are discussed.

Chapter 7 presents a laboratory study on cutting pick selection of unconventional coal driving TBM for frictional ignition prevention. It looks at cutting picks' incendivity from their failure patterns and mechanical performance. Firstly, an introduction of cutting frictional ignition is provided, followed by the description of experimental design and procedures. Then, test results are summarized and analysed. Finally, the significance of the findings on cutting picks selection and design are discussed.

Chapter 8 summarises the results and principal conclusions of the work presented in this thesis. Recommendations for further research are also offered.

2 CHAPTER TWO – HISTORICAL CASES OF TBM APPLICATIONS IN UNDERGROUND COAL MINES

2.1 Introduction

Application of TBMs for underground mine development dates back to the 1960's in Europe (Handewith, 1983). During 1971-1981, more than 40 km of German coal mine roadways were bored by TBMs. The major applications were for construction of access drifts and stone mains (Harding, 1981, Stack, 1982). So far, around 20 underground coal mine TBM projects have been completed in Australia, Canada, Britain and Germany, but mainly in Germany and Britain (Handewith, 1983, Palmer et al., 1985, Athorn and Snowdon, 1986, Donnelly et al., 2014).

This chapter critically reviews some representative cases of application of TBMs in underground coal mines, and extracts lessons and experiences from them to provide guidelines for future projects. The cases considered are Dawdon project in Britain, Grosvenor project in Australia, Donkin-Morien project in Canada, Selby mine project in Britain, Gneisenau mine project in Germany, West Cliff mine project in Australia, and Monopol mine project in Germany.

2.2 Historical cases

2.2.1 Dawdon colliery project

Dawdon colliery sat close to the northeast coastline of County Durham, in England, as shown in Figure 2-1, and indicated by the letter A. In the early 1970s, a cross measure drift was planned to exploit offshore coal reserves under the North Sea, as shown in Figure 2-1. The start point of the drift was from workings in the Hutton seam 476 m below sea level and 449 m below sea bed level. The drift was designed with a gradient of 1 in 400 rising, and the Thyssen FLP 12/35 TBM machine with a diameter of 3.65 m was adopted. The drive commenced in January 1975. This project presents the first modern TBM project in the UK underground coal mining industry (Farmer and Glossop, 1983).

Figure 2-1 Location of Dawdon Colliery project (Courtesy Google Map).

The whole drift can be divided into four sections, as shown in Figure 2-2. The first section starts at approximately 3000 m to the east of the shoreline, and ends until encountering the fault zone with the length of 1040 m; in this section the drift traversed undisturbed and competent coal measure mudstones with fine sandstone laminae and fine-grained white sandstones, with compressive strength ranging from 25 to 155 MPa. The second section is the fault zone with the thickness of 210 m reaching chainage 1250 m, where it encountered sheared and broken zones of coal and shales. At the end of the second section, the drift turned to the direction parallel to the strike of the fault plane; from where the third section came with length of 270 m reaching chainage 1520m. The third section passed through the edge of a dome structure in steeply inclined strata, as shown in Figure 2-3. The fourth section ended at chainage 1692 m with the length of 172 m. Both section 3 and section 4 were in badly disturbed ground associated with the Seaham fault, as shown in Figure 2-3. Sections 1 and 4 were TBM driven sections while section 2 and 3 were driven with drill and blast methods (Farmer and Glossop, 1983).

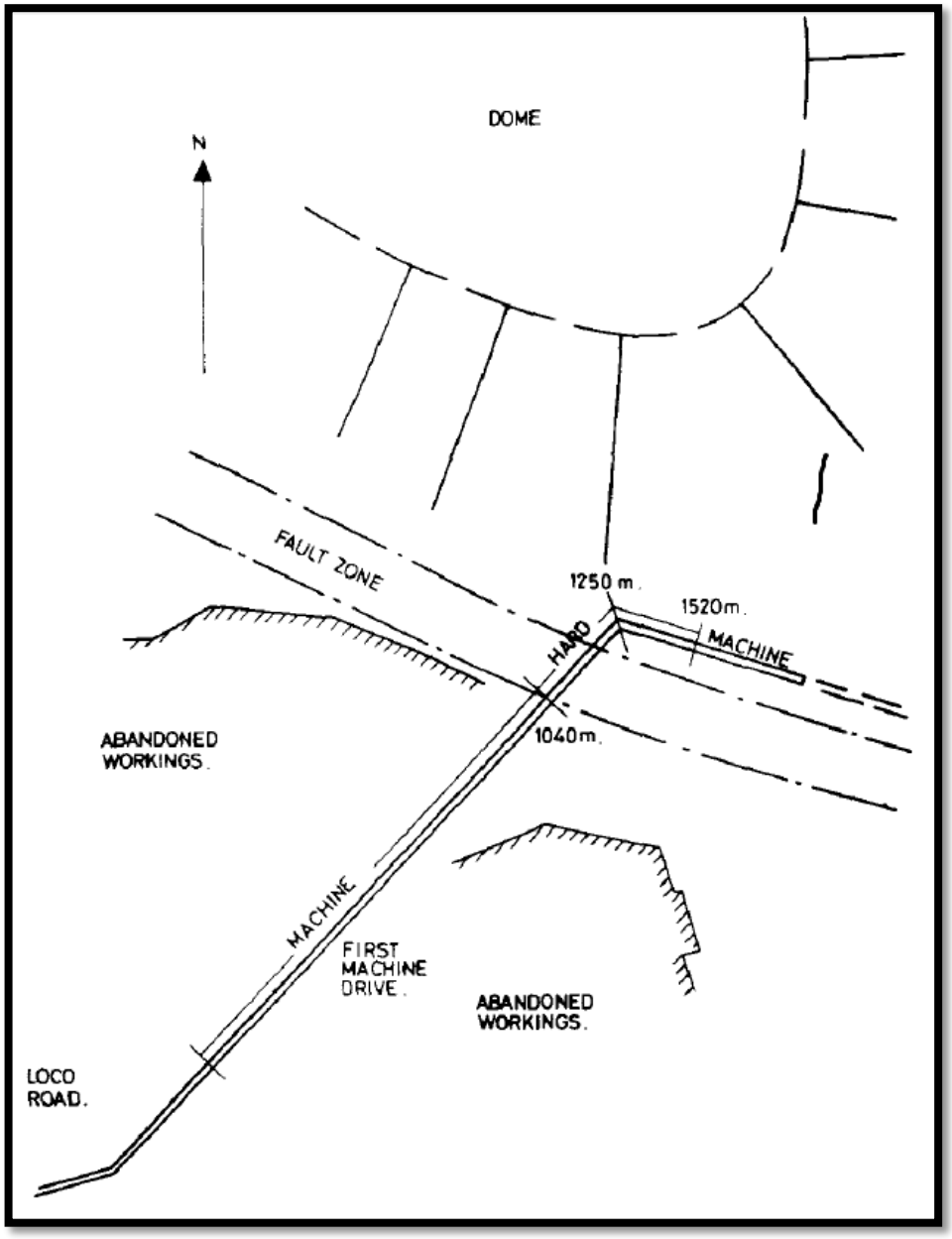

Figure 2-2 Schematic plan of Dawdon Colliery Sea Drift rising at 1 in 400 from the Hutton seam level (Farmer and Glossop, 1983).

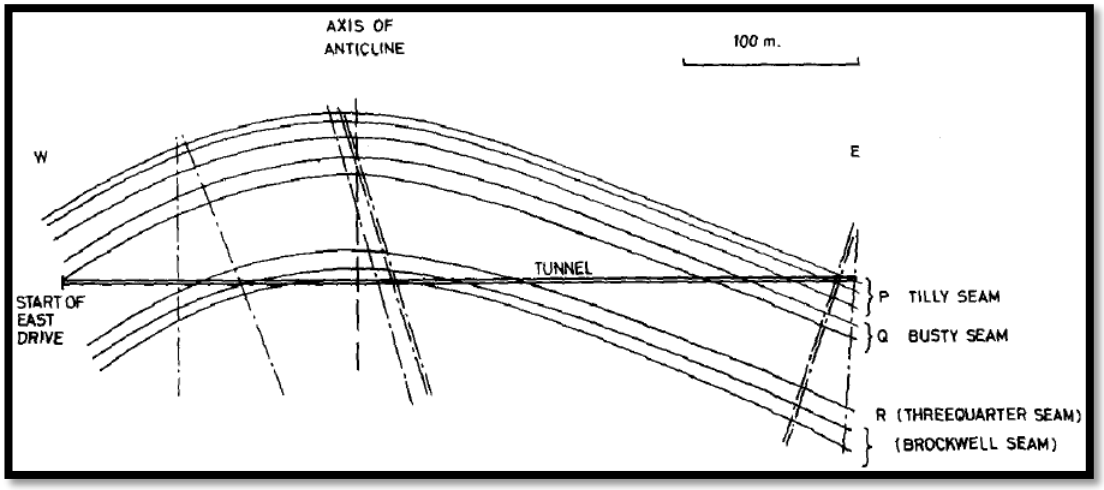

Figure 2-3 Approximate section of the geological structure along the sections parallel to the fault plane (Farmer and Glossop, 1983).

The TBM performed satisfactorily in section 1 with 66.8 m per week and a peak weekly advance of 78 m, under a roster of 3×6 h shifts, seven days per week. By comparing with another drill and blast heading which is in the same geological settings under a similar shift system but over five days per week, TBM's advance rate was 3.9:1 or approximately 2.9:1 when adjusted for volume excavated to its counterpart. But in the second section, its process was slowed by floor penetration and difficulties in supporting the roof above the machine; which eventuated in its being withdrawn. Section 2 and section 3 were finished with drill and blast. Section 4 was excavated with TBM but with very unsatisfactorily results from floor penetration, roof collapse and mucking problems. In this section, the TBM was withdrawn again with only 172 m of drivage (Farmer and Glossop, 1983).

Dawdon colliery project was a partially successful project. The TBM was significantly superior to drill and blast method in advancing rate in competent ground, while it proved to be very sensitive to poor ground conditions, and needed to be withdrawn in weak ground. This demonstrated the importance of geological settings in success of TBM projects.

2.2.2 Grosvenor project

Grosvenor coal project sits on the northern boundary of the town of Moranbah in the Central Queensland Bowen Basin coal precinct, Australia, as shown in Figure 2-4, and indicated by the letter A. It is next to Moranbah North colliery, and shares both coal preparation plant and similar geological settings with it. A two mode Earth Pressure Balance (EPB) machine with 8 m of excavation diameter was adopted to develop the two access declines. The underlying rationale is that a TBM constructed decline holds long enough life expectancy which can eliminate the need of ground support rehabilitation, and the risk of unexpected roof falls during the life of the mine, which have incurred substantial production loss in the Moranbah North mine. These two TBM driven drifts adopt precast concrete segment ring supports which will provide a life expectancy of 50 years (Donnelly et al., 2014).

Figure 2-4 Location of Grosvenor coal project (Courtesy Google Map).

The two decline drifts have lengths of 967 m and 1258 m, with open channel sections of 205 m and 265 m, TBM driven lengths of 762m and 993m, inclination gradient of 1:6 and 1:8 respectively. The overburden depth of the pit bottom is 169 m.The drifts traverse mixed ground conditions ranging from sand and clay to varying grades of hard rock up to 120 MPa of Uniaxial Compressive Strength, as well as stringer coal seams. Some strata are aquifers (Donnelly et al., 2014). Based on the geological

settings, a Robbins hybrid mode- hard rock mode and EPB mode TBM was adopted, as shown in Figure 2-5, and its parameters are shown in Table 2-1 (Willis, 2013, Donnelly et al., 2014). This project is the first one which adopts hybrid TBM to conduct underground coal mine decline drift drivage.

Figure 2-5 Robbins two mode EPB machine for Grosvenor project (Donnelly et al., 2014).

Table 2-1 Grosvenor project TBM specifications (Donnelly et al., 2014)

Bore Diameter	8.0 m
Cutterhead speed	0-3.2 rpm, constant torque range 3.3-6.4 rpm
Maximum thrust	53,018 kN
Stroke	850 mm
Cutters	50, 17” wedge lock, back loading
Power Supply	11 kW

The hybrid TBM is a double shield one, which can work under both hard rock mode and EPB mode through mode conversion. TBM under hard rock mode uses grippers to brace against the hard rock tunnel wall, which can provide anchorage points for the propelling cylinders in the front shield to provide thrust force for the cutter head,

and for the extending of hydraulic cylinders in the rear shield to secure concrete support ring segments. Under this mode, excavation and support installation are undertaken concurrently, which can achieve a faster advancing rate, as shown in Figure 2-6 (a). The TBM under EPB mode idles the grippers and the propelling cylinders in the front shield; only uses hydraulic cylinders in the tail shield to both provide thrust force for the cutter head and provide pushing force for securing installed concrete support ring segments. Under this model, excavation and support installation cannot be conducted simultaneously, as shown in Figure 2-6 (b). Mode conversion consists of changes of cutting tools and mucking system (Willis, 2013).

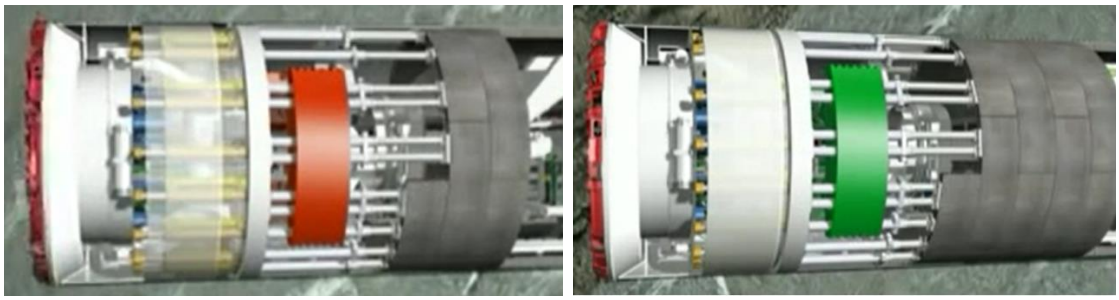

(a) Hard rock mode (b) EPB mode

Figure 2-6 Hard rock/EPB hybrid TBM working modes, red gripper stands for active gripper while green gripper stands for idled gripper (Courtesy Herrenknecht website).

Even though the EPB mode is slower than the hard rock mode, it suits for the broken and water bearing ground, which the hard rock mode is very sensitive to, moreover it can deal with methane gas safely (Willis, 2013). So, the hybrid mode TBM can accommodate mixed ground conditions ranging from competent ground to soft muddy ground, which is a technology breakthrough to boost the application of TBMs in underground coal mines.

Another highlighted feature for the Grosvenor project is its quick TBM retraction system designed for blind drifts. The TBM is able to retract in one piece from its shield, leaving the shield in place, because the core of the machine is a bolted design and separates from the shield, in a process that does not require a cutting torch (Ofiara, 2014). The core of the machine can then walk up the decline tunnel on a set of specially designed transport dolleys and be sent by rail to the second decline

tunnel, where another shield will be waiting for machine assembly prior to launch (Willis, 2013, Ofiara, 2014).

The Grosvenor project commenced from December 2013, the first drift has been completed with successful implementation of the quick retraction system. It is not practical to judge whether the whole project is successful or not, because the whole project has not been completed yet and no performance statistics have been published.

The adoption of a hybrid TBM for mine development is the first trial in the underground coal mining industry in the world. Its novel design of blind drift quick TBM retraction system is also the first trial. This project has set up a milestone for TBMs application in mine construction.

2.2.3 Donkin-Morien project

Donkin-Morien mine is located on the north-eastern shoreline of Cape Breton Island, about 300 km north of Halifax and 25 km east of Sydney, Nova Scotia, Canada, as shown in Figure 2-7, and indicated by the letter A. The coal seams of interest in the mine outcrop on the sea bottom near shore and dip seaward. Decline drifts were adopted to access the coal seams, and one of them was driven by a TBM, the alignment of the proposed declines are shown in Figure 2-8. A 7.6-m diameter full-face shielded TBM was ordered in March 1982 and delivered to site by September 1983. The decline drivage commenced in October 1983. This project is the first case of application of TBM in underground coal mine development in Canada (Palmer et al., 1985).

Figure 2-7 Location of Donkin-Morien mine (Zhao et al., 2010) (Courtesy Google Map).

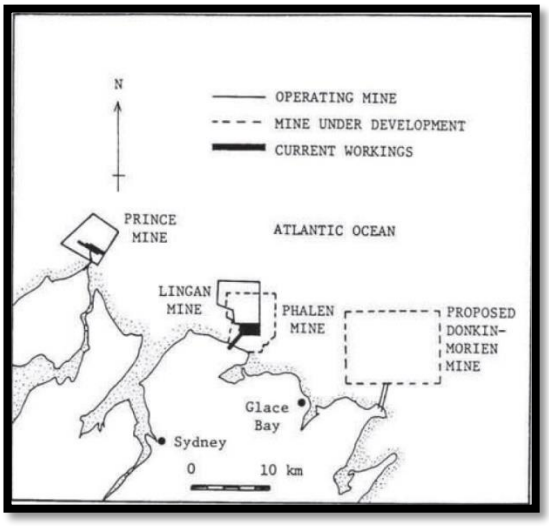

Figure 2-8 Alignment of coal access drifts and the coal mine precinct (Aston et al., 1988).

The tunnel was driven through coal measures strata which consist of interbedded sandstones, siltstones, mudstones and coal seams. The rock along the proposed alignment was expected to vary from 10 to 100 MPa in uniaxial compressive strength. The initial section of the tunnel, which includes the whole declined drift, was driven in a massive sandstone unit, up to 30 m thick, which varies lithologically from laminated to thickly bedded and from fine to coarsely grained, as shown in Figure 2-9.

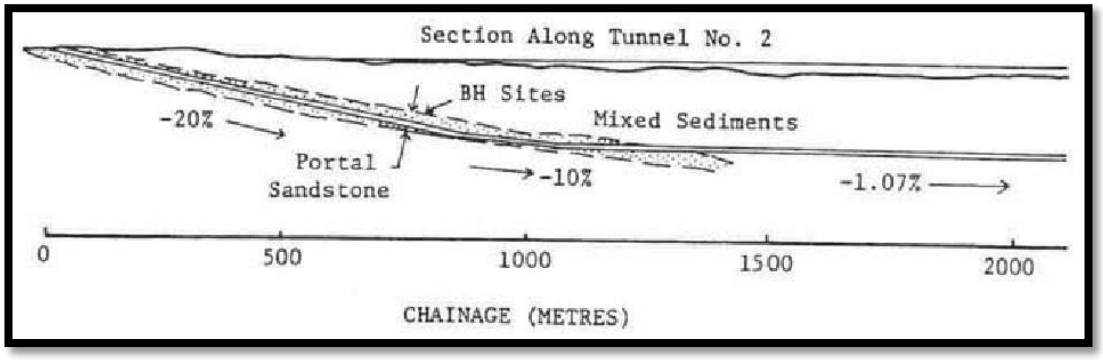

Figure 2-9 Geological conditions along the alignment of the TBM driven drift (Aston et al., 1988).

A fully shielded machine was adopted as weak mudstone and siltstone were encountered along the alignment of the tunnel, which the shield could provide immediate support in the weak ground until the primary lining is expanded into place. The full shield provides good protection to men and equipment. The machine was designed to use disc cutters in the hard rock and rippers in the very soft rock because of the mixed ground conditions with surrounding rock compressive strength ranging from 10 to 100 MPa. A fully articulated and retractable cutter head was designed for this project to provide extra manoeuvrability and lower the risk of being stuck (Palmer et al., 1985). The specific technical data for the TBM are shown in Table 2-2.

Table 2-2 TBM technical data in Donkin-Morien project (Palmer et al., 1985)

Bore diameter	7.6 m
Overall length	6.3 m
Overall weight	350 t
Cutter (all cutters backloading)	39 356-mm Robbins disc 6 330-mm Robbins disc 55 Lovat tungsten carbide ripper teeth
Conveyors	11.5-m primary belt, 122 cm wide 16.5-m secondary belt, 122 cm wide
Connected horsepower	2050
Cutterhead	Fully articulated and retractable Clockwise and counter clockwise rotation Variable-speed hydraulic drive, 0-4 rev/min
Pentechnicon	5 platforms, 6 m long
Propulsion	24 hydraulic jacks 1.7-m stroke Cutting head thrust 1088 t @ 13790 kPa
Pteering	Thrust jacks Articulated cutterhead Stabilizer rollers (also used for control of counter rotation)
Power supply	Main 1100 V, three phase, 60 HZ Lighting 110 V, single phase, 60 HZ
Equipped with mechanical rib erector, rib expander, diamond drill for probing ahead and provision for shotcreting	
Certified intrinsically safe electrics	
Certified for use in coal mines	

The tunnel was driven a total distance of 3579 m, the inclined parts include 780.3 m of -20% decline and 206.8 m of -10% decline as shown in Figure 2-10. Very satisfactory advancing rate of 305 m per month was achieved in the section of -20% decline drivage. There was a -20% decline drift driven by drill and blast method adjacent and parallel to it. Even though the declines cannot be compared exactly because the size and conditions are not identical, general comparison indicates that

the TBM one was heading about four times faster than the drill and blast one; the man-hours expended per meter for the TBM driven decline were of the order of one-third of the counterpart; moreover the quality was superior and overall cost was lower (Palmer et al., 1985). Advancing rates in the horizontal grade section and -10% decline section were higher than that of the -20% decline section, with specific values of 95.2 m per 100 hours and 105 m per 100 hours respectively(Palmer et al., 1985).

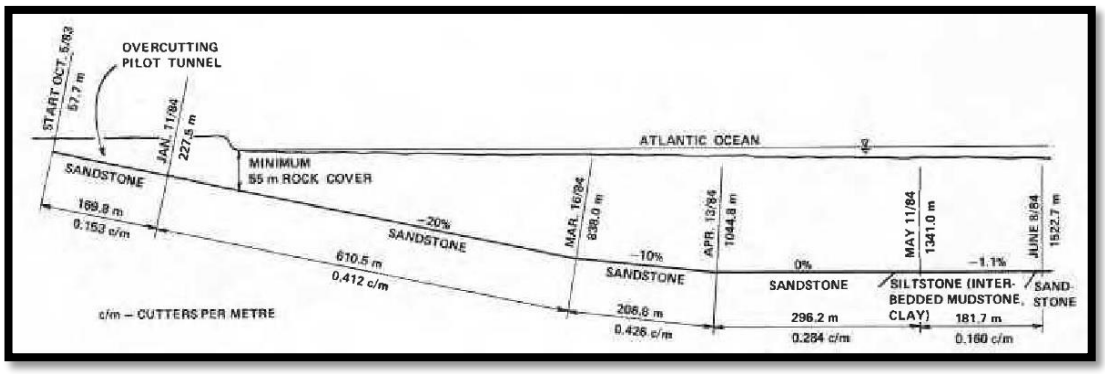

Figure 2-10 Disc cutter consumption along the hard rock section of the TBM driven tunnel (Palmer et al., 1985).

Disc cutter change represented the biggest part of downtime; rock strength and inclination gradient both escalate the disc cutter consumption and downtime. Field statistics showed that cutter change took over one quarter of the total cycle time in the hard rock section and over one fifth in soft ground, which were both the biggest part of downtime sectors. The down time statistics were in line with cutter consumption data as shown in Figure 2-10; in the hard sandstone rock section, the disc cutter consumption was over 0.42 cutters per meter and 0.28 cutters per meter in the decline and horizontal parts respectively; while in softer siltstone (interbedded mudstone clay) horizontal section, that dropped to 0.16 cutters per meter (Palmer et al., 1985). So it is clear that rock strength and inclination will escalate disc cutter wear which will further incur more downtime and lower advancing rate.

The Donkin-Morien project turned out to be successful with higher advancing rate, lower cost and superior quality, as shown in Figure 2-11. It demonstrated the TBMs' capability to accommodate inclination grade for underground coal mine drifts. Even

though the -20% grade caused higher disc cutter use, it did not cause any significant machine operational problem, and the tunnelling performance in the decline was satisfactory (Palmer et al., 1985). Cutter change imposed the biggest downtime factor in all sections of the tunnel, especially in the decline hard rock section, which indicates the importance of conducting further research and improving field management on disc cutter usage.

Figure 2-11 View of completed tunnel - 20% decline section (Zhao et al., 2010).

2.2.4 Selby mine project

The Selby mine situated between Selby and York in North Yorkshire in UK as shown in Figure 2-12, and indicated by the letter A. It was the largest deep mine in the U.K. with a planned output of 10 million tonnes per annum. (Massey and Stenton, 1984, Athorn and Snowdon, 1986, Forrest et al., 1985, Forrest et al., 1983). The whole mine is divided into five working branches; each section have their own shafts for manriding, ventilation and material handling separately; coal was passed from the workings to the main tunnels through staple bunkers across the different branches, and then was transported to the surface through Gascoigne Wood along the two main tunnels using conveyor belts; the main tunnels are 13.5 km long with 70 m distance stretching across the coalfield from Gascoigne Wood to connect all the five branches,

and both housed a single conveyor belt, as shown in Figure 2-13 (Forrest et al., 1983).

Figure 2-12 Location of Selby mine (Courtesy Google Map).

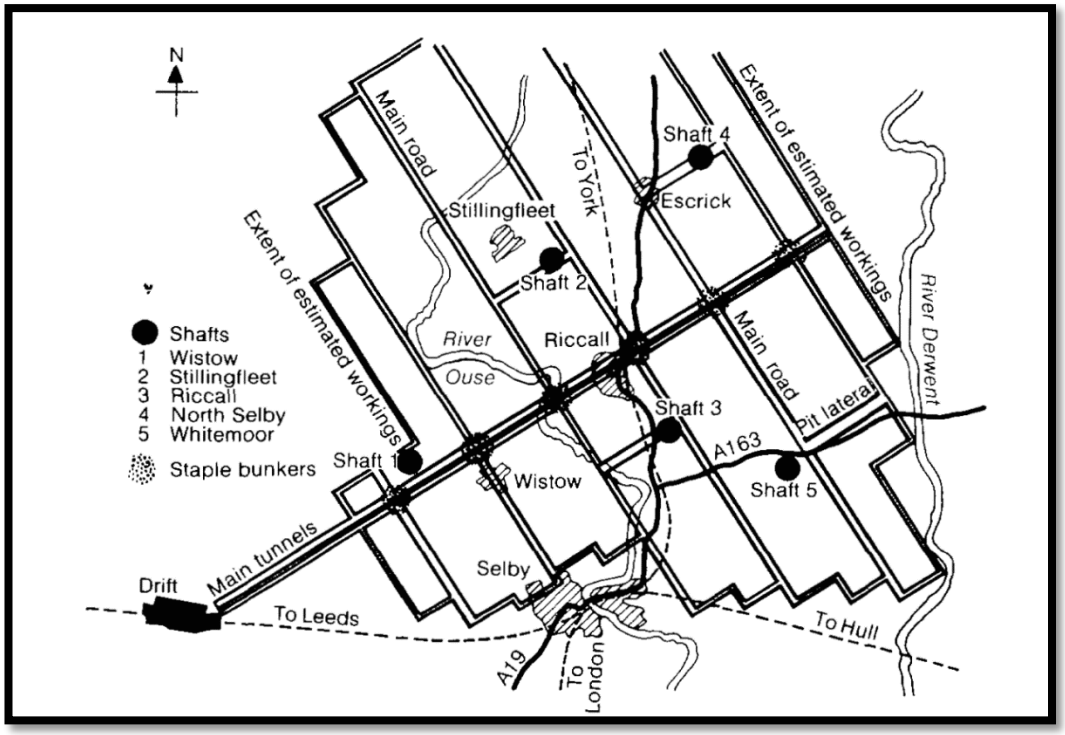

Figure 2-13 The plan of Selby underground coal mine (Forrest et al., 1983).

The mine geological settings are complicated, as shown in Figure 2-14. The overlying strata throughout the field consist of layers of Permian and Triassic overlain by some 20 m of glacial deposits. They are alternating layers of clays and sands, the sands being heavily watered (Massey and Stenton, 1984). The Bunter Sandstone is a major aquifer and in the Selby area is a source of water supply to many industries. Water in the Magnesian Limestone is mostly in the lower part, in crevices and at artesian pressure. The Basal Sands have some hard lenses but in the main consist of fairly loose sand liable to flow (Massey and Stenton, 1984).

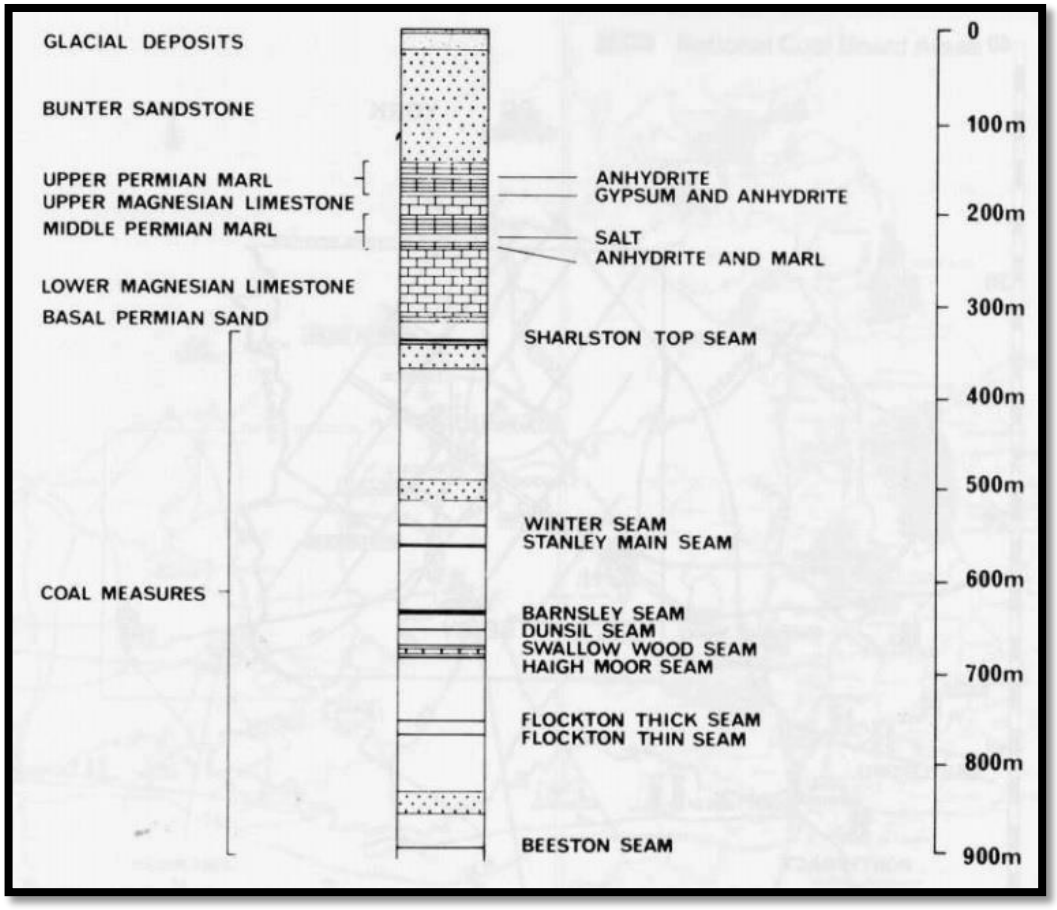

Figure 2-14 General geological section for Selby mine (Massey and Stenton, 1984).

The two spine roadways were constructed by a Robbins TBM and a Titan E134C roadheader respectively. The roadheader was employed to cut the North spine roadway with 5.6 m by 4.0 m horseshoe shaped section; the Robbins 5.8 m diameter TBM was employed for the South one (Athorn and Snowdon, 1986, Massey and

Stenton, 1984). The decline parts of the two roadways dipped at 1 in 4 through the water bearing strata. On reaching the coal measures, the roadways would flatten off and continue right across the coalfield at a horizon some 70 m below the target seam. Pre-treatment of ground was conducted according to the hydrogeology conditions; six dewatering wells were constructed at the portal section, and the basal sands section was frozen from the surface during the drift drivage, as shown in Figure 2-15. Ground support in the water-bearing strata, i.e. from the surface to the coal measures, was spheroidal cast iron segmented lining (tubbing) which provided absolute water-tightness, as shown in Figure 2-16 (Forrest et al., 1983, Massey and Stenton, 1984). Ground support in the sections in coal measures was five piece circular steel arches at 1 m centres and the invert was back-filled to a depth of 1.2 m with debris diverted from the conveyor (Athorn and Snowdon, 1986, Forrest et al., 1983).

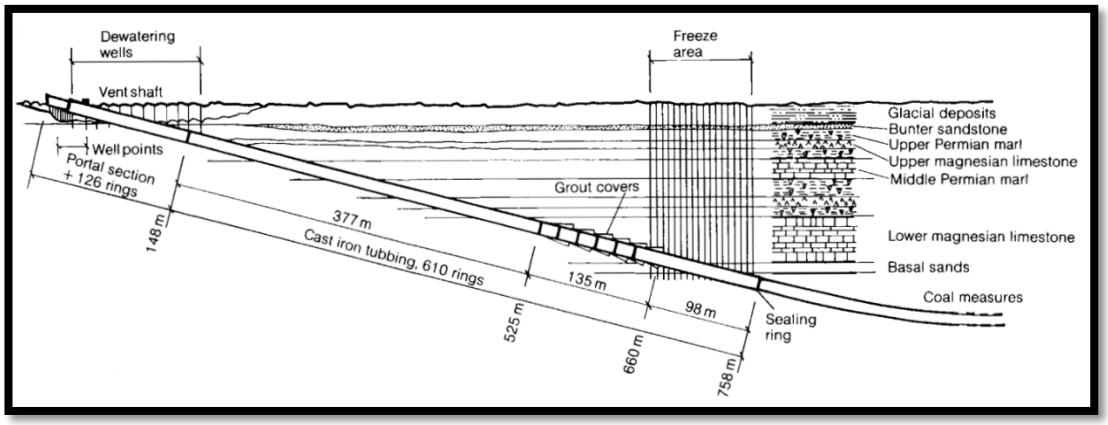

Figure 2-15 Alignment of the TBM driven drift matching with geological stratigraphy (Massey and Stenton, 1984, Forrest et al., 1983)

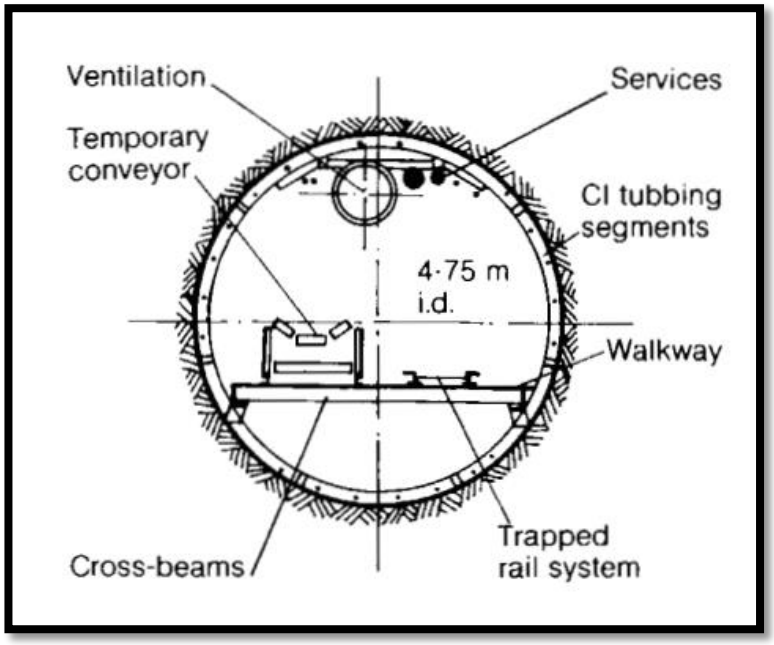

Figure 2-16 Cross section schematic of TBM driven drifts in the water-bearing strata (Massey and Stenton, 1984, Forrest et al., 1983)

The employed Robbins TBM is a hard rock TBM with very short shield and canopy, as shown in Figure 2-17. Average performance of the TBM turned out to be effectively twice the rate of the average achieved with the roadheader in the other roadway (Massey and Stenton, 1984). The TBM achieved the faster heading rate with a best weekly advance of 150 m compared with 72 m for the Titan roadheader: both these rates were achieved in mudstone with a compressive strength of about 45 MPa. The difference between the average weekly advances was somewhat smaller, which were 79.7 m for the TBM and 43.5 m for the roadheader respectively (Athorn and Snowdon, 1986, Forrest et al., 1983).

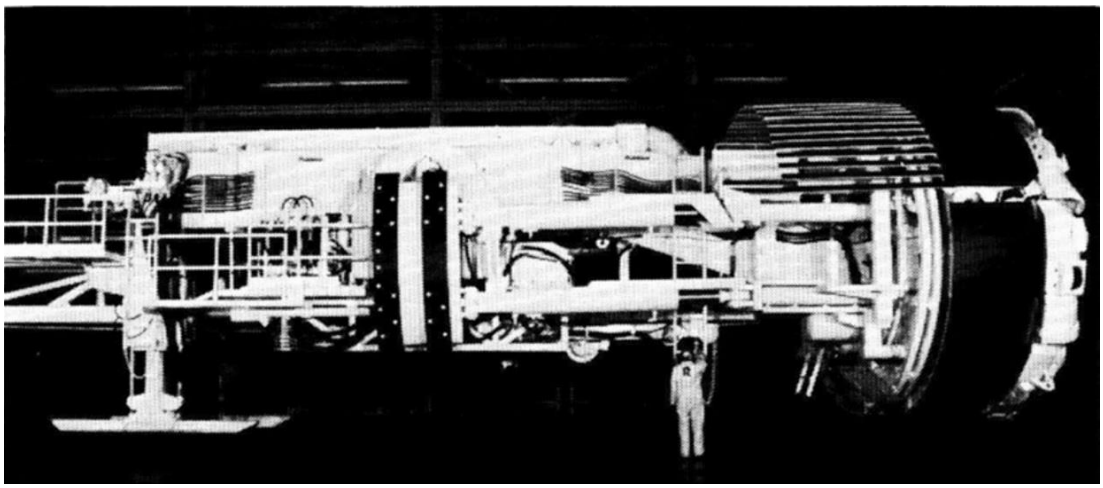

Figure 2-17 Robbins TBM adopted in Gascoigne Wood drift drivage in Selby coal mine (Forrest et al., 1983).

Cost comparing was conducted at specific sections of the drivage, as shown in Table 2-3. The total cost per meter was marginally 16.5% higher for the tunnel driven by the Robbins TBM than for the tunnel driven by the Titan roadheader (Athorn and Snowdon, 1986). But the circular tunnel profile constructed by the Robbins TBM was considerably more stable than the horseshoe-shaped profile produced by the Titan roadheader. The latter was subject to severe floor heave which needed extensive dinting by Hausherr dinting machines. The cost of roadway maintenance can be a source of considerable post-excavation costs and needs to be carefully considered (Athorn and Snowdon, 1986).

Table 2-3 Cost comparing between Roadheader and TBM (Athorn and Snowdon, 1986).

	Titan Roadheader	Robbins TBM
Contractor cost (£/m)	456	400
Materials cost (£/m)	666	718
Machine Parts and Tools cost (£/m)	19	39
Machine cost (£/m)	37	214
Total (£/m)	1178	1371

Selby project demonstrated that the TBM method can accommodate the requirements of deep mine development. Selby project has a big overburden, i.e. the tunnels stretch from the surface and will keep 70 m below the target coal seam to over 1000 m of overburden depth (Athorn and Snowdon, 1986, Forrest et al., 1983, Massey and Stenton, 1984). By the way, conveyor problems posed the biggest factor which adversely influenced the performance of the TBM, which incurred a downtime of 17.5% of the total shift time (Athorn and Snowdon, 1986).

In conclusion, the Selby TBM driven tunnel is a long, deep tunnel, with length of 13.5 km, depth from 0 to over 1000 m, drift sections in ground under complicated hydrogeological conditions. It turned out to be successful with advancing rate twice that of the roadheader, while total cost was just marginally higher than the counterpart of the roadheader. TBM's performance in Selby mine shows that its application in long deep tunnel drivage is practical. The considerable downtime caused by mucking belt conveyor problems reflects the importance of good management of it in long tunnels.

2.2.5 Gneisenau mine project

The Gneisenau mine is sited at Lunen in Westfalia, West Germany, as shown in Figure 2-18, and indicated by the letter A. It was opened in 1873 and closed in 1985. In 1977, a Demag TVM54-58/61H TBM was employed to develop a 4300 m connecting roadway between different levels from 1060 level upward (Hunt, 1978).

Figure 2-18 Location of Gneisenau mine (Courtesy Google Map).

The geological setting was competent for this project apart from an overthrust with thickness of 80 m. The machine encountered sandstone, sandy shale and schist with compressive strength varying from 40 to 160 MPa. Water was also encountered and successfully controlled by grouting (Hunt, 1978). The overthrust did lower the advancing rate but was successfully passed with pre-grouting, and the excavation rate in the overthrust section was 6.5 m per day (Hunt, 1978).

The machine was an open-type hard rock TBM with a diameter of 6.1 m, as shown in Figure 2-19 and Figure 2-20. It has a total power rating of 1000 kW of which 640 kW is available for driving the head. Its stroke was from 0.75 to 1.50 m and it could advance at a maximum rate of 75 mm per minute in favourable rock conditions (Hunt, 1978).

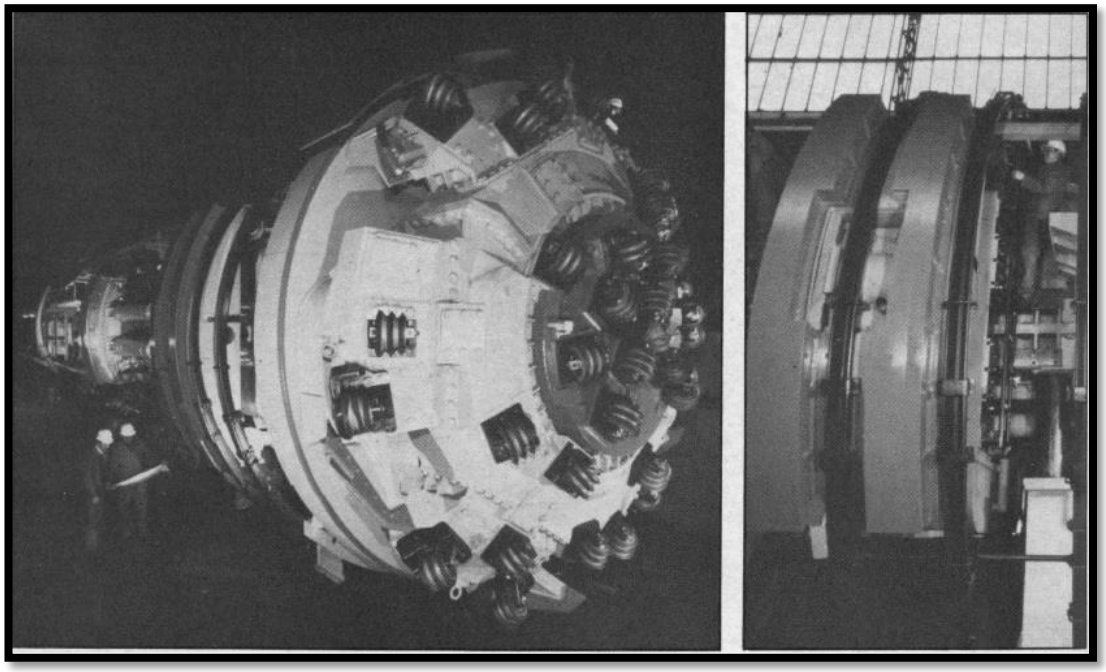

Figure 2-19 The TBM in Demag mine (left), arch erector gear behind the machine head (right) (Gneisenau mine project) (Hunt, 1978).

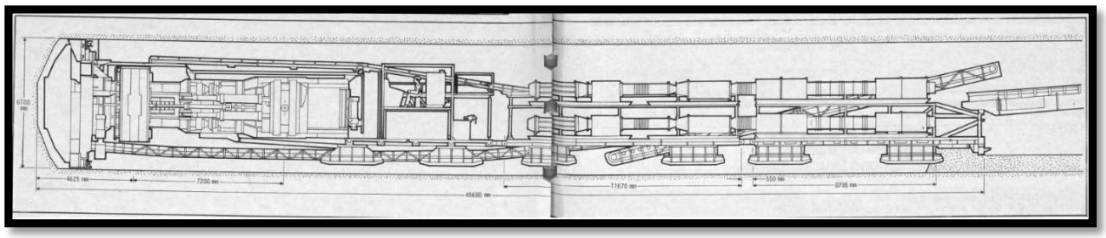

Figure 2-20 Diagrammatic illustration of the full-facer in the tunnel (Gneisenau mine project) (Hunt, 1978).

The TBM was assembled and launched at the 1060 level. Excavated material was carried under the machine on conveyors, as shown in Figure 2-20 (Hunt, 1978). Supports for the tunnel were five pieces steel ring arches with steel mesh forming a continuous layer behind the arches to prevent rock falls and a 130 mm thick sprayed concrete lining (Hunt, 1978). Rigid arches made of steel beam of 29 kg/m were used for the first 800 m of drivage and were then superseded by yielding arches made of steel beam of 34 kg/m (Hunt, 1978). It took 25 minutes to fix a ring of arches into position at 750 mm centres, which was accomplished without stopping the machine (Hunt, 1978).

The TBM achieved satisfactory excavation rates all along the tunnel alignments. The tunnel negotiated two short straight sections and two radial curves with a radius of 150 m before the main cross cut began. Progress on the first straight section was delayed because of overbreak but an advance of 9 m per day was achieved while navigating the first curve, 11 m per day on the second straight section, 13 m per day on the second curve and when the main straight drivage began output built up to the average of 20 m per day or 400 m per month (Hunt, 1978).

The TBM drivage also achieved economic superiority over drill and blast drivage at the main straight drivage section. The cost of the drivage at 400 m per month was DM7000/m which was less than the estimated cost of DM8000/m for the drill and blast approach. The economical break-even point for the full-facer in comparison with drill and blast was estimated to be close to 15 m per day (Hunt, 1978).

In conclusion, the Gneisenau mine TBM project was successful both time wise and economically. The underlying causes included but were not limited to relatively competent geological condition and the long straight tunnel alignment. This project which was as deep as 1060 m set a good reference for the present deep coal mines.

2.2.6 West cliff mine project

The West Cliff mine is about 50 km southwest of Sydney, New South Wales, Australia, as shown in Figure 2-21, and indicated by the letter A. Its men and materials access drift was excavated by a tunnel boring machine. The drift was 1600 metre long with a gradient of 1:3 (White, 1978, Stack, 1982).

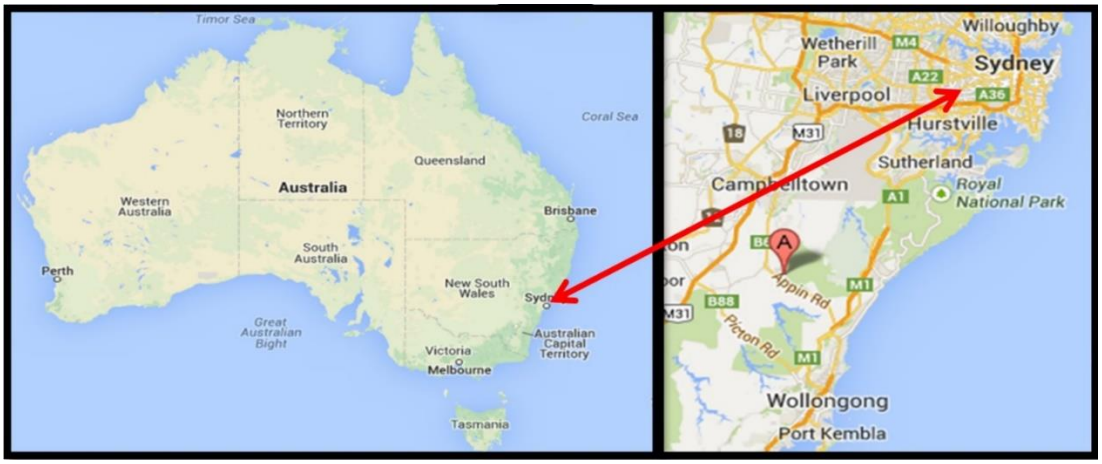

Figure 2-21 Location of west cliff coal mine (Courtesy Google Map).

Geology along the alignment of the decline was reasonable. The decline traversed horizontally bedded sedimentary strata over a vertical distance of 530 meters, as shown in Figure 2-22. Groundwater was encountered, generally in the form of low volume seepage, throughout the Hawkesbury sandstone strata, i.e. over the first 500 meters of drivage, as shown in Figure 2-22. The cumulative inflow over this section of the work amounted to approximately 2250 litres per hour (White, 1978).

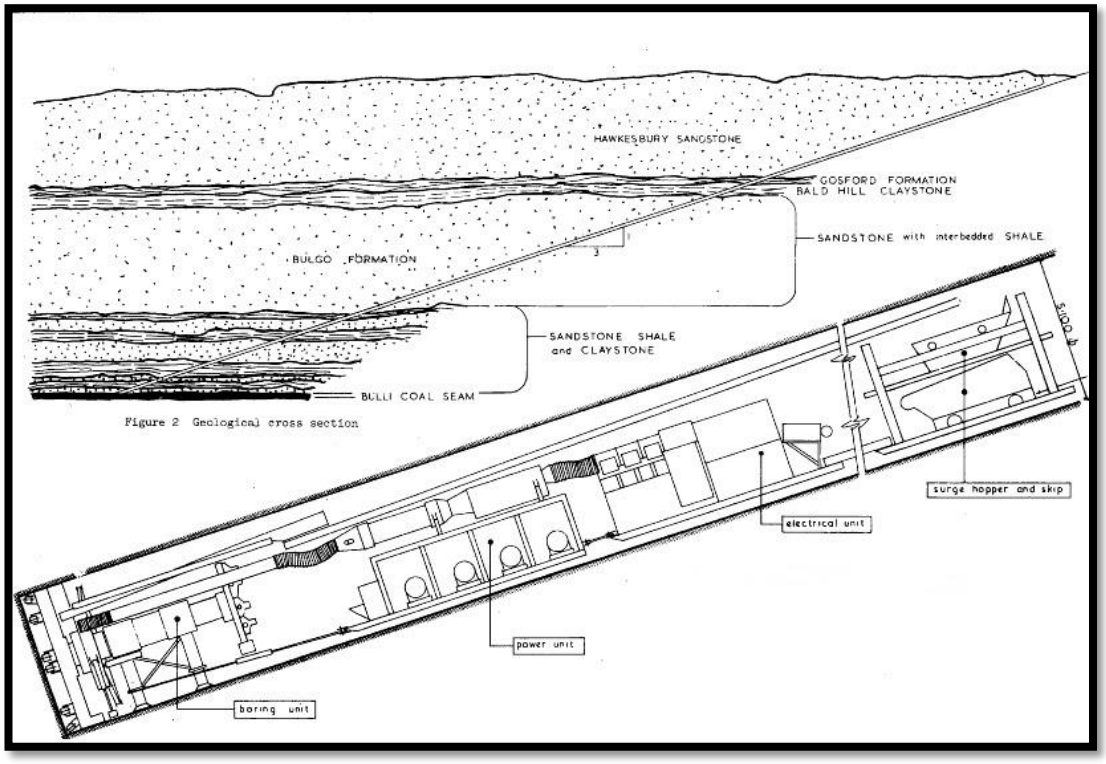

Figure 2-22 Geological cross section of the West Cliff TBM driven decline (White, 1978).

The machine adopted was a Calweld 5.1 meter diameter open-type gripper TBM, as shown in Figure 2-23 (Stack, 1982, White, 1978). The machine was a refurbished one, and was used previously to bore 4572 m of horizontal tunnel in a railway project. To accommodate the 1:3 decline, some modifications had been undertaken, which included but were not limited to the re-orientation of scraper blades which feed spoil to the cutter head muck bucket, the re-build of the machine base for the hydraulic pump units in the power trailer and the re-build of the electrical control unit. Some other machine parameters are shown in Table 2-4 (White, 1978).

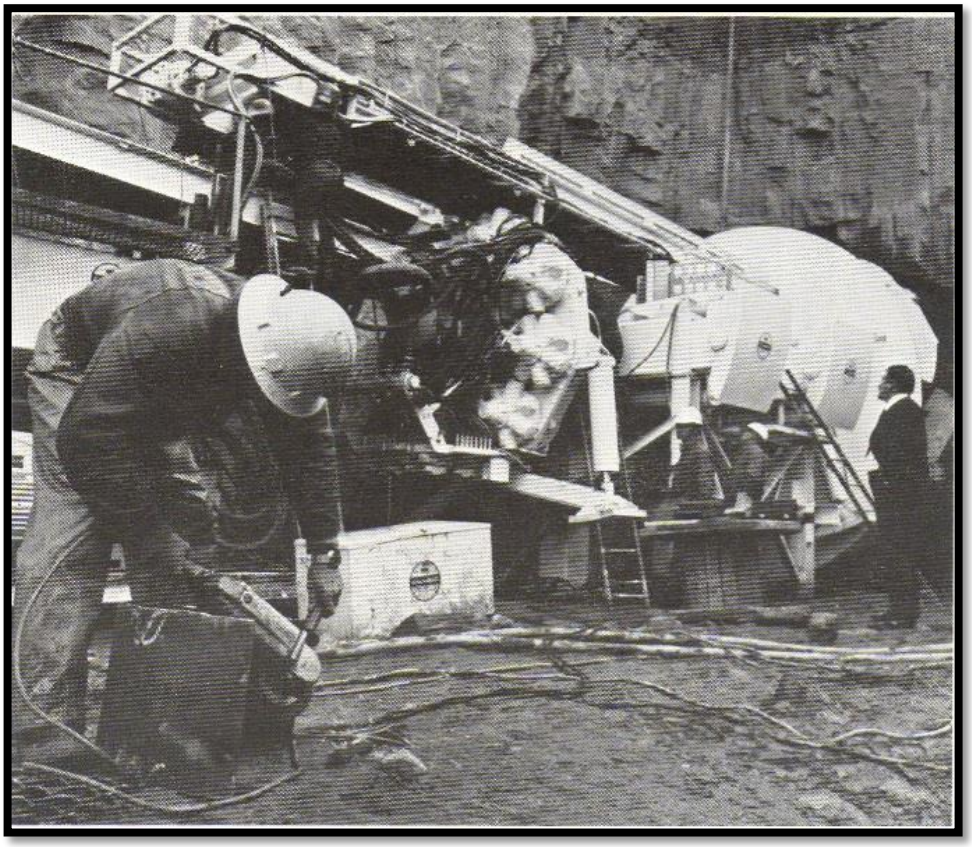

Figure 2-23 The Calweld 5.1 meter diameter TBM employed in West Cliff project (Stack, 1982).

Table 2-4 West Cliff project TBM data (White, 1978)

Head Diameter	5.1 meters
Rotational Speed	4.6 R.P.M
Available Thrust	3.56 MN
Available Torque	880,000 Nm
Cutting Stroke	0.76 meters
Cutters	Centre cutter plus 18 twin kerf disc cutters. Later modified to centre cutter plus 28 single disc cutters.
Power Supply	12 kV

Water bearing strata without being pre-treated and non-water-tight roof bolts and mesh ground support caused problems for the mucking system and ground stability. The conveyor system was employed for mucking at the beginning. Ingress of ground water from the overlying Hawkesbury sandstone made cuttings into slurry. Mucking spillage at transfer points between unit conveyors and penetration of slurry to drive pulleys made the conveyor system completely unmanageable. So after 185 m of drivage, the conveyor system was superseded by a skip system (White, 1978). The interbedded shale and sandstone below the Hawkesbury sandstone gave rise to unstable roof conditions. Delays caused by roof fallout significantly reduced the machine cutting time by approximately 40% (White, 1978).

TBM mechanical breakdowns and hydraulic faults considerably delayed the excavation schedule. At chainage 315 m, the machine suffered main bearing failure. Over six months were taken to get the machine back ready for operation from June

30th 1975 to mid-January 1976. Standstill of three weeks was caused by hydraulic faults during February and March 1975 (White, 1978).

West Cliff coal mine TBM project is the first recorded and steepest application of TBM for drift development in the underground coal mining industry, even though it was not as successful as the later projects. The overall advance rate of only 27.6 m per week was achieved after the re-operation of the TBM in January 1976, which was the favourable period of the project. The reasons for the project failure were mainly but not limited to steep grade, lack of precedent reference and machine mechanical failures.

2.2.7 Monopol mine project

Monopol mine operation sat beneath the Ruhr towns of Kamen and Bergkamen, Germany. In 1979, 11.5 km tunnels was planned to open up a new reserve. The development was 1 km beneath the ground surface.

The tunnels traversed some particularly dangerous ground which included unexpected fault zones. Strata in the faulted zones contained 60 per cent sandy shale, 30 per cent coal and shale and ten per cent sandstone (Harding, 1981).

The adopted machine was a 5.1 meters diameter Robbins TBM. It was purchased in 1969 and first set to work in 1971, the machine was Germany's first ever TBM in a German coal mine and was originally designed for a maximum boring diameter of 5.10 m. It was first used to bore 7 km of 5.1 diameter roadway in another Dortmund mine (Harding, 1981). After satisfactorily completing this task, the machine sat idle for a period until it was decided to use it at Monopol to facilitate the opening up of new reserves (Harding, 1981).

Tunnelling began in 1979 with the roster of 18 hours boring, six hours maintenance per day, and five days a week. A maximum advance rate of 570 m per month and average advance rate of 280 m per month were achieved. Fault zones imposed the major challenge to tunnelling. With only basic seismic surveys carried out, the accurate forecasting of fault zones was out of reach; sometimes one fault, which was

thought to be almost a hundred meters away, turned out to cross the tunnel line. The tunnels received a five-piece, tensioned steel ring support lining at 1.1 m intervals (closer spacing in the fault zones) while heavy steel mesh was used to hold the badly cracked and shattered rock back (Harding, 1981).

Monopol mine TBM project seems to be successful from the perspective of advancing rate, but limited background information including geotechnical and hydrogeological conditions have been accessed through literature review.

2.3 Brief discussion on rock cutting

All the available literature of the seven projects focused on project engineering and management issues, such as advance rate, construction cost, disc cutter wearing, and TBM downtime etc.. Advance rate and construction cost are the two dominating concerns in the feasibility study of a specific TBM project (Balci, 2009). Disc cutter wearing and TBM downtime affect both advance rate and construction cost. According to field experience, disc cutter consumption is very considerable and accounts for nearly 1/5 to 1/4 of the total project cost in normal conditions. In adverse conditions, the cost proportion can reach 1/3, and disc cutters' changing and repairing time will take up to 1/3 of the total TBM down time (Zhang, 2008, Frenzel et al., 2008, Wang et al., 2012). All these project engineering and management issues are closely related to rock cutting (Rostami and Ozdemir, 1993, Ozdemir et al., 1977, Rostami, 2013, Innaurato and Oreste, 2011, Sundin and Wänstedt, 1994).

TBM advance rate is obtained with cutter head penetration multiplied by its rotation speed. The penetration is expressed in mm of advance per rotation. The prediction of cutter head penetration is the prerequisite for TBM advancing prediction. Cutter head is a circular shape disc cutter tool carrier, as shown in Figure 2-24.

Figure 2-24 A typical TBM cutter head.

Penetration is achieved by thrusting the cutter head into the tunnel face at the same time of rotating in a circle. The cutter head rotation takes disc cutters into rolling over the tunnel face, as shown in Figure 2-25. The machine thrust and rotation torque are distributed to disc cutters, and making them penetrate into the tunnel face and form cutting grooves.

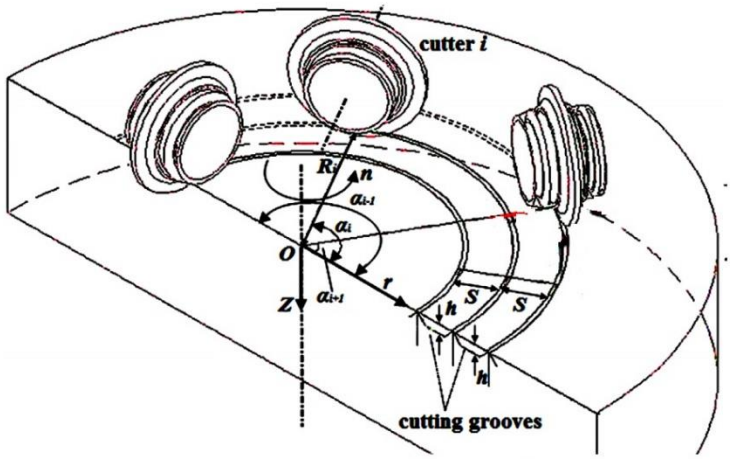

Figure 2-25 Typical disc cutter cutting actions (Xia et al., 2015).

Reacting forces are exerted on the disc cutters from the tunnel face in the cutting actions, as shown in Figure 2-26. The forces include rolling force, normal force and side force. Rolling force is the reacting part to cutter head rotation; normal force is the reacting part to machine thrust; side force is minor and often neglected.

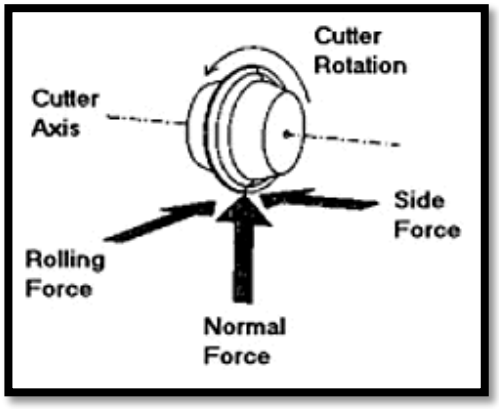

Figure 2-26 The schematic diagram of the forces acting on a disc cutter (Cigla and Ozdemir, 2000).

The cutting forces have direct influences on disc cutter wearing, which is elaborated in the discussions in Chapter 6. As disc cutter wearing affects TBM downtime, construction cost, and advance rate etc., so the cutting forces are influencing factors of all the listed project engineering and management issues. These issues have to be addressed in the course of rock cutting investigation.

For TBM advance rate prediction, cutting forces prediction models derived from the proposed disc cutting mechanisms are employed to calculate the required cutting forces under different penetrations. Then, using the information on the machine thrust and rotation torque, the achievable penetration can be predicted. Combining the achievable penetration and the rotation speed, the TBM advance rate can be predicted.

Studies of rock cutting, which include cutting forces and cutting mechanisms, are the basis for the analysis of the mentioned project engineering and management issues. More details of disc cutting forces and disc cutting mechanisms are provided in Chapter 3 and Chapter 4 respectively.

In addition, the importance of TBM tunnelling in underground coal mines is increasing due to its needs to excavate a large amount of stone roadways to accommodate the stress and gas problems as a result of deeper mining operations. These stone roadways are exposed to high ground stresses as such it calls for a better

understanding of rock-tool interaction in high stress confined strata. However, little knowledge exists about the tool performance in deep tunnels in comparison with shallow excavations. Study of the influence of high ground stresses on dis cutting is elaborated in Chapter 6.

2.4 Conclusions

TBM's have been applied in underground coal mining for over 40 years with cases over America, Asia, Australia and Europe, especially in Britain and Germany. The majority of the historical cases were successful from the perspective of advancing rate, and some of them were even both faster and more economical than conventional methods; although a few ones turned out to fail.

From the perspective of excavation rate, all TBMs outperformed their conventional counterpart in competent geological conditions. In the Donkin-Morien project, the TBM drove four times faster than the drill and blast method in the -20% decline section. In the Selby mine project, TBM's advancing rate was over two times that of roadheader's on both bases of maximum and average. At the long straight section of the Gneisenau mine project, the TBM achieved advancing rate of over 20 meters per day. In the Monopol mine project, with the roster of eighteen hours boring, six hours maintenance per day, five day week, maximum advance rate of 570 m per month and average advance rate of 280 m per month were achieved. Bad performance was also experienced ranging from unsatisfactory advancing rate to withdraw of the machine in adverse geological conditions.

TBM's performance was sensitive to geological conditions, machine reliability and the backup system reliability. Most failures of TBM projects, such as twice withdraw of the machine from the face in Dawdon project, was from the severely faulted ground. The poor performance of TBM in West Cliff project was partly attributed to its main bearing failure and hydraulic faults.

Most TBM projects have higher excavation cost than that of conventional methods. But in favourable conditions, where tunnels were long and straight in competent ground, TBMs could outperform conventional methods. In the Selby mine project,

where two 13.5 km straight tunnels were driven, the total excavation cost of the TBM was just 16.5% higher than that of the roadheader. In the Gneisenau mine project, TBM's overall excavation cost was lower than drill and blast method.

3 CHAPTER THREE –DISC CUTTING FORCE PREDICTION

3.1 Introduction

High advance rate is an important merit which makes TBMs stand out over conventional tunnelling methods for underground coal mines because fast stone roadway drivage is required from the perspectives of mine safety and smooth longwall panel succession. Prediction of advance rates is one of the main concerns in the feasibility study of a specific project (Balci, 2009). Prediction methods are based on the analysis of the forces required to cut a unit volume of rock. So, rock cutting study is the basis for advance rate prediction. In addition, it is also the basis for cutter head design.

TBM rock cutting is accomplished by the cutterhead. The cutting tools on the cutterhead are the parts which interact directly with rocks. Standard cutting tools adopted for TBMs are disc cutters, as shown in Figure 3-1. So, TBM related rock cutting is mainly that under disc cutters.

Figure 3-1 A typical disc cutter which is employed on TBMs.

A disc cutter is made of cutter ring, body, side cap, bearing, and shaft, as shown in Figure 3-2. The cutter ring is the direct interacting part with rocks. During operation the cutter ring edge is forced into the rock surface, and a superimposed translator motion causes the disc to roll along the rock surface. Rock chips form in a lateral direction to the sides of the cutting ring (between adjoining disc cutters).

Figure 3-2 Basic structure of disc cutters.

The first successful use of disc cutters was in 1952 where the machine excavated faulted and jointed shale. Because the rock was weak, it was excavated with low cutter loads. The cutter bearings did not need to be very large and the cutters were kept small which make them easy to handle and change. However, TBMs were soon forced into ever harder rocks, which resulted in unacceptable cutter loads and wear rate on the small cutters, along with a rising number of cutter failures due to catastrophic bearing failure. As a result, over the succeeding years, cutter size and bearing capacity increased, as shown in Table 3-1 (Roby et al., 2008).

Table 3-1 Cutter diameters and loading rate vs. year (Roby et al., 2008).

Diameter（Inch）	Load（kN）	Year Introduced
11	85	1961
12	125	1969
13	145	1980
14	165	1976
15.5	200	1973
16.25	200	1987
17	215	1983
19	312	1989
20	312	2006

According to the geometry of cutter ring, disc cutters can be categorized into V shape disc cutters and Constant Cross Section (CCS) disc cutters, as shown in Figure 3-3 and Figure 3-4.

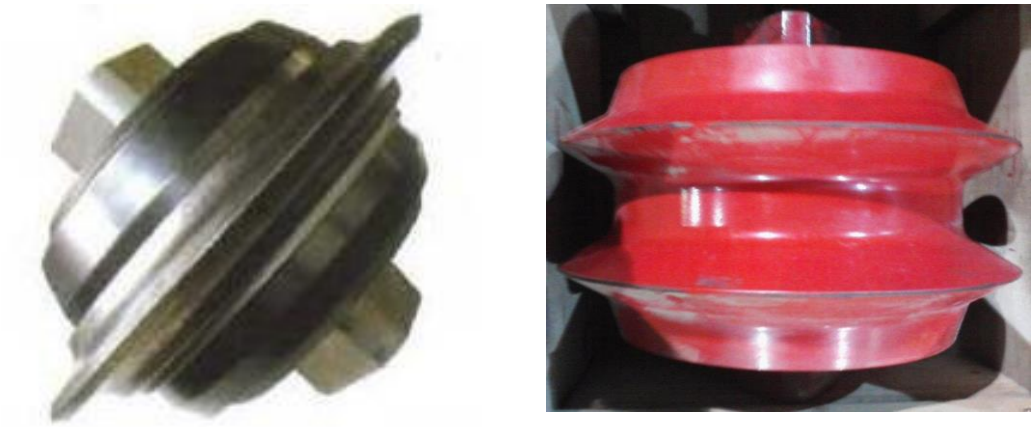

Figure 3-3 V shape disc cutters.

Figure 3-4 CCS disc cutters.

3.2 Disc cutter cutting forces prediction models

In cutting actions, the disc cutter is subject to three orthogonal cutting force components, which are normal force, rolling force and side force, as shown in Figure 2-26. Normal force is provided by the machine thrust, rolling force is provided by the rotational torque of cutterhead. Side force is minor and balanced by cutters placed at different parts of the cutter head. So it is often neglectable compared to normal force and rolling force. Conclusively, the cutting force prediction models focus on normal force and rolling force.

Numerous researchers have attempted to develop accurate cutting force predicting models for disc cutters. A model can be developed basing on postulating a failure mechanism and cutting geometry.

3.2.1 Evans model

Evans proposed a normal force prediction model for V shape disc cutters by assuming that the normal force on a cutter required for penetration is the same in calculation as the passive earth pressure against a retaining wall in soil mechanics (Evans, 1974). The model was formulated as:

$$F_{\mathrm{N}} = \frac{2cp\cos\varphi\sin\left(\frac{\alpha}{2}+\Psi\right)}{\left(\sin\left(\frac{\pi}{4}-\frac{1}{2}\frac{\alpha}{2}+\Psi+\emptyset\right)\right)^{2}} \quad (3\text{-}1)$$

Where:

F_{N} is normal force;

c is cohesion;

φ is rock internal frictional angle;

p is disc cutter penetration;

α is disc cutter included edge angle;

Ψ is angle of friction between wedge and rock.

Evans model is one of the earliest attempts on this topic. However, it does not include disc cutter diameter and cut spacing. Laboratory tests of cutting forces indicate that the theoretical normal forces from Evans model were smaller than the realistic ones (Zhang, 2008).

3.2.2 Roxborough model

Roxborough and Phillips (1975) proposed another theoretical model for cutting force prediction. It is assumed that the resistance to penetration is essentially compressive and that normal force, F_{N}, is equivalent to a compressive stress acting over the projected area of disc contact, A, as shown in Figure 3-5.

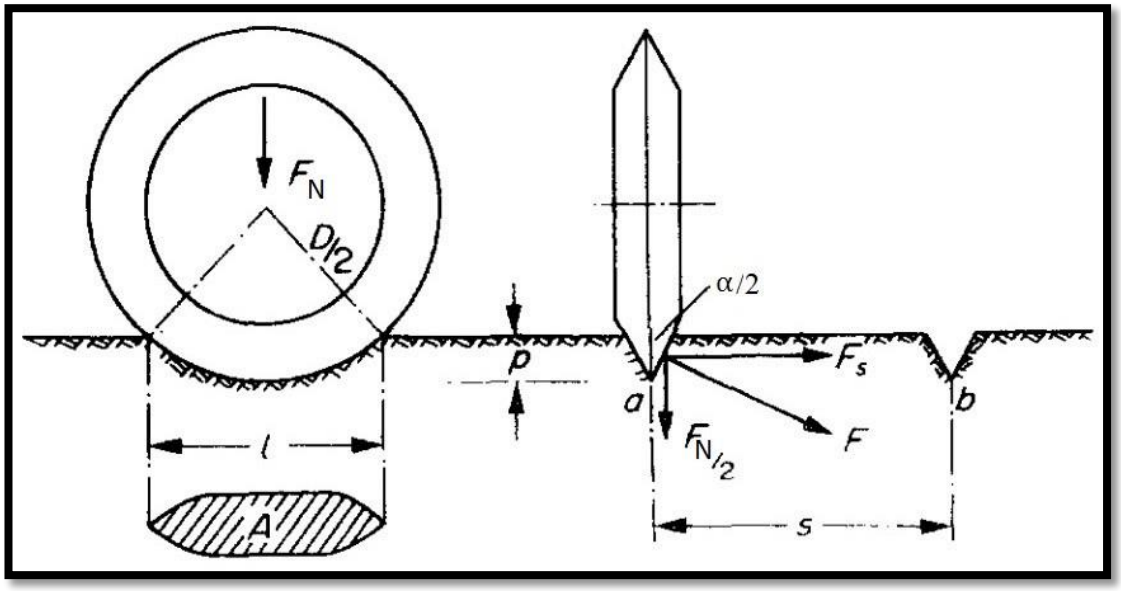

Figure 3-5 Geometry of disc penetration (Roxborough and Phillips, 1975).

The precise determination of area A is complex. Practically, it was simplified with acceptable accuracy as:

$$A = 2pl\tan\frac{\alpha}{2} \qquad (3\text{-}2)$$

Where:

A is the projected area of disc contact;

p is penetration depth;

l is the chord length of contact;

α is disc cutter included edge angle.

The normal force to effect a penetration, p, may, therefore, be written as:

$$F_{\mathrm{N}} = 4\sigma_{\mathrm{c}}\tan\frac{\alpha}{2}\sqrt{Dp^3 - p^4} \qquad (3\text{-}3)$$

Where σ_{c} is the unconfined compressive strength of the rock (Roxborough and Phillips, 1975).

To develop the prediction model of rolling force, F_{R}, Roxborough and Phillips made an assumption and a simplification. The line of action of the resultant force, R, was assumed to pass through the centre of rotation, as shown in Figure 3-6. The cutting action was simplified to be friction free. Ignoring friction poses little influence on the derivation of the rolling force model, since rolling friction is likely to be the most appropriate coefficient and with a value of less than 0.01, which makes the difference negligible.

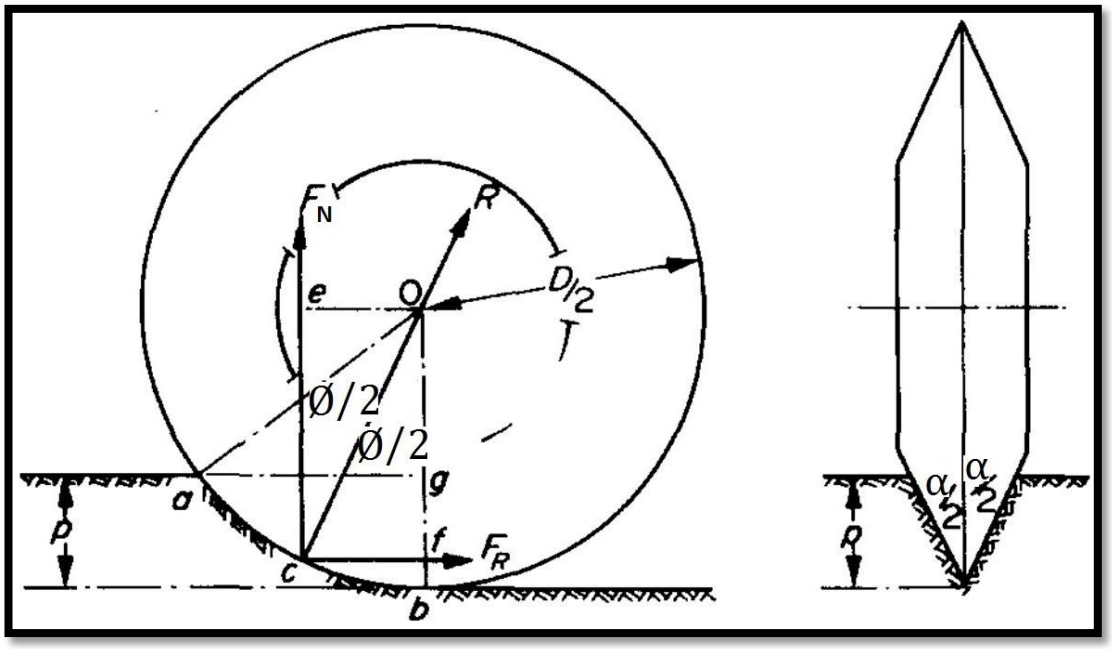

Figure 3-6 Orthogonal forces acting on a disc cutter (Roxborough and Phillips, 1975).

Based on the aforementioned assumption and simplification,

$$F_{\mathrm{R}} \times \overline{of} = F_{\mathrm{N}} \times \overline{oe} \qquad (3\text{-}4)$$

So that:

$$\frac{F_{\mathrm{N}}}{F_{\mathrm{R}}} = \cot\frac{\emptyset}{2} \qquad (3\text{-}5)$$

So:

$$\frac{\overline{og}}{\overline{oa}} = \frac{\frac{D}{2} - p}{\frac{D}{2}} = \cot \emptyset = \frac{1 - \left(\tan \frac{\emptyset}{2}\right)^2}{1 + \left(\tan \frac{\emptyset}{2}\right)^2} \quad (3\text{-}6)$$

Hence:

$$\left(\tan \frac{\emptyset}{2}\right)^2 = \frac{p}{D - p} \quad (3\text{-}7)$$

Thus:

$$\frac{F_{\mathrm{N}}}{F_{\mathrm{R}}} = \sqrt{\frac{D - p}{p}} \quad (3\text{-}8)$$

By substituting the expression of F_{N},

$$F_{\mathrm{R}} = 4\sigma p^2 \tan \frac{\alpha}{2} \quad (3\text{-}9)$$

The Roxborough model provides valuable advancement in establishing the theoretical cutting force model. Validating laboratory tests on a specific sandstone were in good agreement with the proposed theoretical model. However, the assumption that the normal force is equivalent to the compressive stress acting over the projected area of disc contact is based on the assumption that the buried sector of the disc remains in good bearing contact with the surfaces of the cut groove during cutting. But this was not verified by experimental observation. In addition, the parameter cutting spacing is not included in this study and prediction model.

3.2.3 Colorado School of Mines (CSM) model

Ozdemir, Miller, and Wang from the Colorado School of Mines (CSM) proposed the CSM force prediction model based on data from comprehensive and extensive laboratory tests in 1977. The schematic diagram of disc cutting, which the CSM model is based on is shown in Figure 3-7. Aside from all the parameters included in the Roxborough model, spacing of neighbouring cuts, is also taken into consideration.

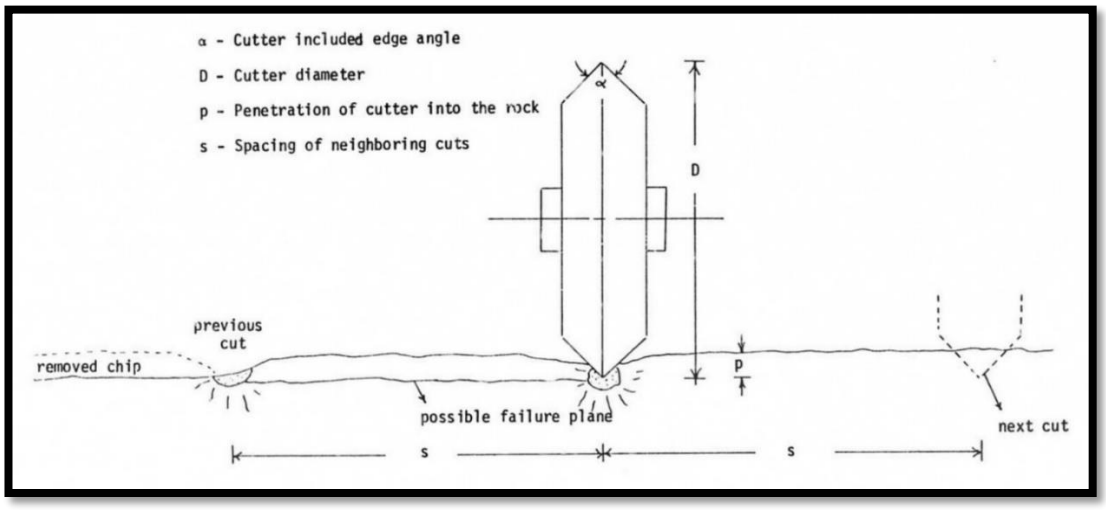

Figure 3-7 Simplified illustration of rock cutting with disc cutter and the nomenclature involved (Ozdemir et al., 1977).

The model development was based on analysis of tests data, as shown in Figure 3-8. It shows that, under fixed penetration, normal force has close correlation with cutting spacing for all disc cutters of different disc diameter and included edge angle. More specifically, vertical cutting force is in linear relationship with the spacing of neighbouring cuts within a medium range of spacing; and changes to be in power function model after a threshold spacing value (Ozdemir et al., 1977).

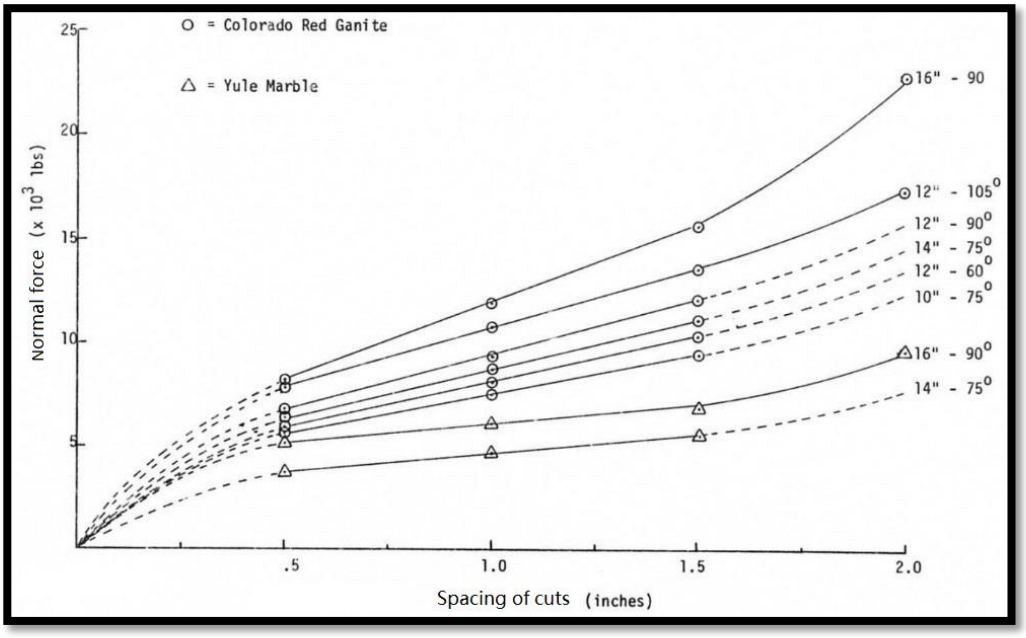

Figure 3-8 Effect of spacing of cuts on normal force at a fixed cutter penetration of 0.1 inches After Ozdemir et al., (1977). Note: the dotted trend lines were extrapolated from known data.

To better visualize the trend, a typical force-spacing relationship for an arbitrary cutter geometry and penetration was abstracted from Figure 3-8, as shown in Figure 3-9. It shows that the force-spacing curve is divided into 3 zones each depicting a distinct mode of increase in forces with increasing spacing of cuts.

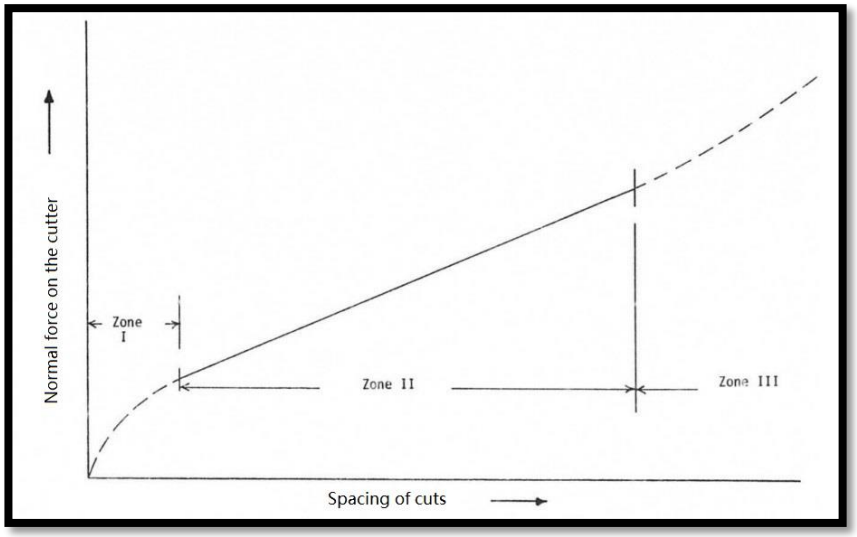

Figure 3-9 A typical normal force-spacing curve for an arbitrary disc cutter geometry and penetration (Ozdemir et al., 1977).

From a practical point of view, zone I is negligible for research because of the small spacing, so only prediction equations for zones II and III are proposed, as follows:

$F_N = a + bs$ for $s < s'$ (zone II) （ 3-10）

And

$F_N = a' + b's^m \; for \; s > s'$(zone III) （ 3-11）

Where:

F_N is normal force;

s' is the optimum spacing;

a, b, a', b' and m are constants.

The assumptions were verified with laboratory testing results on specific energy to spacing trends. The disc cutter rock breaking mechanism was adopted as a combination of uniaxial compressive failure and shear failure, as shown in Figure 3-10.

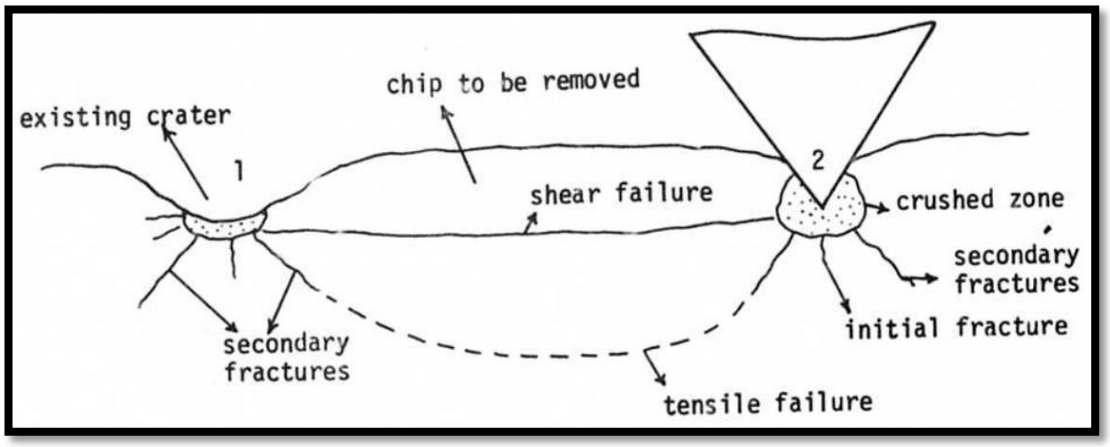

Figure 3-10 The final disc cutter rock breaking mechanisms adopted in the CSM model.

In the CSM model, only the predicting model for Zone II was derived. As discussed above, the prediction equation consists of two parts. The force induced by uniaxial

compressive failure and induced by shear failure are expressed as F_1 and F_2, respectively.

$$\mathrm{F}_1 = \sigma_c \times A_\mathrm{c} \qquad (3\text{-}12)$$

Where:

F_1 is the uniaxial compressive failure induced normal force component;

σ_c is rock uniaxial compressive strength;

A_c is the projected area of disc contact.

This contact area is represented in Figure 3-11.

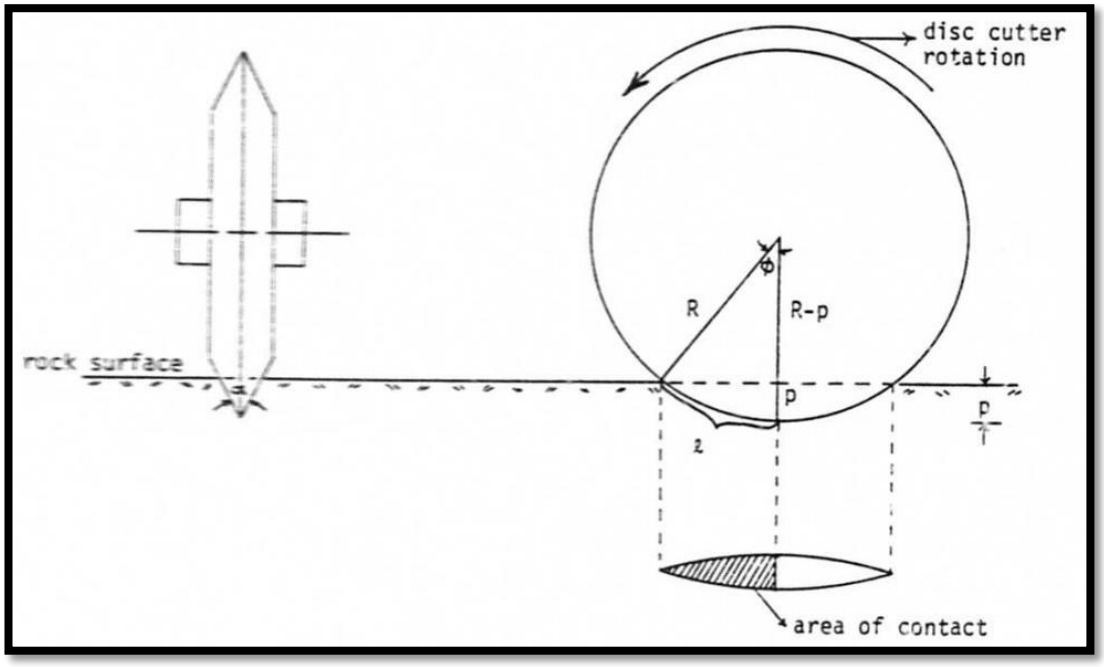

Figure 3-11 Area of contact of disc cutter with rock.

$$\mathrm{A}_c = R^2[\emptyset - \sin\emptyset\cos\emptyset]\tan\alpha/2 \qquad (3\text{-}13)$$

Where:

R is the radius of disc cutter;

$\emptyset$ is the included angle of contact;

α is disc cutter included edge angle.

$$\emptyset = \cos^{-1}(R - p)/R \quad (3\text{-}14)$$

$$F_1 = \sigma_c R^2[\emptyset - \sin\emptyset\cos\emptyset]\tan\alpha/2 \quad (3\text{-}15)$$

F_2 is determined based on the considerations of shear failure of the rock to the adjacent cut(s) and the side force exerted by the cutter to overcome this shear resistance. Considering the idealized multiple cut situation illustrated in Figure 3-12, the cutter is penetrating a rock surface containing two existing cuts equally spaced from the one being formed. To cause shear failure towards the existing cuts, the side force, f_s, exerted by the cutter should have a magnitude to overcome the shearing resistance. That is,

$$f_s = \tau \times A_s \quad (3\text{-}16)$$

Where:

f_s is the slide force;

τ is rock shear strength;

A_s is area of the shear failure surface.

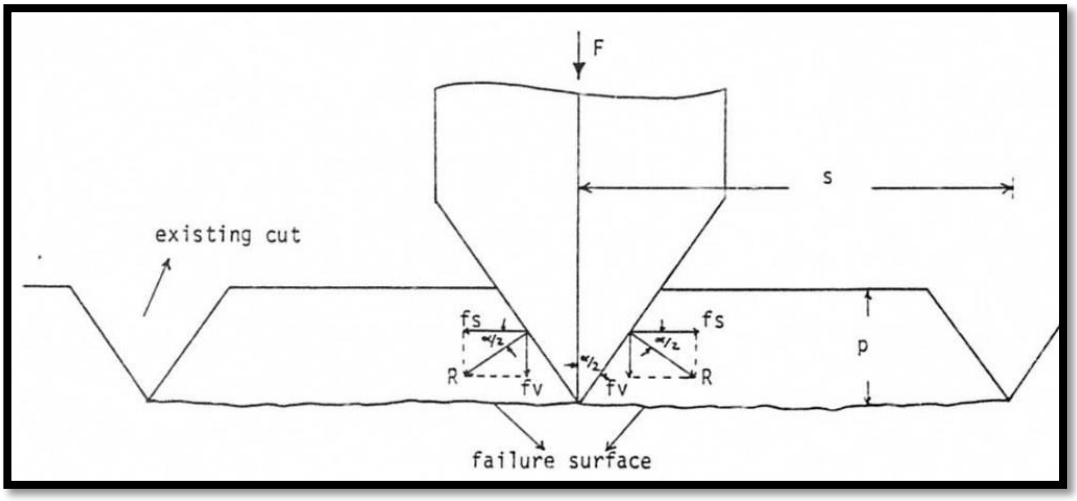

Figure 3-12 Geometry of disc penetration.

At the instant of chip formation, the failure surface is nearly rectangular with ideally a width the same as the cutting spacing and a length approaching the chord length shown as ℓ in Figure 3-11. The expression of ℓ is as follows:

$$\ell = R\emptyset \quad (3\text{-}17)$$

Thus, the area of failure surface becomes:

$$A_s = sR\emptyset \quad (3\text{-}18)$$

$$f_s = \tau \times sR\emptyset \quad (3\text{-}19)$$

$$f_v = f_s \times \tan \alpha/2 \quad (3\text{-}20)$$

$$f_v = \tau sR\emptyset \tan \alpha/2 \quad (3\text{-}21)$$

$$F_2 = 2f_v = 2\tau sR\emptyset \tan \alpha/2 \quad (3\text{-}22)$$

Where:

F_2 is the shear failure induced normal force component;

τ is rock shear strength;

ℓ is the chord length of contact;

f_v is the vertical force.

Considering the fact that a smooth metallic surface is in contact with a finely crushed rock zone at the cutter-rock interface, it is reasonable to expect a relatively small degree of friction so that its effect can be ignored. Before finalizing this equation, the spacing has to be quantified. It should be noted that spacing in the equation is the width of the formed chip(s), i.e. the failure surface width shown in Figure 3-13. However, since real spacing is measured as being the distance between the centerlines of two neighbouring cuts, the actual width of the chip(s) should be less than this value considering the fact that the rock surrounding the penetrating edge of the cutter is locally crushed and the force required to shear this zone should be minute. The width of the crushed zone is assumed to be $2p\ \tan\alpha/2$. So, the width of the chip should be calculated with the real spacing reduced by the width of the crushed zone.

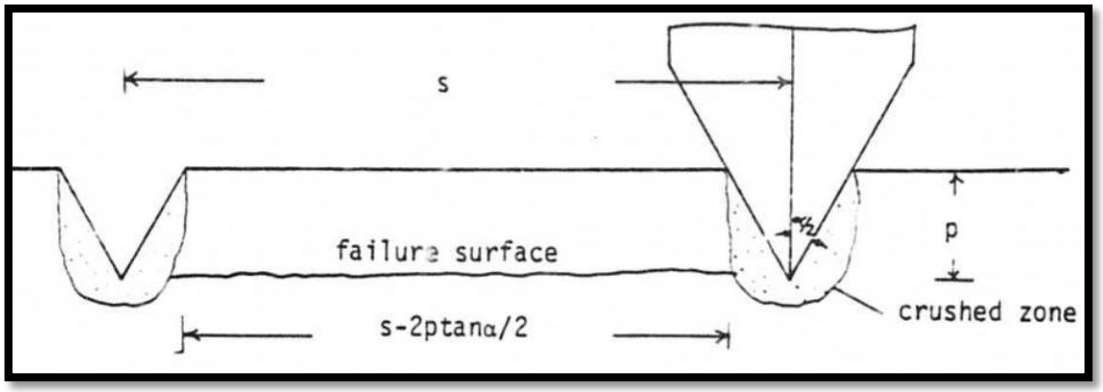

Figure 3-13 The actual chipping length.

Thus, the equation for F_2 was modified as below:

$$F_2 = 2\tau(s - 2p\tan\alpha/2)R\emptyset\tan\alpha/2 \qquad (3\text{-}23)$$

Combining the earlier derived

$$F_1 = \sigma_c R^2(\emptyset - \sin\emptyset\cos\emptyset)\tan\alpha/2 \quad (3\text{-}24)$$

Then

$$F_N = F_1 + F_2 \quad (3\text{-}25)$$

$$F_N = [\sigma_c R^2(\emptyset - sin\,\emptyset\,cos\,\emptyset) + 2\tau(s - 2p\,tan\,\alpha/2)R\emptyset]\,tan\,\alpha/2 \quad (3\text{-}26)$$

Prediction equation (3-26) calculates the expected cutter normal force for given penetration, spacing, cutter geometry, and required rock properties. In practice, it is desirable to estimate the penetration using given normal force and other variables. This can be accomplished by rearranging the equation so that the penetration is the unknown, but with some reasonable approximations for certain terms. And then the rewriting is:

$$F_N = D^{1/2}p^{3/2}\left[\frac{4}{3}\sigma_c + 2\tau\left(\frac{s}{p} - 2\,tan\,\alpha/2\right)\right]tan\,\alpha/2 \quad (3\text{-}27)$$

To establish a rolling force prediction model, a linearly increasing pressure profile at the bearing contact zone was proposed, as shown in Figure 3-14. The contact pressure starts from zero at the surface and increases to its maximum immediately under the disc. The stress at any point on the cutter edge is linearly proportional to depth from the rock surface.

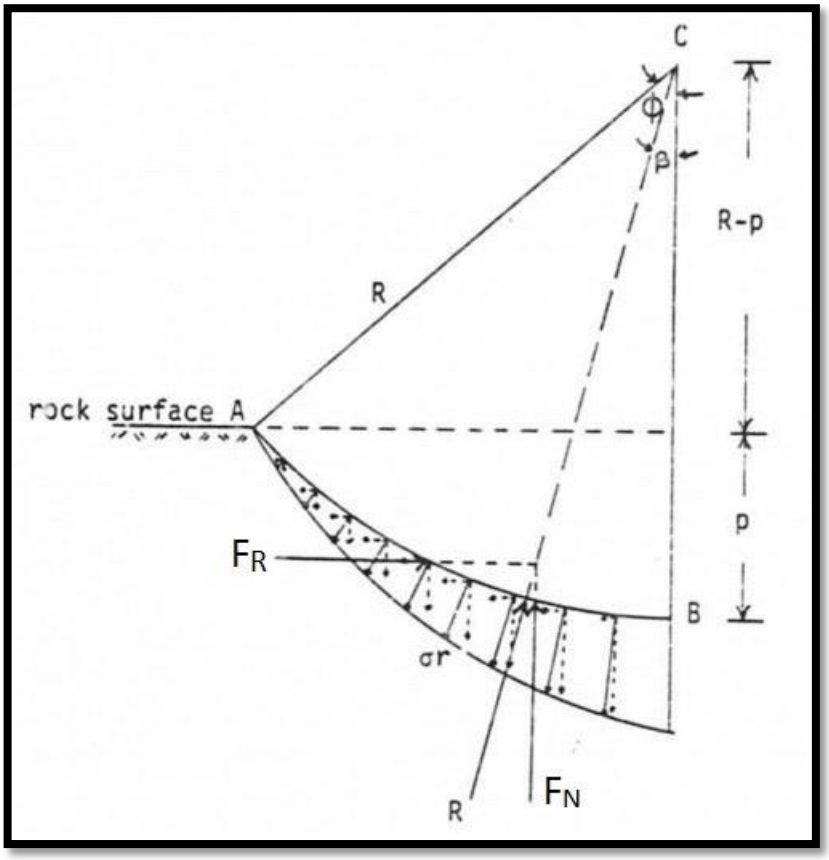

Figure 3-14 Representation of the resultant force and its vertical and rolling components acting on the cutters-rock contact surface in the CSM model (Ozdemir et al., 1977) .

For simplicity, a frictionless cutter was assumed so that the resultant force passes through the center of the cutter. Once the direction of the resultant is determined, the rolling force on the cutter is given as,

$$F_{\mathrm{R}} = F_{\mathrm{N}} \times \tan\beta \qquad (3\text{-}28)$$

Where:

F_{R} is rolling force on the cutter;

F_{N} is normal force on the cutter;

β is the included angle between vertical and resultant line of action (see Figure 3-14).

With the assumed stress distribution profile along the penetrating edge of the cutter and the known geometry of this edge, the direction of the resultant force can be readily calculated, as follows:

$$\tan\beta = \frac{(1-\cos\emptyset)^2}{\emptyset - \sin\emptyset\cos\emptyset} \qquad (3\text{-}29)$$

Where $\emptyset = \cos^{-1}\left(\frac{R-p}{R}\right)$

The predetermined normal force is now substituted into the above equations, giving an expression of the rolling force of the cutter,

$$F_{\mathrm{R}} = \left[\sigma_{\mathrm{c}} p^2 + \frac{4\tau\emptyset(s - 2p\,tan\,\alpha/2)}{D(\emptyset - sin\,\emptyset\,cos\,\emptyset)}\right] tan\,\alpha/2 \qquad (3\text{-}30)$$

In summarizing the preceding theoretical analysis, equations (3-27) and (3-30) were derived for predicting the normal and rolling forces on a sharp disc roller cutter. This model provides reasonably accurate cutting force predictions for V shape disc cutters. Establishment of the CSM model is a vital advancement for cutting force prediction. It was the first practically accepted model in the industry, and is still used.

However, this model is not applicable to disc cutters with large included edge angles, such as the CCS disc cutters as the value will be negative infinite according to the final cutting force calculation formulas. So this model is just applicable to disc cutter with relatively small cutter edge angles. The underlying reason is that this model is established upon laboratory testing data with cutter edge angle not more than 105°.

3.2.4 New CSM model

Along with the development of application of TBMs in hard rock tunnelling, CCS disc cutters had been the standard cutting tools for the applications. All previous cutting force prediction models are not applicable on CCS disc cutters. It is necessary to establish a CCS disc cutter cutting force prediction model for TBM cutterhead

design, optimization and TBM advance rate prediction. To achieve that, Rostami and Ozdemir (1993) tried to introduce a new CSM model.

The forces acting on a disc cutter can be obtained by integrating force elements caused by pressure acting on the disc cutter. For this purpose, the pressure distribution along the periphery of the disc cutter (within the rock-cutter interacting area) was assumed as shown in Figure 3-15. The region of interaction is specified by angle $\emptyset$ which is determined from cutter diameter and penetration as follows:

$$\emptyset = \cos^{-1}\left(\frac{R-p}{R}\right) \qquad (3\text{-}31)$$

Where:

R is cutter radius;

p is penetration depth.

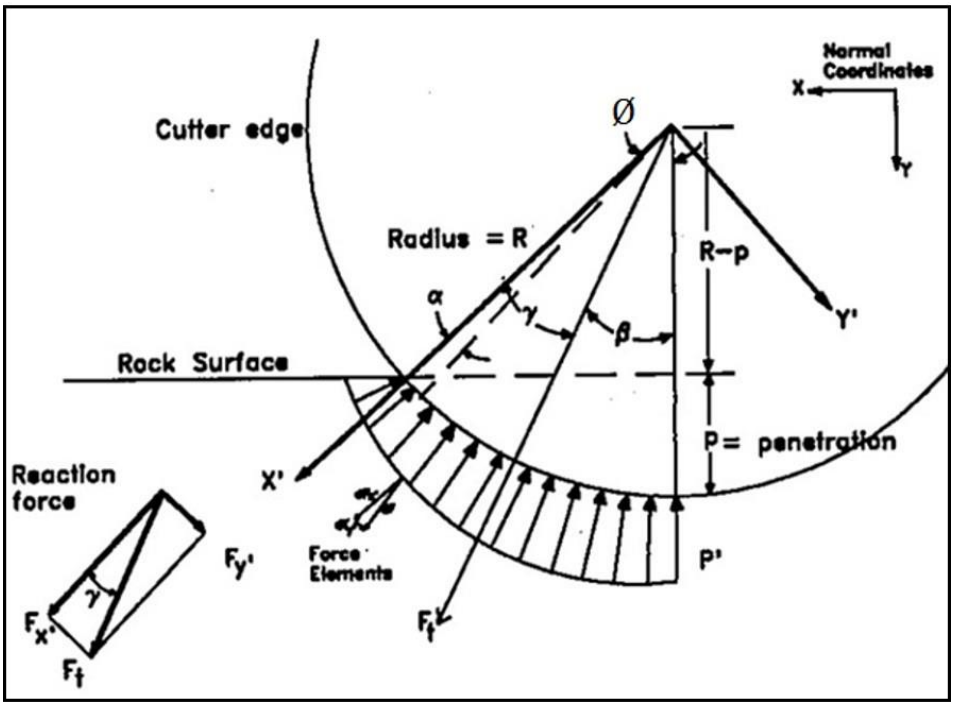

Figure 3-15 Proposed pressure distribution along the disc cutter periphery (Rostami and Ozdemir, 1993).

The pressure, P, at any point is a function of the angle θ and the base pressure, P'. This function can be written as:

$$P = P'\left(1 - \frac{\theta}{\emptyset}\right)^{\psi} \quad (3\text{-}32)$$

Where:

P is pressure at the point of angle θ;

P' is base pressure;

θ is the angle from the normal to face, ranging from 0 to $\emptyset$.

This function may generate different pressure distributions by different power ψ. For a linear distribution starting from zero in front of the cutter and reaching its maximum value, P', under the cutter in a linear pattern with $\psi = 1$. A value of $\psi = 0$ generates a uniform or constant pressure distribution along the cutter penetration edge.

The angle of resultant force with normal to the cutting face (or Y axis), β, is determined by estimating cutting coefficient (CC) as follow:

$$\beta = \tan^{-1}\left(\frac{F_{\mathrm{R}}}{F_{\mathrm{N}}}\right) = \tan^{-1}(CC) \quad (3\text{-}33)$$

In order to determine the cutting forces and CC in a general case with the power function, a new coordinate system, X'-Y', was used to simplify calculations as in Figure 3-15. Using a new positioning angle α, the pressure was expressed as:

$$P = P'\left(\frac{\alpha}{\phi}\right)^{\psi} \quad (3\text{-}34)$$

Thus force components in the system can be determined as:

$$dF = TPR\mathrm{d}\alpha = TRP'\left(\frac{\alpha}{\phi}\right)^{\psi} d\alpha = \frac{TRP'}{\phi} t^{\psi} dt \quad (3\text{-}35)$$

Where:

T is cutter tip width;

t is a slack variable replacing $\frac{\alpha}{\phi}$.

$$F_{y'} = \int_0^{\phi} dF_{y'} = \int_0^{\phi} dF \sin\alpha \quad (3\text{-}36)$$

And

$$F_{x'} = \int_0^{\phi} dF_{x'} = \int_0^{\phi} dF \cos\alpha \quad (3\text{-}37)$$

Since the above integrals do not have an analytical solution, a numerical approach based on Taylor series is used to determine the forces. The results of the integration are:

$$F_{x'} = \sum_1^n (-1)^{i-1} \frac{\emptyset^{2i+\psi}}{(2i+\psi)(2i-2)!} \quad (3\text{-}38)$$

And

$$F_{y'} = \sum_1^n (-1)^{i-1} \frac{\emptyset^{2i-1+\psi}}{(2i-1+\psi)(2i-2)!} \quad (3\text{-}39)$$

Herein, "n" is the number of iterations needed to get the desired degree of accuracy in numerical estimation (usually $n \geq 5$ is enough). The angle of resultant force, γ, is

$$\gamma = \tan^{-1}\left(\frac{F_{y'}}{F_{x'}}\right) \quad (3\text{-}40)$$

This angle can be related to β and the CC can be expressed as:

$$\mathrm{CC} = \tan\beta = \tan(\emptyset - \gamma) \quad (3\text{-}41)$$

Laboratory tests showed that, for CCS and blunt (or worn) cutters, ψ is close to zero and decreases with increase of the tip width. A nominal value of $\psi = 0$ can be used for most cases in which CCS cutters with a tip width of about 12.5 mm (0.5 in.) are used. Using this value, the following equations can be obtained:

$$\beta = \frac{\emptyset}{2} \quad (3\text{-}42)$$

And

$$\mathrm{CC} = \tan\frac{\emptyset}{2} \quad (3\text{-}43)$$

The cutting forces, F_N and F_R, are determined by using the total force F_t and CC or β:

$$F_t = \frac{P'RT\emptyset}{\psi + 1} \quad (3\text{-}44)$$

$$F_{\mathrm{N}} = F_{\mathrm{t}} \cos \beta \qquad (3\text{-}45)$$

And

$$F_{\mathrm{R}} = F_{\mathrm{t}} \sin \beta \qquad (3\text{-}46)$$

To estimate the base pressure, P', a database of measured forces from laboratory linear cutting tests was used. An empirical calculation model of base pressure was established using parameters of cut spacing and penetration, cutter diameter and tip width, and the uniaxial compressive and tensile strengths of the rock. Subsequently, the cutting forces can be calculated with Equations (3-44), (3-45) and (3-46).

This new CSM model made material progress to predict the cutting force for CCS disc cutters. It provides the basis for the CCS disc cutter equipped TBM cutterhead design, optimization and advance rate prediction.

However, simplicity in the model makes its applicability arguable. Firstly, this model did not consider the rock breaking mechanism along with disc cutting. Moreover, the foundation of the model is the empirical formulae of base pressure estimation. The empirical formulae base on the cutting force database was obtained from laboratory linear cutting tests. However, linear cutting tests cannot stand for realistic field rotary cutting. In addition, the tested rock categories were limited.

In addition, the proposed stress distribution in the contact area between rock and disc cutters was not validated by laboratory test measurements; the only verification was the value of cutting coefficient. Recent laboratory tests focusing on pressure distribution within the crushed zone in the contact area between rock and disc cutters have shown a notably different result, as shown in Figure 3-16 (Rostami, 2013). There is an area of no load within the theoretical contact area in front of the high pressure zone, and another no loading area directly underneath the disc. So the assumption base for this new CSM model is arguable.

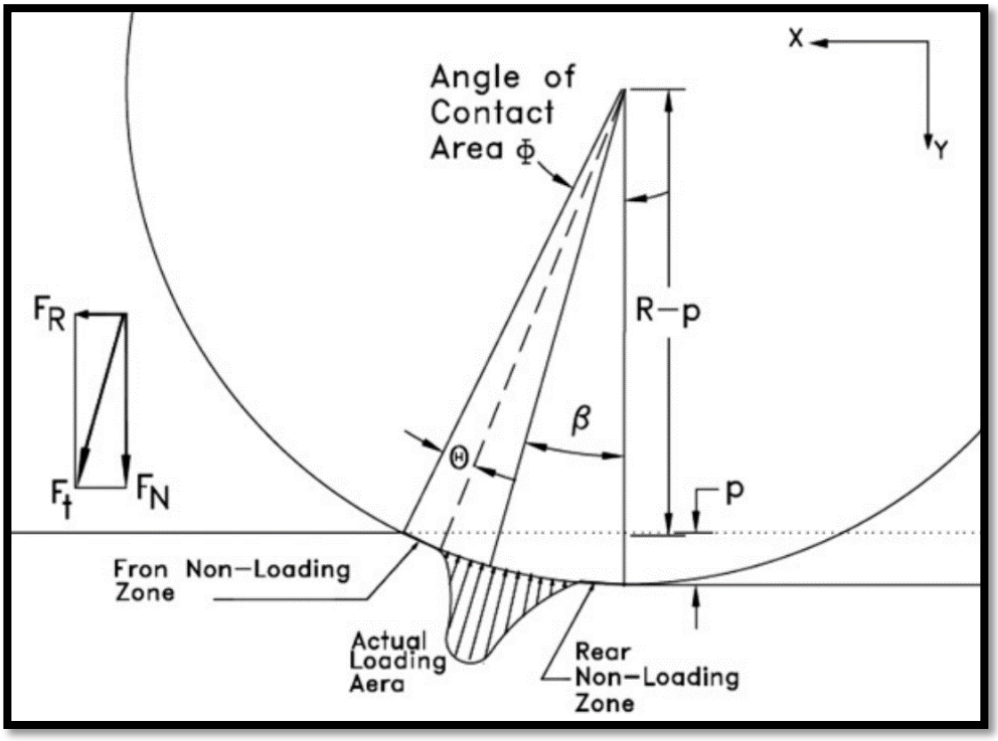

Figure 3-16 Laboratory tested stress field (Rostami, 2013).

3.2.5 H. P. Sanio model

Although most researchers chose shear failure mechanism to establish cutting force prediction models, there is still considerable debate about the mode of failure in disc cutting. Radial cracks and some other observations suggest tensile failure while the presence of shear forces and shear faces in chips suggest shear failure. In contrast to the prediction models based on shear failure, Sanio (1985) from Ruhr University Bochum proposed a prediction model based on tensile failure, which can be explained as shown in Figure 3-17.

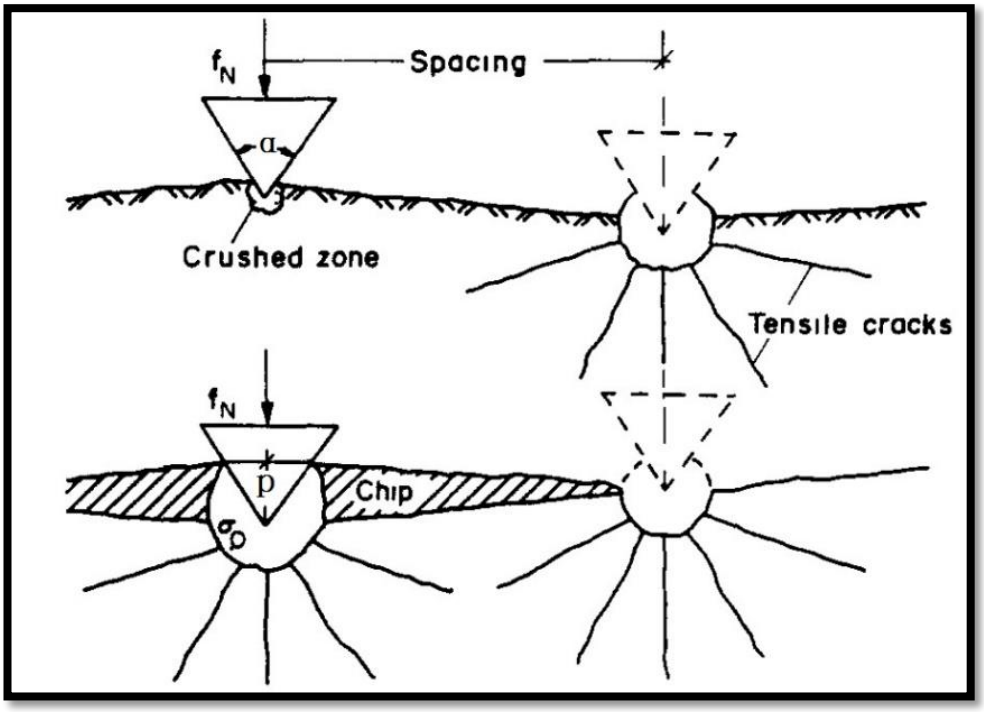

Figure 3-17 Schematic of wedge penetration and chip forming process (Sanio, 1985).

The proposed process of rock cutting consists of three phases. The first one is the formation of a crushed zone below the tool when the rock surface is compressed with approximately hydrostatic high level stress. The second phase is the initiation of the tensile cracks; i.e. the crushed zone exerts stress in the surrounding undamaged rock. When the stress reaches the tensile strength of the rock, tensile cracks would be initiated from the cutting edge. The third phase is the chip formation. Along with the penetration, tensile cracks propagate. When tensile cracks reach the surface or coalesce with tensile cracks formed under the neighbouring groove, chips form (Sanio, 1985).

For simplification, the crushed zone is assumed to be circular in shape, and its radius is to be a constant ratio q of the penetration depth p. The hydrostatic pressure within the crushed zone is to be a critical characteristic of the rock. Then the penetration force f_N can be obtained through multiplying the hydrostatic pressure by the projected area of contact between the tool and the rock, as shown in Figure 3-17.

$$f_{\mathrm{N}} = 2p \tan\left(\frac{\alpha}{2}\right)\sigma_0 \text{ (force per unit width)} \quad (3\text{-}47)$$

Where:

f_{N} is penetration force;

p is penetration depth;

α is cutter edge angle;

σ_0 is hydrostatic pressure in the crushed zone.

Equation (3-47) shows that, as long as σ_0 is known, the normal force f_N can be obtained. To calculate σ_0, a formula in rock blasting fracture mechanics was introduced, as shown in Equation (3-48). It describes correlation between the length of the cracks, the radius of the hole and σ_0 for a pressurized circular hole with pressureless radial cracks in an infinite plate, as shown in Figure 3-18 (Ouchterlony, 1973).

$$2\sigma_0 r = kc^{0.5} \quad (3\text{-}48)$$

Where:

r is radius of the hole;

k is critical stress intensity factor, dependent on the rock and the number of cracks;

c is length of cracks.

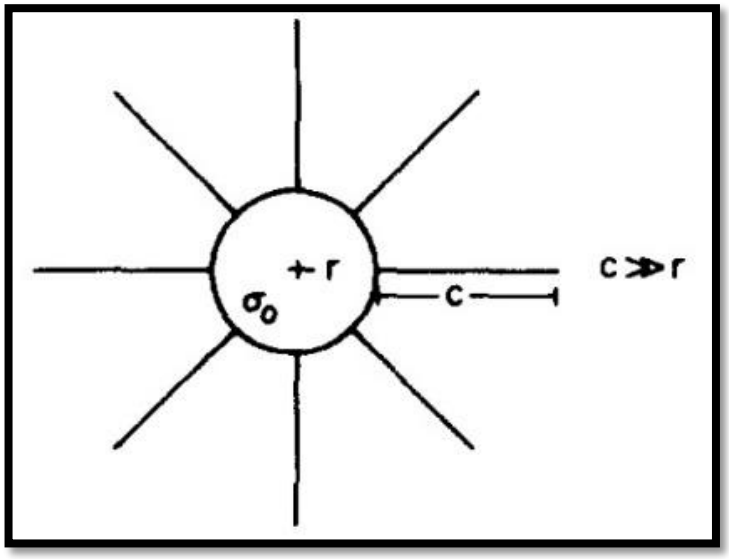

Figure 3-18 Crack propagation from a circular hole in an infinite plate (Ouchterlony, 1973).

For simplicity, the influence of the free surface of the rock on the state of stress at the crack ends is neglected, a combination of Equations (3-47) and (3-48) and $r = qh$ results in:

$$f_{\mathrm{N}} = \frac{k}{q}\tan\left(\frac{\alpha}{2}\right) c^{0.5} \qquad (3\text{-}49)$$

Assuming the cutting is a process as shown in Figure 3-19, the normal force F_{N} at the tool can be derived as follows:

$$F_{\mathrm{N}} = \int_0^{(dp-p^2)^{0.5}} f_{\mathrm{N}}(x)\, dx \qquad (3\text{-}50)$$

$$F_{\mathrm{N}} = \frac{k}{q}\tan\left(\frac{\alpha}{2}\right) \int_0^{(dp-p^2)^{0.5}} [c(x)]^{0.5}\, dx \qquad (3\text{-}51)$$

Where:

F_N is normal force;

d is diameter of disc cutter;

p is penetration of the tool.

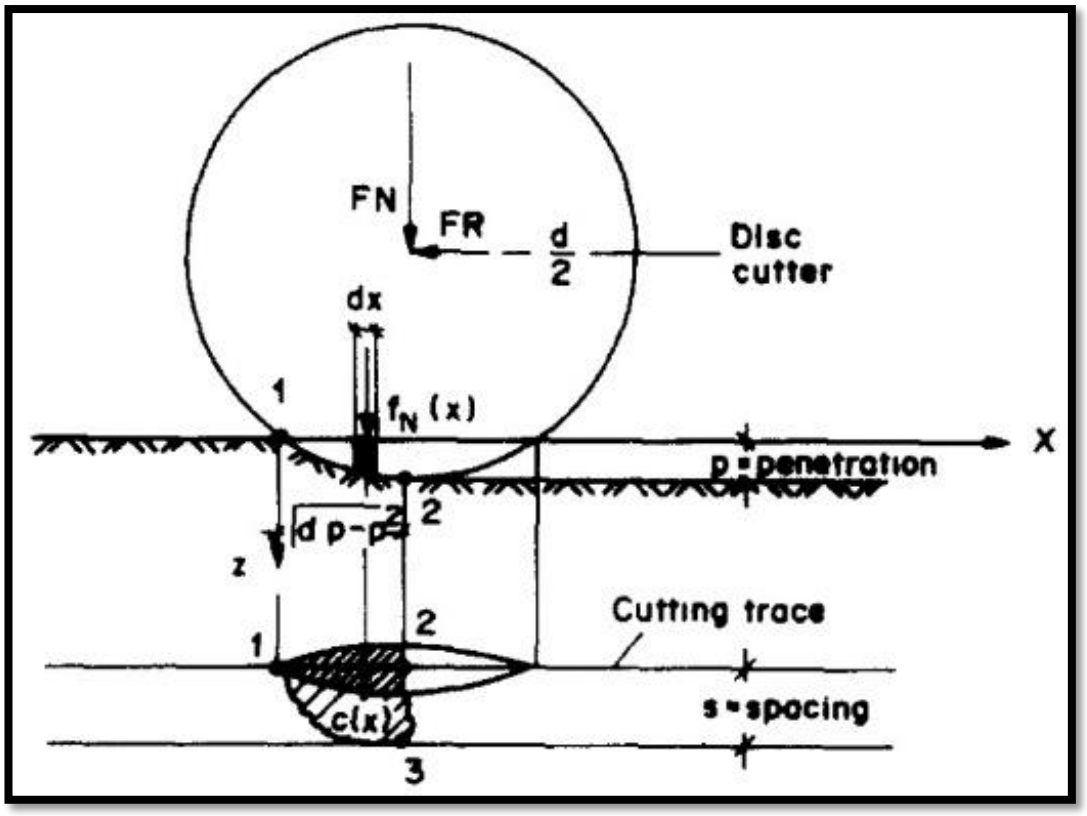

Figure 3-19 Illustration of cutting process of a disc cutter (Sanio, 1985).

As shown in Figure 3-19, a single wedge element starts its penetration at point (1) where the length of the crack is "0". The wedge element at point (2) has to generate cracks of length s in order to enable continuous removal of rock between two neighboring cuts. Assuming that the length of the cracks increases between points (1) and (2) approximately linearly with x, the following is attained:

$$c(x) \cong \frac{s}{(dp - p^2)^{0.5}} x \qquad (3\text{-}52)$$

By incorporating Equation (3-52) into (3-51) and integrating over the area of contact between tool and rock one finally obtains

$$F_{\mathrm{N}} = \frac{2k}{3q} \tan\left(\frac{\alpha}{2}\right) (dp - p^2)^{0.5} s^{0.5} \qquad (3\text{-}53)$$

For simplicity, the friction at the bearing of the tool is neglected, the resultant force of F_{N} and F_{R} must pass through the rotation centre of the tool, as shown in Figure 3-20. Consequently, the moment around the tool axis must be zero

$$F_{\mathrm{N}} h + F_{\mathrm{R}} t - F_{\mathrm{R}} \frac{d}{2} = 0 \qquad (3\text{-}54)$$

With:

$h = (dp - p^2)^{0.5} - \mathrm{b}$

It follows:

$$F_R = \frac{[(dp - p^2)^{0.5} - b] F_N}{\left(\frac{d}{2} - t\right)} \qquad (3\text{-}55)$$

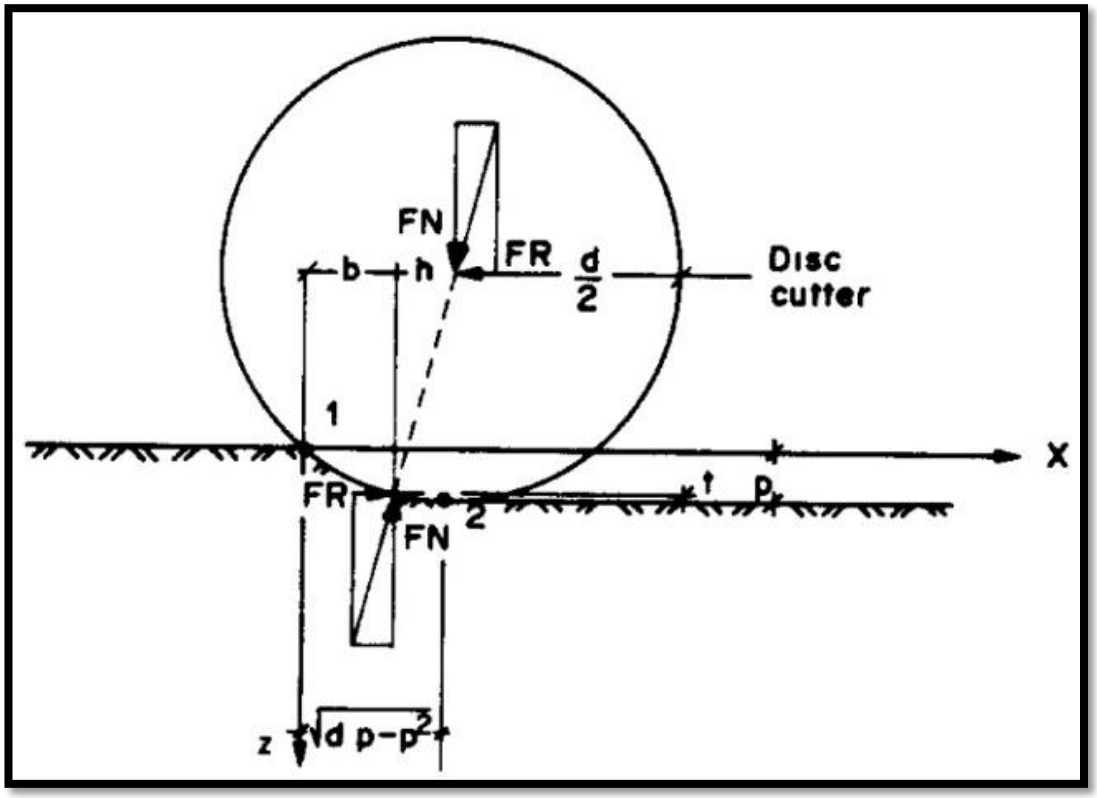

Figure 3-20 State of equilibrium of a disc cutter (Sanio, 1985).

Since the resulting normal force F_N must yield the same static moment around point (2) in Figure 3-20 as the sum of all moments generated by the normal forces of the infinitesimal small wedges, the length b can be derived as:

$$b = \frac{1}{F_N} \cdot \int_0^{(dp-p^2)^{0.5}} f_N(x) \cdot dx \qquad (3\text{-}56)$$

Then

$$F_R = \frac{2}{5} \cdot \frac{(dp-p^2)^{0.5}}{\left(\frac{d}{2}-t\right)} \cdot F_N \qquad (3\text{-}57)$$

As a result, the following equations for calculating F_{N} and F_{R} can now be derived if $\frac{d}{2} \gg t,\ \mathrm{dp} \gg p^2$.

$$F_{\mathrm{N}} = \frac{2k}{3q}(dsp)^{0.5} \cdot \tan\frac{\alpha}{2} \qquad (3\text{-}58)$$

$$F_{\mathrm{R}} = \frac{4}{5} \cdot \left(\frac{p}{d}\right)^{0.5} F_N \qquad (3\text{-}59)$$

Sanio's model adopts the tensile failure mechanism to establish the model. However, tensile strength is not included in the prediction formulae. The rock property included in the formulae is the critical stress intensity factor, k, which depends on the rock and the number of cracks, but its calculation was not given in the model. Another parameter of the model, q, is defined as a constant value of the crushed zone radius divided by the penetration depth. Its calculation was also not given. The model assumed that the value of k/q is a constant for fixed rocks, and can be obtained with laboratory experiments; however, tests on limited rocks could not justify its applicability.

This model could not be used to predict cutting forces for CCS disc cutters. The equations of cutting forces (3-58) and (3-59) indicate that when the cutter edge angle α is 180° (CCS disc cutter), the calculated normal force and rolling force will both be infinite. It is not true in reality.

One of the simplifications of this model is that, the crushed zone is assumed to be circular in shape. However, it has not been substantiated by laboratory studies. As a result, the circular hole assumption used in blasting fracture mechanics cannot be justified to simulate the fracture layout under disc cutter.

3.3 Conclusions

In conclusion, numerous efforts have been made to develop accurate cutting force predicting models for disc cutters. These models are mainly based on some

theoretical analysis combined with laboratory test verification. However, an extensive model for all disc cutters and rocks has not been developed.

Evans model does not include disc cutter diameter and cut spacing into calculations, and the calculated normal force values are often smaller than that of realistic ones. The compressive failure mechanism proposed in the Roxborough model was not verified. Cutting spacing was not taken into consideration in the model either, which made it not able to be used in the cutterhead layout design.

The most widely accepted model in the industry is the CSM model. It provides acceptable accuracy for cutting force prediction of V shape disc cutters. However, it is not applicable for CCS disc cutters as the calculated force will be negative infinite according to the formulae. For CCS disc cutters, there is no commonly accepted model developed to provide reasonably accurate predictions. This might be due to the lack of knowledge of the rock breaking mechanism of CCS disc cutters. The shear failure mechanism has facilitated the most accepted model for V shape disc cutters, i.e. the CSM model. However, its modified version for CCS disc cutter prediction is not widely accepted by the industry.

The introduction of tensile failure mechanism is a distinctive feature for the Sanio model. It raises the argument on the rock failure mode in disc cutting, especially for CCS disc cutters. The Sanio model is also not applicable for CCS disc cutters as well. It suggests that a combined failure mode of shear and tensile would better represent the cutting mechanism reality for CCS disc cutters.

Last but not least, the aforementioned models lag behind the advance of industrial requirements. Aside from the wide spreading applications of TBM in shallow tunneling projects, they have also been used to excavate deep tunnels, for example the long Trans-Alpine tunnels in Europe with overburden higher than 2000 meters. Application of TBMs in underground coal mines also mainly focus on deep tunnel excavation. Deep tunnels are exposed to high stress regime. However, so far, there is no cutting force prediction model taking due consideration of the factor of confining stress.

4 CHPTER FOUR – DISC CUTTING WORKING MECHANISMS

4.1 Introduction

Understanding the mechanism of disc cutting is the prerequisite for establishing the accurate models for cutting force prediction and furthering the TBM performance prediction models. Disc cutting is the result of the interaction between disc cutter and rock. Rock fracturing mechanism under a single disc cutter is the basis. Rock fragmentation under a disc cutter is mainly the function of thrust force. So, a disc cutter can be simplified as an indenter, and the tool rock interaction can be treated as an indentation process.

The indentation process includes different phases, namely stress build-up, formation of crushed zone, and initiation and propagation of fractures, as shown in Figure 4-1. The research on indentation process mainly focuses on these three phases. Researchers conducted theoretical and experimental studies on the indentation process for decades. Evolution of computing sciences has made numerical simulation a practical study methodology. It extends the study to more variables such as joint set. This chapter provides a critical review of research from perspectives of the three methodologies.

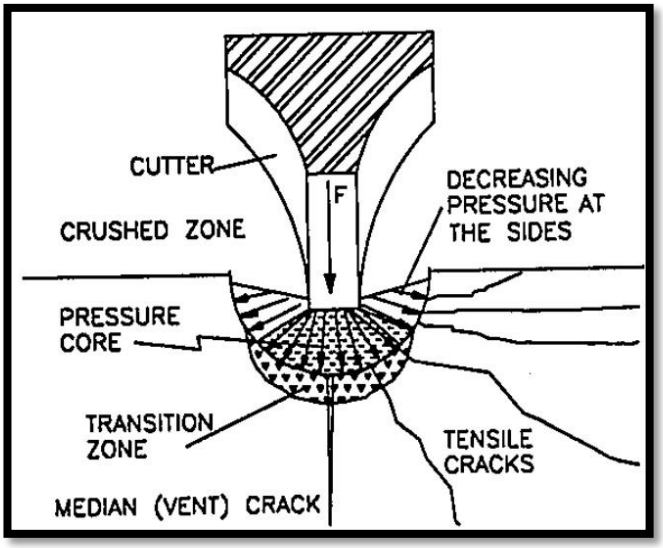

Figure 4-1 Schematic diagram of indentation under disc cutter (Rostami and Ozdemir, 1993).

4.2 Analytical study

An analytical study regarding disc cutting mechanisms mainly focused on the stress field caused by the applied load, which is the first step to a sound treatment of the indentation analogy. Based on the stress field, the fracture zones could be determined by applying rock failure criteria. Two classical analytical studies were conducted and published by Wagner (1971) and Lindqvist (1984).

Wagner (1971) proposed a theoretical analysis of the stress field under a flat-ended circular indenter. This study was based on the assumption of linear, isotropic, and elastic behaviour. Under this simplification, the indentation was analysed as a contact problem with the theory of elasticity, of the kind generally known as the Boussinesq problem. The studied rock was Witwatersrand quartzite.

Both elastic and rigid indenters were considered. The analytical solution of the maximum principal stress, σ_{11}, and the minimum principal stress, σ_{33}, were plotted, as shown in Figure 4-2. It shows that the minimum principal stress value decreased with the depth increasing from the contact and converted to tensile stress beyond the indenter's sides; and the tensile stress increased as it approached the surface. The maximum principal stress decreased with depth increasing but would not convert to tensile stress. It also demonstrated the distinct stress distribution contours under elastic and rigid indenters. However, no attention was payed to intermittent principal stress and shear stresses although they are also significant in indentation problems.

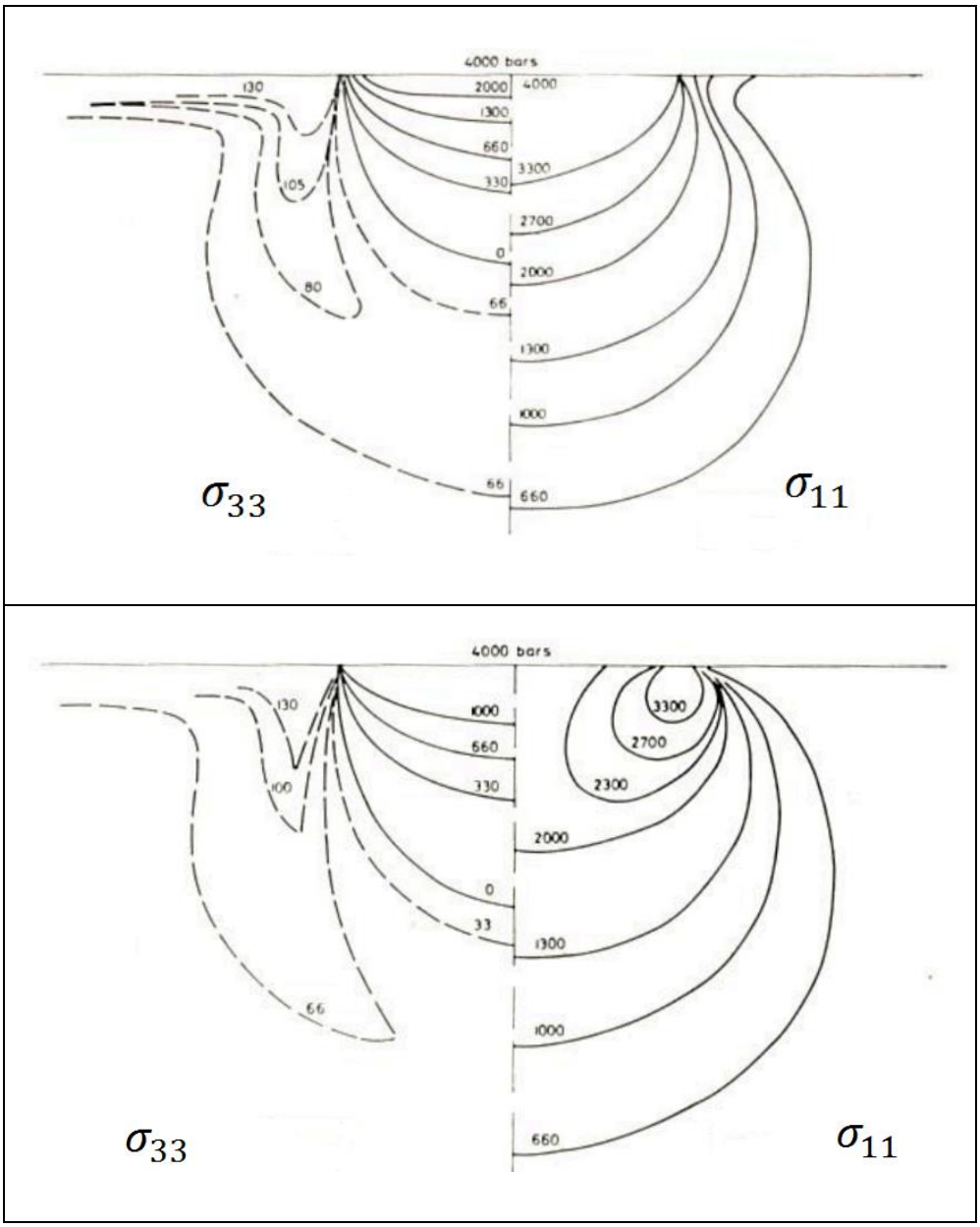

Figure 4-2 Distribution of maximum and minimum principal stresses; elastic stamp (above), rigid stamp (below) (Wagner, 1971).

By applying the failure criterion of Witwatersrand quartzite, the fracture zones of the rock samples were obtained, as shown in Figure 4-3. It shows that tensile failure zones initiated from the side corner of indenter and propagated outwardly. Failure zone increased with load mounting on both length and depth. Rigid indenter failure zone has distinctive feature comparing to the elastic one. It was deeper but shorter than the failure zone under elastic indenter.

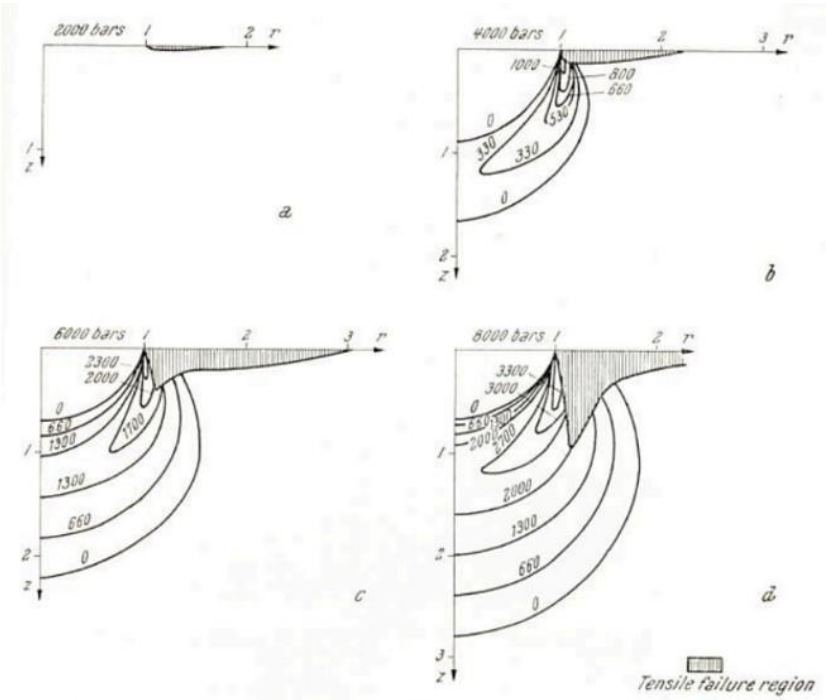

(a) Elastic stamp

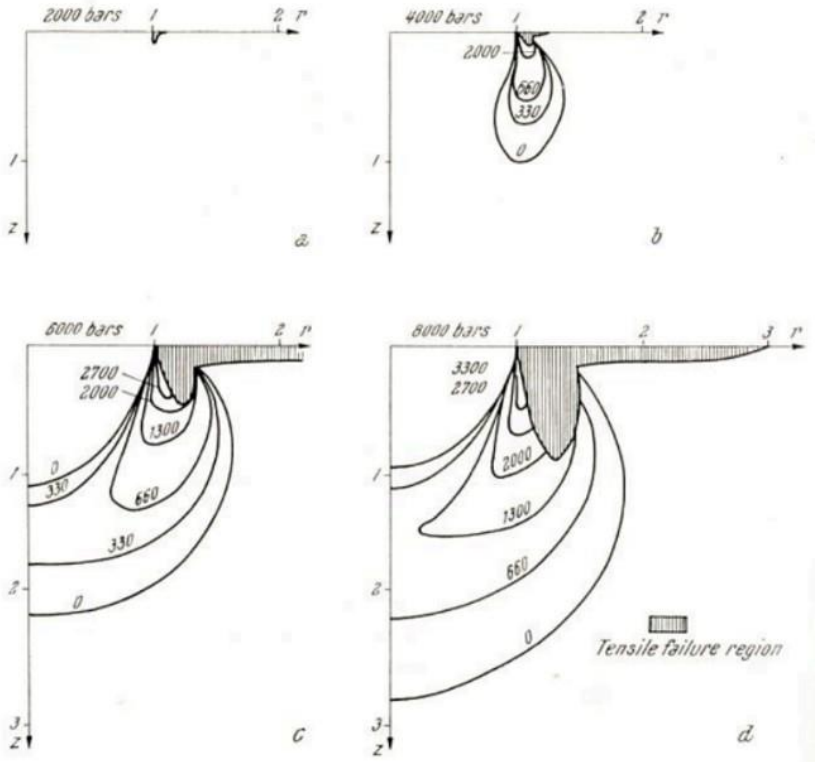

(b) Rigid stamp

Figure 4-3 Fracture zones for four different contact stresses; elastic stamp (above), rigid stamp (below) (Wagner, 1971).

Wagner's model was an early attempt at an analytical approach with limited laboratory and field verification. Although it presented a reasonable prediction of crack propagation, the proposed failure pattern did not agree well with the realistic indentation process. This model does not predict the presence of median cracks, which have been verified with laboratory observations, as shown in Figure 4-1. In addition, the crushed zone was not considered in the model. Conclusively, Wager's model can hardly be applied to a disc cutting problem directly but represents a good attempt and reference.

Lindqvist (1984) proposed a two dimensional analytical solution to the stress field of indenting on a linear elastic half-space. The stresses were normalized with the mean contact pressure under the indenter to make the study be of general interest and presented in general form. By defining the tensile stress as negative, and taking 0.20 as the poison's ratio, the calculation results were shown in Figure 4-4.

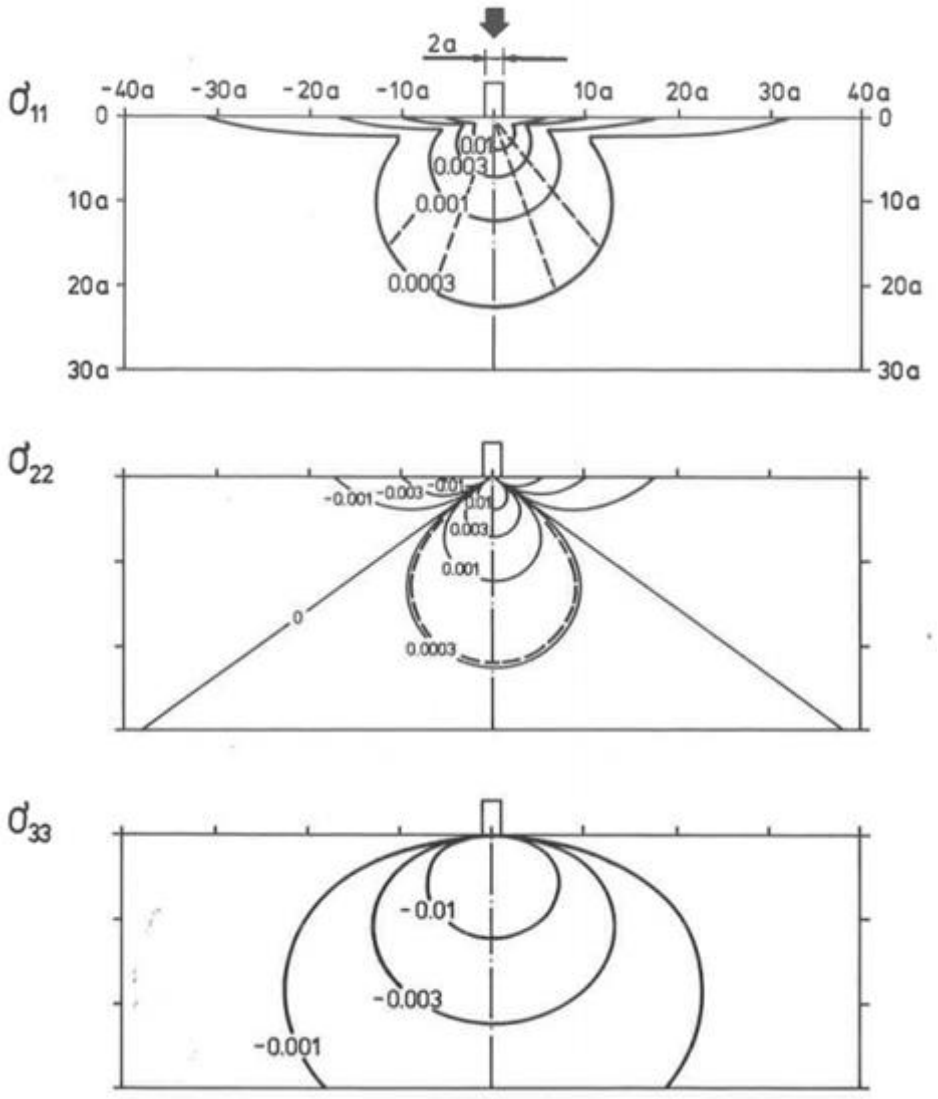

Figure 4-4 Contours of principal normal stresses. Broken lines indicate possible cracks (Lindqvist, 1984).

Figure 4-4 shows that stresses σ_{11} and σ_{33} are compressive and tensile respectively, while σ_{22} is tensile at the outward-upward region of the indenter edges but compressive elsewhere. Aside from the stress field, this model also provided a prediction of the crack pattern as mainly median and cone cracks. Although it calculated the three principal stresses, no attention was payed however for shear stress. In addition, the lateral cracks, which are crucial for the rock removing process were not included in this model. Conclusively, this model is also not applicable to real disc cutting problems but represents a good reference.

The aforementioned works were both about two dimensional indentation processes, which made a considerable simplification of the realistic disc cutting process because of the complexity of the tool-rock interaction in reality. They were limited by the simplification of linear, isotropic, and elastic behaviour. With the advance of laboratory testing technologies, experimental studies designed to closely represent the realistic cutting actions of disc cutters had been undertaken to justify and supersede analytical studies.

4.3 Experimental study

Experiment with the assistance of optical apparatus is the most direct means to observe the crushed zone and crack development caused by the indentation in rock, and to further improve the understanding of the mechanisms in disc cutting. Using experimental results, the analytical models and numerical models can be verified and justified. Based on experimental data, reliable mechanical models could be established for cutting force prediction and TBM performance prediction.

Lindqvist et al. (1984) conducted laboratory tests to observe the indentation process with assistance of a Scanning Electron Microscope (SEM). The tests were carried out in a JEOL JSM-50A SEM. The test specimens and indenters were placed on a loading stage, as shown in Figure 4-5. The specimen is loaded at one edge and observations were made on the adjacent surface. Two wedge-type tungsten carbide indenters were used. One wedge is sharp and the second type is truncated, giving a width of the flat of 0.38 mm. the length of the wedges is approximately 5.0 mm and the included wedge angle $77°$ (Lindqvist et al., 1984).

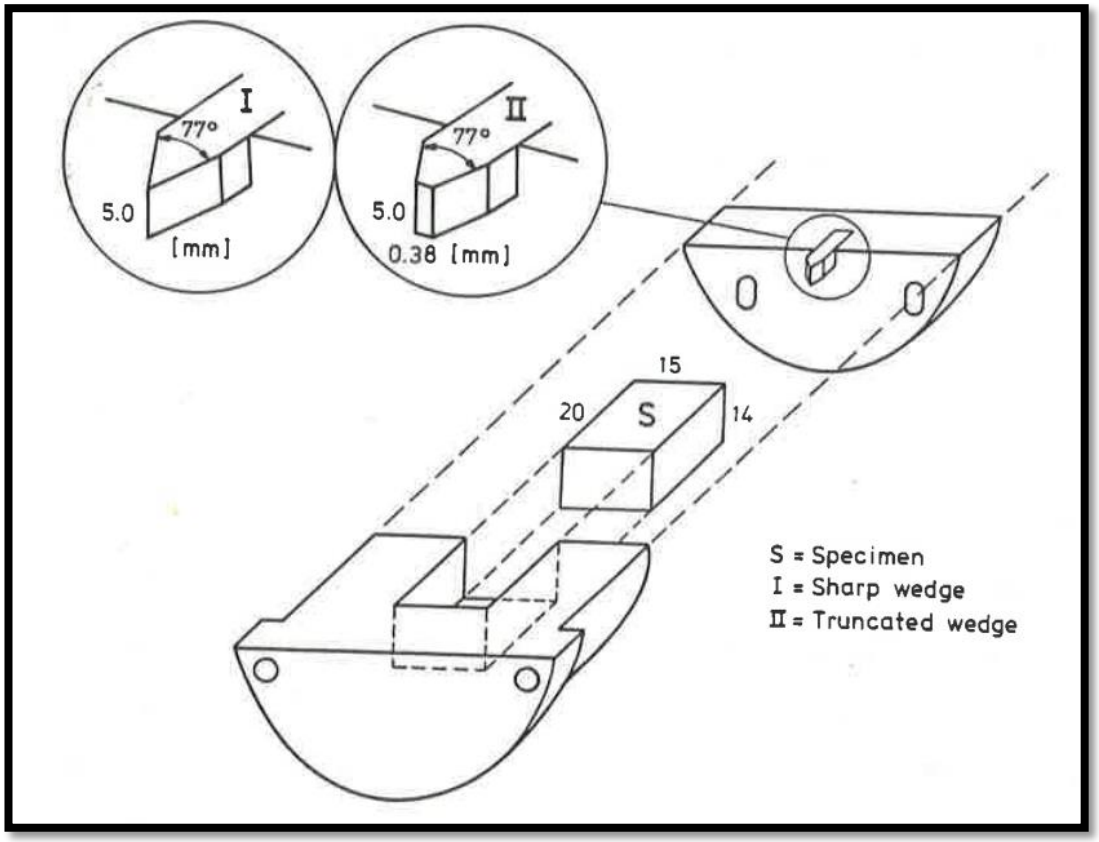

Figure 4-5 Exploded view of the indentation fixture (Lindqvist et al., 1984).

Three types of Swedish rocks are tested, namely Red Oland limestone, Ekeberg marble and Stripa granite. The specimens were cut from cores with a diamond saw and polished on two adjacent surfaces, with dimensions of $20 \times 15 \times 14$ mm (Lindqvist et al., 1984). Two typical post-test rock samples are presented in Figure 4-6, in which the crushed zones and cracks are clearly illustrated.

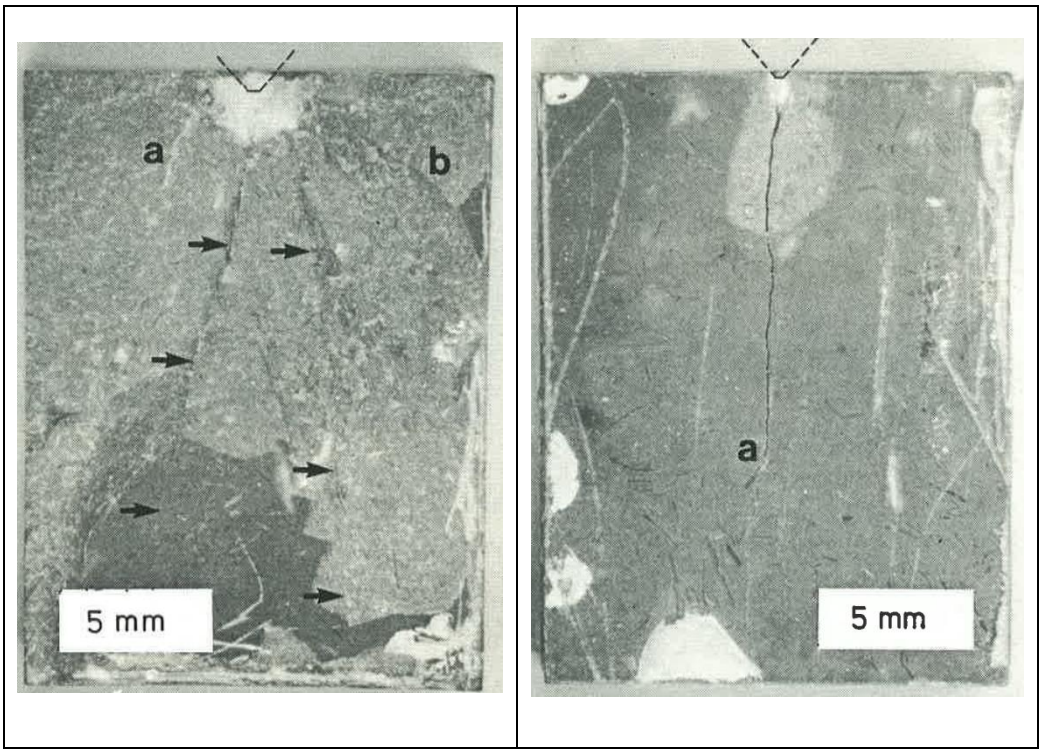

Figure 4-6 Two tested Red Oland limestone samples, after completion of SEM test (Lindqvist et al., 1984).

The tested rock samples were all of small dimensions and un-confined, therefore did not reflect the field realities. The test results as shown in Figure 4-6 show that the rock samples did not have side chipping, i.e. lateral cracks, which is the major contributing part of disc cutting. This is a notable discrepancy from reality and might be caused by the small dimensions of the samples and lack of confinement.

Howarth and Bridge (1988) designed laboratory indentation tests to reveal the fracture pattern under CCS disc cutters. The experiments were conducted on a 3600 kN capacity Avery compression machine, as shown in Figure 4-7. Rock specimens were cut to dimensions of $400 \times 200 \times 200$ mm. Only one side of each block was used for the indentation experiments to avoid the possibility of an overlapped crack system that may make analysis and interpretation of the results difficult.

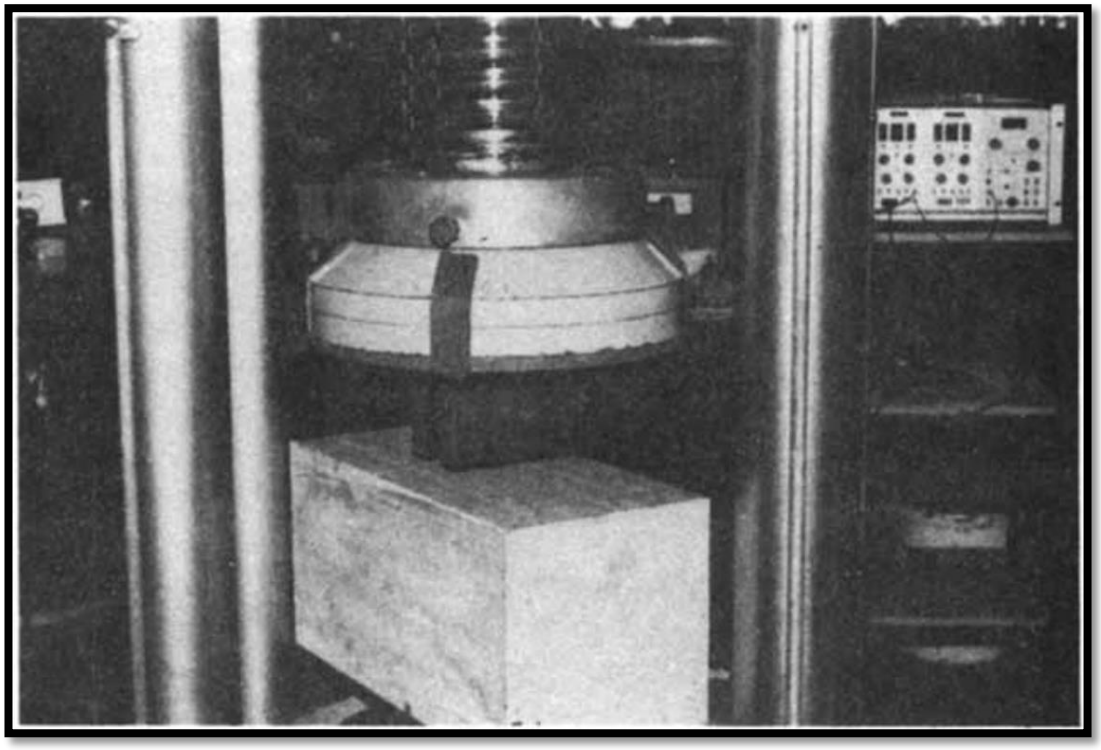

Figure 4-7 The laboratory test set up (Howarth and Bridge, 1988).

Two kinds of rocks were tested, namely microsyenite and granite. Each rock sample had two cuts, the pre-conditioning (first) cut and the secondary cut. The pre-conditioning cut was made by indenting the disc cutter into the rock to the required load (200-250 kN). The penetration was recorded for the pre-conditioning cut. The secondary cut was indented at a required spacing, which was determined by the pre-conditioning cut penetration and the selected spacing-penetration ratio. The penetration of the secondary cut was to be the same as the first one, and the cutting load for the secondary cut was recorded accordingly. Tested rock samples were then cut to observe the subsurface crushed zone and cracks. Some typical images are presented in Figure 4-8.

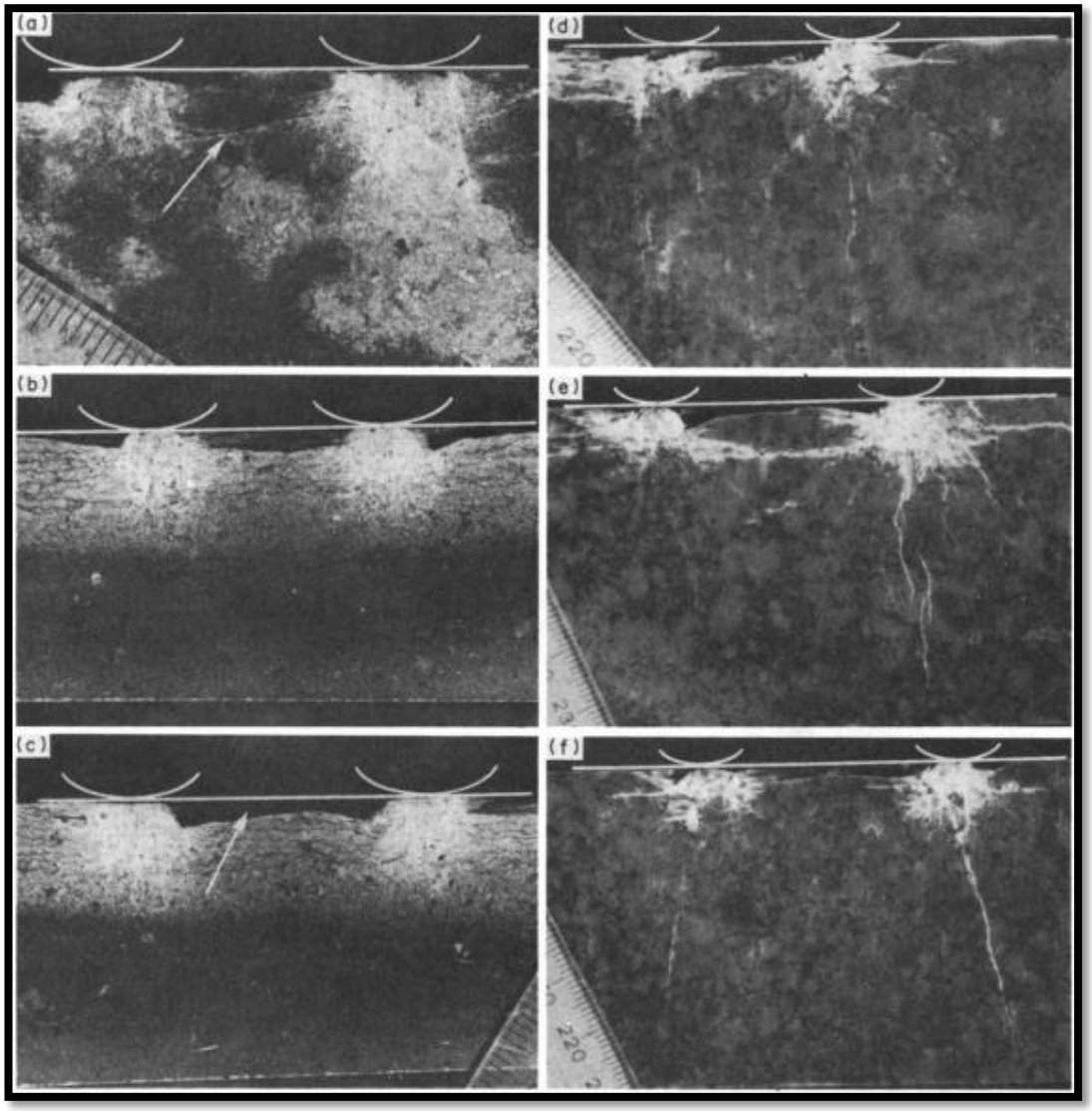

Figure 4-8 Subsurface crushed zone and crack systems development (Howarth and Bridge, 1988).

Figure 4-8 shows images for both crushed zones and cracks. The horizontal white line denotes the original surface, and the curved lines indicate the positions of the disc cutter. The direction of loading was normal to the plane of the original surface; the white arrows were plotted to point the interacting lateral cracks, and a millimeter scale is shown in the lower right or the lower left corners of the photographs. Image (a) was for microsyenite with 1.45 mm penetration and spacing-penetration ratio of 16:1; image (b) was for microsyenite with 1.2 mm penetration and spacing-penetration of 20:1; Image (c) was for microsyenite with 1.2 mm penetration

and spacing-penetration ratio of 25; Image (d) was for granite with 1.05 mm penetration and spacing-penetration ratio of 25; Image (e) was for granite with 1.15 mm penetration and spacing-penetration ratio of 35; Image (f) was for granite with 1.05 mm penetration and spacing-penetration ratio of 40.

Howarth and Bridge's tests were closer to reality than Lindqvist's, from both perspectives of indenter and rock sample. Howarth and Bridge's cutting tool was designed and fabricated based on a commercially available TBM disc cutter design. It incorporates the commercial cutter tip geometry, but was downsized from 432 mm diameter to that as shown in Figure 4-9, which is much closer to real indenter than that of Lindqvist's design as shown in Figure 4-5. The rock sample used in the experiment by Howarth and Bridge was $400 \times 200 \times 200$ mm, which was also much larger than that of Lindqvist's specimens of $20 \times 15 \times 14$ mm.

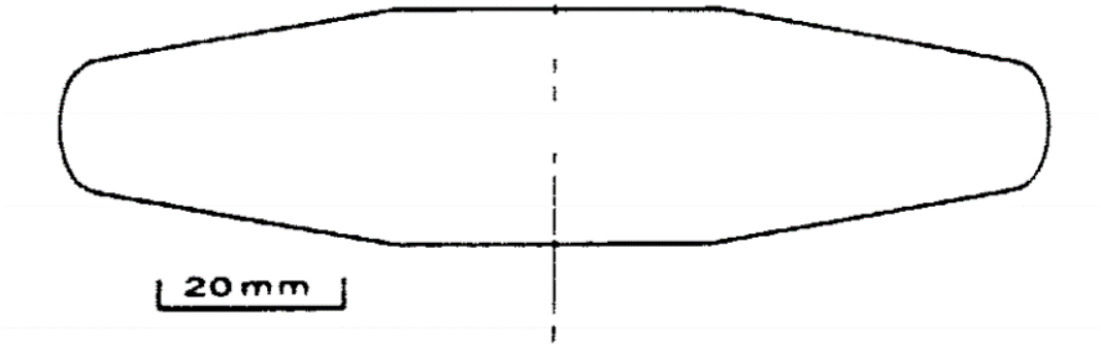

Figure 4-9 Howarth and Bridge's experimental cutting tool (Howarth and Bridge, 1988).

Tests by Howarth and Bridge improved the understanding of disc cutting mechanisms by observing the lateral cracks, which were absent in Lindqvist's tests. This might be caused by the difference of the sample dimension.

Shallow penetration and lack of confinement make the results from Howarth and Bridge deviate from reality. The penetrations adopted in the tests were not more than 1.45 mm, while the field penetrations might be up to 10 mm. Considering the on-going failure modes argument between tensile failure and shear failure, the conclusions drawn from shallow penetrations are questionable in real penetration

scenarios. Tunnel faces are confined by surrounding rocks in reality. The confinement increases the resistance to rock deformability, which is related to the formation of crushed zones and cracks. Lack of confinement is a discrepancy from field reality, and limits the applicability of the research outcomes.

Confinement's influence on disc cutting was taken into consideration by Innaurato et al. in 2007. The background was the increasing application of TBMs in deep tunnels, for example the excavation of long Trans-Alpine tunnels in Europe. It requires a better understanding of disc cutting mechanisms to optimize the TBM cutting system and achieve accurate TBM performance prediction (Innaurato et al., 2007).

Indentation tests were adopted to conduct the research. The experiments were conducted on a compression machine, as shown in Figure 4-10. To simulate confining stress, a flat-jack was used to apply compression load on the rock samples. Rock samples were placed in a steel frame, and the flat-jack was positioned vertically between the rock sample side and the steel frame internal side. Two kinds of rocks were tested in the experiment, which were limestone (Botticino from Brescia) and granitoid rock (Diorite from Vico) (Innaurato et al., 2007).

The indenter was a parallel cut realistic TBM disc cutter. Rock specimens were diamond sawn to rectangular blocks with dimensions of $150 \times 150 \times 200$ mm. The adopted confinement pressure values were 0, 5, and 10 MPa respectively. The indenter was placed in the middle of the upper face of the sample (Innaurato et al., 2007).

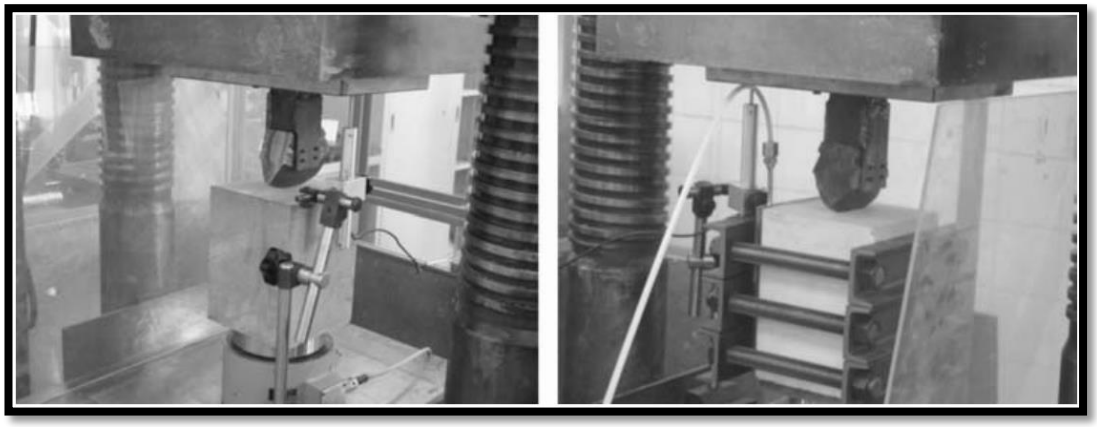

Figure 4-10 Experimental set up for Innaurato's tests (Innaurato et al., 2007).

Each rock sample had only one cut. Maximum load, ultimate load, and maximum penetration were recorded. Modes and types of fractures on tested rock samples were observed from the side and top surfaces. A typical image is presented in Figure 4-11.

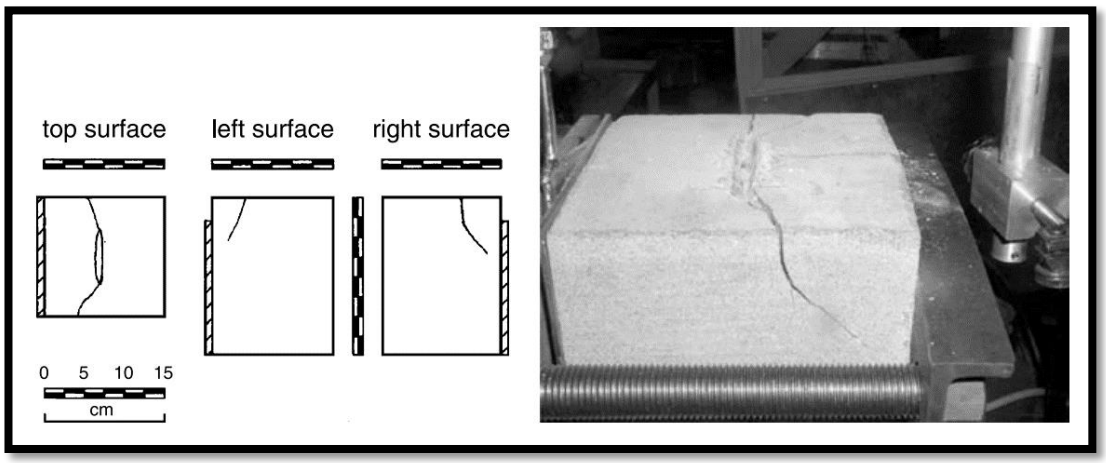

Figure 4-11 A typical post-test sample of Innaurato's indentation tests (Innaurato et al., 2007).

This research was a successful attempt to look into the influence of confinement on disc cutting from the perspectives of cutting forces and fracture patterns, especially cutting forces. However, the fracture patterns were observed from surfaces only; subsurface crushed zone and crack systems were not studied by cutting the post-tested rock specimens, as had been conducted in Howarth and Bridge's tests.

In conclusion, considerable experimental studies concerning disc cutting mechanisms had been conducted. The research results improved the understanding. However, due

to limitations of the experimental designs, it is questionable if they were applicable in real field scenarios. The rock sample dimensions were small in Lindqvist's experiments, and they were not confined, which can hardly represent field conditions. The SEM scanning in the study also showed that the rock samples did not have side chipping, as shown in Figure 4-6, which is a notable discrepancy from reality. Howarth and Bridge (1988) studied the fracture pattern with shallow penetration not more than 1.45 mm, whereas the field penetrations might be up to 10 mm. Absence of confinement is another discrepancy from field reality for Howarth and Bridge's study. The discrepancies render the research conclusions questionable for real scenarios. Innaurato et al. (2007) considered the confinement stresses' influence in their experimental design with penetrations up to 7 mm, which is an advance towards real scenarios. However, the fracture patterns were studied from surfaces only, i.e. it did not study the subsurface crushed zone and crack systems using a similar manner conducted in Howarth and Bridge's tests.

Based on the critical analysis of the previous experimental studies, a new experimental study with confinement stresses, penetrations up to 9 mm, and observation on subsurface crushed zone and crack systems, has been designed and conducted. Experimental details and results of the study are presented in the following chapters.

4.4 Numerical study

A large scale experimental study is capable of closely simulating field conditions. However, it requires elaborate equipment, tedious sample handling and preparation, which is costly and time consuming. Analytical studies have to make some simplifications, and sometimes these simplifications ignore important factors influencing the material behaviour, for example, rock heterogeneity.

Numerical simulation has been a practical, cost effective and time saving approach to conduct in-depth research on disc cutting due to the rapid development of computing technologies. Numerical studies do not need rock sample preparation. It can also

avoid simplification of important factors, for example, rock heterogeneity. Therefore, it can provide a better description of the mechanical behaviours of disc cutting.

Liu et al. (2002) used a numerical code R-T^{2D} (Rock-Tool interaction) to study the rock cutting process induced by indenters. This is a two dimensional simulation simplified to a plain strain condition. A plane passing through the central axis of the indenter was taken as the concern. A displacement increment control model of 0.005 mm/step was applied on the indenters and a confining pressure of 20 MPa was applied to the rock specimen. The model was set up as shown in Figure 4-12 (Liu et al., 2002).

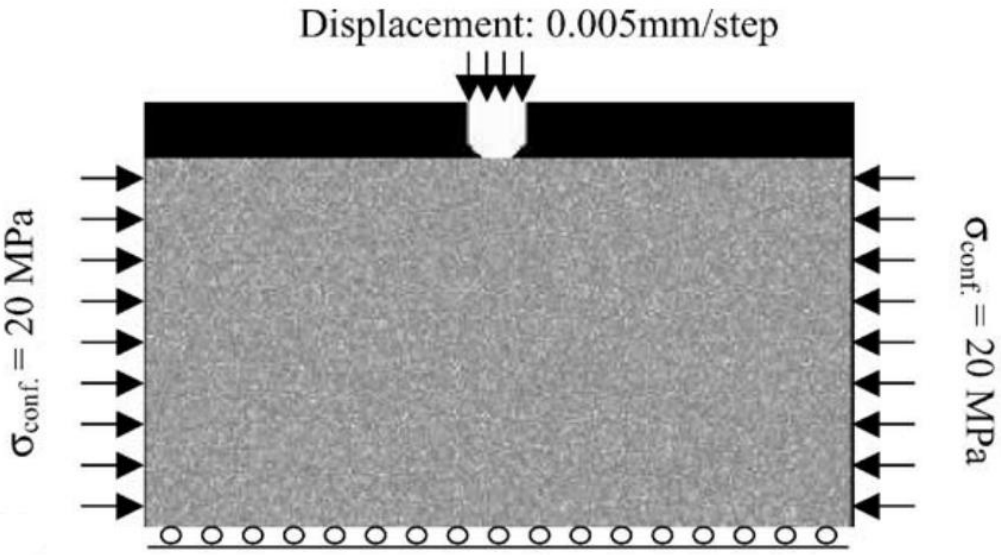

Figure 4-12 Numerical simulation model in Liu's study (Liu et al., 2002).

The process of penetration of an indenter into the rock starts with the development of a stress field beneath the indenter. Getting clear ideas of the stress field caused by the applied load is the first step to a sound treatment of the indentation problem. Liu et al.'s model computed the stress regime of each element; and the results are presented in Figure 4-13. It shows that the stresses were extremely large at the loading point and decreased rapidly with increasing distance from the loading point (Liu et al., 2002).

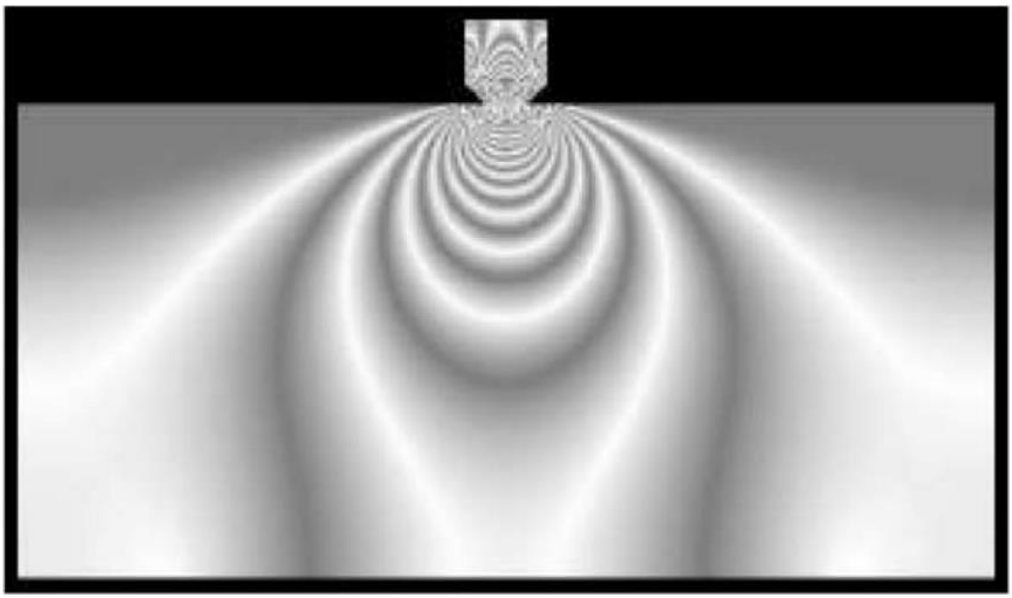

Figure 4-13 Computed stress field pattern induced by indenter (Liu et al., 2002).

Aside from the stress field, the model also provided an insight to the dynamic fracturing process for the indentation, which is shown in Figure 4-14. The initiation and propagation of cracks was clearly demonstrated in the simulated results. In the early phases, the stress intensity built up; cracks began to initiate from the two corners of the indenter and propagated laterally, as shown in Figure 4-14 (A)~(E). As loading displacement increased, the lateral cracks propagated until reaching the surface; and the cone cracks run downward as shown in Figure 4-14 (F)~(J).

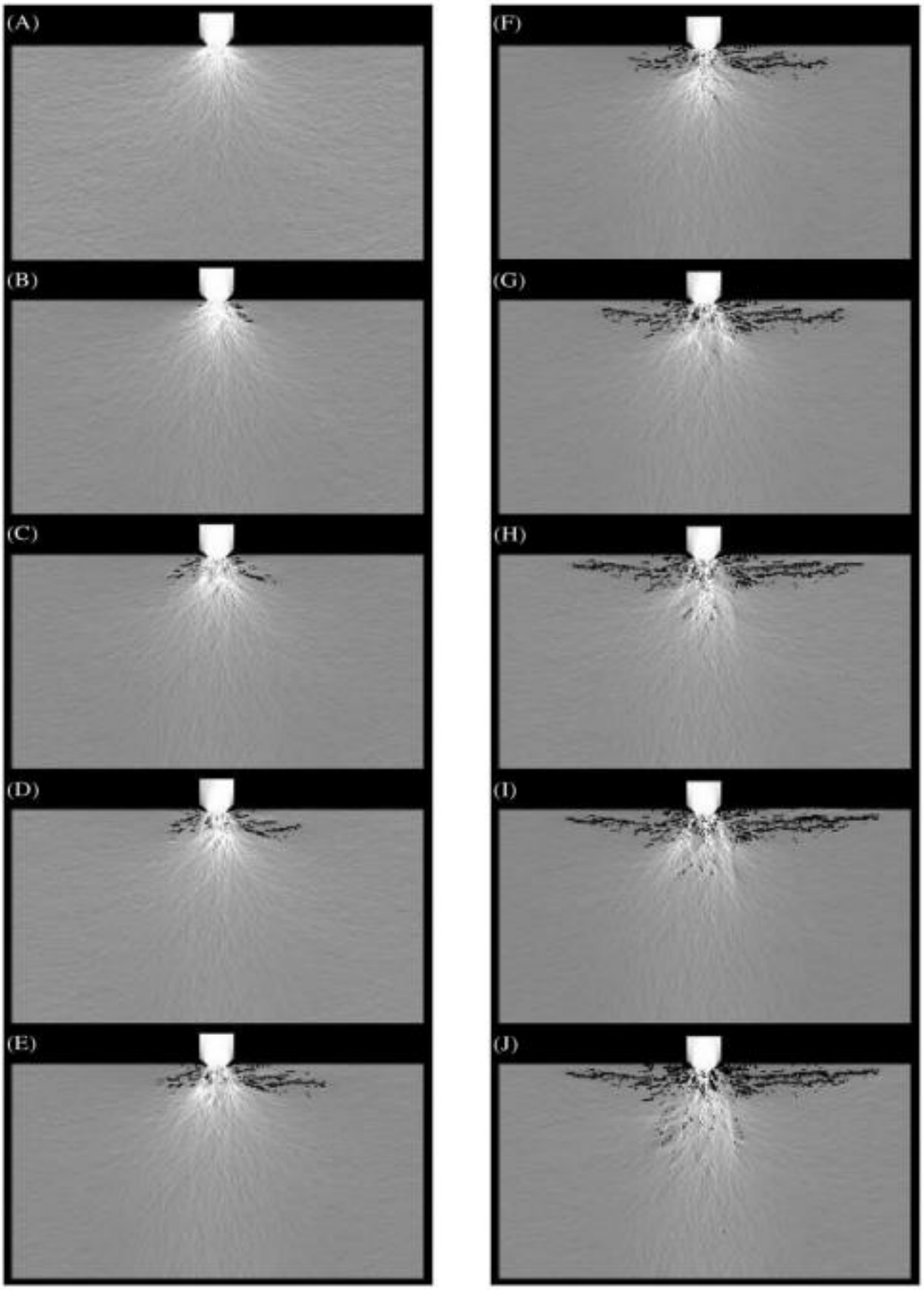

Figure 4-14 Simulated results for the dynamic fracturing process (Liu et al., 2002).

Liu et al.'s research provided insights into the stress field pattern and fracturing process for indentation. However, indenters adopted in this study had different

shapes and sizes from disc cutters. So the conclusions drawn from this study are questionable if applied to disc cutter scenarios. In addition, the numerical simulations were not validated by laboratory tests. Conclusively, the study is a valuable reference for the future numerical studies, although the results' applicability is questionable.

Mo et al. (2012) studied the disc cutting mechanisms by adopting the real cutter geometry. Both V shape disc cutters and CCS disc cutters were included, with different cutter ring thickness, as shown in Figure 4-15. The two dimensional numerical model was set up with the commercial software UDEC (Universal Distinct Element Code). In addition, rock strength and joint orientation were also included in the study, as shown in Figure 4-16 (Mo et al., 2012).

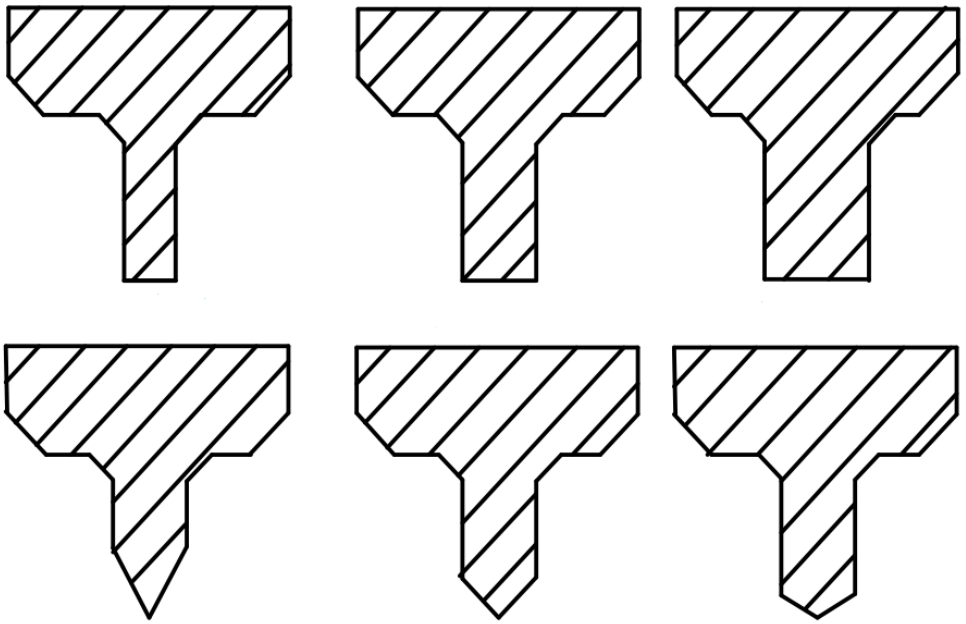

Figure 4-15 Cutter ring cross-section shapes included in Mo's study (Mo et al., 2012).

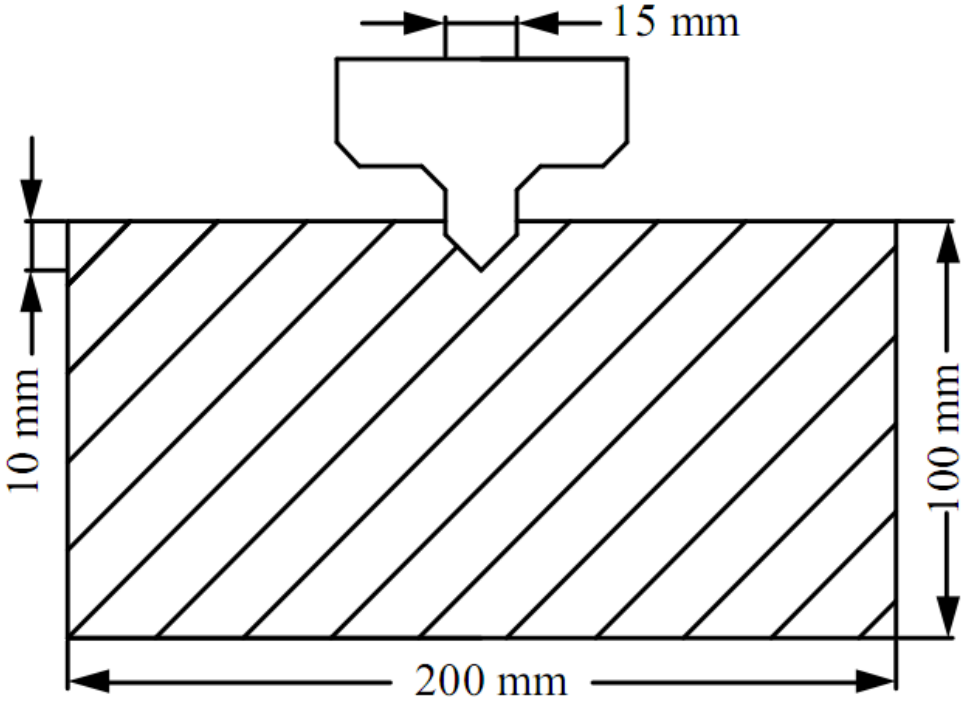

Figure 4-16 Mo's UDEC model (Mo et al., 2012).

The results show that rock breaking mechanism is a combination of shear failure and tensile failure. Tensile failure is the major reason for crack initiation and propagation, as shown in Figure 4-17 (Mo et al., 2012). It suggests that CCS disc cutters generated more lateral cracks and radial cracks than vertical cracks, the larger cutter thickness, the fewer vertical cracks; V shape disc cutters generated more vertical cracks than CCS ones, the smaller the wedge angle, the more vertical cracks were generated. The influence of joints and rock strength on disc cutter were also elaborated in the study.

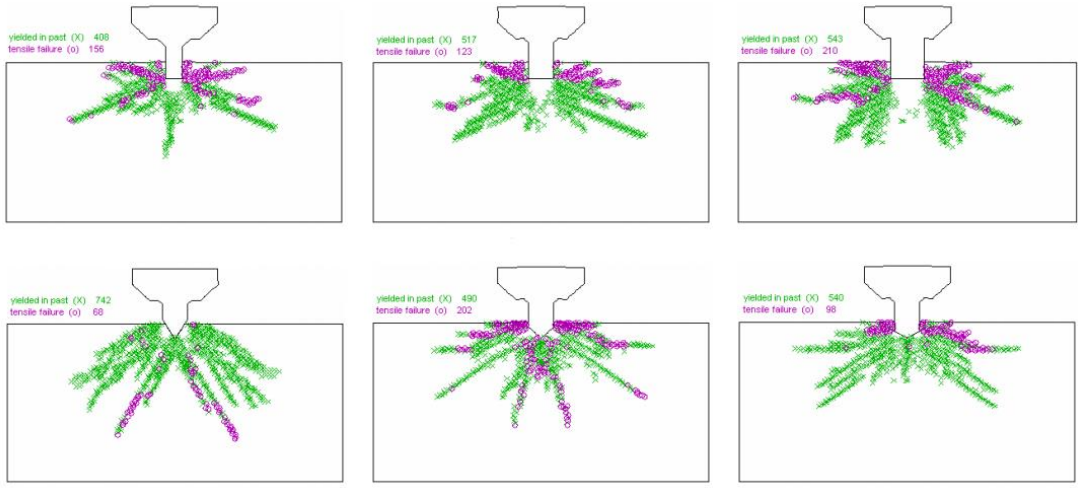

Figure 4-17 Numerical simulation results (Mo et al., 2012).

The study by Mo et al. was a successful early attempt to evaluate the influence of disc cutter patterns on disc cutting mechanisms. The research outcome provided guidelines for designing and optimizing disc cutters. However, in this study, confining pressure was not taken into consideration, which is a discrepancy from field reality. In addition, there were no specified laboratory tests conducted to validate the numerical study results. Conclusively, Mo's study can be improved by adding the confining pressure into the model along with validating laboratory studies.

Peng (2014) conducted a numerical study to analyse the influence of the confining pressure on disc cutting. The two dimensional numerical model was set up using UDEC, as shown in Figure 4-18 (Peng, 2014). Confinement pressures of 0, 1.0, 2.5, 4.5, 9.0, and 15.0 MPa were adopted and Mohr-Coulomb failure criterion was employed in the model.

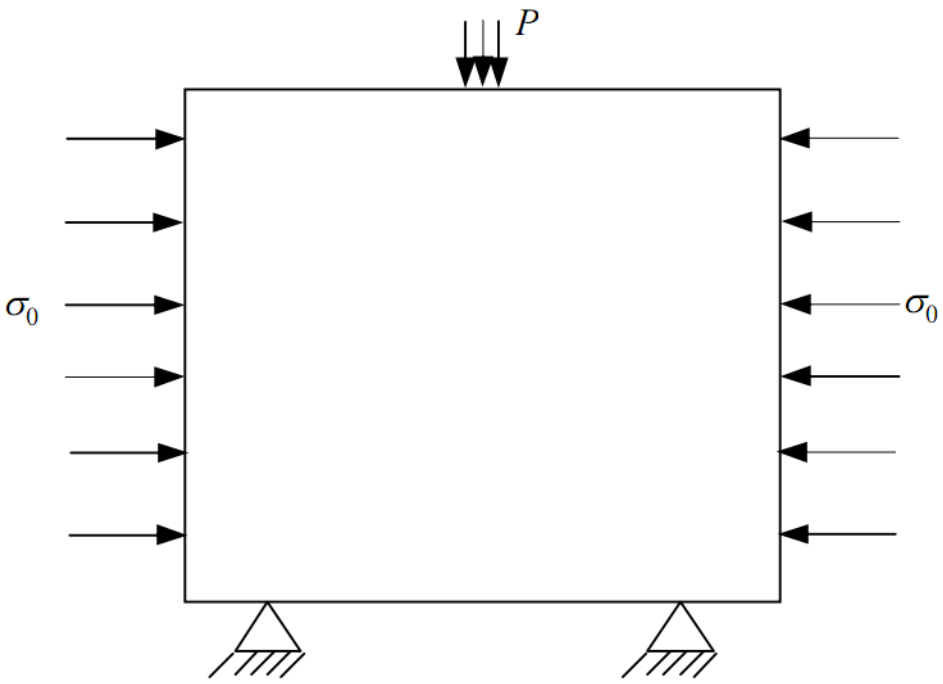

Figure 4-18 UDEC model (Peng, 2014).

The results show that confining pressure has a considerable influence on both crushed zone and crack development, as shown in Figure 4-19. It demonstrates that increasing of confining pressure restraints the propagation of the crushed zone, which is a crucial source for dust generation. So, the confining pressure could reduce dust exposure at the tunnelling face. Increasing confining pressure also impedes the development of vertical and radial cracks, and convert radial cracks to lateral directions. In addition, lateral crack propagation is augmented by rising confining pressure, which is favourable for side chipping.

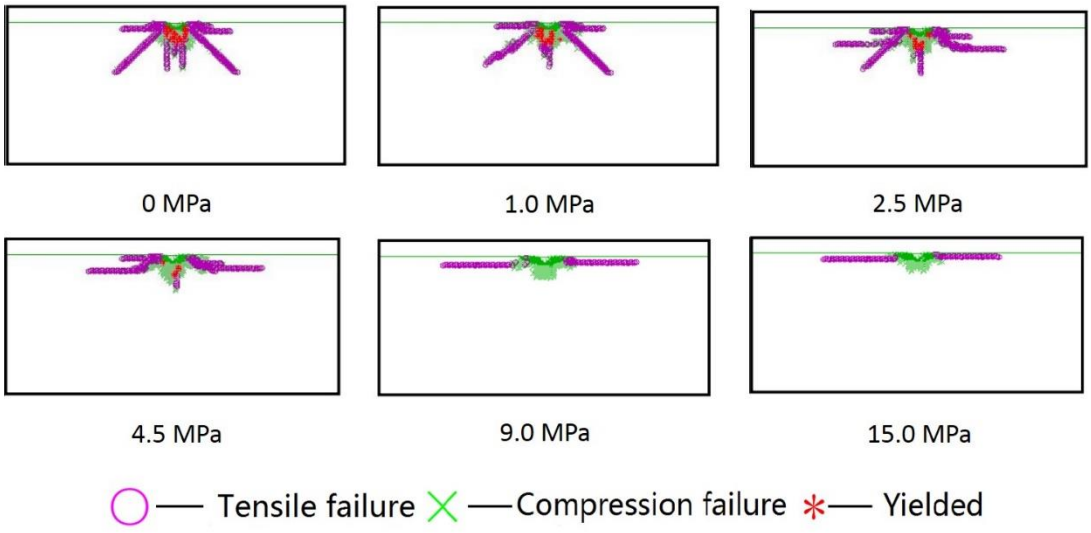

Figure 4-19 Comparison of rock failure patterns under different confining pressures (Peng, 2014).

Peng's study advanced the understanding of the influence of confining pressure on disc cutting. However, the model did not take the disc cutter cross-sectional shape into consideration. It simplified the indentation to an evenly distributed load, which only represents the rigid CCS disc cutters, but not V shape disc cutters. In addition, the research results regarding the development of crushed zone and cracks were not validated with laboratory tests.

In conclusion, a number of researchers have been using numerical analysis to study the crushed zone and cracks development in disc cutting. With the improvements of computing technologies and simulation software, the numerical studies has evolved from simplified scenarios with general indenters to more realistic scenarios with different disc cutter shapes. Although, the numerical simulation is a powerful way to trace the crushed zone and cracks development, the validating laboratory tests were rarely conducted to justify the simulation results.

4.5 Conclusions

Since the introduction of disc cutters, there have been numerous studies to look at disc cutting mechanisms. Analytical, experimental and numerical approaches were all employed to conduct the researches. It is commonly accepted that disc cutting

consists of three different phases, stress build-up, formation of crushed zone, and initiation and propagation of fractures. Researchers have been studying disc cutting mechanisms from these facets.

Analytical analysis was employed to predict the stress field and failure zone caused by the applied load. However, the analytical models have to be simplified as linear, isotropic and elastic scenarios, which is a discrepancy from the complex tool-rock interaction associated with realistic disc cutting. Some important factors were ignored in the analytical studies, such as rock heterogeneity and crushed zone. In addition, the early analytical analysis lacked experimental verification. With the improvement of laboratory testing power, researchers turned to experimental studies.

Experimental studies improved the understanding of the disc cutting mechanisms by avoiding linear, isotropic and elastic simplifications. In addition, they are essential for validating the analytical and numerical studies. Experimental studies have evolved from the perspectives of test scale, applied confinement pressure, and the observation of sub-surface crushed zone and crack development. However, only a few experimental studies take all these factors into consideration as large scale experiments with confinement and sub-surface observation are costly and time consuming.

Numerical study turned out to be a practical, cost effective and time saving approach to improve the knowledge of disc cutting, based on the rapid improvement of computing power and with no need for physical experimental preparation. It is convenient to trace the crushed zone and crack development, so it can provide a better description of the mechanical behaviour of disc cutting than other methods. In addition, numerical studies can also avoid important factor simplifications, such as rock heterogeneity. However, the numerical study results are questionable without validation of experimental tests.

Literature review shows that there is still considerable debate about the disc cutting mechanisms. This is mainly because of the discrepancies between an experimental set up and field realities. To advance the understanding of disc cutting mechanisms,

based on the critical analysis of the previous experimental and numerical studies, a more realistic experimental study was conducted. Confining stresses, penetrations up to 9 mm, and observation of subsurface crushed zone and cracks are taken into consideration. Details and results of the study is presented in the following chapters of this thesis.

5 CHAPTER FIVE – CHARACTERIZATION OF THE TESTED ROCK

5.1 Introduction

Rock cutting is a complicated phenomenon, rocks break under different mechanisms. Howarth and Bridge （1988） conducted laboratory indentation tests with CCS disc cutters on microsyenite and granite, which confirmed the different rock breaking mechanisms, as shown in Figure 5-1. Rock properties pose considerable influence on the disc cutting mechanism, which limits the research outcomes' applicability for rock types. So, rock property characterization is essential for research study to indicate the applicable range of the proposed research outcomes.

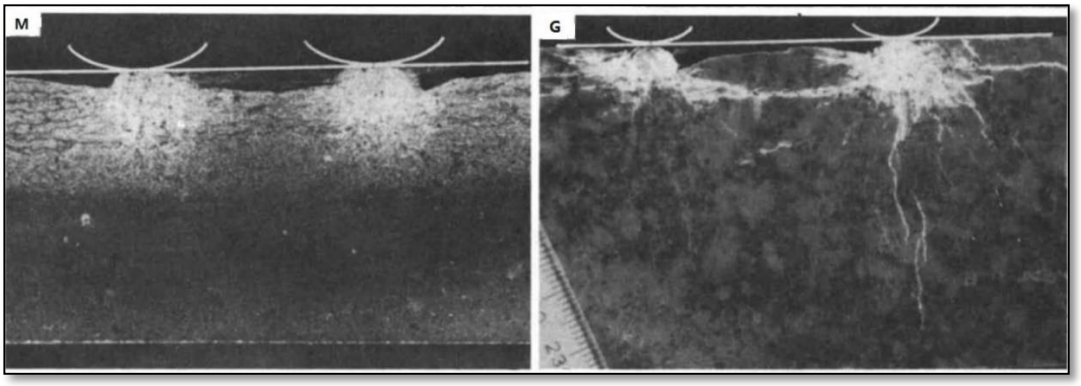

Figure 5-1 Different rock failure patterns for Microsyenite [left] and Granite [right] under CCS disc cutter (Howarth and Bridge, 1988).

In addition, rock properties are also parameters of the cutting force prediction models. Evans model included rock cohesion, c, and rock internal friction angle, φ (Evans, 1974). Roxborough and Philips (1975) considered Unconfined Compressive Strength (UCS), σ_c, in their prediction model. Ozdemir et al. (1977) and Rostami and Ozdemir (1993) added shear strength, τ, in the Colorado School of Mines (CSM) models.

Rock physical and mechanical properties are also prerequisite input parameters for numerical simulation. Numerical simulation is the only way currently to trace the development of sub-surface crushed zone and crack systems. Characterization of the tested rock properties is an important preparation for numerical simulation.

In this chapter, characterization techniques for physical and mechanical properties of the tested rock are described. Typical properties of tested rock, including density, UCS, Brazilian tensile strength, shear strength, cohesion, Young's modulus, and Poisson's ratio were measured in the laboratory according to suggested methods of the International Society of Rock Mechanics (ISRM).

5.2 Test preparation

All the tested samples were in cylinder shape. They were cored from intact sandstone blocks, as shown in Figure 5-2. The samples for UCS and deformability tests were 54 mm in diameter and 120 mm in height; for double shear tests they were 38 mm in diameter and 120 mm in height; and in Brazilian tests, specimens were prepared 54 mm in diameter and 28 mm in height. The sample diameter was controlled by choosing different drill bit diameters, while a diamond saw was employed to cut samples to the required height, as shown in Figure 5-3. All the samples were dried before tests. And the displacement control mode with a loading rate of 1.0 mm/min was utilized for all the tests.

Figure 5-2 Coring machine under operation.

Figure 5-3 Diamond saw for Brazilian testing sample preparation.

5.3 Specific density

To determine the specific density of the tested sandstone, six blocks were sampled. The sampled sandstone blocks were dried to avoid the influence of moisture, as shown in Figure 5-4.

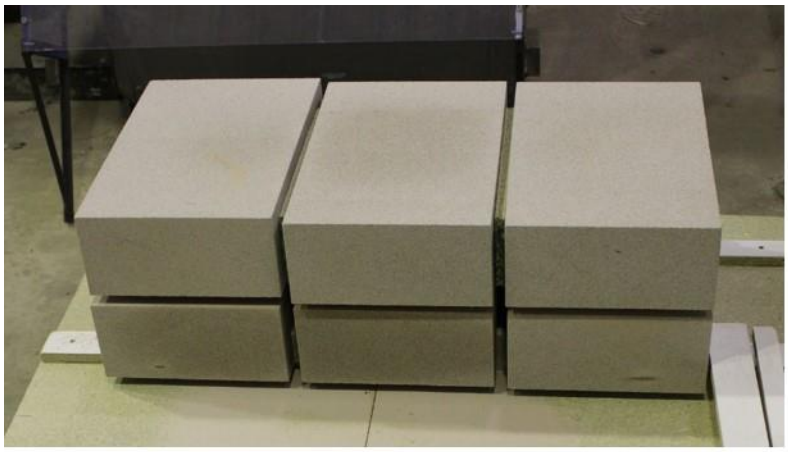

Sampled sandstone blocks

Blocks drying up

Figure 5-4 The sandstone blocks for specific density characterization.

The mass and size of the sandstone blocks were recorded, as listed in Table 5-1. The specific density values of the sampled blocks were 2233.98, 2230.66, 2239.55, 2225.45, 2229.59, and 2230.45 kg/m^3, respectively. By calculation, the average specific density of the sandstone was 2231.62 kg/m^3.

Table 5-1 Mass and dimensional characterization of sampled sandstone blocks.

Sample No.	Mass (kg)	Mean length (mm)	Mean breadth (mm)	Mean height (mm)	Specific density (kg/m^3)
1	28.19	401.2	260.8	120.6	2233.98
2	28.13	400.3	261.0	120.7	2230.66
3	28.23	400.9	260.5	120.7	2239.55
4	28.17	401.3	260.9	120.9	2225.45
5	28.19	400.2	261.1	121.0	2229.59
6	28.15	400.6	260.8	120.8	2230.45

5.4 Uniaxial compressive strength

The UCS testing of rock samples was conducted on an Instron loading machine, as shown in Figure 5-5. The test samples were cored from a sandstone block, and then the two ends were polished to be parallel and smooth. The dimension of all samples is 54 mm in diameter and 120 mm in height. UCS tests were carried on the prepared samples according to the ISRM suggested methods (Ulusay and Hudson, 2007).

Figure 5-5 Uniaxial compression strength tests on an Instron loading machine.

Ten samples were tested to obtain UCS strength. The samples' typical failure pattern and loading characteristics are shown in Figure 5-6. The peak load and sizes of the tested samples are listed in Table 5-2. The UCS values of the samples were 37.37, 33.73, 41.03, 39.36, 41.03, 36.97, 41.95, 37.68, 40.79, and 34.34 MPa, respectively. By calculation, the average uniaxial compressive strength of the tested sandstone was 38.43 MPa.

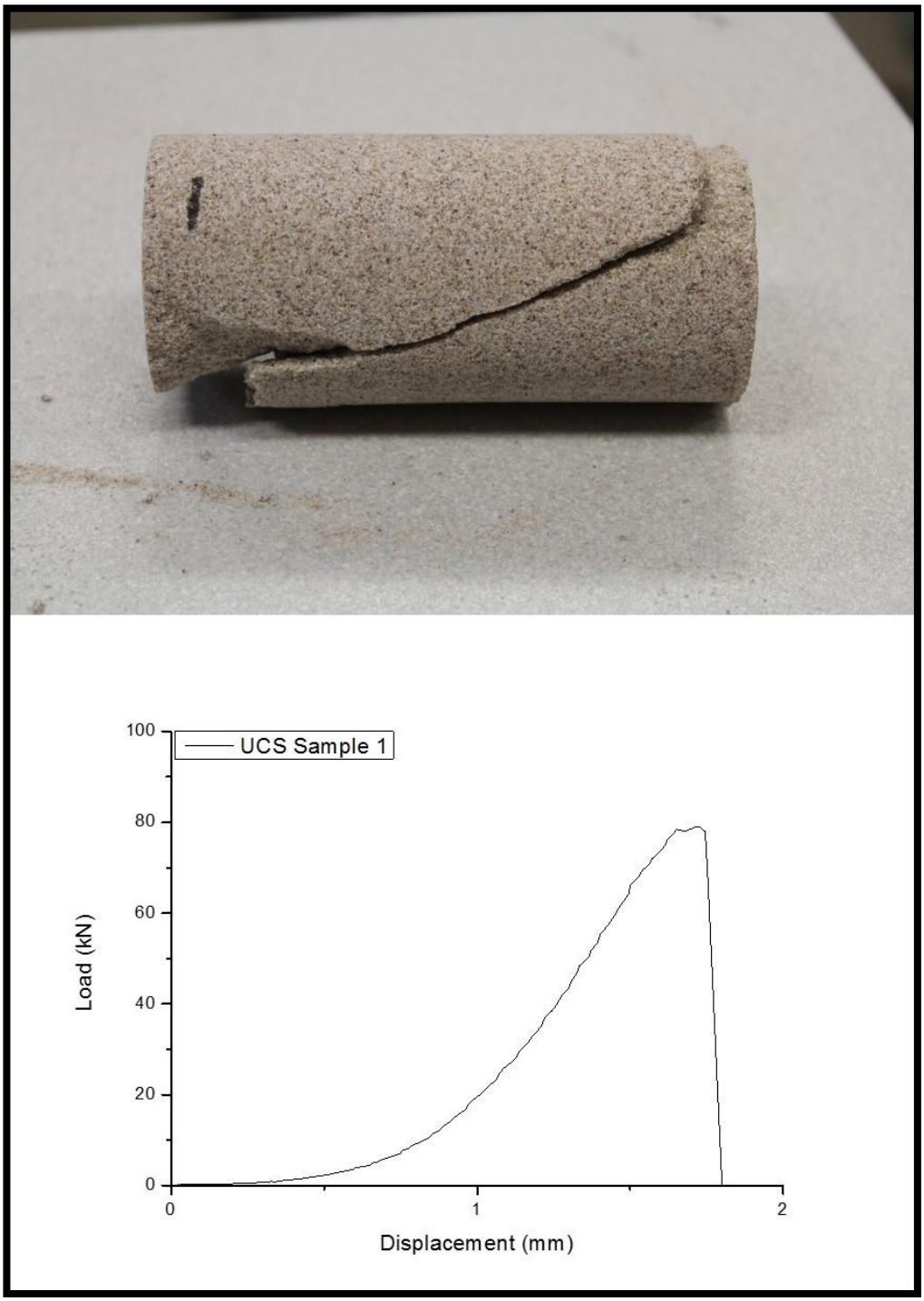

Figure 5-6 Typical failure pattern and loading characteristics for UCS tests.

Table 5-2 Summary of UCS strength of tested samples.

Sample No.	Diameter 1 (mm)	Diameter 2 (mm)	Mean diameter (mm)	Peak load (kN)	UCS (MPa)
1	54.16	54.25	54.205	86.21	37.37
2	54.21	54.20	54.205	77.81	33.73
3	54.02	54.08	54.05	94.09	41.03
4	54.16	54.19	54.175	90.68	39.36
5	54.23	54.28	54.255	94.82	41.03
6	54.17	54.19	54.18	85.19	36.97
7	54.25	54.18	54.215	96.79	41.95
8	54.13	54.15	54.14	86.70	37.68
9	54.20	54.22	54.21	94.11	40.79
10	54.16	54.19	54.175	79.12	34.34

The calculated UCS value is for samples with specific dimension. The sample size has a significant influence on the UCS of rock. The influence of sample size upon rock strength has been widely discussed in geotechnical literature and it is generally assumed that there is a significant reduction in strength with increasing sample size, as shown in Figure 5-7 (Hoek and Brown, 1980).

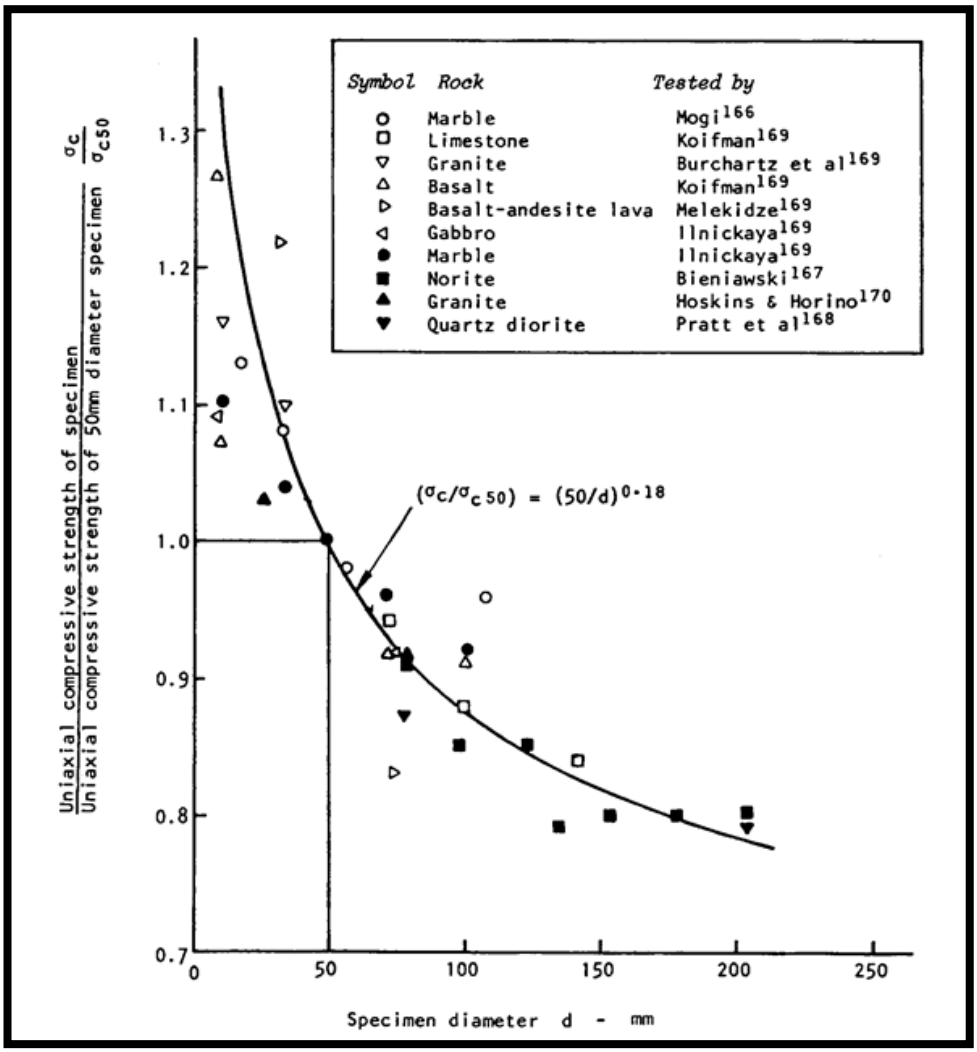

Figure 5-7 Influence of specimen size upon the strength of intact rock (Hoek and Brown, 1980).

Researchers employed different sample dimensions in their tests. To compare the strength under different sizes, it is important to generalize UCS data to their corresponding values under standard size. Based upon an analysis of extensive published data, Hoek and Brown (1980) proposed a formula to generalize the tested strength to the standard value under 50 mm diameter, as shown below.

$$\sigma_{cd} = \sigma_{50}\left(\frac{50}{d}\right)^{0.18} \qquad (5\text{-}1)$$

Where:

σ_{50} is the uniaxial compressive strength of a specimen of 50 mm diameter;

d is the diameter of the specimen;

σ_{cd} is the uniaxial compressive strength of a specimen with diameter of d.

5.5 Tensile strength

Several methods, direct or indirect, are available to test tensile strength of rocks. The Brazilian test, which is an indirect tensile test, is a commonly used method. In the test, a solid rock disc of diameter, d, and thickness, t, is placed between platens of the testing machine and a compressive load, p, is applied across the diameter. Rupture usually occurs along the loading line with a complicated stress distribution in the specimen. At the centre of the disc, the tensile stress is given by:

$$\sigma_T = \frac{2p}{\pi dt} \qquad (5\text{-}2)$$

Where:

σ_T is the Brazilian tensile strength;

p is the compressive load;

d is the dimeter of rock disc;

t is the thickness of rock disc.

The Brazilian method was employed in this study. It was conducted on an Instron loading machine, as shown in Figure 5-8.

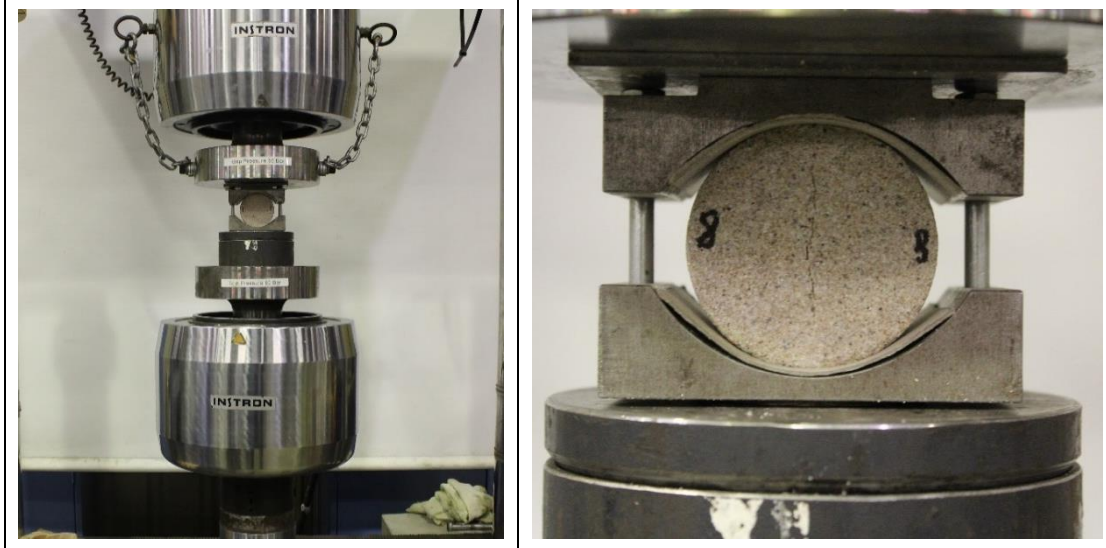

Figure 5-8 Brazilian indirect tensile test on an Instron loading machine.

Eight samples were tested to obtain Brazilian tensile strength. The samples' typical loading characteristics and failure pattern is illustrated in Figure 5-9. The peak load and sizes of the tested samples are listed in Table 5-3. The tensile strength values of the samples were 6.38, 5.89, 4.18, 6.94, 4.78, 4.91, 4.22, and 5.03 MPa, respectively. By calculation, the average Brazilian tensile strength of the tested sandstone was 5.29 MPa.

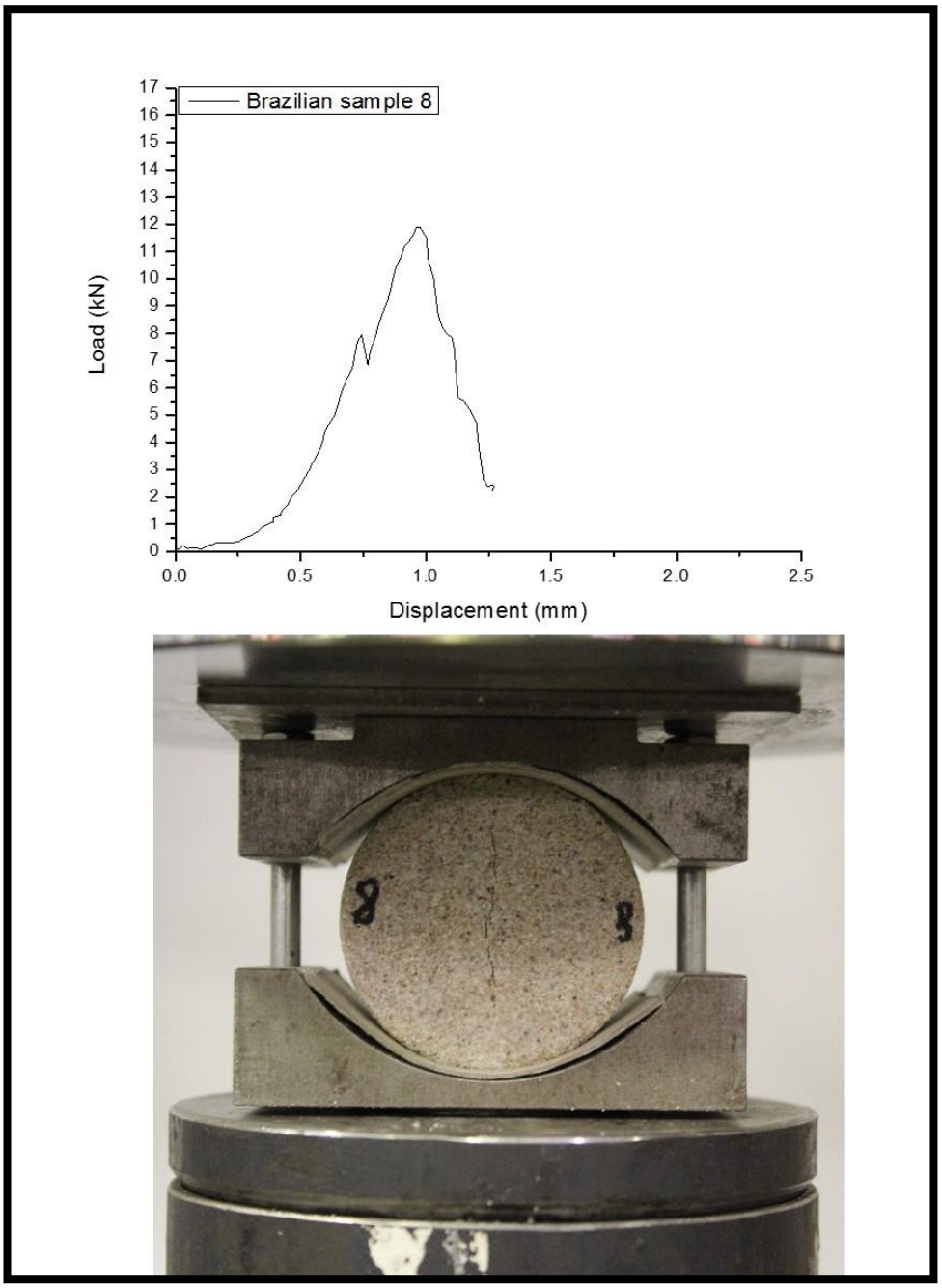

Figure 5-9 Typical loading characteristics and failure pattern for Brazilian tensile tests.

Table 5-3 Summary of test results for Brazilian indirect tensile test.

Sample	Thickness (mm)	Diameter (mm)	Peak load (kN)	Tensile strength (MPa)
Sample No.1	29.75	54.13	16.12	6.38
Sample No.2	28.73	54.16	14.38	5.89
Sample No.3	29.09	54.17	10.35	4.18
Sample No.4	28.83	54.25	17.03	6.94
Sample No.5	28.50	54.20	11.59	4.78
Sample No.6	27.49	54.18	11.49	4.91
Sample No.7	29.76	54.18	10.69	4.22
Sample No.8	27.86	54.13	11.91	5.03

5.6 Shear strength

Rock's shear strength can be obtained with direct shear tests which include single shear test and double shear test. Double shear was adopted in this study. For double shear test, a specimen is clamped in a double shear box, and shear load is applied through a double edged platen with a cylindrical groove at the bottom of the platen fitting the specimen. The specimen is sheared along two parallel planes, as shown in Figure 5-10 (Nemcik, 2013).

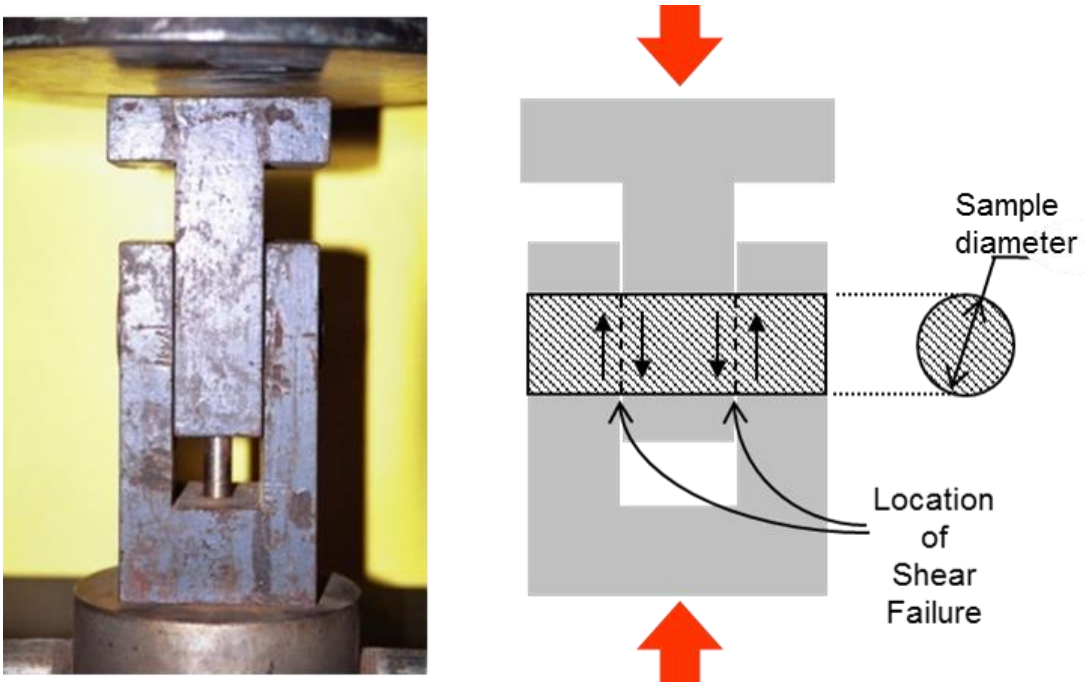

Figure 5-10 Graphic demonstration of double shear tests (Nemcik, 2013).

The shear strength is given by Equation (5-3):

$$\tau = \frac{S}{2A} \qquad (5\text{-}3)$$

Where：

τ is shear strength;

S is the load;

A is the cross sectional area of rock sample.

Eight samples were tested to obtain shear strength. The typical loading characteristics and failure pattern is illustrated in Figure 5-11. The peak load and size of the tested samples are listed in Table 5-4. The shear strength values of the samples were 6.22, 6.94, 6.27, 5.76, 4.99, 5.17, 6.94, and 5.04 MPa, respectively. By calculation, the average shear strength of the tested sandstone was 6.22 MPa.

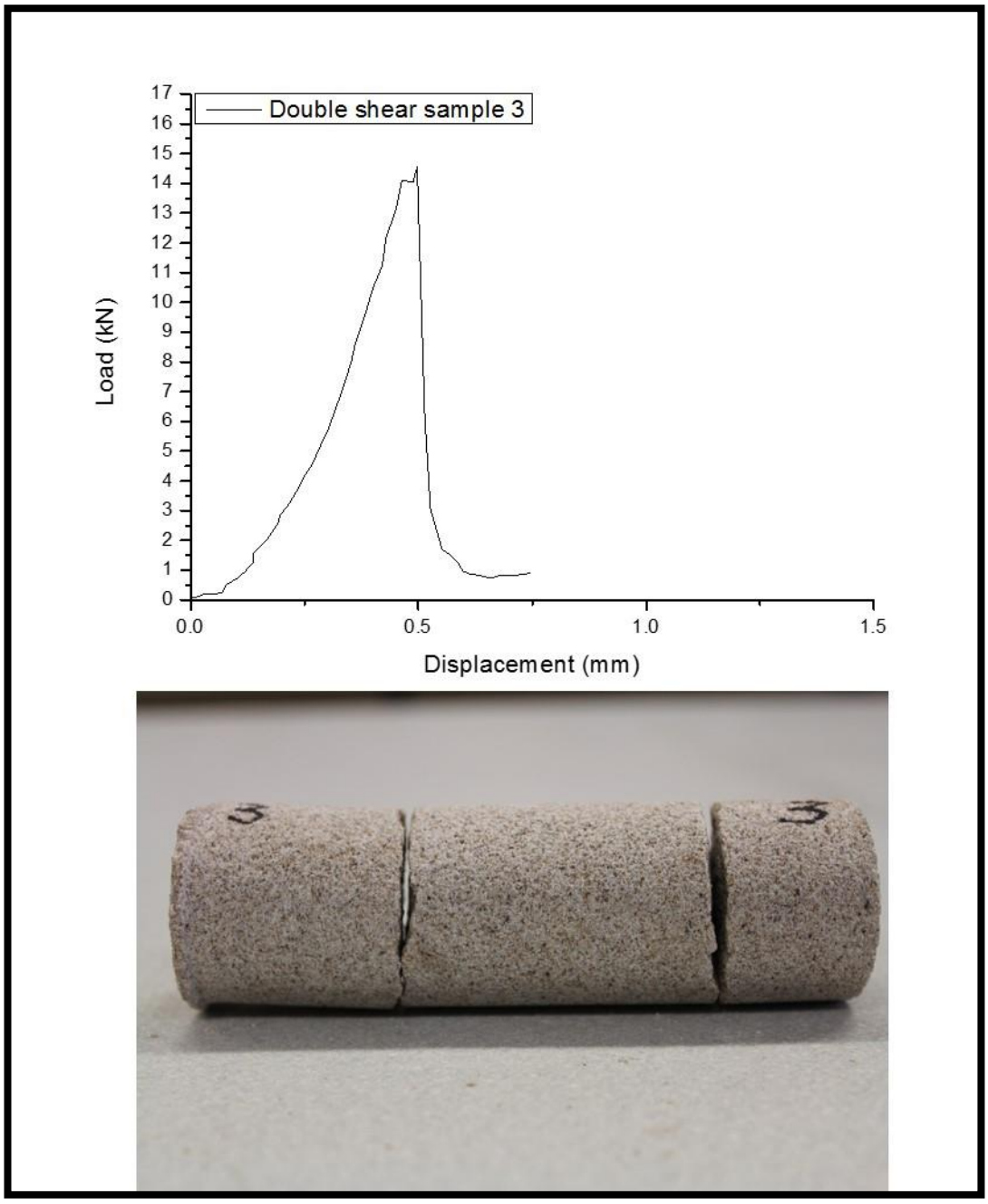

Figure 5-11 Typical loading characteristics and failure pattern for double shear tests.

Table 5-4 Double shear test results.

Sample	Diameter 1 (mm)	Diameter 2 (mm)	Mean diameter (mm)	Peak load (kN)	Shear strength (MPa)
1	38.19	38.34	38.265	14.30	6.22
2	38.23	38.20	38.215	15.91	6.94
3	38.33	38.57	38.45	14.55	6.27
4	38.17	38.21	38.19	13.18	5.76
5	38.18	38.19	38.185	11.43	4.99
6	38.20	38.23	38.215	11.86	5.17
7	38.24	38.27	38.255	15.94	6.94
8	38.16	38.16	38.16	11.52	5.04

5.7 Tri-axial compression tests

The tri-axial compressive strength test is similar to the UCS test but with confining stresses applied to the sides of the samples. There are two kinds of tri-axial compression tests – true tri-axial compression test and the traditional tri-axial compression test. In true tri-axial compression tests, two horizontal confining stresses are applied independently and different magnitudes can be assigned. This is similar to the field stress situation. However, the true tri-axial compression apparatus is fairly expensive and the preparation of the test is also time-consuming. In

traditional tri-axial compression tests, the sample is usually confined by pressurized oil and the two confining stresses are equal in magnitude, as shown in Figure 5-12.

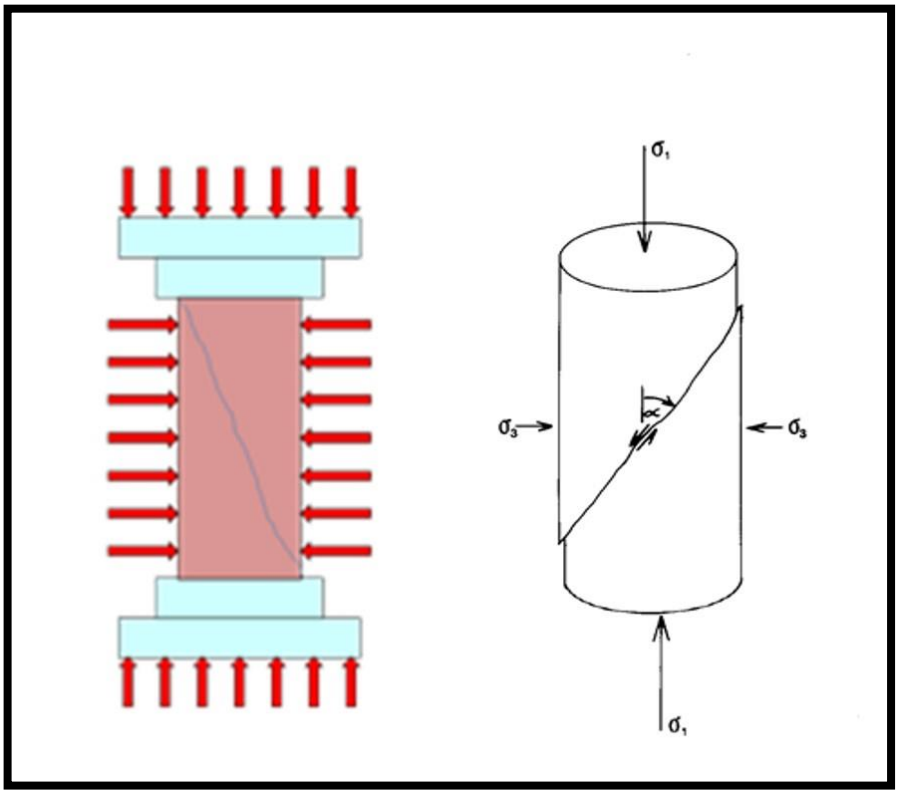

Figure 5-12 Schematic diagram of traditional tri-axial compression test (Nemcik, 2013).

The traditional tri-axial compression test is used to determine cohesion and the internal friction angle of the rock. It was conducted on an Instron loading machine, as shown in Figure 5-13. A Hoek-Brown tri-axial cell was used to apply confining stresses, as shown in Figure 5-14. To keep in line with the confining pressure of disc cutting tests, the confining pressures were adopted as 3 MPa, 6 MPa and 9 MPa in the tri-axial compression tests.

Figure 5-13 Tri-axial compression tests on an Instron loading machine.

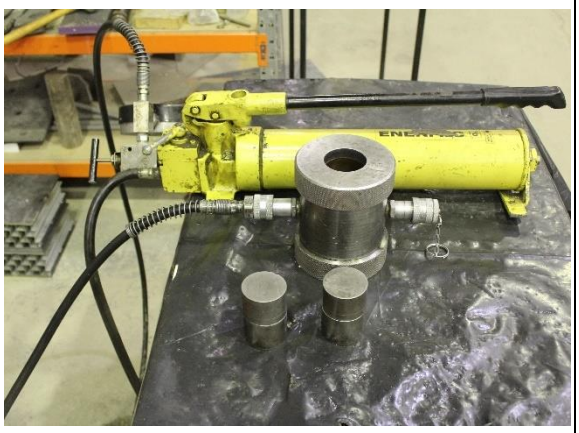

Figure 5-14 Hoek-Brown tri-axial cell and the oil supply pump.

Rock cohesion and the internal friction angle are important mechanical properties included in cutting force prediction models. Traditional tri-axial compression tests are the basis to obtain these parameters. There are two approaches to determine them from the test data, which are the $\sigma - \tau$ diagram method, and the σ_1-σ_3 diagram method.

For the $\sigma - \tau$ diagram method, rock cohesion is determined as the intercept of the shear stress axis, τ, with Mohr's failure envelope, as shown in Figure 5-15. Mohr's envelop is a common tangent through all the Mohr's circles of stress. Mohr's circles

are plotted with the values of the confining stresses and the failure stresses in a set of tri-axial compression tests. Additionally, the internal friction angle is the slope angle of the Mohr's envelop.

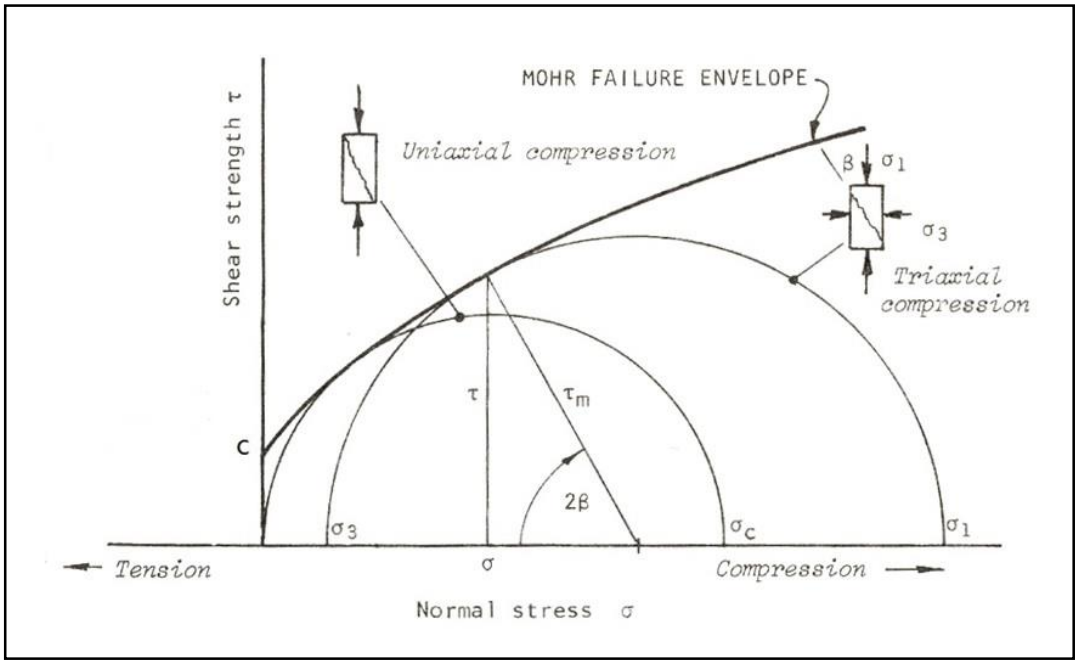

Figure 5-15 Determination of rock cohesion (Hoek and Brown, 1980).

For the σ_1-σ_3 diagram method, the determination of rock cohesion and internal friction angle is achieved through an intermediate step of plotting the σ_1-σ_3 diagram, as shown in Figure 5-16. The σ_1-σ_3 diagram can be expressed with the following formula:

$$\sigma_1 = \sigma_c + (\tan\beta) \times \sigma_3 \qquad (5\text{-}4)$$

Where:

σ_1 is axial stress;

β is the slope angle of σ_1 and σ_3 curve;

σ_c is uniaxial compressive strength of rock;

σ_3 is confining pressure.

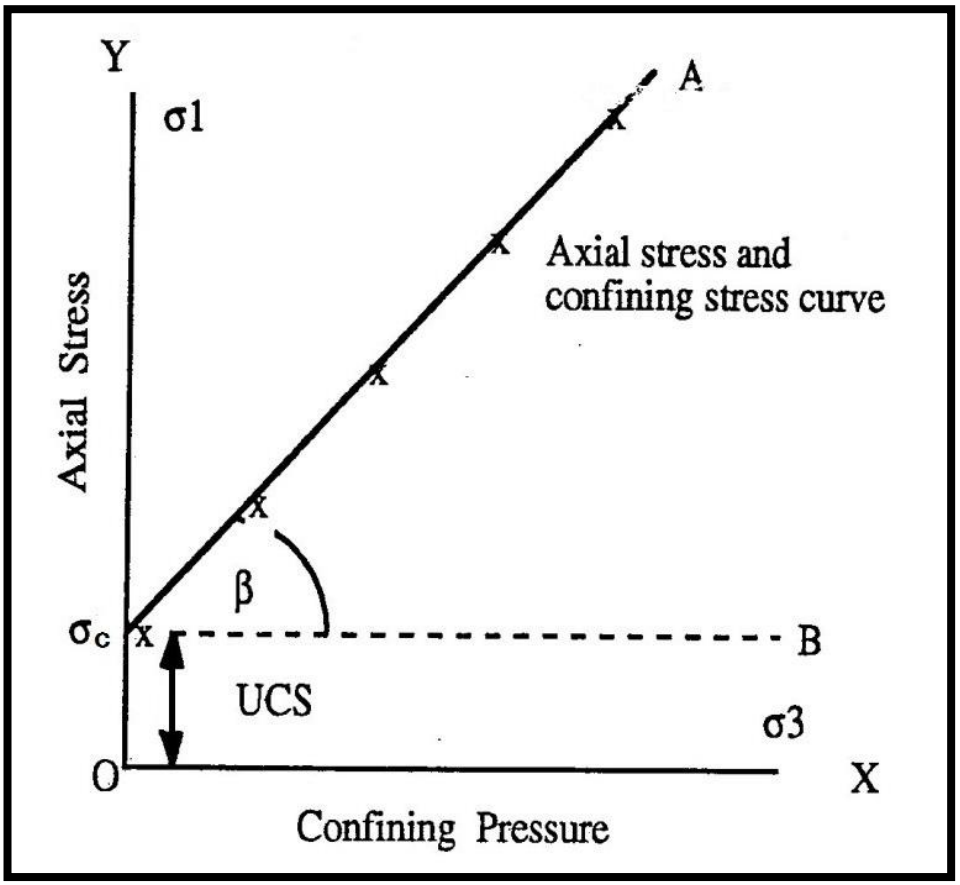

Figure 5-16 The σ_1-σ_3 diagram based on tri-axial compressive test data (Nemcik, 2013).

By plotting the tri-axial tests data onto a graph, and drawing a regression line; the intercept of the regression line and σ_1 axis is taken as σ_c, and β is determined as the included angle between the regression line and the σ_3 line. With the values of σ_c and β, the cohesion c and internal friction angle φ can be calculated with the following formulae:

$$\tan\varphi = \frac{(\tan\beta - 1)}{2(\tan\beta)^{1/2}} \qquad (5\text{-}5)$$

$$\sigma_c = \frac{(2c\cos\varphi)}{(1-\sin\varphi)} \qquad (5\text{-}6)$$

Three samples were tested for each confining pressure value, i.e. a total of nine samples were tested. The samples' typical failure pattern is shown in Figure 5-17.

Figure 5-17 Typical failure pattern for tri-axial compression tests.

The peak load and size of the tested samples are listed in Tables 5-5, 5-6, and 5-7 for confining pressure of 3, 6 and 9 MPa, respectively. The tri-axial compressive strength values for 3 MPa were 66.42, 61.93, and 64.99 MPa; those for 6 MPa were 84.28, 85.54, and 84.10 MPa; and those for 9 MPa were 98.27, 94.74, and 100.12 MPa. By calculation, the average tri-axial compressive strength values for 3, 6, and 9 MPa were 64.45, 84.64, and 97.71 MPa, respectively.

Table 5-5 Peak load of samples with 3 MPa confining pressure.

Sample No.	Diameter 1 (mm)	Diameter 2 (mm)	Peak load (kN)	Tri-axial compression strength (MPa)
1	54.19	54.16	153.10	66.42
2	54.23	54.25	143.10	61.93
3	54.18	54.19	149.87	64.99

Table 5-6 Peak load of samples with 6 MPa confining pressure.

Sample No.	Diameter 1 (mm)	Diameter 2 (mm)	Peak load (kN)	Tri-axial compression strength (MPa)
1	54.17	54.15	194.17	84.28
2	54.22	54.18	197.35	85.54
3	54.16	54.20	193.89	84.10

Table 5-7 Peak load of samples with 9 MPa confining pressure.

Sample No.	Diameter 1 (mm)	Diameter 2 (mm)	Peak load (kN)	Tri-axial compression strength (MPa)
1	54.19	54.16	226.53	98.27
2	54.20	54.18	218.50	94.74
3	54.22	54.17	230.95	100.12

Based on the tri-axial compression tests data, both aforementioned analysing approaches were adopted to calculate the rock cohesion and internal friction angle. Firstly, the σ_1-σ_3 diagram approach was conducted, as shown in Figure 5-18. The laboratory determined UCS value was also plotted on the graph, which is regarded as the tri-axial compressive strength with the confining pressure of 0 MPa.

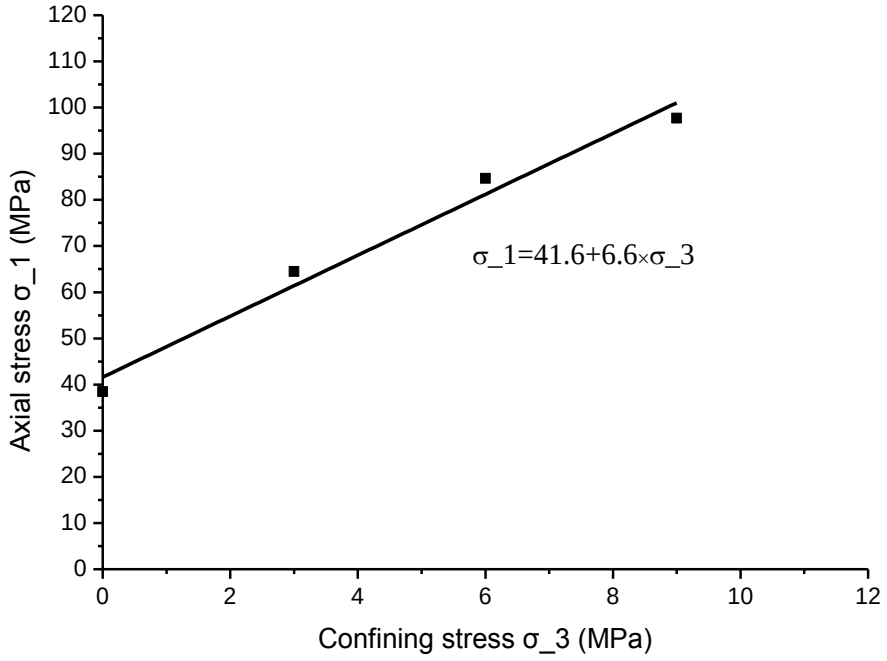

Figure 5-18 The σ_1-σ_3 diagram based on the tri-axial compression test data.

According to Figure 5-18,

$$\tan\beta = \frac{1+\sin\varphi}{1-\sin\varphi} = 6.6$$

By calculation, it can be obtained that,

$$\tan\varphi = \frac{(\tan\beta - 1)}{2(\tan\beta)^{1/2}} = 1.09$$

Then the value of φ can be obtained as $\varphi = 47.47°$. Where, β is the slope angle of the regression line; φ is the internal friction angle.

Based on the equation

$$\sigma_c = \frac{2c\cos\varphi}{1-\sin\varphi}$$

By substituting $\sigma_c = 41.6$ MPa and $\varphi = 47.47°$, i.e.

$$41.6 = \frac{2c\cos 47.47°}{1-\sin 47.47°}$$

Then $c = 8.10$ MPa.

Conclusively, the values of cohesion and internal friction angle were 8.10 Mpa, and 47.47° respectively, according to the σ_1-σ_3 diagram approach.

The $\sigma - \tau$ diagram method was also used to determine the cohesion and internal friction angle. The first step was to plot the $\sigma - \tau$ diagram basing on the tri-axial compression test data, as shown in Figure 5-19. In the figure, Mohr's circles of stress are plotted with the values of the confining stresses and the failure stresses; Mohr's failure envelop is a common tangent through all the Mohr's circles.

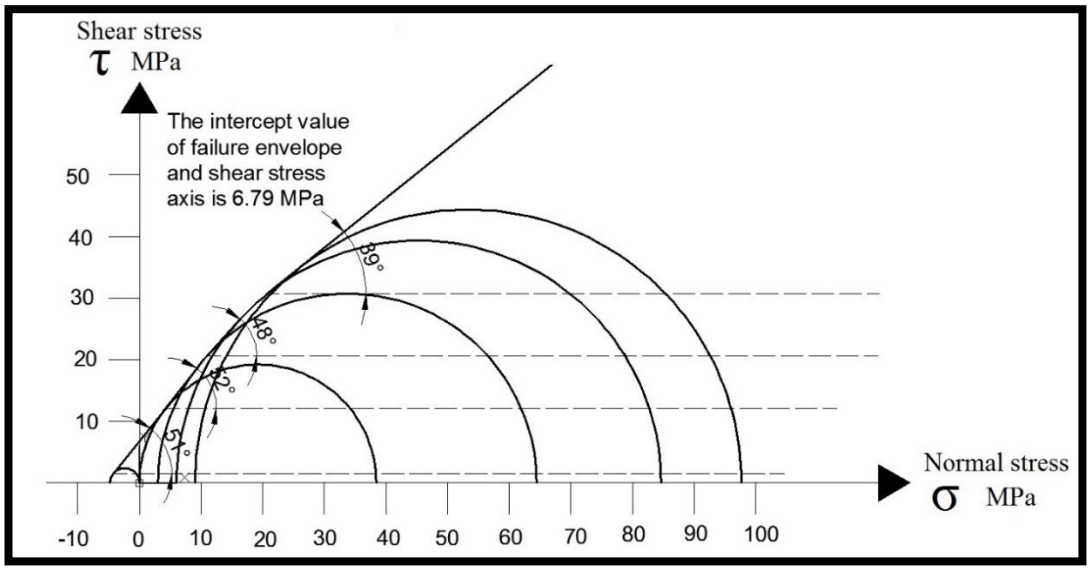

Figure 5-19 $\sigma - \tau$ diagram based on the tri-axial compression test data.

Figure 5-19 shows that the intercept value of the failure envelope and the shear stress axis is 6.79 MPa. While the failure envelope slope angle varied with different confining pressures. The values were 51°, 52°, 48°, and 39° for confining pressures of 0, 3, 6 and 9 MPa, respectively. By taking the mean value, the internal friction angle was determined as $47.50°$.

In conclusion, the tri-axial compression tests were conducted with confining pressure values of 0, 3, 6 and 9 MPa. Based on the testing data, two methods were employed to calculate rock cohesion and internal friction angle. With the σ_1-σ_3 diagram method, the rock cohesion was 8.10 MPa, and the internal friction angle was $47.47°$; with the $\sigma - \tau$ diagram method, the rock cohesion was 6.79 MPa, and the internal friction angle was $47.50°$.

5.8 Deformability tests

Rock deformability accounts for its deformation characteristics when loaded. Deformability parameters include Young's modulus, E, Poisson's ratio, υ, shear modulus, G, and bulk modulus, K. Young's modulus, E, is the ratio of the stress to the strain along an axis in the elastic phase. It is a measure of material stiffness in the elastic phase. Poisson's ratio, υ, is the ratio of diametric strain to the axial strain in

the direction of the applied load. Shear modulus, *G*, describes a material's response to shear strain; and bulk modulus, *K*, describes a material's response to uniform pressure. For homogenous, isotropic materials, the shear modulus, *G*, and bulk modulus, *K*, can be functionally expressed by Young's modulus, E, and Poisson's ratio, v:

$$G = \frac{E}{2(1+v)} \qquad (5\text{-}7)$$

$$K = \frac{E}{3(1-2v)} \qquad (5\text{-}8)$$

Young's modulus, *E*, and Poisson's ratio, v were determined through deformability tests, which are similar to the uniaxial compressive test, but assisted with electrical resistance strain gauges, as shown in Figure 5-20 and Figure 5-21. 4 strain gauges were mounted for every tested samples, i.e. a couple of axial ones and a couple of diametric ones. Both axial and diametric strain gauges were mounted on the centre of the specimen.

Figure 5-20 Deformability test on an Instron loading machine.

Figure 5-21 Deformability test samples with mounted strain gauges.

The applied axial stress on a test sample is calculated by:

$$\sigma = \frac{P}{A} \qquad (5\text{-}9)$$

Where:

σ is axial stress;

P is applied force;

A is cross sectional area of tested sample.

Both axial and diametric strains were obtained from a data logger, as shown in Figure 5-20. With the stress and strain values, the stress/strain curve can be plotted, as shown in Figure 5-22. In addition, the plotted strain values were the mean values of strain gauge couples. Young's modulus is calculated with the stress and strain values at 50% of the compressive strength. Poisson's ratio, υ, is also calculated with the values at 50% of the compressive strength.

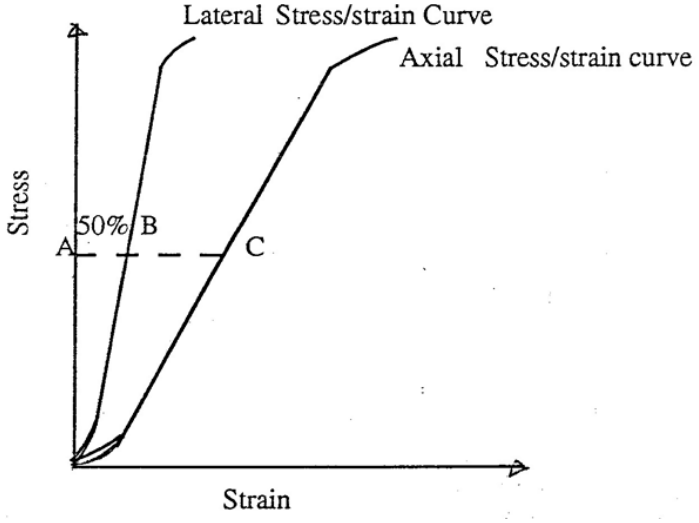

Figure 5-22 Calculation of Young's modulus and Poisson's ratio (Nemcik, 2013).

Four samples were tested to acquire Young's modulus and Poisson's ratio. The samples' typical loading characteristics and failure pattern are shown in Figure 5-23. The strain-stress curves were plotted for tested samples, as shown in Figures 5-24 to 5-27. It should be noted that test data for sample 1 was invalid. So it was excluded from the subsequent calculations. By calculation, Young's modulus values were 49.60, 47.68 and 48.52 GPa respectively for the samples; and Poisson's ratio values were 0.15, 0.17 and 0.16 respectively. Conclusively, by taking the mean value, the sandstone's Young's modulus value is 48.60 GPa, and Poisson's ratio value is 0.16.

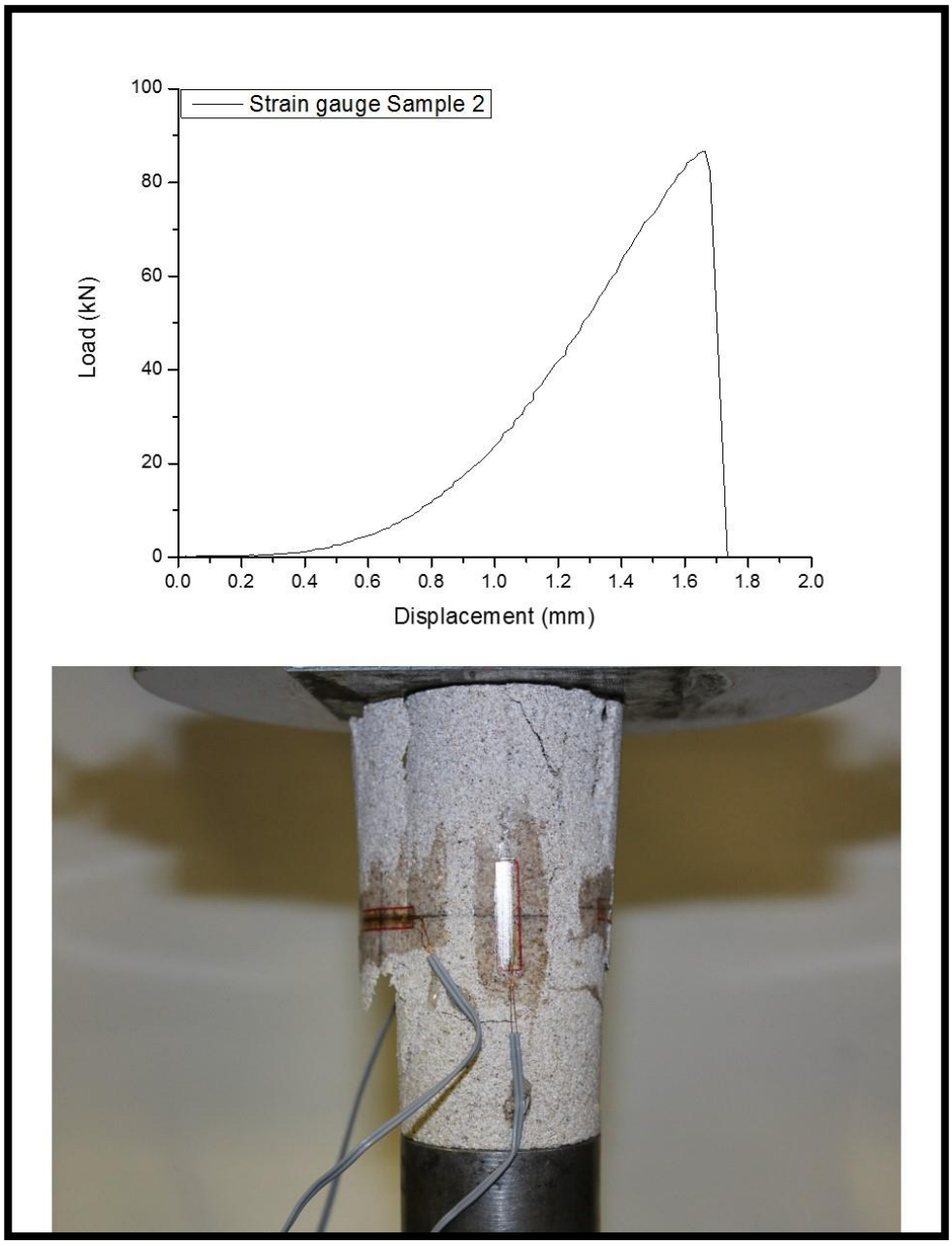

Figure 5-23 Typical loading characteristics and failure pattern of deformability test samples.

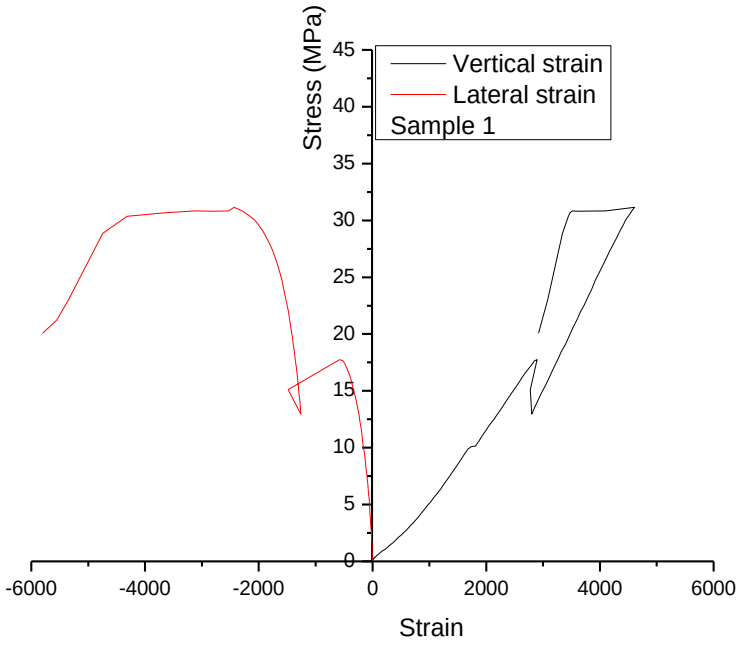

Figure 5-24 Strain-stress curve for deformation test of sample 1.

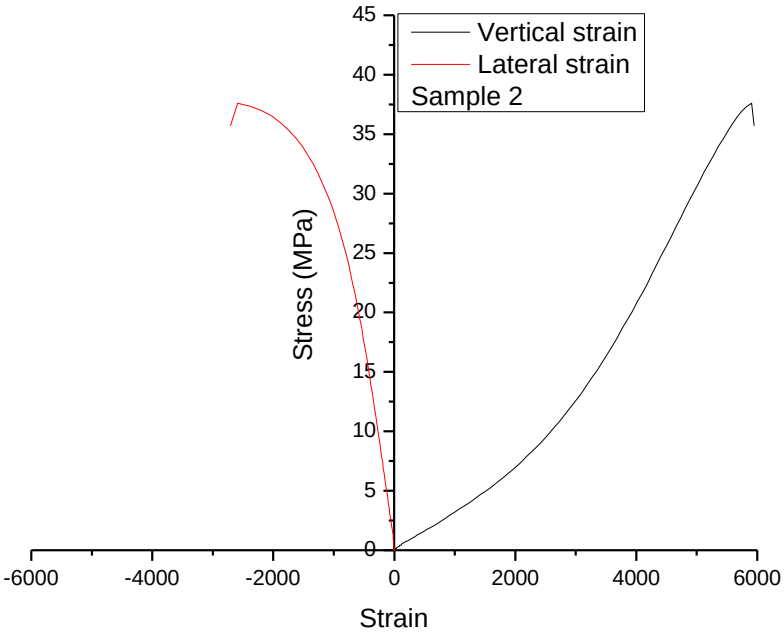

Figure 5-25 Strain-stress curve for deformation test of sample 2.

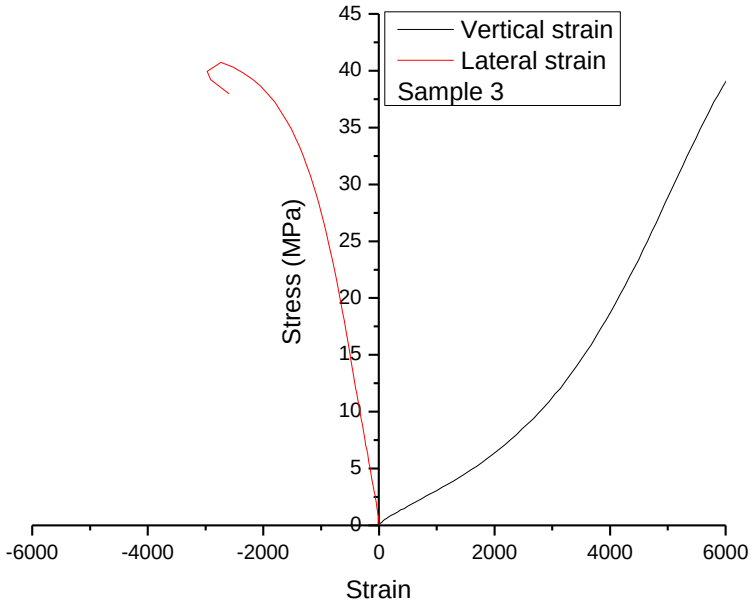

Figure 5-26 Strain-stress curve for deformation test of sample 3.

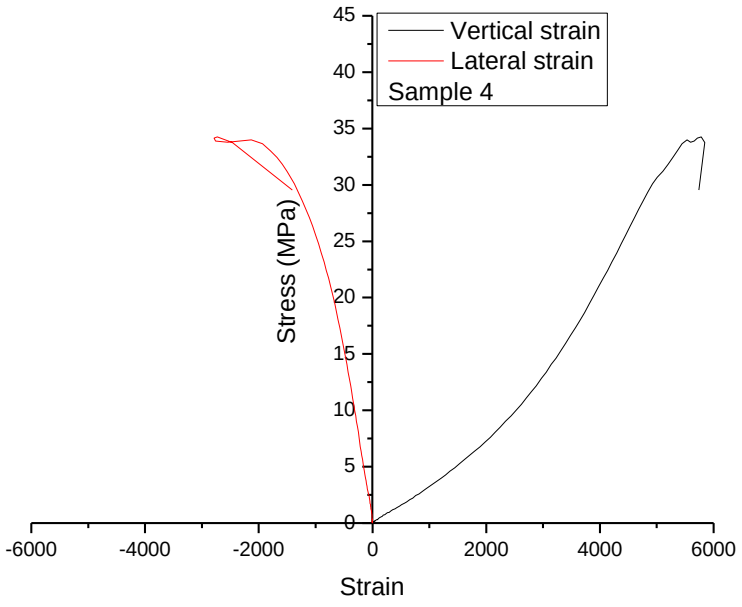

Figure 5-27 Strain-stress curve for deformation test of sample 4.

5.9 Summary

Rock physical and mechanical properties impose a considerable influence on the disc cutting mechanism. They are also parameters of the cutting force prediction models, and necessary for TBM performance prediction. In addition, they are prerequisite input parameters for numerical simulation. This chapter described the characterization techniques for rock properties. The tested rock's properties were determined by the described methods. The rock properties results are summarized in Table 5-8.

Table 5-8 Summary of rock properties.

Rock property titles	Property values
Specific density	2231.62 kg/m^3
Uniaxial compressive strength (UCS)	38.43 MPa
Brazilian tensile strength	5.29 MPa
Shear strength	6.22 MPa
Cohesion	6.79/8.10 MPa
Internal friction angle	47.50°/47.47°
Young's Modulus	48.60 GPa
Poisson's ratio	0.16

6 CHAPTER SIX –LABORATORY STUDY ON CUTTING FORCE AND CUTTING MECHANISMS

6.1 Introduction

TBM has promising application in deep underground coal mines. However, unlike shallow tunnels, TBM performance prediction for deep tunnels is not really reliable. Lack of reliable prediction imposes difficulties on risk and cost management, which can deter their applications.

Deep tunnels are exposed to high ground stress conditions, which influences rock breaking of TBM disc cutters. So far, the influence of ground stresses influence on disc cutting is not clear. Researchers have proposed different mechanisms; but sometimes, they conflict with each other. Tarkoy and Marconi (1991) proposed an unfavourable influence of high confinement stresses on rock boreability by referring to an exceptionally poor penetration rate of less than 0.12 m/h for Star Mine tunnels driven with 1200-2000 m overburden. Klein et al. (1995) in contrast with those described by Tarkoy and Marconi, proposed favourable effects of high confining stresses on the TBM boring based on four TBM tunnelling projects' field data of Field Penetration Index. Cook et al. (1984) argued that increasing confinement stress would cause higher cutting force and lower penetration by experimental studies on rock fragmentation under a circular flat stamp indenter. Liu et al. (2002) numerically simulated rock fragmentation under a truncated cone indenter, and proposed similar conclusions to Cook et al. Innaurato et al. (2007) conducted laboratory tests on two very hard rocks, with UCS of 142 MPa and 234 MPa respectively, and found that the influence of confinement was notable and increased with the increment of spacing. Conclusively, the influence of confinement stress on disc cutting is not yet fully explored, although it is notable.

Rock fragmentation and cutting forces are the major concerns of disc cutting studies. From these two perspectives, the influence of ground stresses on disc cutting needs to be conducted. Rock fragmentation under a disc cutter mainly includes forming a crushed

zone and crack development. The crushed zone reflects subsurface stress distribution under the disc cutter; it is also related to dust generation, which influences occupational health and disc cutter lifespan (Rostami and Ozdemir, 1993, Innaurato and Oreste, 2011, Rostami, 2013). Crack development patterns reflect the mode of failure; radial cracks are often caused by tensile failure, while lateral cracks, i.e. side chipping, indicate likely shear failure. Observation of crack development patterns under confining stresses would improve the understanding of the influence of confining stresses on failure mode, which is a prerequisite for refinement of cutting force prediction models with the consideration of confining stresses.

Laboratory study on the influence of confining stresses on cutting forces has both practical and theoretical meanings. Practically, it would provide direct and reliable guidelines for new TBM cutter-head design, and performance prediction of given TBMs, for deep tunnel projects. Theoretically, it enriches the reliable database for verification of proposed cutting force prediction models.

In conclusion, the lack of knowledge of the influences of ground stress to disc cutting limits the application of TBMs in deep underground coal mines. This chapter aims to offer new insights onto this issue with laboratory tests. More specifically, this laboratory study focuses on the influence of ground stresses on crushed zone formation, crack development and cutting forces.

6.2 Disc cutter indentation tests

Disc cutting is the result of interaction between the disc cutter and rock. It is mainly the function of thrust. So a disc cutter can be considered as an indenter, and the cutter and rock interaction can be treated as an indentation process. In indentation tests, ground stresses can be simulated as confinement pressures.

Indentation test methodology was used to study cutter-rock interaction of a single cutter, without the influence of contiguous cuts. Ozdemir et al. (1977) conducted indentation

tests by pushing six inch disc cutters into the rock samples which were contained in six inch (152.4 mm) ID steel pipes. The 6 inch disc cutter is too small compared to mining industry employed ones; rock specimens were also small with only 152.4 mm diameter; and confinement pressure was not considered in the study. Lindqvist et al. (1984) conducted indentation tests by placing $14 \times 15 \times 20$ mm rock samples in a loading stage, as shown in Figure 4-5. In this study, indenters were different from real disc cutters on both shape and size; and rock specimens were too small to avoid dimensional influences. In addition, confinement pressure was not applied.

Howarth and Bridge (1988) refined the indentation tests using an AVERY compression machine, as shown in Figure 4-7. They improved the indenter design using the same shape of industrial adopted disc cutter. Rock specimens were also upsized to dimensions of $400 \times 200 \times 200$ mm. The rock samples were cut twice on the same surface. However, the factor of confinement pressure was still not considered in Howarth and Bridge's tests.

Innaurato et al. (2007) further refined the indentation set up by taking confinement's influence into consideration, as shown in Figure 4-10. The background of this study was the application of TBMs in deep tunnels, i.e. the excavation of long Trans-Alpine tunnels in Europe, which needs better understanding of disc cutting mechanisms to optimize the TBM cutting system and to achieve more accurate TBM performance prediction. Indenter was also refined to a parallel cut realistic TBM disc cutter.

According to the aforementioned literature review, indentation tests preparations include indenter selection, test specimen preparation, and test platform design. To get meaningful results, indenters need to be similar to real disc cutters, rock specimen should be prepared as large as possible based on laboratory treating capacity, tests should be designed to provide realistic confinement pressure regimes. Details of the proposed indentation tests on these three aspects are explained below.

6.2.1 Disc cutter design

According to cutter ring shape, disc cutters can be categorized into V shape disc cutters and CCS disc cutters, as shown in Figure 3-3 and Figure 3-4. Various disc cutters have been developed for different applications, depending on machine types, sizes and specific geological operating conditions. For applications in the mining industry, where the tunnel diameters are often in the range of 3~8m, both V shape and CCS shape disc cutters are utilized.

Diameter and thickness are two important parameters for cutter rings. According to mining industrial applications, cutter rings with diameters of 17 inches [431.8 mm], 19 inches [482.6 mm] and 20 inches [508.0 mm] are employed. Furtherly, 17 inch and 19 inch cutter rings are the most widely used, as shown in Figure 6-1 (Roby et al., 2008). Figure 6-1 shows the real values of industrial adopted cutter ring dimensions. To align with reality, 450 mm and 30 mm were selected as the cutter diameter and thickness respectively in this study.

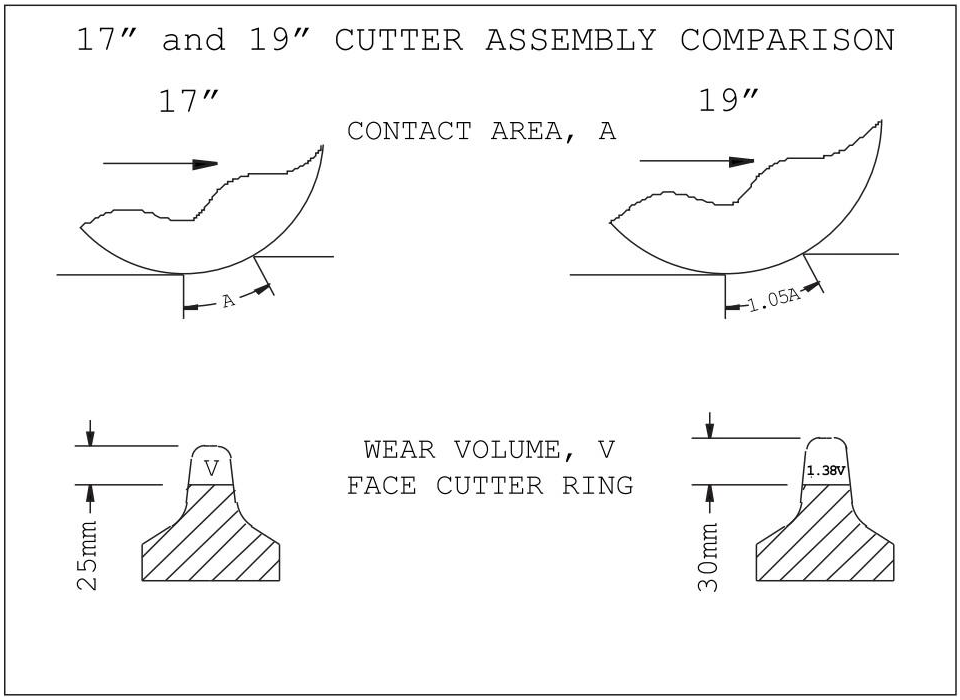

Figure 6-1 Schematic diagram of classical Robbins disc cutter rings (Roby et al., 2008).

Included edge angle is another important parameter for V shape cutter rings. Various included angle values have been adopted from 60° to 105°, as shown in Figure 3-8 (Ozdemir et al., 1977). To represent the most common scenarios, the cutter included edge angle adopted in the laboratory tests was 80°.

In conclusion, the dimeter of cutter rings was 450mm, the thickness was 30mm, and the included edge angle for V shape cutter rings was 80°. Based on the parameters, the V shape and CCS cutter rings were designed as shown in Figures 6-2, 6-3, and 6-4.

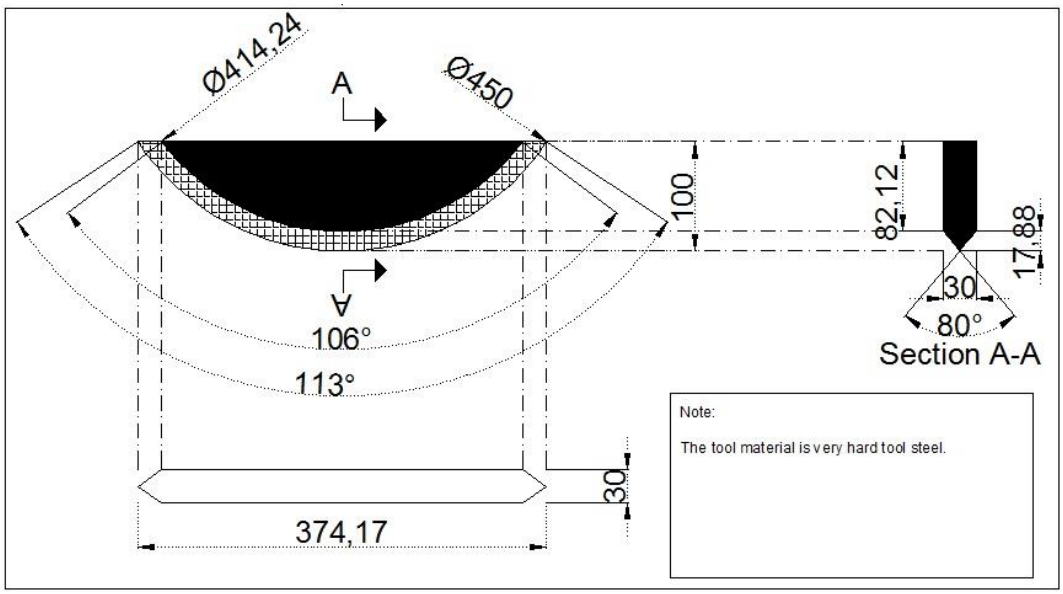

Figure 6-2 Fabricating drawing for V shape cutter ring.

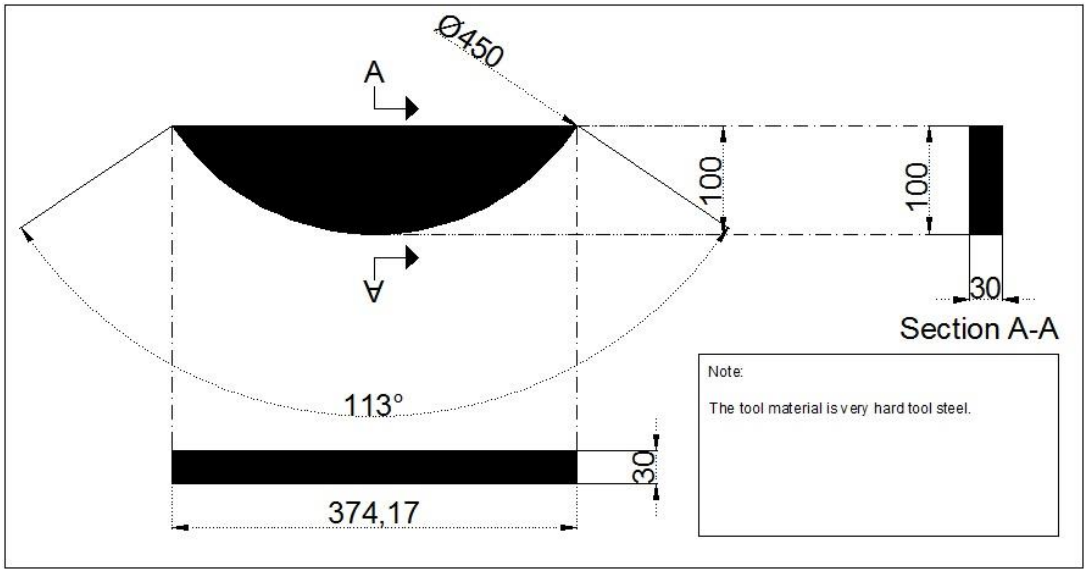

Figure 6-3 Fabricating drawing for CCS cutter ring.

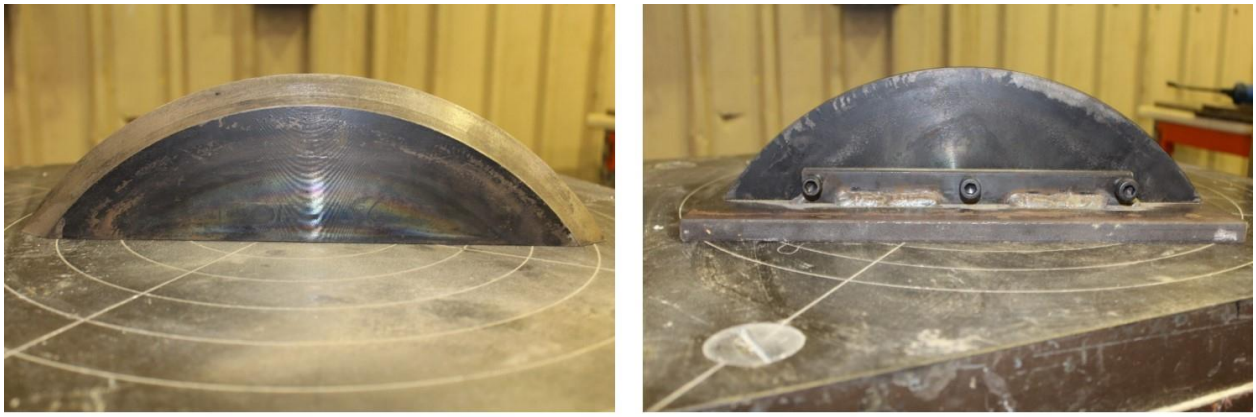

(a) V Shape cutter ring (b) CCS cutter ring

Figure 6-4 Fabricated cutter rings

6.2.2 Preparation of tested rock

The context of this laboratory study is the application of TBMs in underground coal mines. Sandstone is the most common surrounding rock in underground coal mines. As different rock types have distinctive failure patterns under disc cutting due to the complexity of the rock properties in nature; it is hard to generalize a specific research outcome applicable for all rocks. To obtain meaningful guidelines for application of TBMs in underground coal mines, sandstone was chosen as the tested rock in this study.

To ensure that the tested sandstone blocks have consistent physical and mechanical properties, all rock blocks were cut from a single large lump, which was from a quarry in Wollongong. They were diamond sawn into a specified dimension of $400\ \text{mm} \times 260\ \text{mm} \times 120\ \text{mm}$, as shown in Figure 6-5. Dimension of the rock samples were determined by the maximum capacity of the diamond saw in the laboratory, as shown in Figure 6-6, which was used to cut the sandstone blocks to examine the subsurface crushed zone and crack development after the indentation tests.

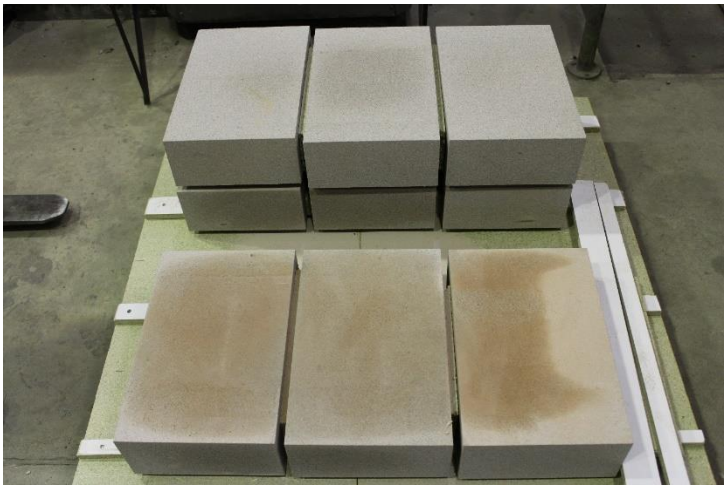

Figure 6-5 Sandstone blocks tested in the experiment.

Figure 6-6 Diamond saw used in the tests.

Sandstone blocks had moisture from quarrying and sawing. To eliminate the influence of moisture, they were dried in a drying cell, as shown in Figure 6-7.

Figure 6-7 Drying of sandstone blocks before laboratory tests.

Rock property tests were carried out according to ISRM recommendations, and the results are listed in Table 5-8.

6.2.3 Test platform set up design

The field ground stresses were simulated as confinement pressures in laboratory tests. Confining pressure applied in the literature was in one direction. However, stress regimes of face rock in deep tunnels were two directional, i.e. vertical and lateral. To apply the two directional confinement on sandstone blocks, a confining box was designed to accommodate the sandstone blocks. The sandstone block was positioned at a corner of the box, and then two steel plates were placed against the two open sides of the sandstone block. Two hydraulic flat jacks were placed between the box and steel plates to apply confining pressure, as shown in Figure 6-8.

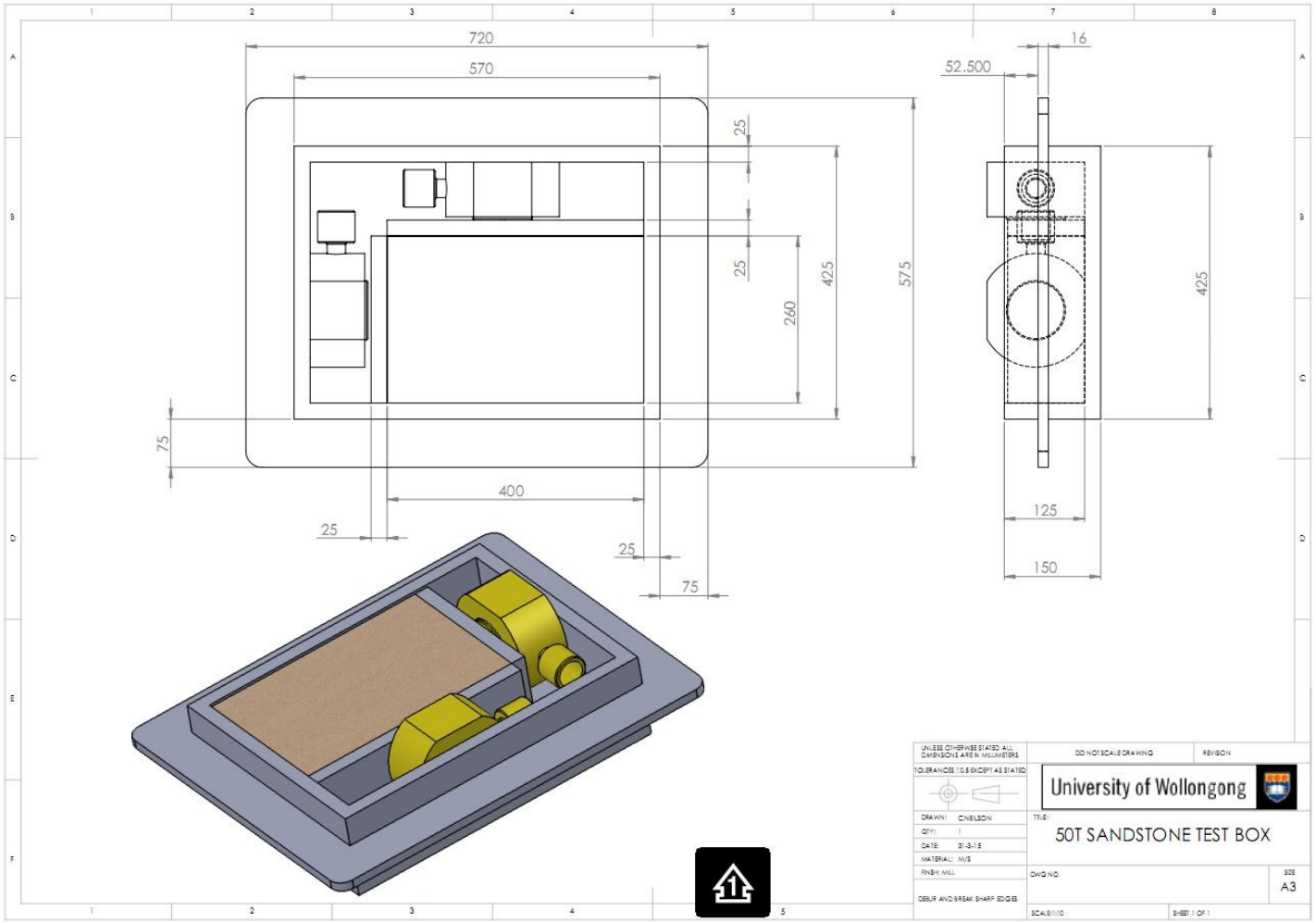

Figure 6-8 Steel box to apply confining pressure (Courtesy of Cameron Neilson).

Figure 6-8 shows that the two compartments used to accommodate the hydraulic jack cylinders had a width of 90 mm ($425 - 25 \times 3 - 260 = 90$) and 95 mm ($570 - 25 \times 3 - 400 = 95$) respectively. With these dimensions, general hydraulic cylinders cannot be employed, so the flat jack cylinders were considered. The accessible flat jack cylinders are listed Figure 6-9.

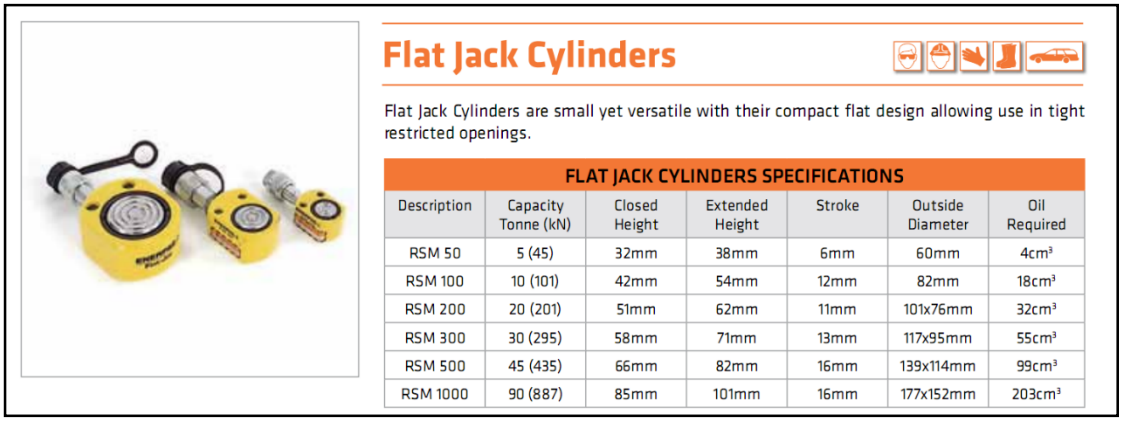

Flat Jack Cylinders

Flat Jack Cylinders are small yet versatile with their compact flat design allowing use in tight restricted openings.

FLAT JACK CYLINDERS SPECIFICATIONS

Description	Capacity Tonne (kN)	Closed Height	Extended Height	Stroke	Outside Diameter	Oil Required
RSM 50	5 (45)	32mm	38mm	6mm	60mm	4cm³
RSM 100	10 (101)	42mm	54mm	12mm	82mm	18cm³
RSM 200	20 (201)	51mm	62mm	11mm	101x76mm	32cm³
RSM 300	30 (295)	58mm	71mm	13mm	117x95mm	55cm³
RSM 500	45 (435)	66mm	82mm	16mm	139x114mm	99cm³
RSM 1000	90 (887)	85mm	101mm	16mm	177x152mm	203cm³

Figure 6-9 The parameters of flat jack cylinders (after online Coates hire product brochure).

Considering the limited space of the confining compartments, and the parameters of the accessible flat jack cylinders, the highest capacity cylinder that can fit in the confining box was the RSM500, i.e. the 45 t (435 kN) flat jack cylinder. The RSM1000, i.e. the 90 t (887 kN) flat jack cylinder, was not available because its height was over 95 mm. With the available load capacity, it can be calculated that the maximum confining pressure is 9.0625 MPa ($435\ \text{kN} \div 400\ \text{mm} \div 260\ \text{mm} = 9.0625\ \text{MPa}$). Consequently, 9 MPa was adopted as the highest confining pressure.

The indentation tests were set upon an AVERY computer controlled electro-hydraulic servo machine with load capacity of 5000 kN, as shown in Figure 6-10. The confining box was placed on the bottom platen while the disc cutter was

placed at the upper platen. The two flat jacks were inflated with two hydraulic hand pumps.

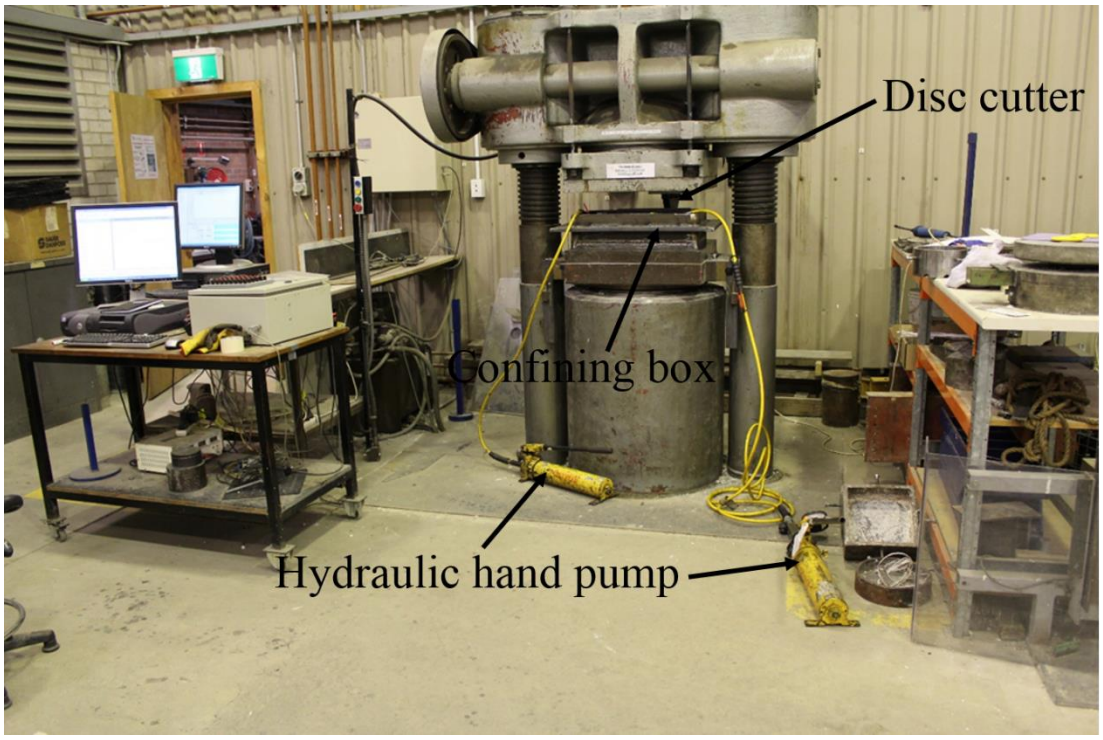

Figure 6-10 The indentation test platform.

Indentation cut positioning was another issue to be determined. Two sequential cuts were planned for each rock specimen on the top surface, as shown in Figure 6-11. Determination of each cut's position was based on the reviewing of research outcome on spacing- penetration ratio. The spacing- penetration ratio is normally less than 10. The first cut's penetration is 6 mm, the second cut's penetration is 9 mm. By adding a safety factor, the first cut's spacing was adopted as 85 mm, while the second cut's spacing was adopted as 125 mm; the spacing between the two cuts was 160 mm, as shown in Figure 6-11.

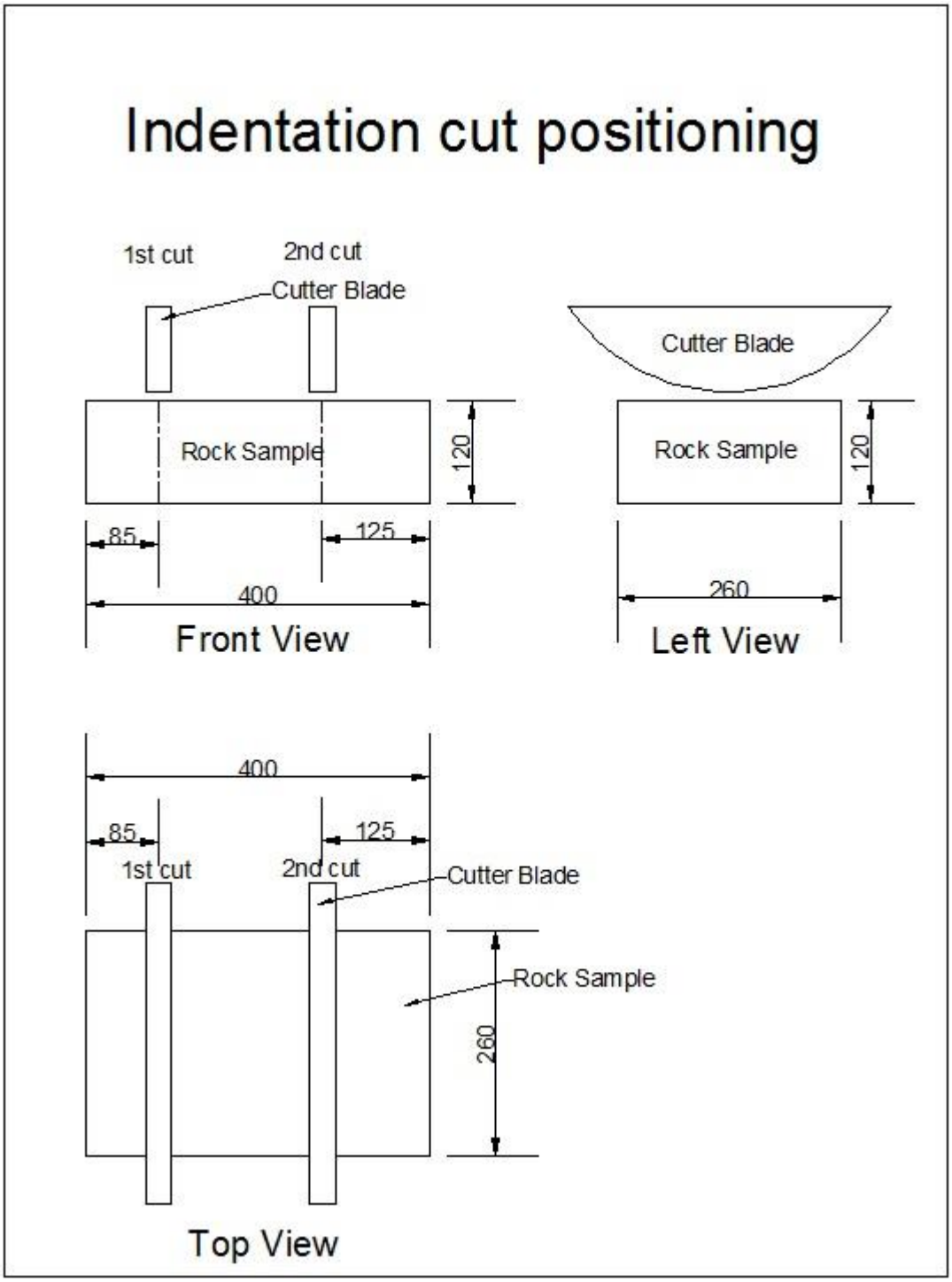

Figure 6-11 Positioning of the indentation cuts.

As aforementioned, the influence of confinement pressure on disc cutting was a focus of this study. Confinement pressure was applied with flat jacks and hydraulic

hand pumps, as shown in Figure 6-10. Four confinement pressure values were adopted, which were 0, 3, 6, and 9 MPa. Eight sandstone specimens were tested, with four confinement pressure values and two disc cutter shapes. In the indentation tests, the indenter penetration and load forces were measured using the built-in sensor of the AVERY compression machine. After placing the indentation cuts, the rock specimens were diamond sawn into four pieces to study the subsurface crushed zone and crack development under the disc cutter, as shown in Figure 6-12.

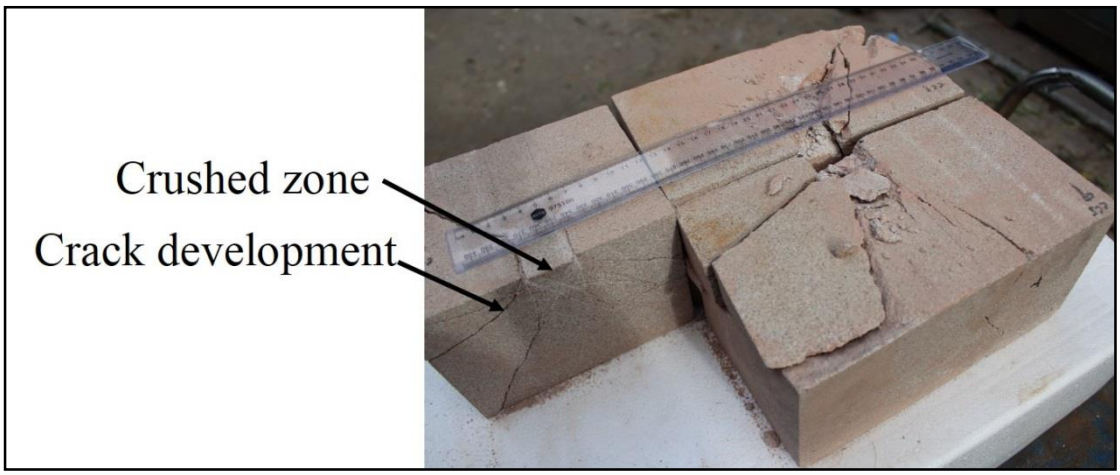

Figure 6-12 Crushed zone and cracks development observation.

6.3 Test results and analysis

Eight rock specimens were tested, with four specimens using a CCS disc cutter and four specimens using a V shape disc cutter, as shown in Figure 6-13 and Figure 6-14. As aforementioned, the variable parameters of the study are disc cutter patterns and confinement pressures. The major concerns are their influence on cutting forces, cracks development and crushed zone formation. These issues were compiled and analysed separately as shown below.

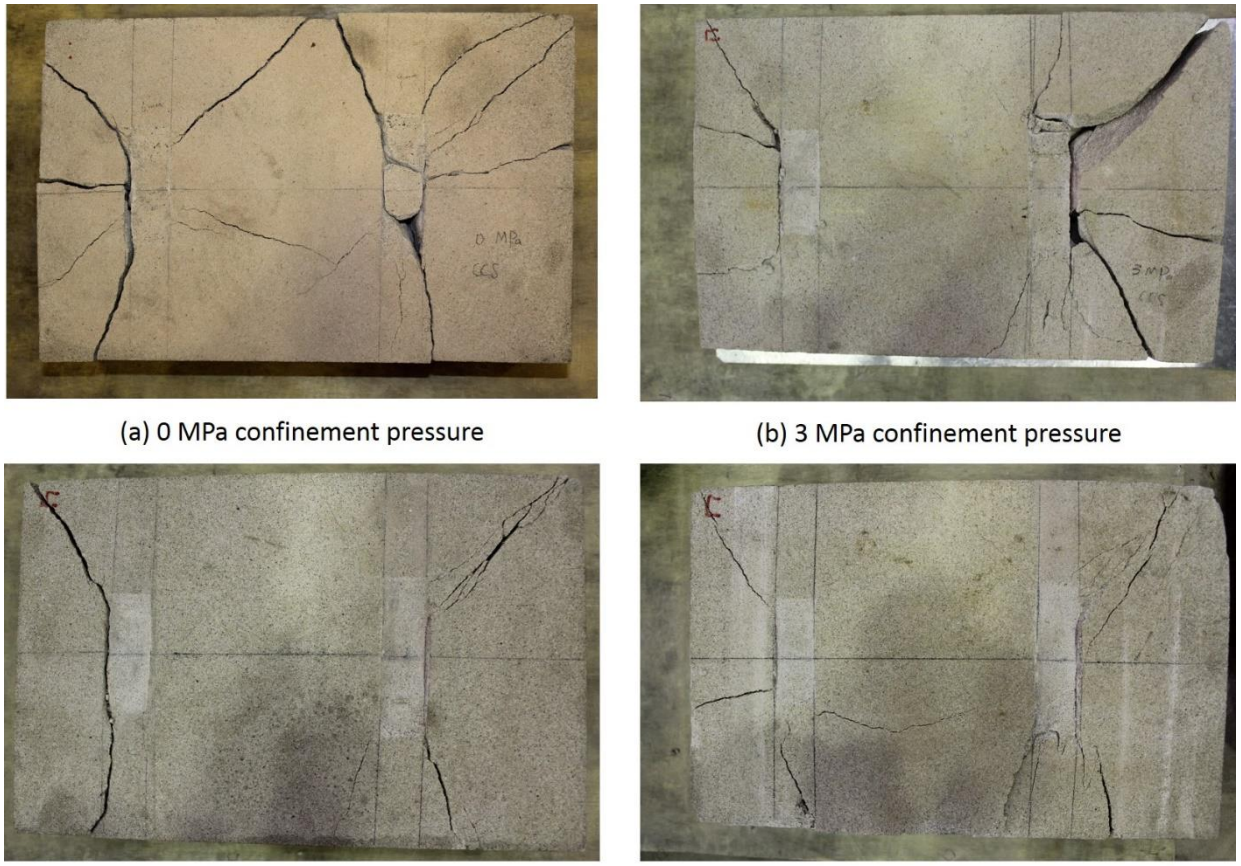

(a) 0 MPa confinement pressure

(b) 3 MPa confinement pressure

(c) 6 MPa confinement pressure

(d) 9 MPa confinement pressure

Figure 6-13 CCS disc cutter indentation specimens.

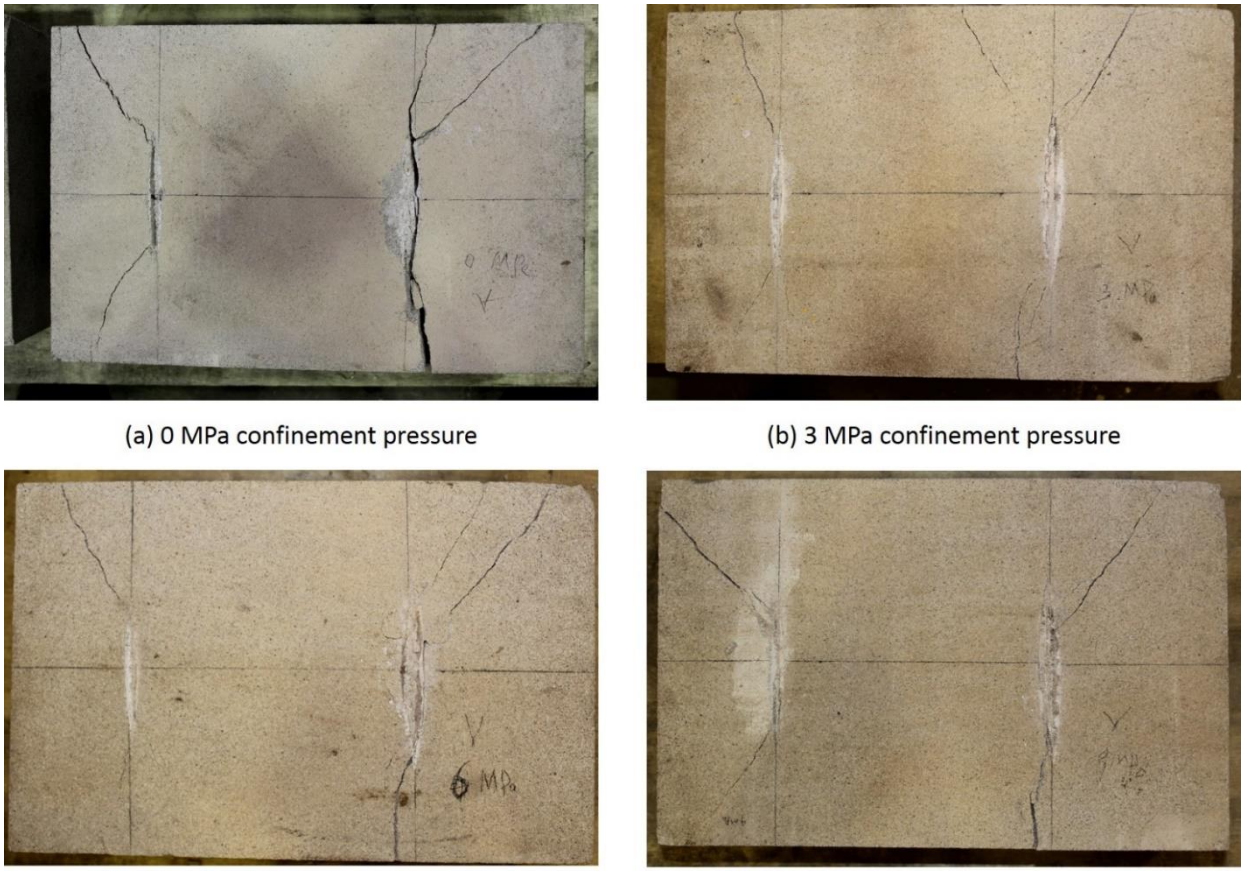

Figure 6-14 V shape disc cutter indentation specimens.

6.3.1 Confinement pressure's influence on cutting forces

A good understanding of cutting forces is the base for both TBM performance prediction and design and optimization of cutter head layout. Several cutting parameters have been studied and incorporated into cutting force prediction models, including spacing, penetration, disc diameter, disc tip width and rock properties. However, the influence of the confining pressure is rare and it was not incorporated into cutting force prediction models.

The CCS disc cutter and the V shape disc cutter had distinctive penetration-force characteristics. The influence of confining pressure on cutting forces was separately studied with different disc cutters. For the CCS disc cutter, four different confining pressure values were studied in the laboratory tests, which were 0 MPa, 3 MPa, 6 MPa and 9 MPa. The penetration-force characteristics with penetration up to 6 mm under these confinement pressures are shown in Figure 6-15.

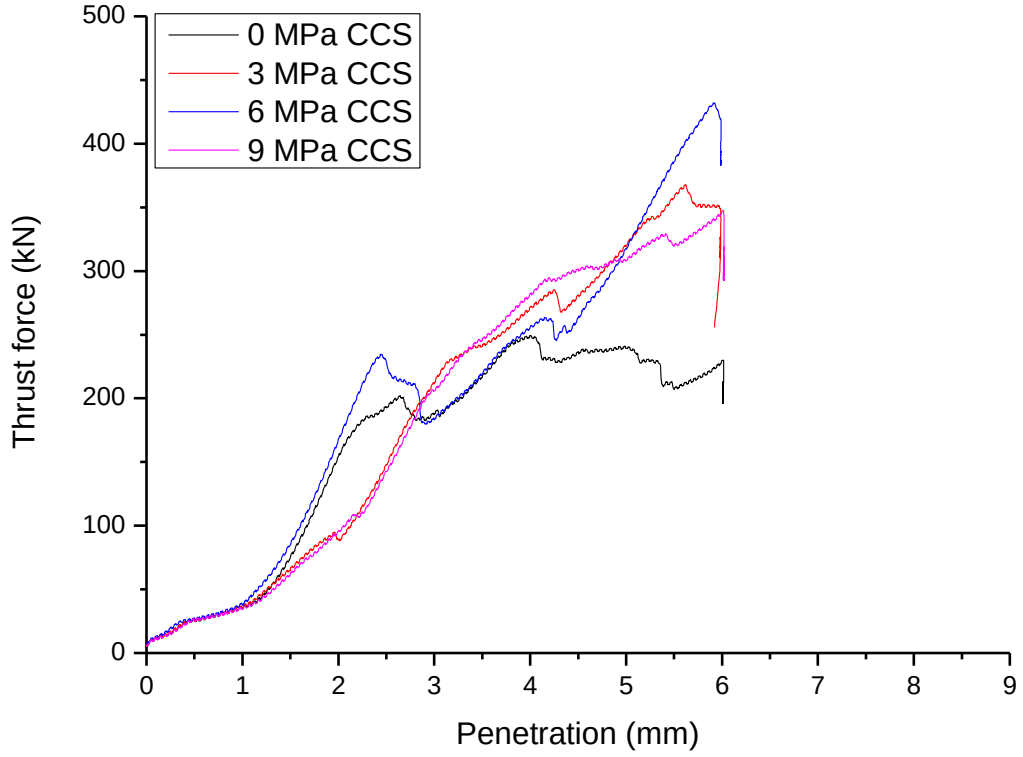

Figure 6-15 CCS disc cutter cutting force curves with penetration up to 6 mm.

Figure 6-15 shows the CCS disc cutter cutting force evolution patterns under confining pressures of 0, 3, 6, and 9 MPa with penetration up to 6 mm. The cutting force disparities among different confining pressures were of a marginal extent and irregular with penetration up to 4.5 mm. The disparities increased and became notable when penetration approached 6 mm.

TBM thrust capacity is simply a multiplication of single cutter normal force by the number of cutters. So, getting the maximum load for a single cutter is the basis for determining the thrust capacity for the TBM propelling system design. From this point of view, the influence of confinement pressures on maximum load is of great interest, and was analysed and presented as shown in Figure 6-16.

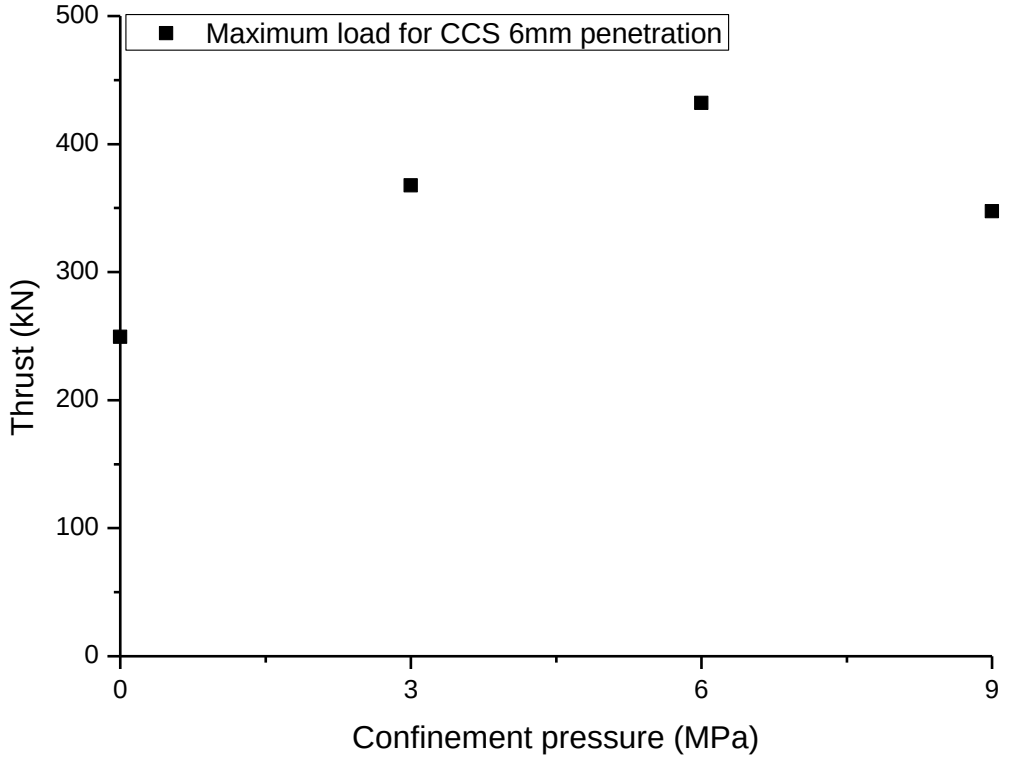

Figure 6-16 Maximum load for CCS disc cutter with 6mm penetration.

Figure 6-16 shows the maximum load values for the CCS disc cutter with a penetration of 6mm. The maximum load reached 249.4, 367.7, 432.2, and 347.6 kN under confinement pressures of 0, 3, 6, and 9 MPa respectively. Positive correlation existed between confining pressure and maximum load with confinement less than 6 MPa. While maximum load began to decrease from some point between 6 and 9 MPa confinement.

For the CCS disc cutter indentation tests with penetration up to 9 mm, the penetration-force characteristics under these confinement pressures are shown in Figure 6-17. It indicates that the cutting force disparities among different confining pressures were irregular but generally increased with increasing confinement

pressure up to penetration of 3 mm. The disparities were higher than that of 6 mm ultimate penetration.

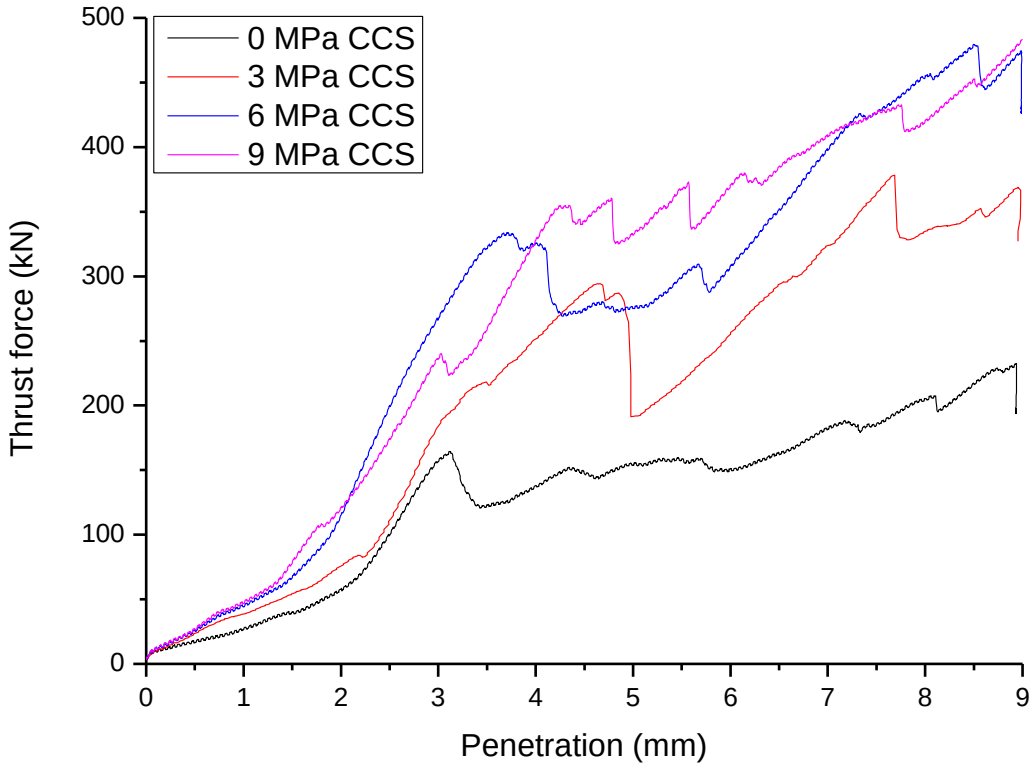

Figure 6-17 CCS disc cutter cutting force curves with penetration up to 9 mm.

Figure 6-18 shows the maximum load values for the CCS disc cutter with the ultimate penetration of 9 mm. It shows that the load reached 232.6, 378.2, 479.6, and 483.7 kN under confinement pressures of 0, 3, 6, and 9 MPa respectively. Positive correlation existed between confining pressure and maximum load with confinement lower than 6 MPa. While the maximum load began to flatten from some point between 6 and 9 MPa confinement.

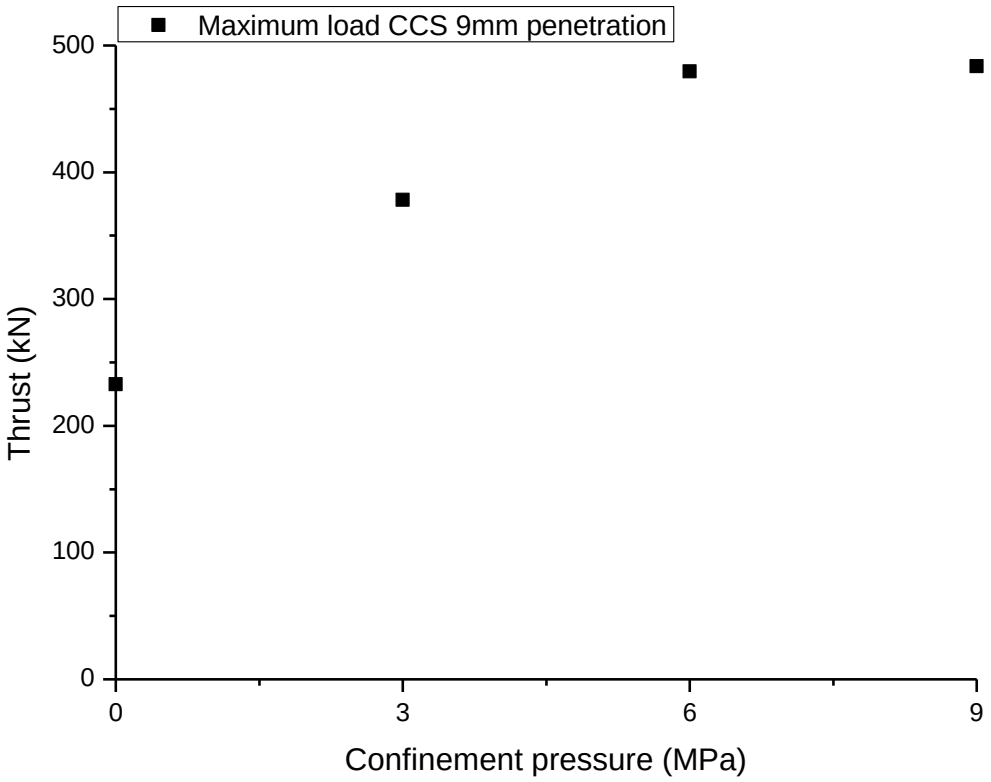

Figure 6-18 Maximum load for CCS disc cutter with 9mm penetration.

Four different confining pressure values were studied in the V shape disc cutter indentation tests, which were 0 MPa, 3 MPa, 6 MPa and 9 MPa. For indentation tests with penetration up to 6 mm, the penetration-force characteristics under these confining pressures are shown in Figure 6-19.

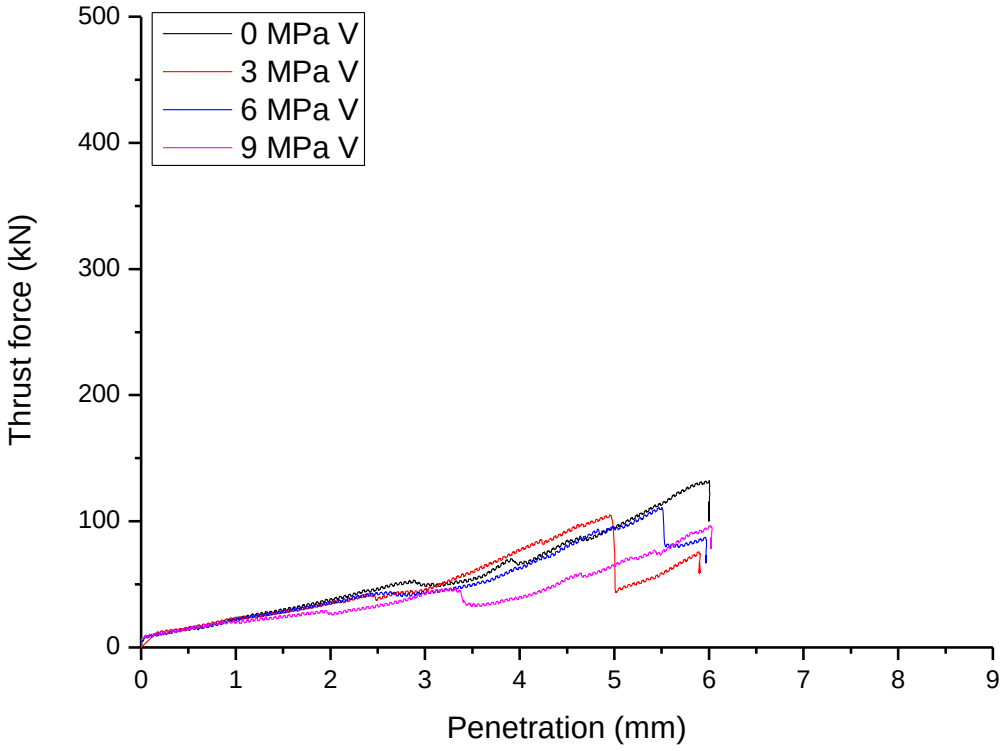

Figure 6-19 V shape disc cutter cutting force curves with penetration up to 6 mm.

Figure 6-19 shows the V shape disc cutter cutting force curves under confining pressure of 0, 3, 6, and 9 MPa with penetration up to 6 mm. The cutting force disparities among different confining pressures were of marginal extent and irregular with penetration up to 3.3 mm. Notable drops appeared for 9 MPa, 3 MPa and 6MPa at 3.3, 5 and 4.4 mm afterwards respectively, which causes very irregular disparity patterns.

The maximum load values for V shape disc cutters with the ultimate penetration of 6 mm are shown in Figure 6-20. It shows that the load reached 132.3, 105.1, 110.9, and 96.6 kN under confining pressures of 0, 3, 6, and 9 MPa respectively. No correlation was found between confining pressure and maximum load.

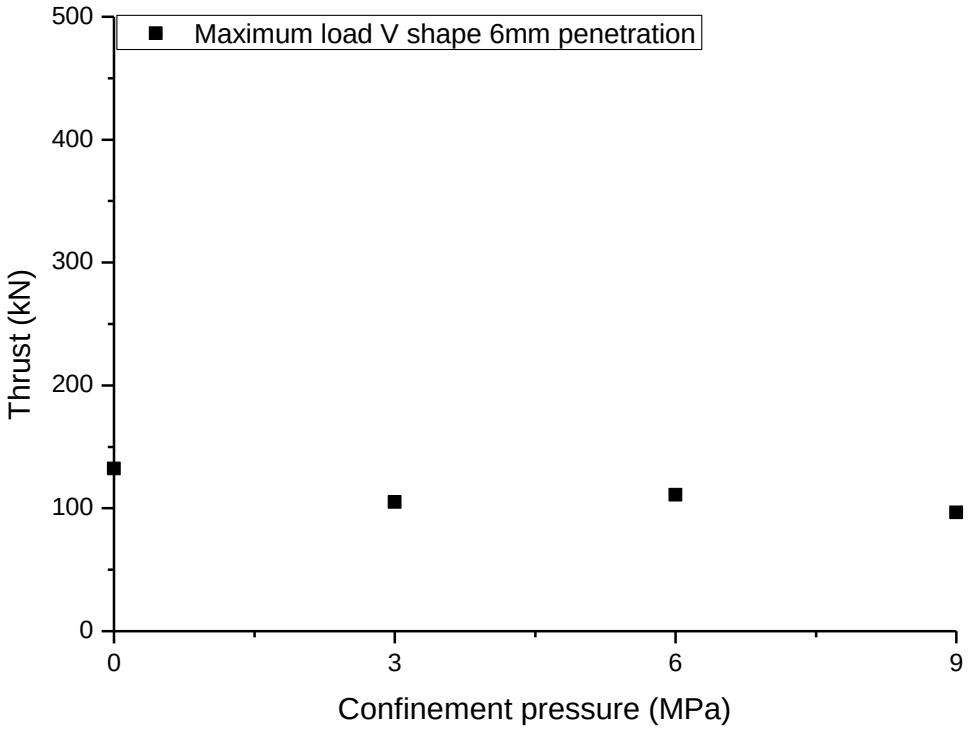

Figure 6-20 Maximum load for V shape disc cutter with 6mm penetration.

Figure 6-21 shows the V shape disc cutter cutting force curves under confining pressures of 0, 3, 6, and 9 MPa with penetration up to 9 mm. The cutting force disparities among different confining pressures were irregular but generally increased with increasing confinement pressure, which is different from that of 6 mm ultimate penetration. The most notable change was the drop at 6.5 penetration for 0 MPa confinement.

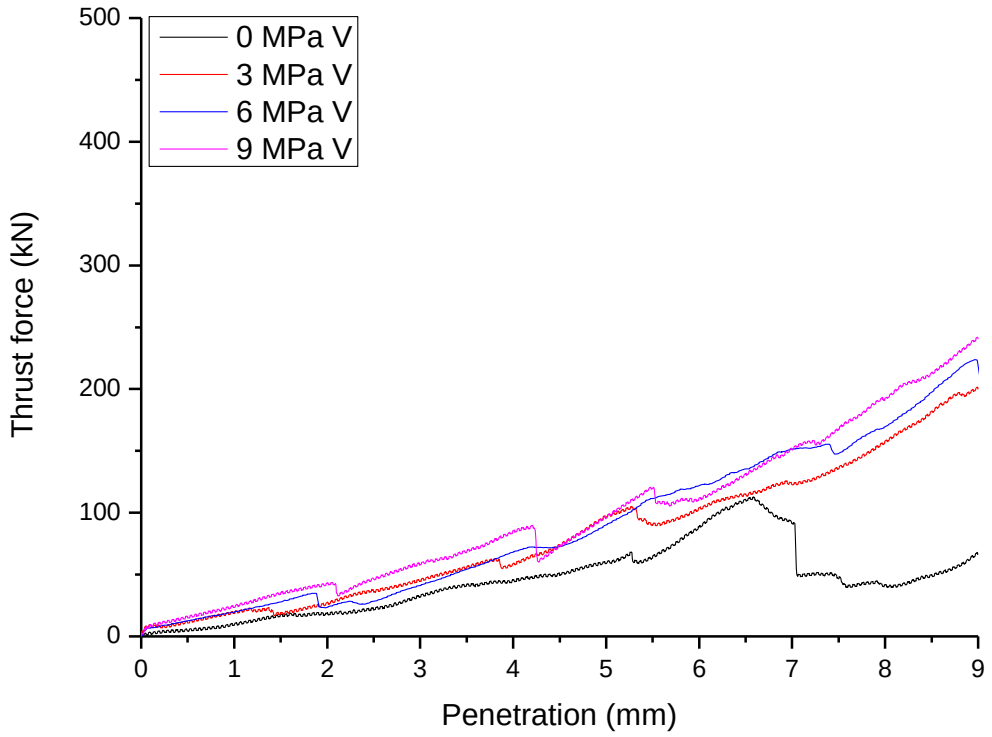

Figure 6-21 V shape disc cutter cutting force curves with penetration up to 9 mm.

The maximum load values for the V shape disc cutter with the penetration of 9mm are shown in Figure 6-22. It shows that the load reached 112.7, 201.6, 223.7, and 241.9 kN under confining pressures of 0, 3, 6, and 9 MPa respectively. Positive correlation existed between confinement pressure and thrust load with confinement up to 9 MPa.

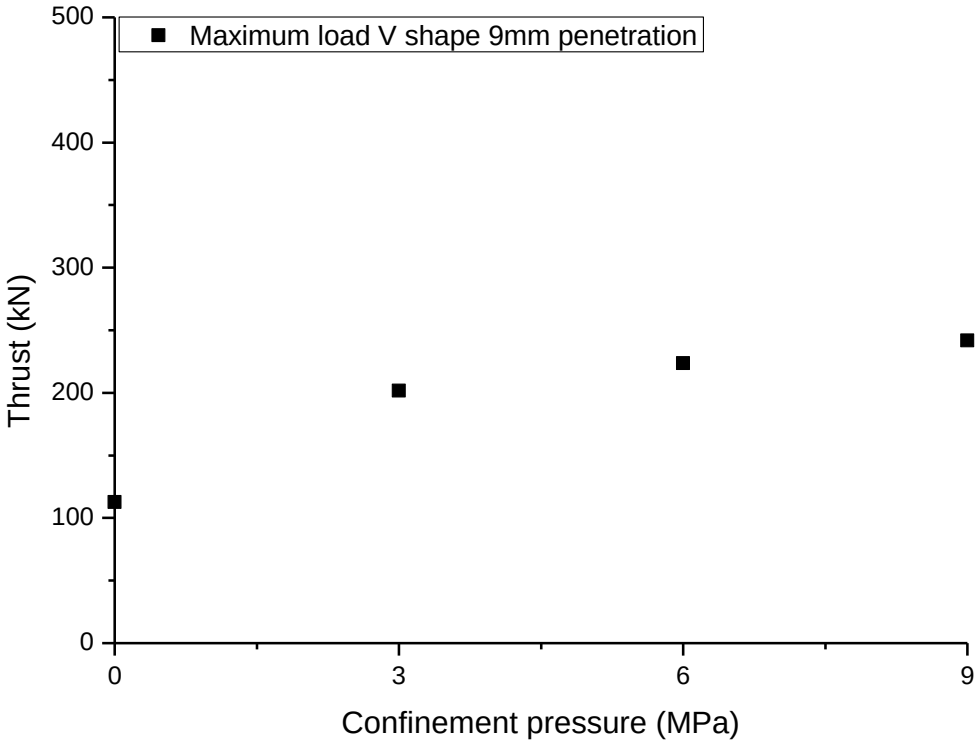

Figure 6-22 Maximum load for V shape disc cutter with 9mm penetration.

In conclusion, the confining pressure's influence on V shape disc cutters' cutting forces is more irregular, unpredictable and marginal than those of CCS's.

6.3.2 Disc cutter patterns' influence on cutting forces

Figure 6-23 shows cutting force curves with different cutters but both under 0 MPa confining pressure. It indicates that CCS disc cutter thrust forces were significantly higher than that of V shape disc cutter. The maximum loads were 112.7 and 232.6 kN for the V shape disc cutter and the CCS disc cutter, respectively. The maximum load value for the CCS disc cutter was 206.4% of that of the V shape disc cutter.

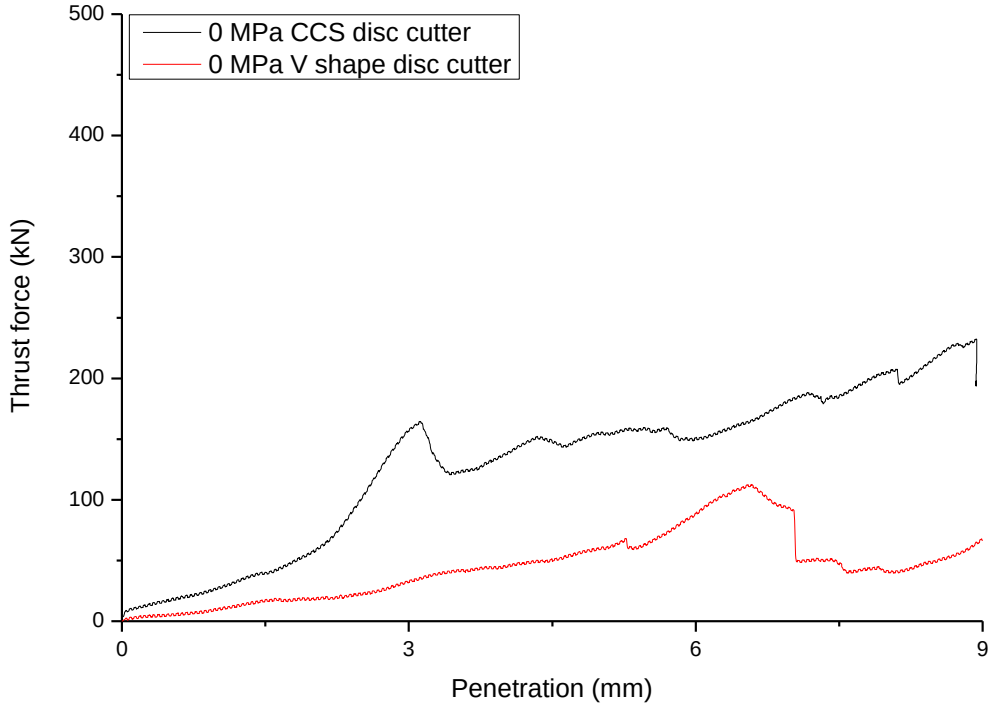

Figure 6-23 Comparison of thrust forces between CCS and V shape disc cutters under 0 MPa confinement pressure.

Figure 6-24 shows cutting force curves with different cutters but both under 3 MPa confining pressure. It indicates that the CCS disc cutter thrust forces were significantly higher than that of the V shape disc cutter. The maximum loads were 201.6 and 378.2 kN for the V shape disc cutter and the CCS disc cutter, respectively. The maximum load value for the CCS disc cutter was 187.6% of that of the V shape disc cutter.

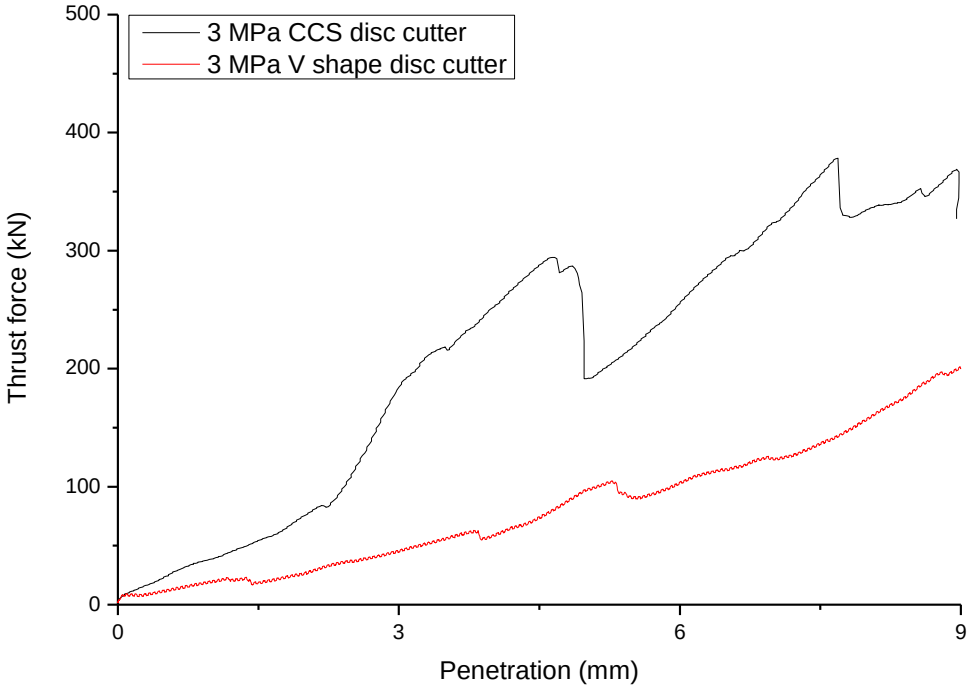

Figure 6-24 Comparison of thrust forces between CCS and V shape disc cutters under 3 MPa confinement pressure.

Figure 6-25 shows cutting force curves with different cutters but both under 6 MPa confining pressure. It indicates that the CCS disc cutter thrust forces were significantly higher than that of the V shape disc cutter. The maximum loads were 223.7 and 479.6 kN for the V shape disc cutter and the CCS disc cutter, respectively. The maximum load for the CCS disc cutter was 214.4% of that of the V shape disc cutter.

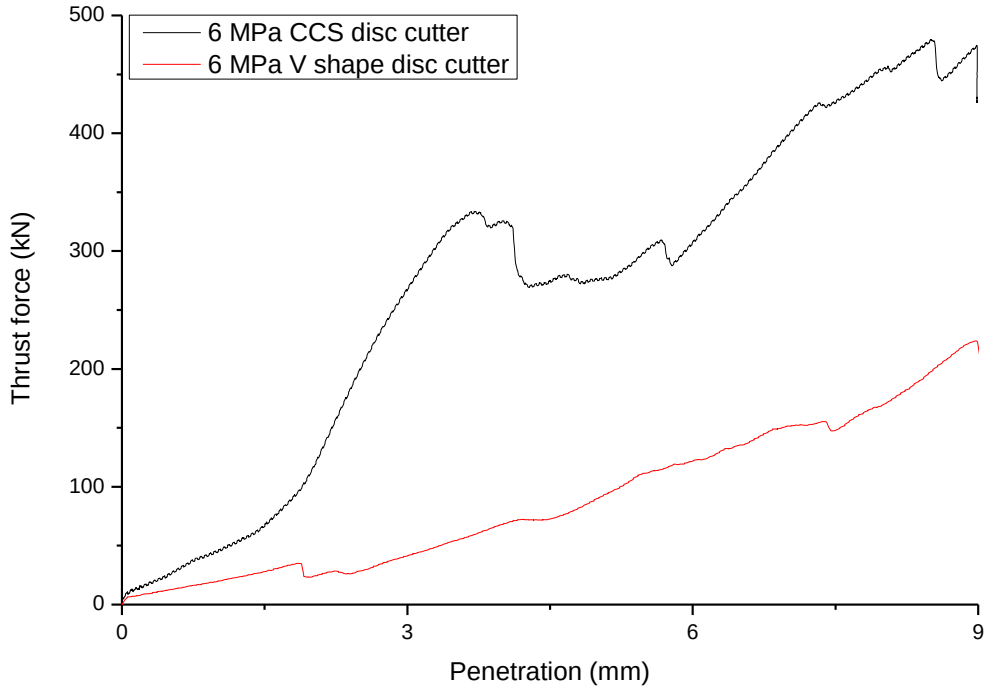

Figure 6-25 Comparison of thrust forces between CCS and V shape disc cutters under 6 MPa confinement pressure.

Figure 6-26 shows cutting force curves with different cutters but both under 9 MPa confining pressure. It indicates that the CCS disc cutter thrust forces were significantly higher than that of the V shape disc cutter. The maximum loads were 241.9 and 483.7 kN for the V shape disc cutter and the CCS disc cutter, respectively. The maximum load for the CCS disc cutter was 200.0% of that of the V shape disc cutter.

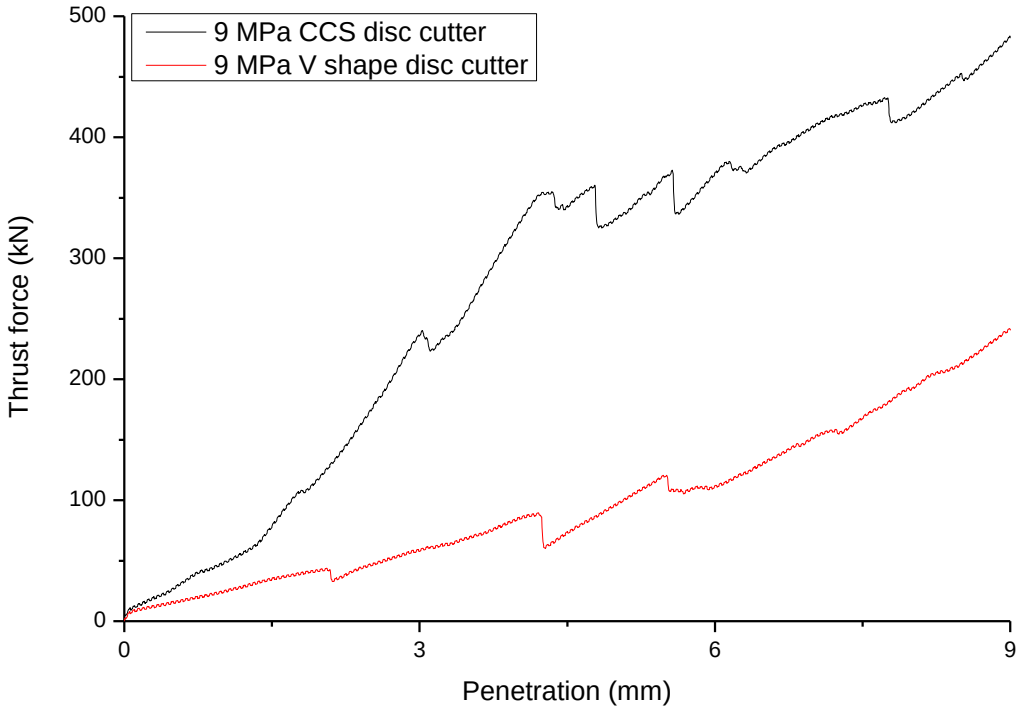

Figure 6-26 Comparison of thrust forces between CCS and V shape disc cutters under 9 MPa confinement pressure

Conclusively, Figures 6-23 to 6-26 show that thrust load for the CCS disc cutter was nearly two times of that of the V shape disc cutter under the given experimental set up.

6.3.3 Confinement pressure's influence on crack system development

After indentation tests, the sandstone blocks were diamond sawn to examine the subsurface crack development under different disc cutter patterns and confinement pressures, as shown in Figure 6-27 and Figure 6-28.

0 MPa - 9mm	3 MPa - 9mm
	
0 MPa - 6mm	**3 MPa - 6mm**
	

Figure 6-27 Subsurface crack development under CCS disc cutter.

Figure 6-27 shows that both confinement pressure and penetration depth influence crack development under the CCS disc cutter. Firstly, from the perspective of penetration, when it was 6 mm, most cracks initiated from the contact corner of the disc cutter, in both the radial and lateral directions. More specifically, for confinement pressures of 0, 3 and 6 MPa, all the cracks initiated from the contact corners; while one radial crack initiated beneath away from that under 9 MPa confinement. When the penetration increased to 9 mm deep, aside from the propagation of readily existed cracks, the most highlighted feature was the initiation and propagation of vertical cracks, which can be observed for all the four confinement scenarios. So, rock fragmentation initiated with radial and lateral cracks at the tool-rock contact corner; vertical cracks initiated with penetration surpassing 6 mm.

Secondly, confinement pressures influence the crack number and orientation. By comparing the crack systems under the same penetration with different confinement pressures, it clearly shows that radial and lateral crack numbers increased with mounting confinement; although the vertical crack numbers did not change. In addition, radial crack orientation turned more laterally with confining pressure increasing.

In summary, with penetrating of disc cutters, radial and lateral cracks initiated from the rock-cutter contact corner ahead of vertical cracks. Vertical cracks did not appear until the penetration reached a value between 6 mm and 9 mm. Confining pressure can boost crack development by increasing the crack number. It also influenced the crack orientation by turning them laterally, except for vertical cracks.

Figure 6-28 shows the crack development with different confinement pressures and penetration depth under the V shape disc cutter. The rock-tool contact under the V shape disc cutter was a line aligned with the cutter tip, which is not like the face contact under the CCS disc cutter. Figure 6-28 shows that all cracks initiated from the cutter tip contact. Confinement pressure variation did not show a considerable influence on crack development

from the perspectives of crack number and orientation. In addition, incrementing of penetration increased the crack numbers in some scenarios.

0 MPa - 9mm	3 MPa - 9mm
	
0 MPa - 6mm	**3 MPa - 6mm**
	

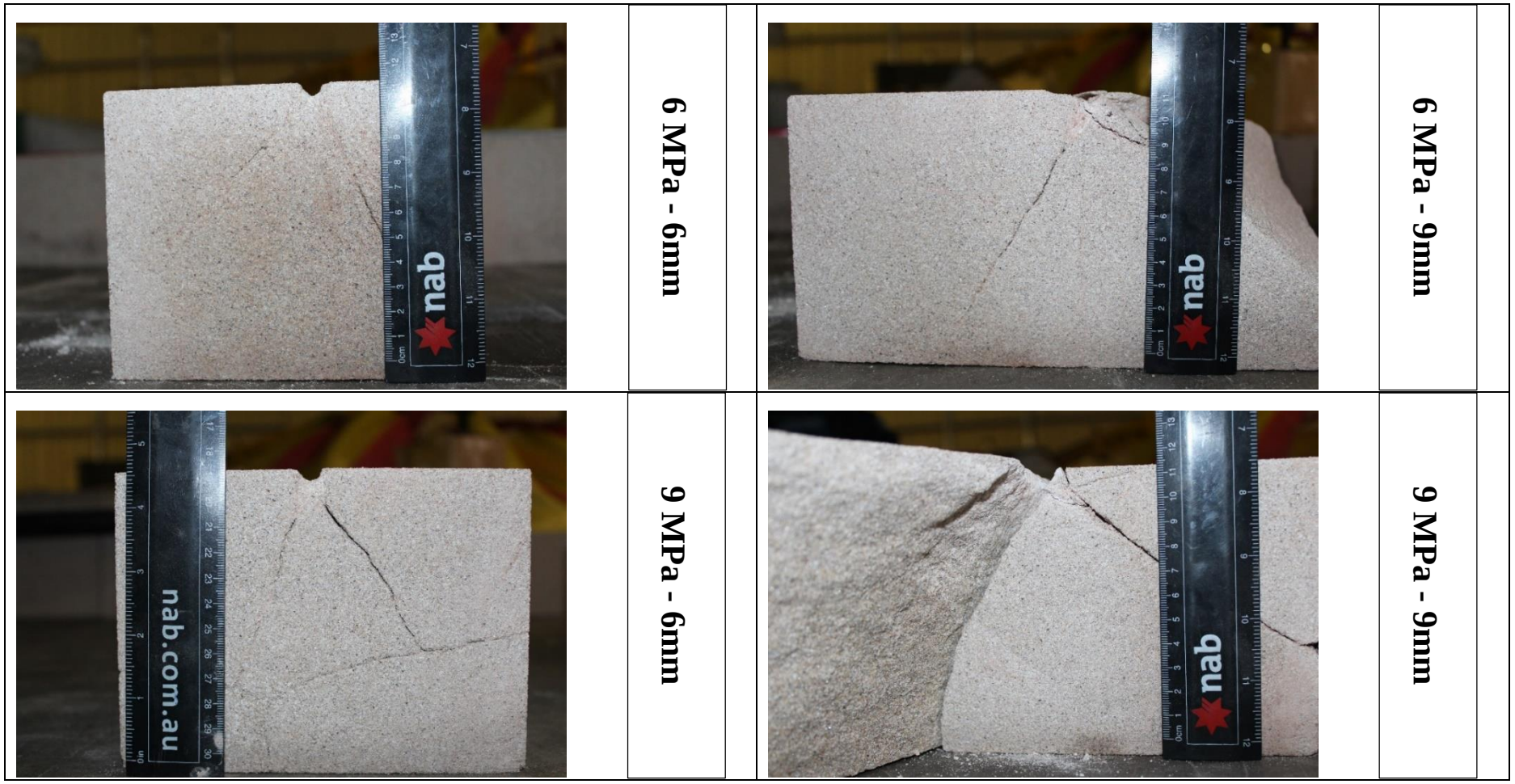

Figure 6-28 Subsurface crack development under V shape disc cutter.

By comparing the crack development under different disc cutters, the V shape disc cutter indentation had smaller crack numbers and its cracks were more vertical. In addition, the V shape disc cutter indentation was less sensitive to confinement pressure than the CCS one, which was reflected in both crack numbers and crack orientation. With incrementing of confinement pressure, the CCS cutter indentation induced more cracks and turned cracks laterally. While both of them did not change greatly under the V shape disc cutter indentation.

In summary, indentation under different disc cutters induced distinctive crack patterns with the same penetration and confinement pressure, as shown in Figure 6-27 and Figure 6-28. The CCS disc cutter indentation had denser cracks and the crack orientation was more lateral, which is favourable for rock cutting. The V shape disc cutter indentation was less sensitive to confining pressure, with no notable increase of crack number and crack re-orientation.

6.3.4 Confinement pressure's influence on crushed zones

The crushed zone consists of fine grained crushed rock, which is developed due to high stress concentration in the area immediately under the cutter. It provides the means of transferring stresses into the rock medium. It is often assumed to be circular for the purpose of simplicity, as shown in Figure 4-1.

The development of the crushed zone is of significance for disc cutting. The size of the crushed zone is related to disc cutting efficiency and dust generation. Reducing its size would decrease the amount of generated dust and increase the cutting efficiency, i.e. reduce the specific cutting energy of cutting, as fine particles consume

more cutting energy (Rostami and Ozdemir, 1993). So, it is of significant interest to study the crushed zone development under different cutting scenarios.

To study crushed zones, high resolution close-up photos were taken, as shown in Figure 6-29. A transparent ruler with millimetre units was placed close to the crushed zones to help appreciate the size of the crushed zones.

0 MPa - 9mm	3 MPa - 9mm
	
0 MPa - 6mm	**3 MPa - 6mm**
	

Figure 6-29 Subsurface crushed zone development under CCS disc cutter.

Figure 6-29 shows the crushed zones with different confinement pressures and penetration depth under the CCS disc cutter. It presents highlighted crushed zone features from the perspectives of shape and dimension.

Crushed zones were all in wedge shapes. All of them had the top width of 30 mm, which is the same as the thickness of disc cutter. However, the height of crushed zones varied with changes of penetration depth and confinement pressure. Deepening of penetration increased the height of crushed zones, while increasing confining pressure decreased it.

More specifically, under 6 mm penetration, the crushed zone height was 30, 25, 25, and 23 mm for confinement pressures of 0, 3, 6, and 9 MPa, respectively. Under 9 mm penetration, the crushed zone height was 42, 37, 40, and 33 mm for confinement pressures of 0, 3, 6, and 9 MPa, respectively, as shown in Figure 6-30. It indicates that the propagation of crushed zone was energized by penetration deepening and constrained by confinement increasing.

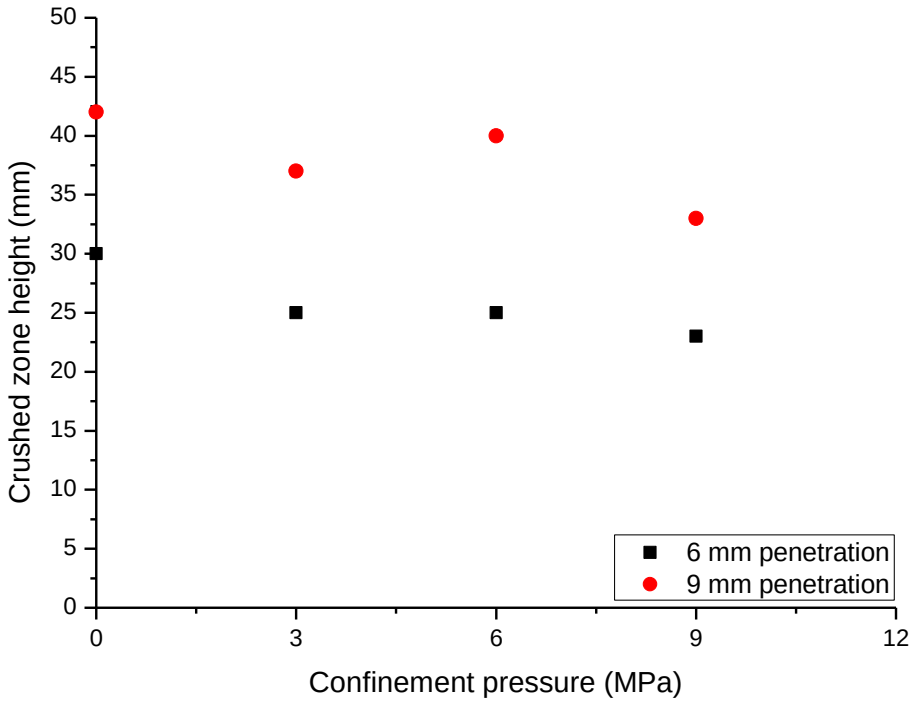

Figure 6-30 Crushed zone height values under different confining pressure and penetration.

Another highlighted feature is that the crushed zone boundaries were enclosed by shear failure cracks, as shown in Figure 6-29. In addition, the crushed zone initiated from shear cracks. The crushed zones under 6 mm penetration were slim belts along the shear cracks but propagated both upwards and downwards with penetration increasing, and covered the whole wedge area when the penetration reached 9 mm.

Figure 6-31 shows the photos focused on the crushed zones under the V shape disc cutter with different confining pressure and penetration. The crushed zones under the V shape disc cutter were of much less significance in size comparing to those under the CCS disc cutter. Their shapes are irregular. However, the enlargement of crushed zones with increasing of penetration and confinement pressure was appreciable.

0 MPa - 9mm	3 MPa - 9mm
	
0 MPa - 6mm	**3 MPa - 6mm**
	

Figure 6-31 Subsurface crushed zone development under V shape disc cutter.

In summary, the study on crushed zones revealed that they were in wedge shapes under the CCS disc cutter, which overturned the circular shape simplification in some theoretical studies. They had the same width with cutter thickness. However the wedge height changed with varying confinement pressure and penetration. Deepening of penetration increased the height of the crushed zones, while increasing confining pressure decreased it. In addition, the crushed zone boundaries were enclosed by shear failure cracks, and they initiated from shear cracks. For the V shape disc cutter, the crushed zones were of little significance from both shape and size perspectives. However, their enlargement with increasing of penetration and confining pressure was appreciable.

6.3.5 The findings on disc cutting mechanisms

Figure 6-32 shows the photos of failure faces of lateral cracks, wedge cracks, and radial cracks. The presence of scrubbing surface shows that the wedge crack was induced by shear failure; while the rough fresh surfaces indicated that lateral and radial crack were induced by tensile failure.

Combining with the crack development patterns, it is reasonable to deduce the crack development procedure. Shear stress induced wedge cracks initiated at the corners of rock-cutter contact area. Tensile stress induced lateral cracks might initiate at the corners as well; they were influenced by confining pressure, and did not initiate under low confining pressure. Tensile stress induced radial crack initiated from both rock-cutter contact corners and wedge crack ends, the higher the confinement pressure, the more radial cracks appeared. Finally, vertical cracks initiated and propagated from the bottom tip point of wedge shaped crushed zone.

Figure 6-32 Fracture face of lateral crack, wedge crack, and radial crack under CCS cutter.

6.4 Discussions

6.4.1 Significance on refinement of cutting force prediction models

The highlighted feature for the CCS disc cutter cutting force evolution was the flattening and decreasing from some point between 6 and 9 MPa confinement, which is different from the findings of previous similar experiments conducted by Innaurato et.al. (2007), as shown in Figure 6-33.

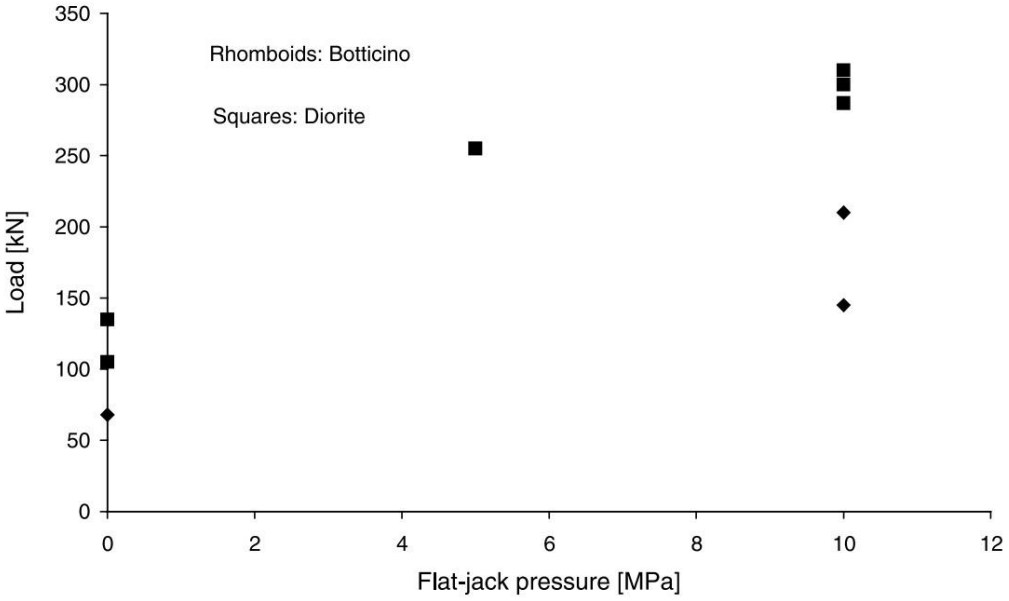

Figure 6-33 Maximum indentation load vs. flat-jack confinement pressure for Botticino (rhomboids) and Diorite (squares) under the given settings (Innaurato et al., 2007)

Figure 6-33 shows that the maximum load values increase with confinement mounting for up to 10 MPa, i.e. the flattening and decreasing of maximum load did not present. By comparing the experimental set up, there were two differences between Innaurato et al.'s test and this test. One is that only one directional confinement was applied in Innaurato's test, as shown in Figure 4-10, while two directional confinement was applied in this one. The other difference is the rock properties of the tested rock samples. The tested sandstone's cohesion was between 6.7 and 8.1 MPa. While those in Innaurato et al.'s tests were 16 and 23 MPa, as shown in Table 6-1. By relating cohesion values to the maximum indentation loads, it is reasonable to deduce that the cohesion value is the turning key point for the

flattening and decreasing of load from some point between 6 and 9 MPa confinement.

Table 6-1 Physical and mechanical properties of the two rock types adopted in Innaurato et al.'s laboratory tests.

	Botticino	Diorite
Specific weight ($\mathbf{kN/m^3}$)	26.5	27.8
Young's modulus (MPa)	67000	30000
Poisson's ratio	0.3	0.2
Uniaxial compressive strength (MPa)	142	234
Cohesion (MPa)	16	23
Internal friction angle (°)	57	61
Brazilian tensile strength (MPa)	7.2	9.3

The decreasing and flattening load pattern was also substantiated by field database collected and compiled by Klein et al., as shown in Figure 6-34 (Klein et al., 1995). Field TBM performance regarding cutting force is assessed with a normalized parameter of Field Penetration Index (FPI), which is defined as the cutter loading divided by the penetration rate (Nelson, et al., 1983). Figure 6-34 shows the correlation between FPI and the ratio of overburden pressure to UCS of rock mass. This finding indicates that, with fixed rock, higher confining pressure would cause lower thrust for given disc penetration. It supports the load trend between 6 MPa and 9 MPa confining pressure for the tested sandstone.

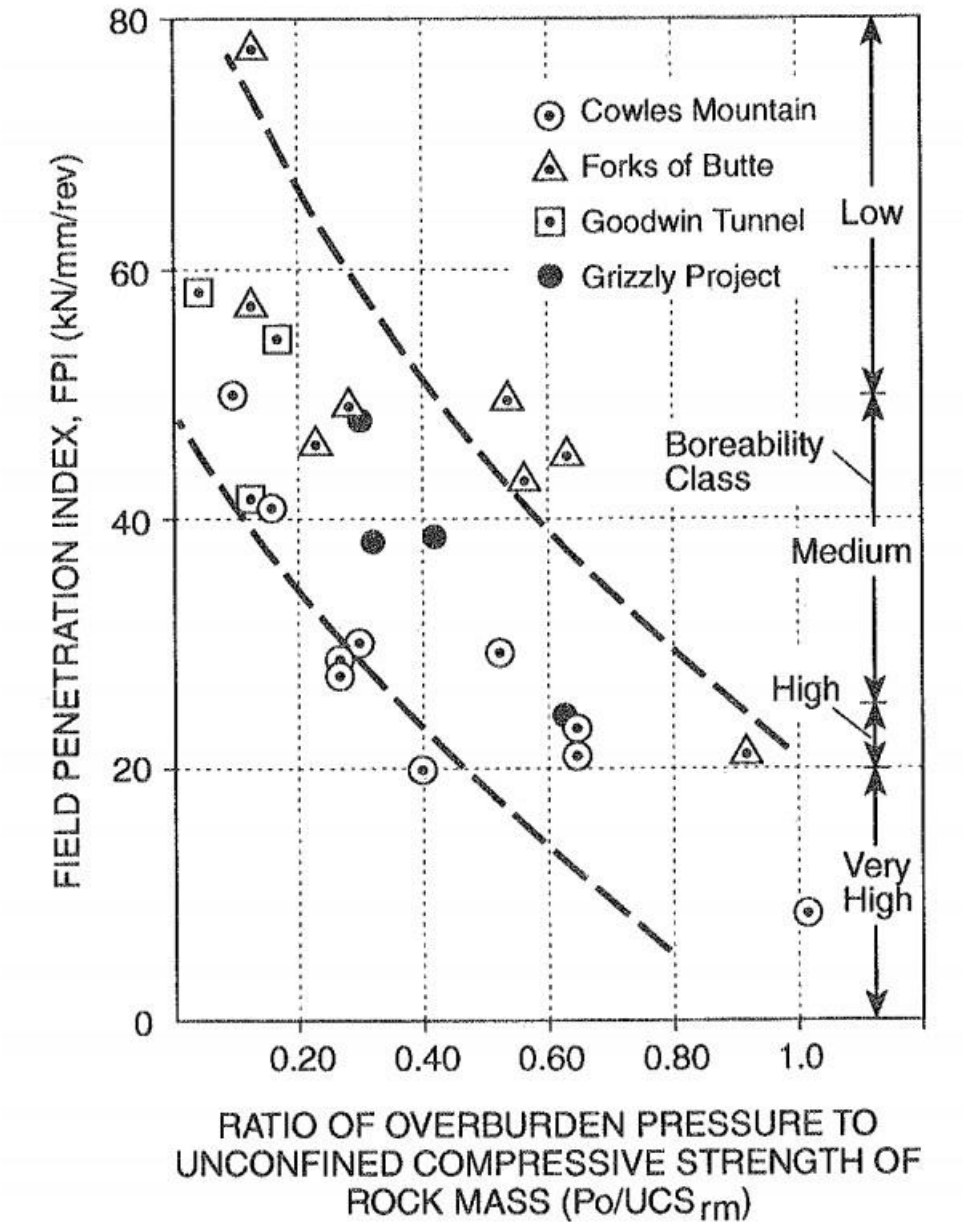

Figure 6-34 Field Penetration Index correlation with the ratio of overburden pressure divided by UCS of rock mass (Klein et al., 1995).

The flattening and decreasing thrust pattern was not found in Innaurato et al.'s tests, because the cohesion of the tested rocks was much higher than the maximum confining pressure. Cohesion value is normally 0.1~0.2 times the rock UCS value. Klein et al.'s data shows that FPI decreased from overburden pressure values of 0.1~0.2 times the UCS value. So, Klein et al.'s finding supports the assumption that cohesion value is the turning key point for the flattening and decreasing of load.

Cutting forces are the basis of TBM performance prediction and cutter head design. The new findings regarding the cutting forces will provide guidelines for TBM performance prediction in tunnels with high overburdens, and the cutter head design of new TBMs for the designated tunnels.

The experimental study in this chapter confirms the significant influences of confining stresses on disc cutter cutting forces and cutting mechanisms. While there has been no cutting forces prediction model that takes the confining stress factor into consideration. It is of interest to the industry to establish cutting forces prediction models incorporating the confining stress factor.

Incorporating the confining stress factor is a significant advance for the evolution of cutting force prediction models, which will need considerable efforts. Take the widely accepted CSM model for example, it was based on at least three major efforts. The first one is the laboratory work conducted by Miller, as described in his PhD thesis in 1974. The second one is the combination of laboratory and field work by Ozdemir, as described in his Master thesis in 1975. The third one is the joint laboratory and theoretical work contributed by Ozdemir, Miller and Wang, as described in a research project report supported by the US National Science Foundation in 1977 (Ozdemir et al., 1977).

This study made a contribution to the development of a practical cutting force prediction model with the consideration of confining stress factor. However, more research efforts, including laboratory experiments, field investigation, theoretical analysing, and industrial support, are needed to build such a model, which is beyond the scope of this study.

6.4.2 Significance on cutter-head layout design and disc cutter selection

Advance rate and construction cost are the two dominating criteria for TBM applicability. Proper selection and optimum layout of disc cutters for TBM cutter heads significantly influences TBM advance rates and excavation costs.

From the perspective of TBM advance rate, it is often deteriorated by machine downtime. Disc cutter replacement caused delays take up a substantial proportion of downtime. In the cases of catastrophic cutter failures, the project can be stopped completely for a long period (Roby et al., 2008).

From the perspective of excavation cost, according to field experience, disc cutters consumption is very considerable and it accounts for nearly 1/5 to 1/4 of the total project cost in normal conditions; in adverse conditions, the proportion can reach 1/3 (Zhang, 2008, Frenzel et al., 2008, Wang et al., 2012).

Disc cutters consist of several mechanical parts. Every part has its own load limits, especially for the roller bearing. The whole disc cutter has its loading limit as well. For selection and layout of disc cutters, the manufacturers provided the rated load values. The higher the cutting force, the more risk to cause disc cutter failures. So, higher thrust loads would incur more disc cutter consumptions. This has been verified by reported field data. Innaurato and Oreste (2000) collected and analysed disc cutter consumption data with respect to cutter head total thrust, as shown in Figure 6-35. It shows clearly that a higher thrust corresponds a larger tool consumption (Innaurato and Oreste, 2000, Innaurato et al., 2007).

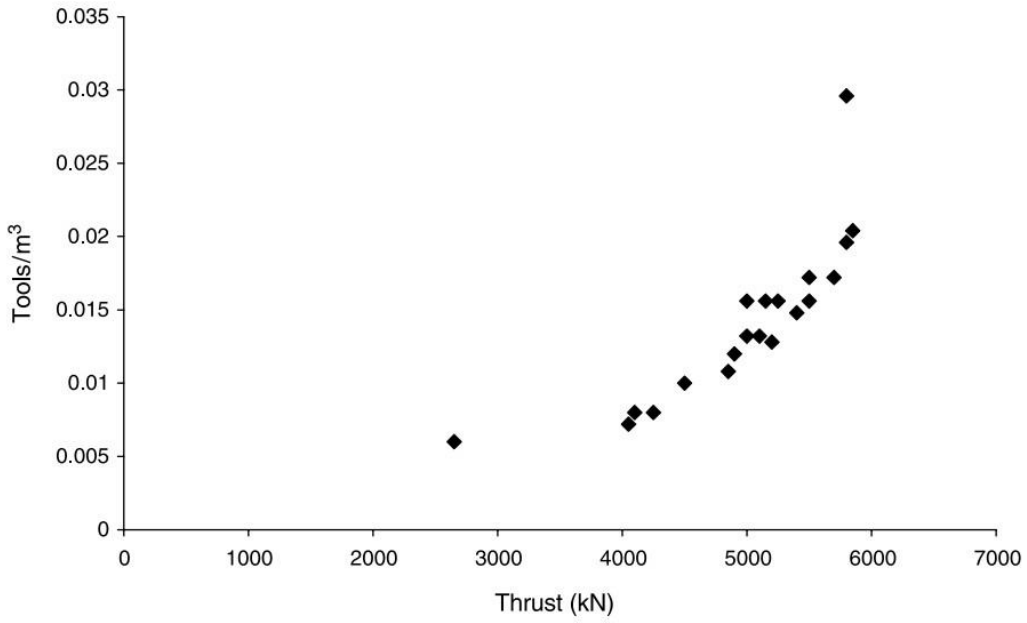

Figure 6-35 Disc consumption of a TBM (tools/m^3 of rock bench) vs. total thrust (Innaurato and Oreste, 2000, Innaurato et al., 2007).

Based on the aforementioned correlation between disc cutter consumption and load forces, it is reasonable that confining pressure would influence the disc cutter consumption via influencing the thrust loads. The influence can be favourable or unfavourable, which depends on the magnitude of confinement. When the confining pressure is lower than rock cohesion, increasing confinement would uplift the disc cutter thrust load; when the confinement pressure is higher than rock cohesion, then increasing confinement would decrease the disc cutter thrust load.

It is of significance to incorporate the *in situ* stress regime, i.e. confinement pressure, to cutter head design. For new cutter head design, the spacing should be down sized to achieve the same penetration in an intermediate confinement pressure regime to avoid damaging thrust load, and should be up sized in a high confinement pressure regime.

6.5 Summary

A set of refined disc cutter indentation tests considering bi-lateral confinement pressures was presented in this chapter. The findings of the study improved the

understanding of the cutting force development and disc cutting mechanisms of the TBM excavation. They are summarized as follows.

For the CCS disc cutter, the cutting force disparities among different confining pressures were of marginal extent and irregular with shallow penetration. The disparities increased and became notable with deepening penetration. Positive correlation existed between confining pressure and the maximum load with confinement less than 6 MPa. While the maximum load began to flatten or even decrease from some point between 6 and 9 MPa confinement.

For the V shape disc cutter, the cutting force disparities among different confining pressures were irregular but generally increased with increasing confinement pressure. While compared with the CCS disc cutter, the confinement pressure's influence on the maximum load was more marginal and irregular.

From the perspective of disc cutter pattern, the thrust load under the same confining pressure and penetration was always substantially lower for the V shape disc cutter than that of the CCS one. The maximum load for the CCS disc cutter was nearly constantly two times that of the V shape disc cutter under the given experimental set up.

Post indentation test observation of subsurface crack development revealed that indentation under different disc cutters induced distinctive crack systems with the same penetration and confining pressure. The CCS disc cutter indentation had denser cracks and the crack orientation was more lateral, which is favourable for rock chipping. The V shape disc cutter indentation was less sensitive to confining pressure, with no notable increase in crack number and crack re-orientation.

The study on crushed zones revealed that they were in wedge shapes under the CCS disc cutter, which overturned the circular shape simplification in theoretical studies. The crushed zones had the same width as cutter thickness. However, the wedge height changed with varying confinement pressure and penetration. Deepening of penetration increased the height of crushed zones, while increasing confining pressure decreased that height. In addition, the crushed zone boundaries were

delimited by shear failure cracks, and they initiated from shear cracks. For the V shape disc cutter, the crushed zones were of little significance from both shape and size perspectives. However, their enlargement with increasing penetration and confinement pressure was appreciable.

The findings of confining pressure's influence on cutting forces partly explained the conflicting opinions about ground stresses' influence on disc cutting. The ground stresses could either unfavourably or favourably influence boreability. It depends on the ground stresses magnitude and rock strength. When ground stress is lower than a threshold value, it would unfavourably influence boreability; after surpassing the threshold value, its influence could convert to favourable.

The aforementioned findings provide guidelines for cutter head design, by incorporating the *in situ* stress regime into consideration. More specifically, disc cutter spacing should be decreased to achieve the same penetration in an intermediate ground stress regime to avoid large thrust load, while that can be increased in high stress regimes.

7 CHAPTER SEVEN – CUTTING PICK SELECTION OF UNCONVENTIONAL COAL DRIVING TBM FOR FRICTIONAL IGNITION PREVENTION

7.1 Introduction

7.1.1 Cutting frictional ignition

Ignition of firedamp or methane gas is one of the most serious hazards for underground coal mining, as it may trigger a more violent and catastrophic dust and gas explosion. Numerous mining disasters of such explosions have been reported and caused considerable casualties in recent years; for example U.S. Upper Big Branch coal mine disaster in 2010 with 29 fatalities. The Governor's Independent Investigation Panel identified that it was the fire ignited by the shearer's cutting on a sandstone roof that triggered the catastrophic explosion in Upper Big Branch mine (McAteer et al., 2011).

Every ignition needs an igniting source. There are several categories of igniting sources: cutting friction, shot-firing, spontaneous combustion, open flame and exposed electrical circuits. The statistics of occurrences of firedamp ignitions show that cutting friction is the dominant igniting source (Philips, 1996, Philips, 1997, Department of Mineral Resources New South Wales, 1998, Krog and Schatzel, 2009, Browning, 1988, Courtney, 1990). Aside from the Upper Big Branch disaster, another one of the most catastrophic mining disasters was the Pike River mining explosion, which also claimed 29 lives among a total of 31 underground shift miners. According to the Royal Commission on the Pike River Coal Mine Tragedy (2012), the mine had several cutting frictional ignitions since 2007. Combined with the Upper Big Branch accident, it is clear that cutting frictional ignition is a major threat to underground coal mining industry.

Cutting frictional ignitions have been one of the major hazards for the underground coal mining industry for more than half a century. The statistics of UK underground coal mining firedamp ignitions is shown in Figure 7-1. There was a clear trend of rising incidence of cutting frictional ignitions from 1950s to late 1960s. Thereafter,

cutting frictional ignitions took up the majority of the firedamp ignition incidents (Philips, 1996).

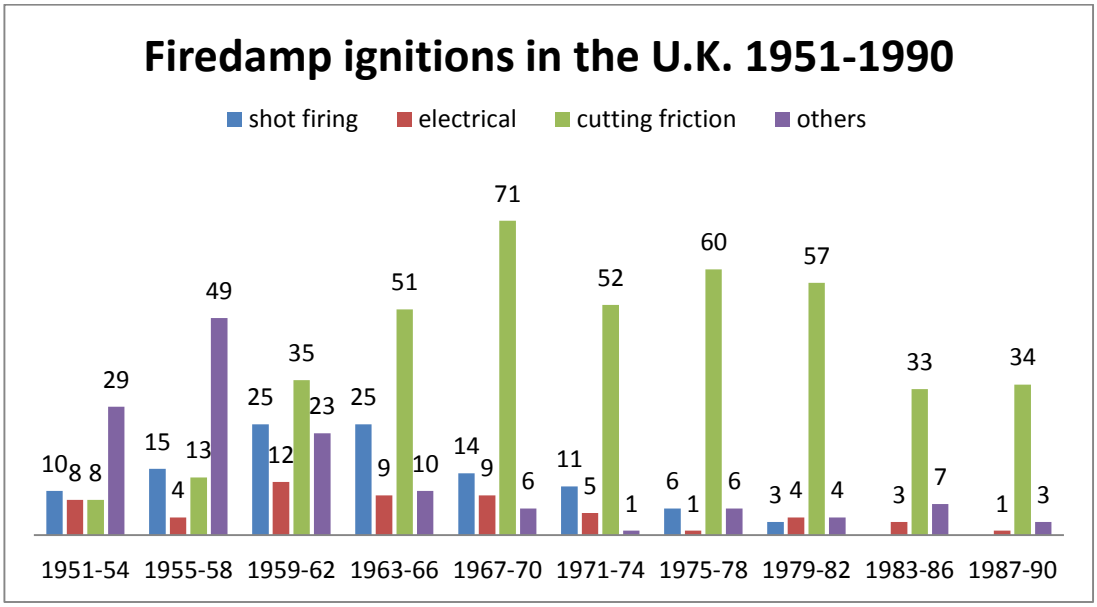

Figure 7-1 Firedamp ignition occurrences in U.K. 1951-1990 (Philips, 1996).

Cutting frictional ignitions also are the major part of firedamp ignition occurrences in South Africa. Ten-year national statistics of cutting frictional ignitions between 1984 and 1993 was conducted and the results are demonstrated in Figure 7-2. It shows that cutting frictional ignitions account for 68 percent of the firedamp ignitions with determined causes in South Africa over the period (Philips, 1996).

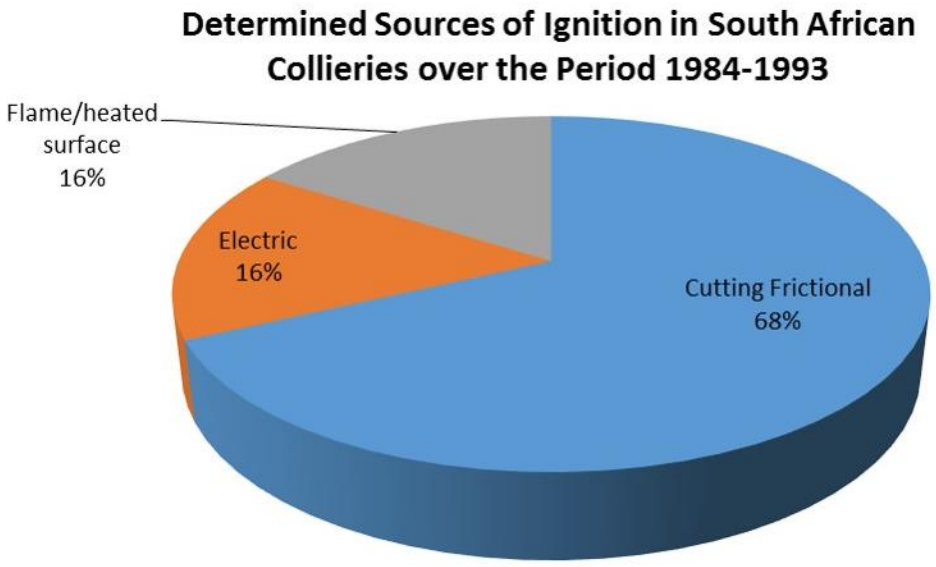

Figure 7-2 Determined Sources of Ignition in South African Collieries over the Period 1984-1993 (Philips, 1996).

Cutting frictional ignition is one of the major hazards for the Australian underground coal mining industry. According to the Department of Mineral Resources in New South Wales, there were 40 firedamp ignition incidences reported between 1st July 1987 and 1st July 1998, among which 34 were caused by cutting frictional ignition associated with shearers and continuous miners, as shown in Figure 7-3 (Department of Mineral Resources New South Wales, 1998). In 2011, with only 12 Longwall faces operating in Queensland, 2 cutting frictional ignition incidents associated with shearers were reported (Taylor and Watson, 2011, Bell, 2012).

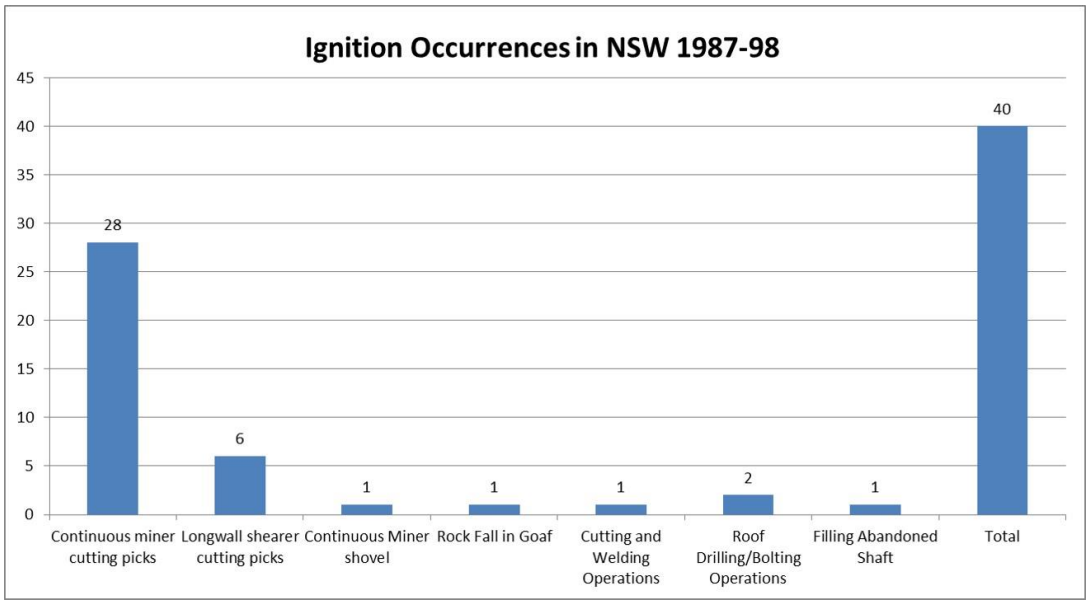

Figure 7-3 Reportable ignitions of methane in NSW underground coal mines 1987-1998(Department of Mineral Resources New South Wales, 1998).

U.S. underground coal mining industry is also under threat of cutting frictional ignitions. A statistical study of available data regarding frictional ignitions in the United States from 1983 to 2005 was conducted by the National Institute for Occupational Safety and Health (NIOSH) to determine and define conditions controlling their occurrences. Over the study period, 13 states out of a total of 17 underground coal producing states reported the occurrences of cutting friction ignition, covering 155 different coal mines. U.S. has 17 states which have underground coal mines, among them, Arkansas, Montana, New Mexico have only 1 underground coal mine, and Oklahoma has 2 underground coal mines. It is clear that all major underground coal mining states have the cutting frictional ignition problem. The occurrences of cutting frictional ignition always accounted for the majority of ignitions, with more than 65%, as shown in Figure 7-4 (Krog and Schatzel, 2009).

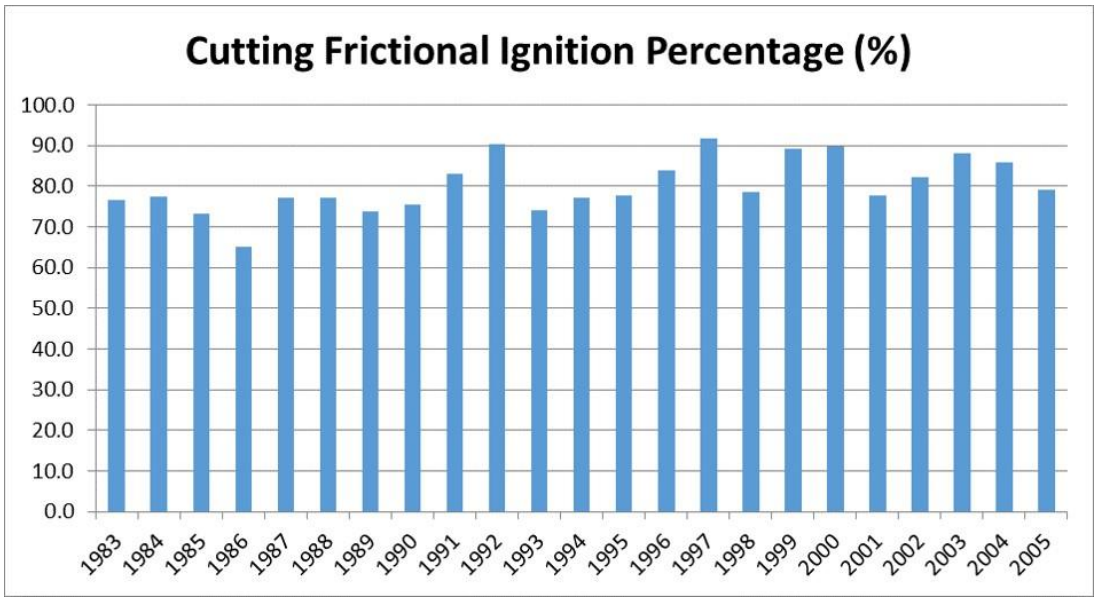

Figure 7-4 Cutting Frictional ignition proportion of total ignitions in U.S.A over the period of 1983-2005 (Krog and Schatzel, 2009).

Correlation between mechanization and cutting frictional ignition has been found from statistical data. For example, cutting frictional ignitions increased rapidly from the 1950's to the late 1960's in UK, as shown in Figure 7-1, which was also the period of mechanization of the UK underground coal mining industry, indicated by increasing applications of shearers and roadheaders equipped with drag cutters. Since then, cutting frictional ignition had been the majority of firedamp ignition incidents. The occurrence of frictional ignitions decreased from the 1970s in the UK, it was caused by shrinkage of the mining industry rather than a decline of mechanization (Philips, 1996； Browning, 1988).

Longwall operations were found to have a high frequency of cutting frictional ignitions. The 17 mines with the most frictional ignitions were all longwall mining operations (Krog and Schatzel, 2009). The total longwall faces in U.S. ranged from 38 to 88, while the occurrences of shearer frictional ignition reached up to 26, as shown in Table 7-1.

Table 7-1 U.S. longwall operation numbers and shearer cutting frictional ignition occurrences breakdown between 1989 and 2005 (Krog and Schatzel, 2009, Weir International, 2010).

Year	U.S. Longwall Face	Shearer FI Number
1989	38	18
1990	42	26
1991	42	11
1992	45	24
1993	39	3
1994	52	25
1995	56	8
1996	67	20
1997	72	25
1998	77	18
1999	75	22
2000	78	11
2001	76	11
2002	75	10
2003	79	21
2004	88	18
2005	87	13

It should be noted that longwall operations have a higher chance of incurring cutting frictional ignitions than that of other mining methods. U.S. statistics show that 1365 ignitions occurred in longwall operations and 224 ignitions occurred in room and pillar operations between 1983 and 2005. The 17 mines with the most frictional ignitions were all longwall mining operations. Furthermore, longwall development headings produced more frictional ignitions than longwall faces (Krog and Schatzel, 2009).

The high propensity for frictional ignition in longwall development headings can be explained by its firedamp environment. A longwall gateroad heading can operate up to 5 km in virgin coal seams, developing quickly and deeply into coalbed methane reservoir. Methane bleeds into the longwall gateroad from the virgin coal on both ribs and face, while a multi-entry room-and-pillar section has barrier pillar ribs that most likely have been degassed of methane. In addition, the development rate of a longwall gateroad is much higher than that of a multi-entry room-and-pillar section, so it cannot provide sufficient time for degassing for longwall development (Krog and Schatzel, 2009).

In conclusion, cutting frictional ignition is one of the major hazards for the underground coal mining industry. Longwall operations have a high frequency of cutting frictional ignitions. Longwall development headings are most likely to incur frictional ignitions.

7.1.2 Mechanism of cutting frictional ignition

The occurrence of cutting frictional ignition relies on the presence of an incendive igniting source and an air-methane mixture. The incendive air-methane mixture is when the methane concentration ranges between 5% ~ 15%. The presence of airborne coal dust can extend the incendive range; for example a 4.2 per cent methane air admixture could be ignited with the presence of 150 g/m^3 airborne dust (Dawood, 2011). Ventilation at the cutting zone is poor, which makes the presence of an incendive methane-air admixture highly probable; and in most cases, the incendive methane-air admixture is there. Researchers conducted measurements of

maximum and mean methane concentration inside the cutting zone of a shearer for a typical methane release rate of 5.5 L/s over a range of airflows, as shown in Figure 7-5. It shows that methane concentration was above the lean explosive limit even at the highest velocity of nearly 8 m/s, although methane concentration was in reverse proportion with air velocity (Browning, 1988). Aside from methane, coal dust generated and emitted from cutting also disperses into the cutting zone, which enhances the incendivity of the environment in and around the cutting zone. Considering the more confining environment for continuous miner cutting drums and TBM cutter heads, which impedes the dilution of methane, they are more likely to be in incendive environment. In conclusion, for shearers, continuous miners and TBMs in coal seams, their cutting zones are often in an incendive environment.

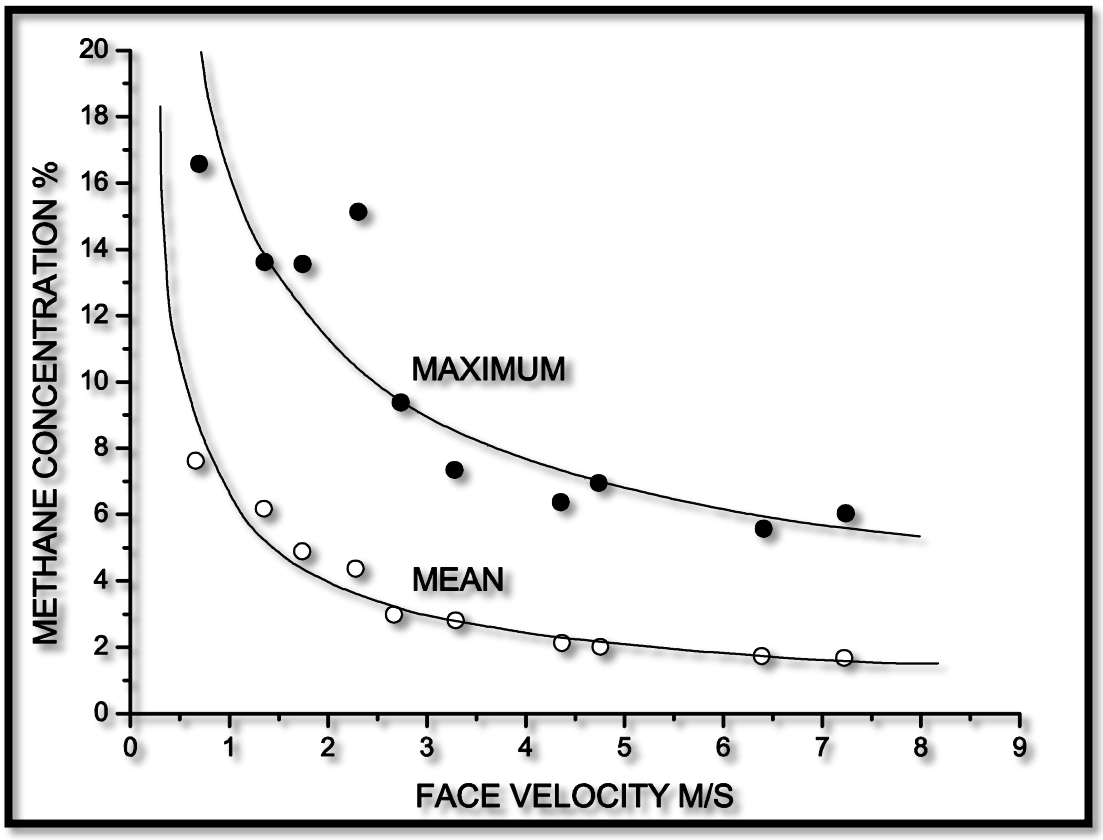

Figure 7-5 Shearer cutting zone methane concentration pattern measured by researchers (Browning, 1988).

The cutting frictional igniting source is the hot streak at the trail of the cutting picks (Powell and Billinge, 1975, Ward et al., 2001). When cutting bits strike incendive

rocks, the friction at the contact generates thermal energy, which would heat up both the bit and rock interfaces. If the contact face temperature reaches the lower solidus temperature of the rubbing materials, hot streaks would appear on the trails of the cutting picks. The hot streaks are incendive if they have sufficient area, high enough temperature and long enough life time. So the likelihood of presence of an igniting source depends on the incendivity of rock, cutting bits and their interaction.

A rock's incendivity varies with its quartz content and quartz particle size. Powell from UK Safety in Mines Research Establishment (SMRE) conducted extensive and comprehensive tests to investigate the influence of quartz content and particle size on frictional ignition with colliery rocks, and reported the results as shown in Figure 7-6. It indicates that, under the testing conditions, the rocks with 10 micron plus quartz particle content less than 20 percent could not produce ignitions, while the rocks with that size quartz particle content more than 40 percent could surely produce ignitions. Therefore, the chance of frictional ignitions is closely related to quartz content (Powell and Billinge, 1975a).

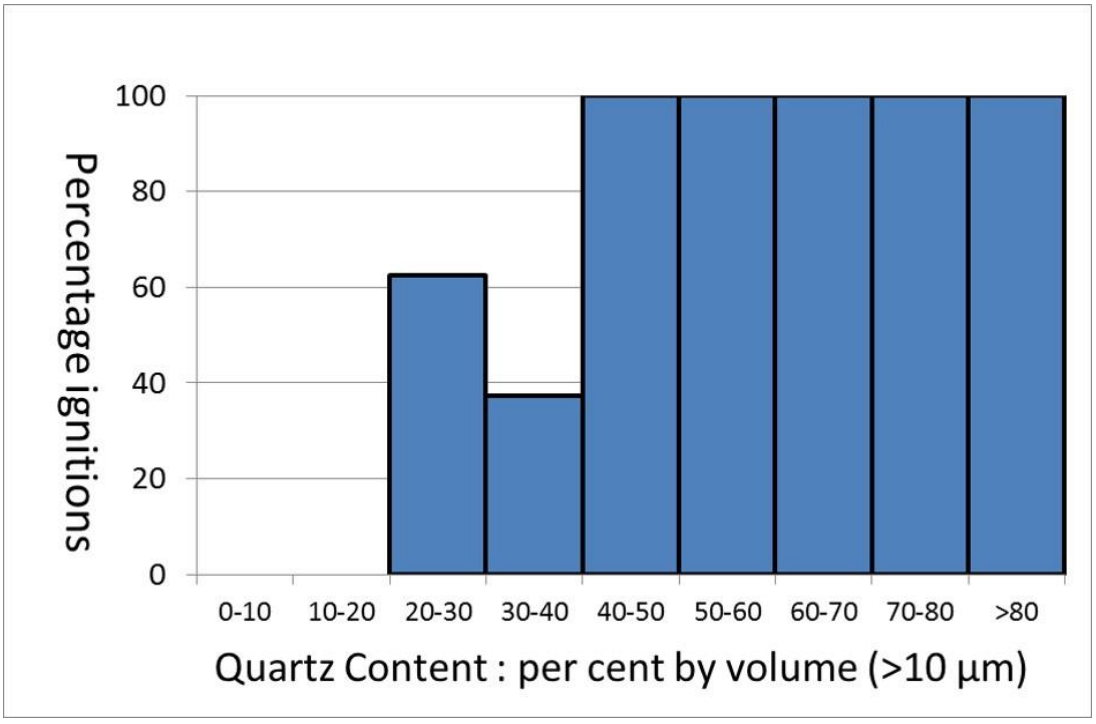

Figure 7-6 The influence of quartz content on incidence of frictional ignition (Powell and Billinge, 1975).

The influence of mineral composition on the incidence of frictional ignitions is also confirmed by field statistics. Surrounding rocks of coal measures are typically conglomerate, sandstone, mudstone, shale and claystone. Conglomerate and sandstone contain more than two thirds of quartz by volume but with different grain size; while mudstone and shale contain quartz from one third to two thirds by volume, and similar with grain size; and claystone contains quartz by no more than one third. The statistical data of ignitions in New South Wales between 1987 and 1993 showed that conglomerate had the highest incendivity with 8 out of 25 ignitions were caused when picks strike on conglomerate, followed by sandstone (Ward et al., 2001).

According to field observations and laboratory tests, for tungsten carbide tipped cutting picks, the steel body of the cutting pick needs to be exposed and rubbed to generate an incendive hot streak. Figure 7-7 shows results of laboratory tests of the influence of steel exposure on the incidence of frictional ignitions, conducted by U.S. Bureau of Mines (Courtney, 1990).

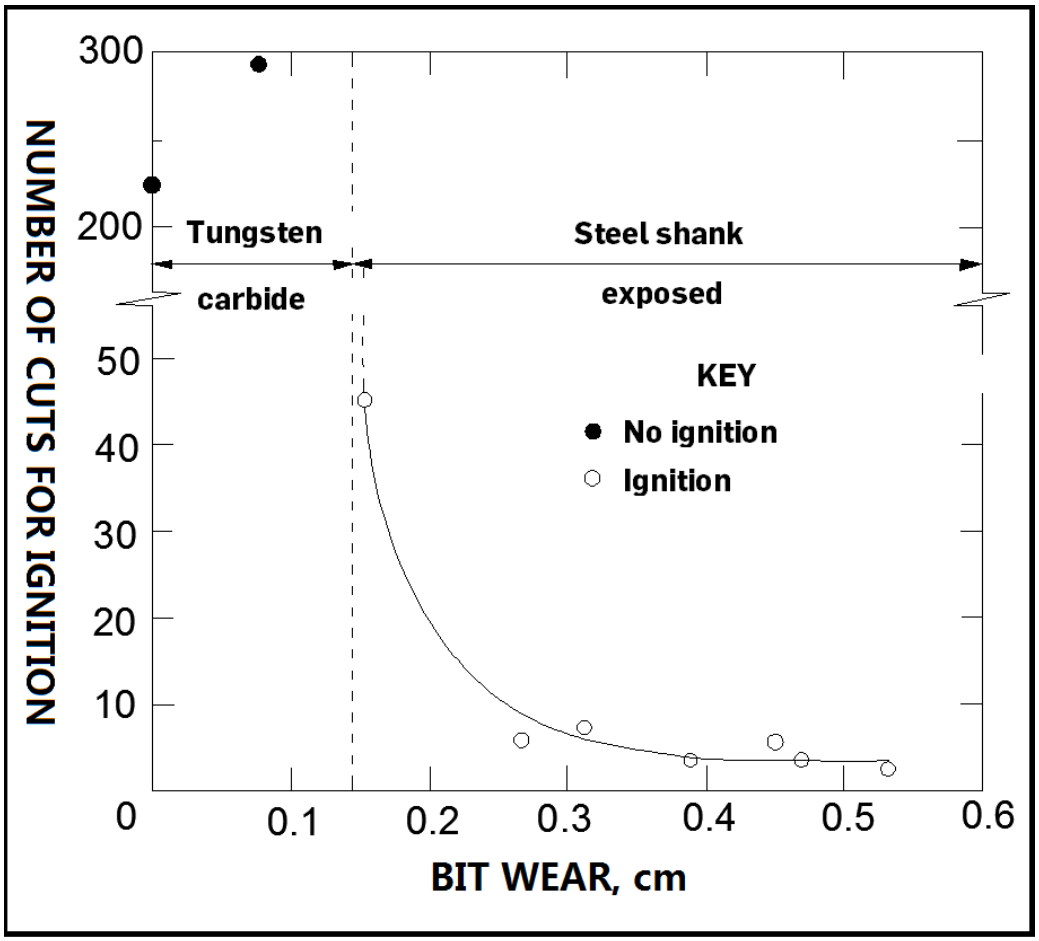

Figure 7-7 Effect of bit wear on frictional ignition with a specific pick type (Courtney, 1990).

Figure 7-7 shows that the cutting picks without steel body being exposed did not yield ignition with up to 300 cuts. When the steel shank of the cutting picks is exposed, however, frictional ignitions might occur within 10 cuts. In addition, the more steel body is exposed, the less number of cuts are needed to produce ignitions (Courtney 1990). As the tungsten carbide protects the cutting picks from frictional ignition, so, the worst scenario with regard to frictional ignition prevention is that tungsten carbide tip is completely lost in the cutting action, which is termed detipping. Detipping occurs suddenly during cutting, and is often not detected until the next pick inspection. Detipped picks are the most incendive ones in practical underground cutting regimes. McStravick (1989) studied optimum water spray configuration for detipped picks to minimise ignition occurrence. However, there is little research on optimum pick design or selection with respect to frictional ignition prevention for coal cutting machinery.

7.1.3 Frictional ignitions associated with TBMs

Underground coal mine TBM drivage is more prone to incur frictional ignitions. During the period 1980-1986 there were 40 ignitions in underground coal mines of the Federal German Republic. Among them, 17 were caused by shearers, 14 by boom-type roadheaders and 9 by full-face tunnelling machines. However, from the viewpoint of machine numbers, shearers, boom-type roadheaders and TBM accounted for 0.020, 0.015 and 0.196 ignitions per machine per year, respectively (Browning, 1988), i.e. the incidence of frictional ignition risk for TBM is around tenfold that of the shearers and thirteen fold that of roadheaders. In other countries, the industrial considerations in TBM design and construction have substantiated this hazard, even though no TBM frictional ignitions statistics are accessible. In Canada at the Donkin-Morien project, a maximum cutterhead peripheral speed was specified to control the risk of frictional ignition (Palmer et al., 1985).

Unconventional TBMs have been employed for longwall gateroad drivage. And have achieved a remarkable advance rate of 132 meters per day, 3088 meters per month. Based on the aforementioned mechanism of cutting frictional ignitions, especially the high incendivity of longwall gateroads development, it is reasonable to assume that coal driving TBMs have a higher risk of frictional ignition than both shearers and continuous miners.

The higher risk can be explained from two aspects, a more incendive methane environment and a more incendive cutting action. The first one is caused by full face cutting profile, single-entry development pattern and high advance rate. Full face cutterhead blocks ventilation to the cutting zone, which makes the methane dilution deteriorated. Single-entry development patterns with high advance rates cause high gas emissions and less time for degassing. The second one is that its cutting action is more incendive because the cutting picks have continuous sliding cutting against rocks rather than the intermittent ones like shearers and continuous miners, which makes the heat accumulation more likely.

In addition, cutting frictional ignition occurrences in coal drivage are easier to escalate to serious disasters than that in stone headings. Coal headings are rich of coal dust and gas emission, which add fuel for fire expanding or even escalating to an explosion. So, it is important to minimize the chance of cutting frictional ignitions associated with coal headings using TBMs.

The occurrence of cutting frictional ignition relies on the co-presence of an incendive methane environment and ignition sources. The presence of incendive methane environment is not avoidable. Then, the feasible way to control the risk of cutting frictional ignitions is eliminating the presence of igniting sources. Incendive rocks and incendive cutting picks are needed for the presence of igniting sources. As underground geology is uncontrollable, incendive rocks are frequently encountered. So, the practicable way to avoid ignition sources would be avoiding incendive cutting picks.

Detipped picks are the most incendive ones in practical underground cutting regimes. However, there are few research studies on optimum pick design or selection with respect to detipping and frictional ignition prevention for coal cutting machinery. This chapter presents an experimental study to identify detipping and frictional ignition risks of cutting picks based on their failure patterns. The load-displacement characteristics have also been analysed quantitatively to provide a guideline for cutting pick selection in gassy environment.

7.2 Experiment

Five types of drag cutting picks commonly used in the underground coal mining industry were selected and three specimens were tested for each kind of pick. The nominated cutting depth of all tested picks was 28 mm; and the pick shank dimensions were all the same 100 mm ×50 mm ×30 mm. All specimens consisted of tungsten carbide tip, pick body, heel, water channel, extraction point, shank and rib lock; the terminology and dimensions of the cutting picks are shown in Figure 7-8 and Figure 7-9.

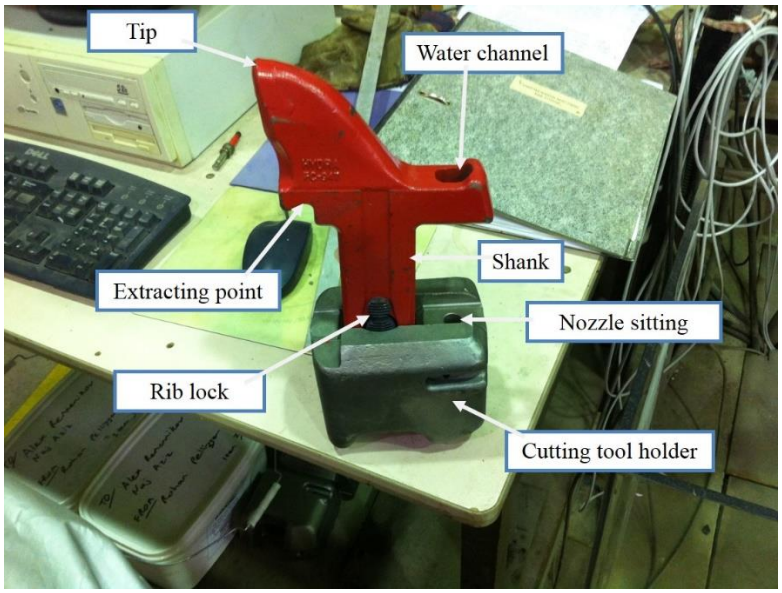

Figure 7-8 Terminology of radial cutting pick.

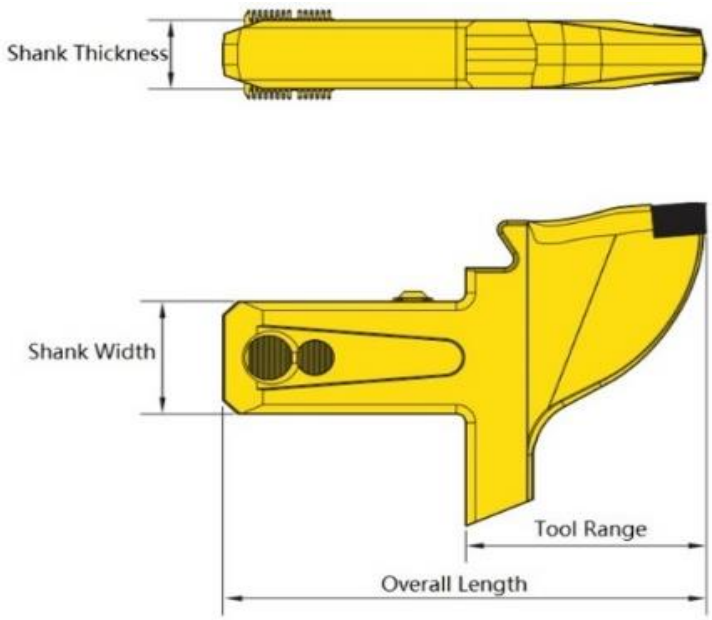

Figure 7-9 Dimensions of radial cutting pick.

With respect to the tungsten carbide tip attachment, three patterns were identified as slotted, slug and laid-on, as shown in Figure 7-10. The length of pick tool range is an important parameter for failure pattern analysis. To investigate its influence on frictional ignition, picks I, IV and V were all slotted picks but had different tool range lengths of 100, 110 and 140 mm, respectively. The specifications of tested cutting picks are listed in Table 7-2.

Figure 7-10 Studied cutting tip attachment patterns, from left to right: slotted, slug and laid-on.

Table 7-2 Specifications of tested cutting picks.

Pick	Tip attachment	Tool range (mm)
I	Slotted tip	100
II	Laid-on tip	130
III	Slug tip	100
IV	Slotted tip	110
V	Slotted tip	140

The testing platform was set up on an AVERY machine, as shown in Figure 7-11. It was run under displacement control mode with the displacement rate of 1.0 mm per minute. The data were automatically recorded and saved in the affiliated computer. Tests continued till the picks failed, as shown in Figure 7-12. The details of the failure pattern were then recorded.

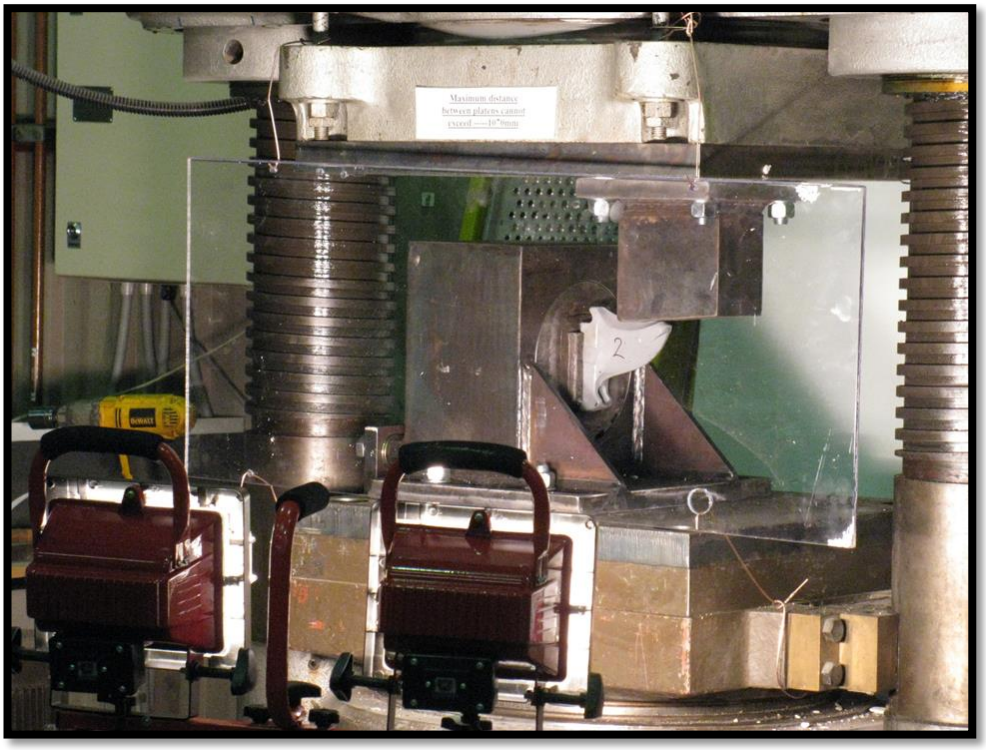

Figure 7-11 The close-up view of test set up.

Figure 7-12 A close-up of the pick failure.

7.3 Results

In the laboratory tests, failure of the specimens may occur at the tip (i.e. detipping) or at the shank or both of them. Figure 7-13 shows typical failure patterns in the experiment. From the view point of frictional ignition prevention, pick failure at the shank is favourable as a detipped pick greatly increases the frictional ignition risk. More specific results about the tests are given below.

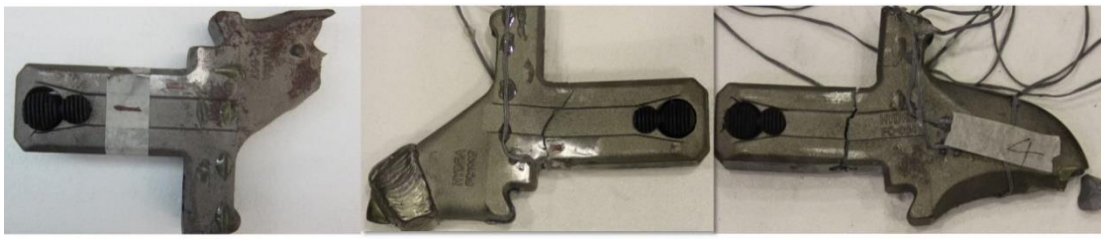

Figure 7-13 Cutting picks failure patterns, from left to right: at tip (detipping), at shank and at tip and shank simultaneously.

7.3.1 Pick I testing results

Three Pick I cutting picks all detipped, as shown in Figures 7-14 to 7-19. This failure pattern incurs adverse incendive cutting actions. Their strength values were 330 kN, 372 kN and 469 kN respectively, with the mean value of 390 kN.

Figure 7-14 Failure pattern of Pick I-1.

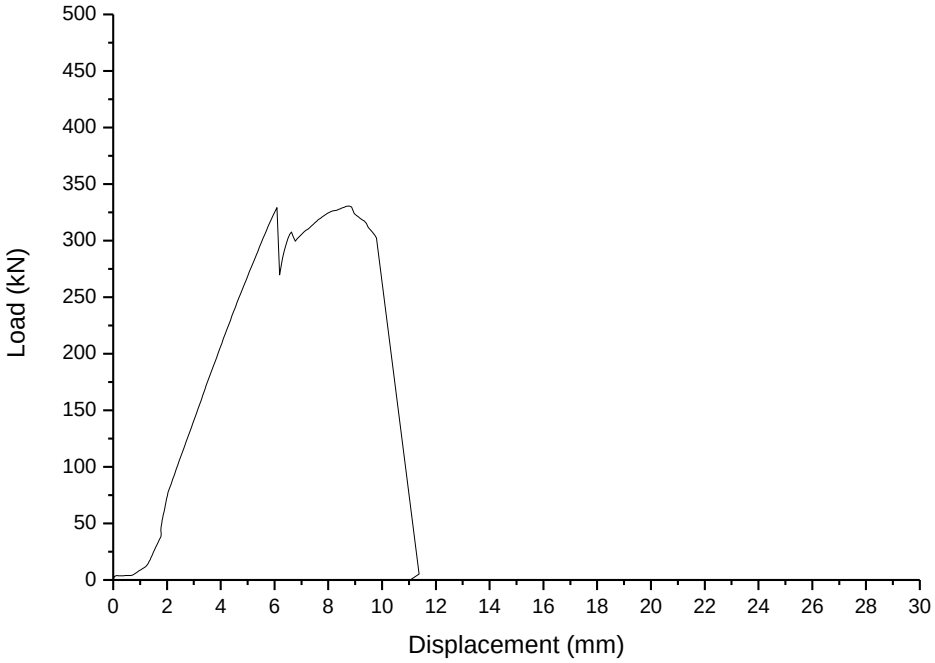

Figure 7-15 Loading characteristic of Pick I-1.

Figure 7-16 Failure pattern of Pick I-2.

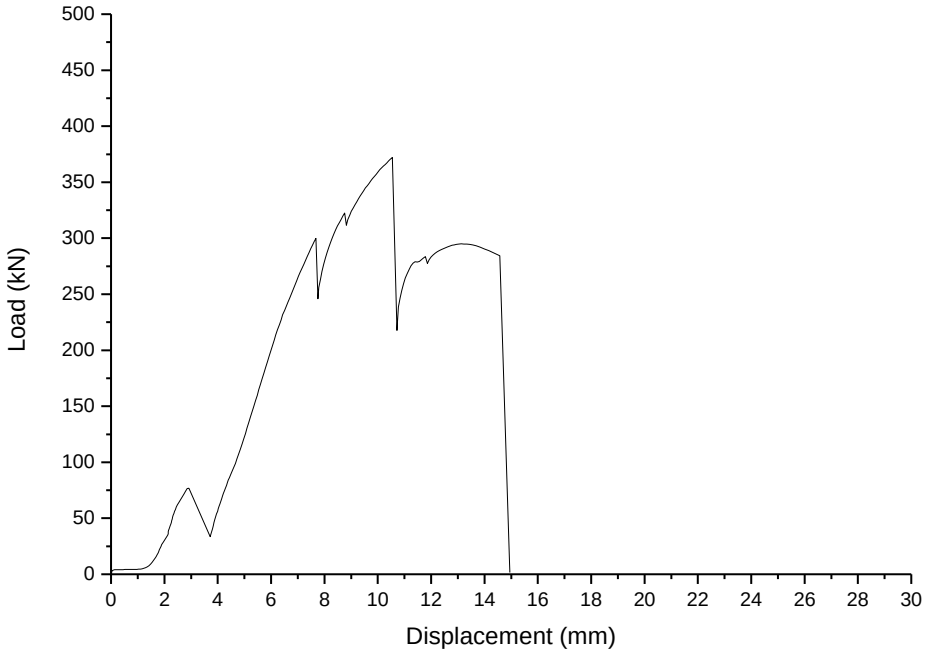

Figure 7-17 Loading characteristic of Pick I-2.

Figure 7-18 Failure pattern of Pick I-3.

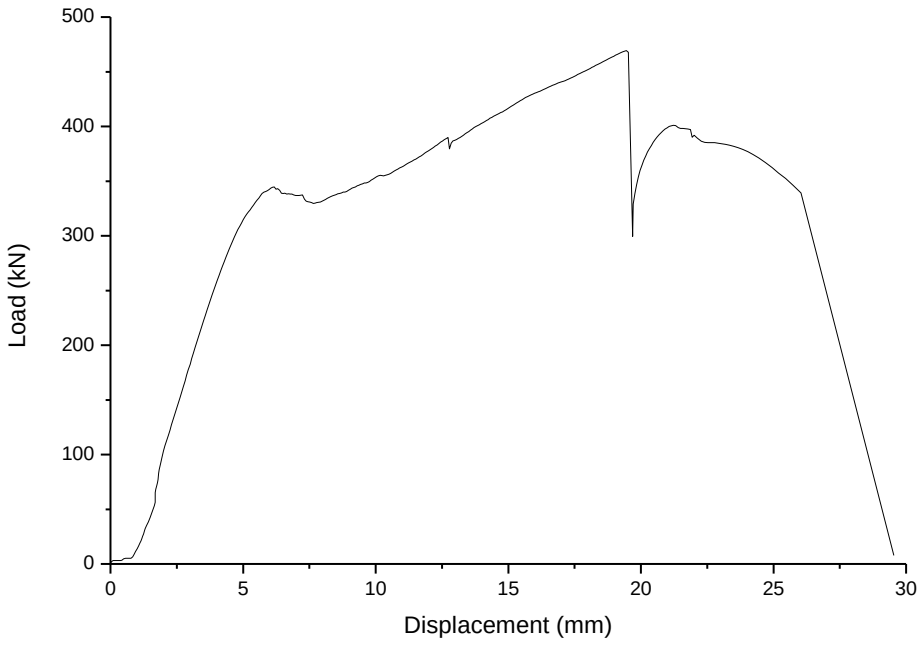

Figure 7-19 Loading characteristic of Pick I-3.

7.3.2 Pick II testing results

Three Pick II cutting picks had different failure patterns, two failed at both shank and tip while the third one failed at the shank only, as shown in Figures 7-20 to 7-25.

Their strength values were 449 kN, 407 kN and 323 kN respectively, with the mean value of 393 kN.

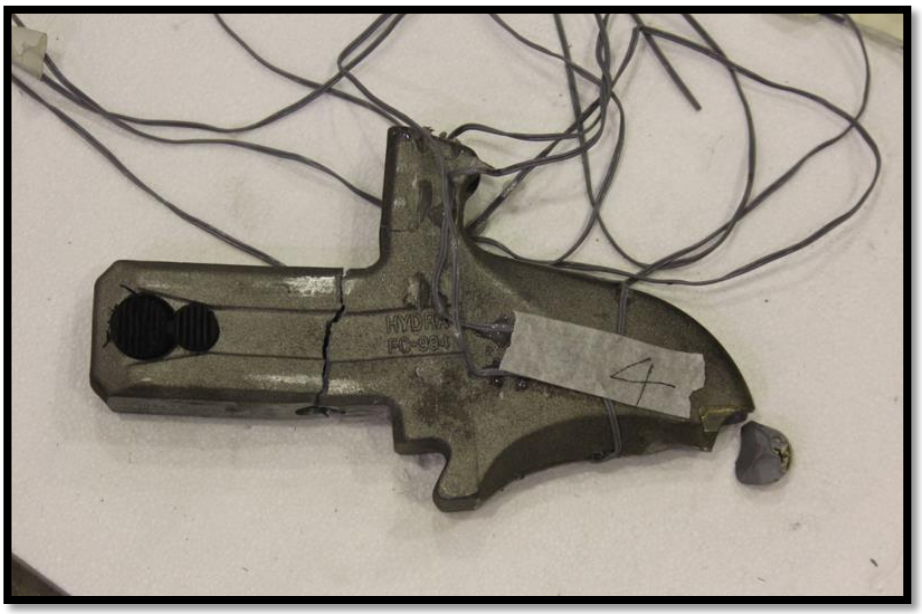

Figure 7-20 Failure pattern of Pick II-1.

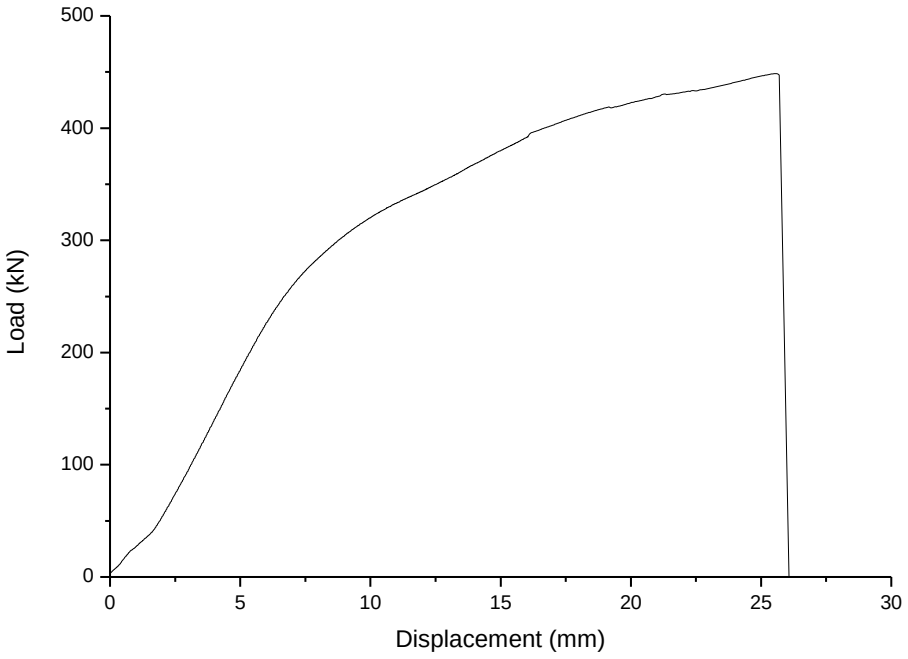

Figure 7-21 Loading characteristic of Pick II-1.

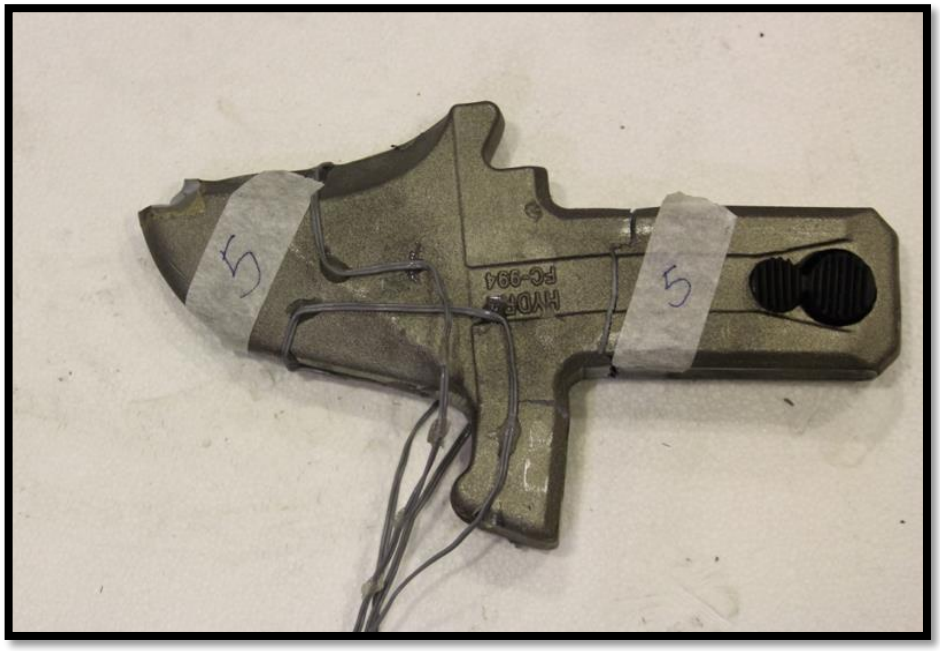

Figure 7-22 Failure pattern of Pick II-2.

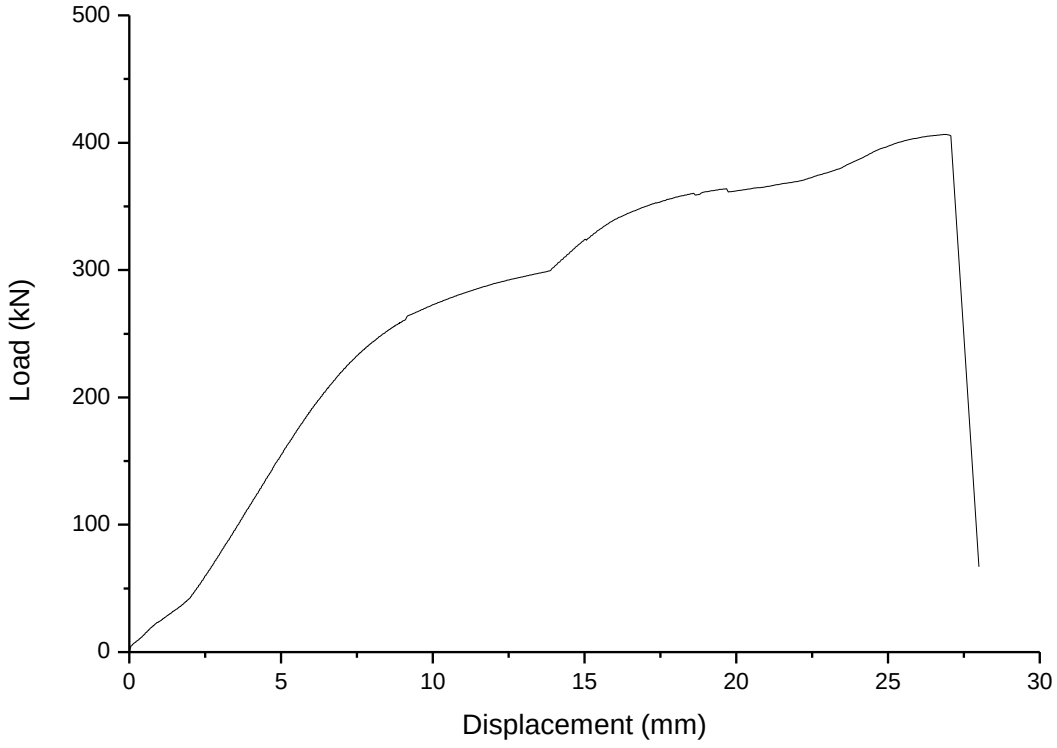

Figure 7-23 Loading characteristic of Pick II-2.

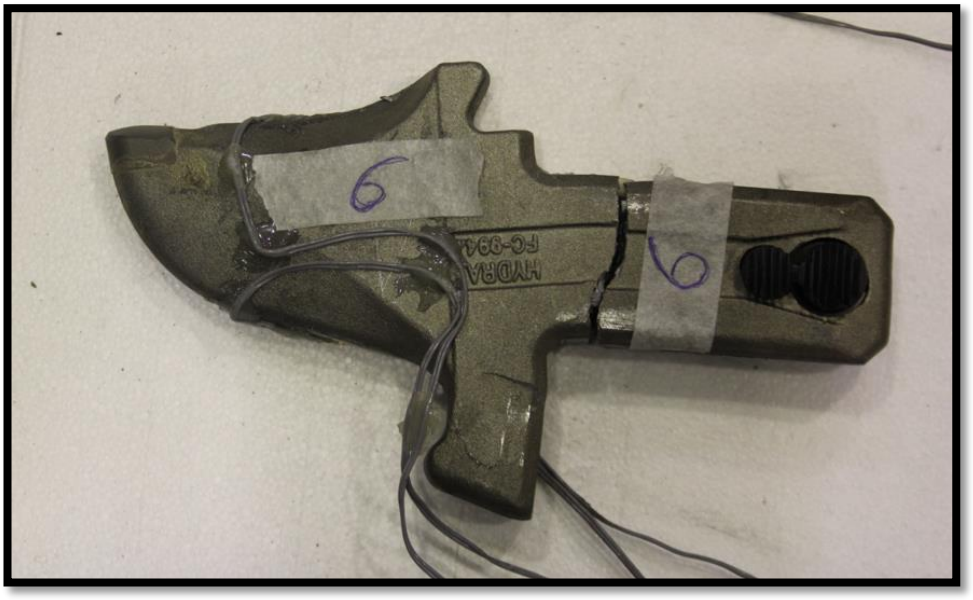

Figure 7-24 Failure pattern of Pick II-3.

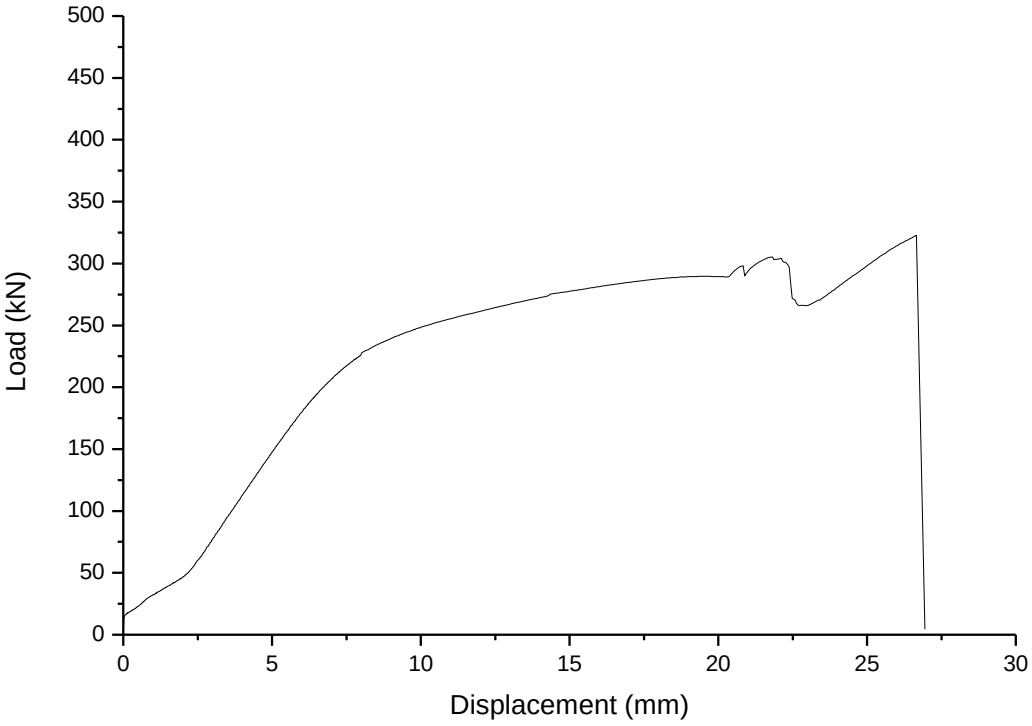

Figure 7-25 Loading characteristic of Pick II-3.

7.3.3 Pick III testing results

Three Pick III cutting picks failed at different parts, one failed at the shank, while two others failed at the tip, as shown in Figures 7-26 to 7-31. Their strength values were 466 kN, 479 kN and 471 kN respectively, with the mean value of 472 kN.

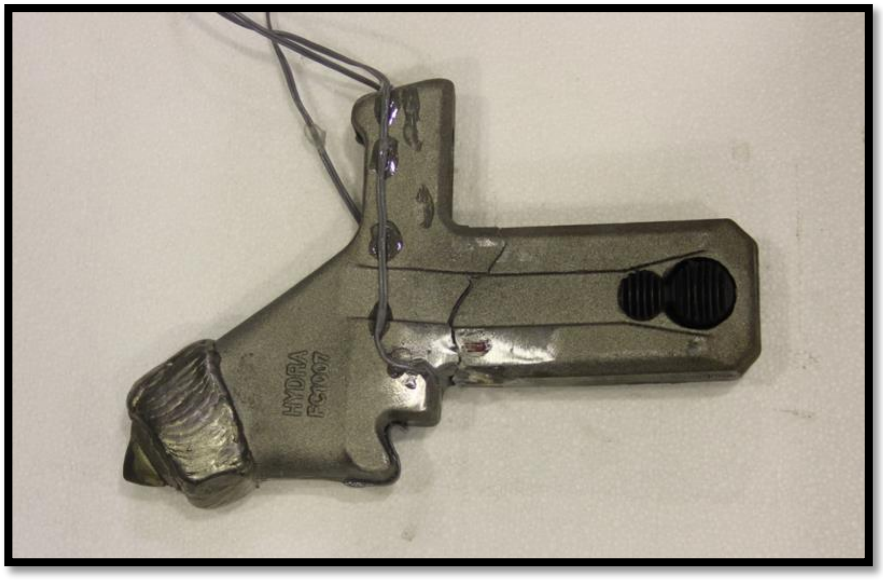

Figure 7-26 Failure pattern of Pick III-1.

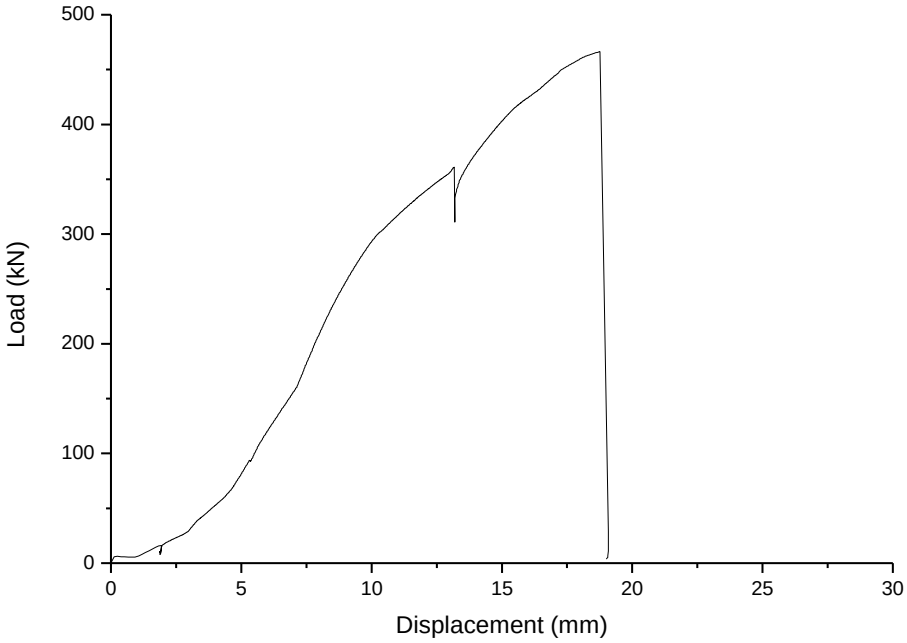

Figure 7-27 Loading characteristic of Pick III-1.

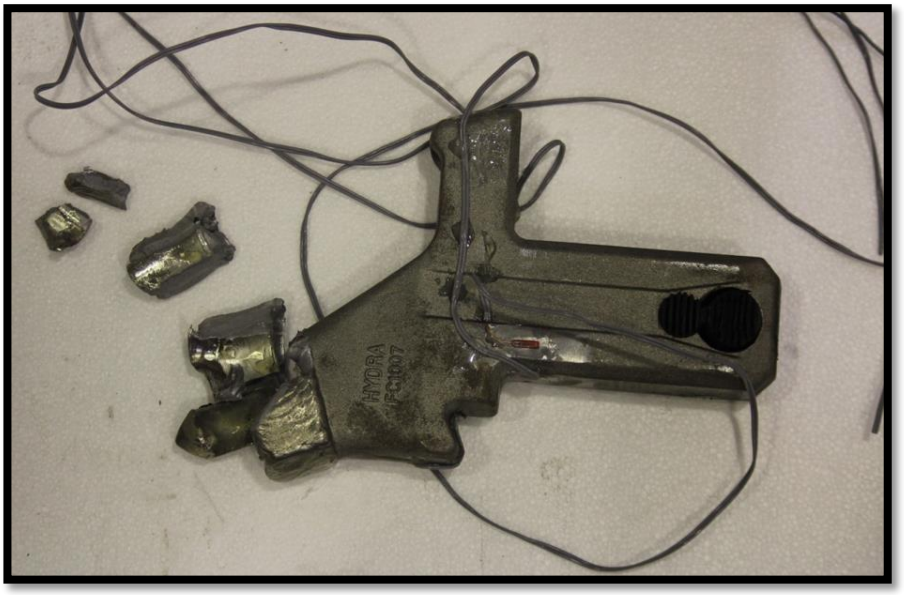

Figure 7-28 Failure pattern of Pick III-2.

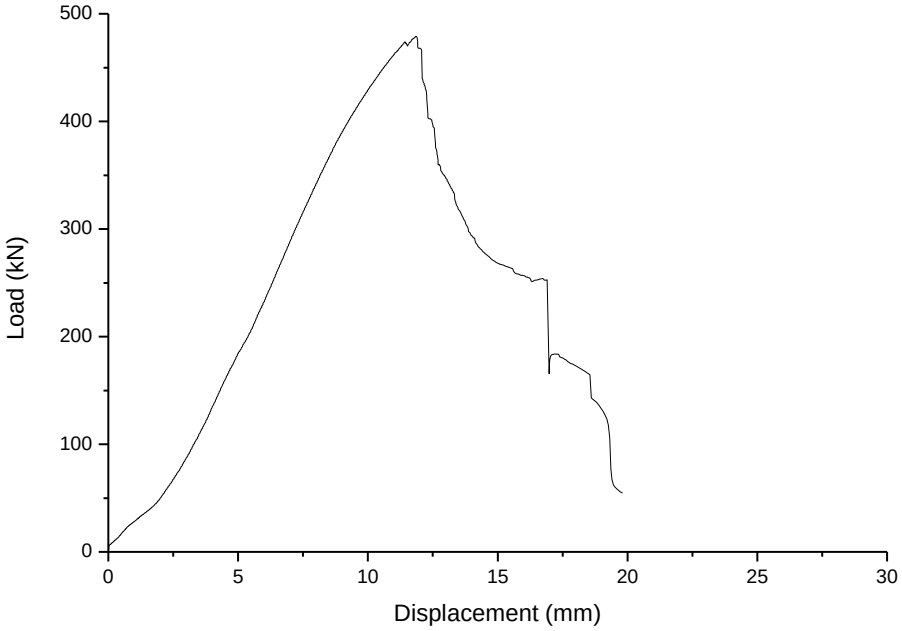

Figure 7-29 Loading characteristic of Pick III-2.

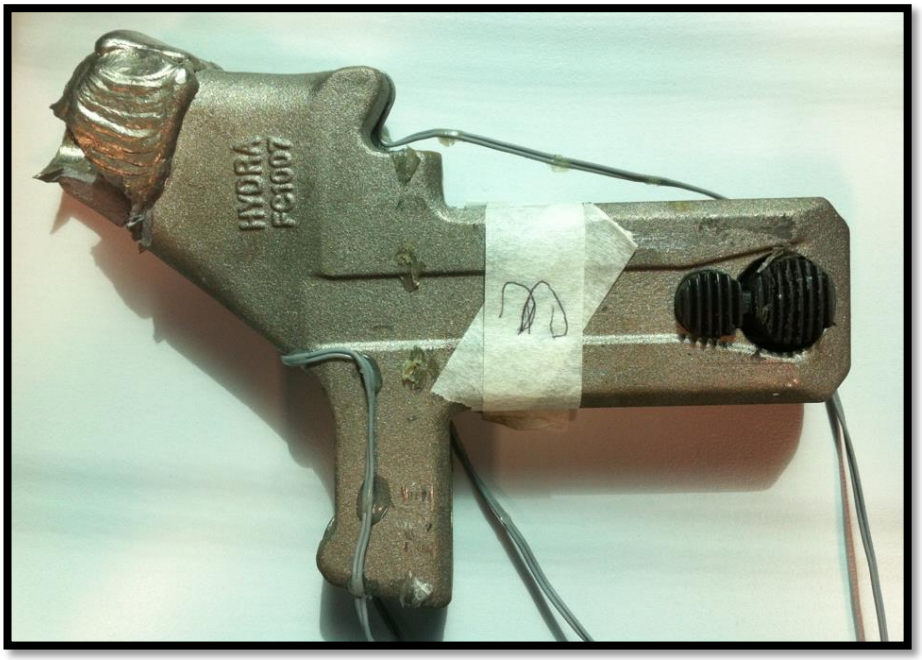

Figure 7-30 Failure pattern of Pick III-3.

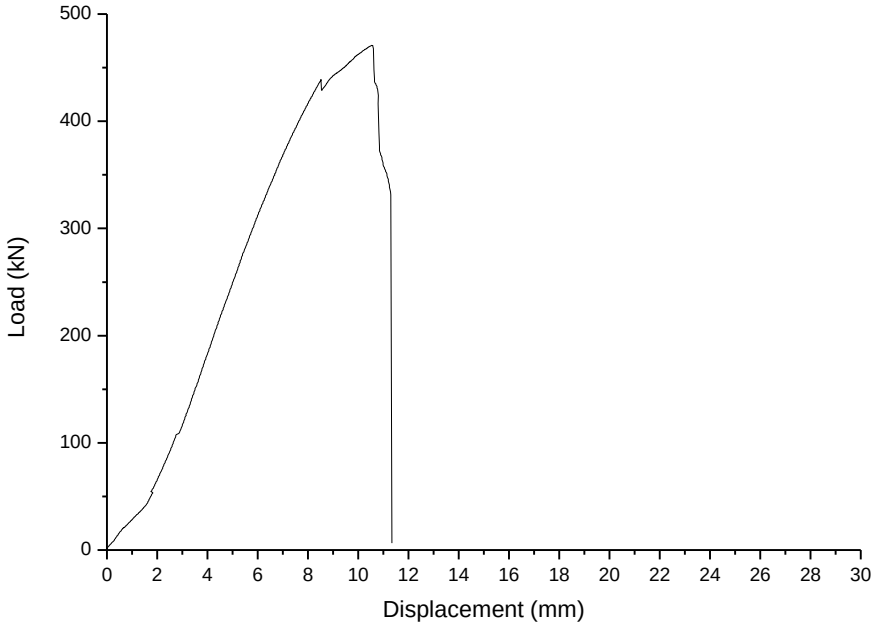

Figure 7-31 Loading characteristic of Pick III-3.

7.3.4 Pick IV testing results

The test results show that three Pick IV cutting picks all failed at the tip, as shown in Figures 7-32 to 7-37. Their strength values were 364 kN, 421 kN and 443 kN respectively, with the mean value of 409 kN.

Figure 7-32 Failure pattern of Pick IV-1.

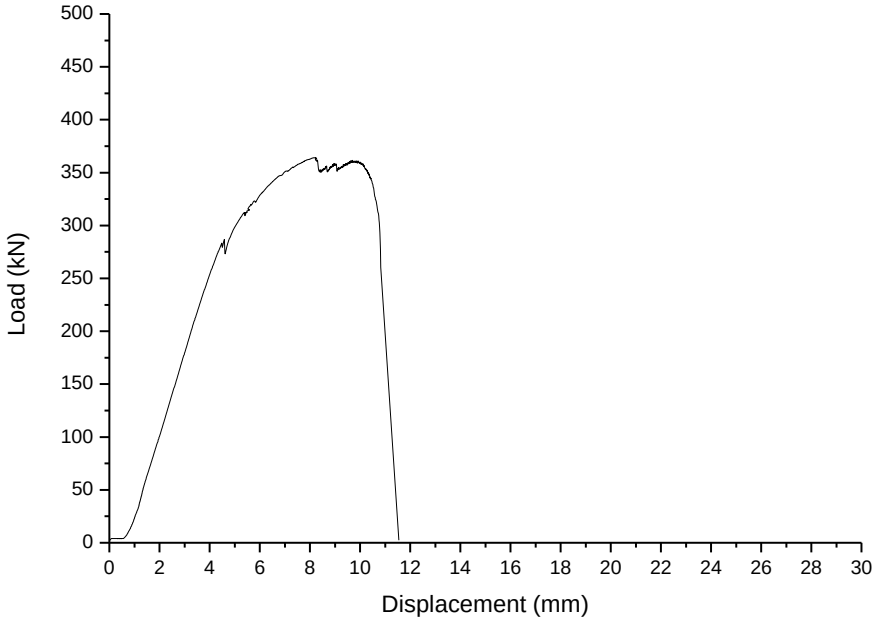

Figure 7-33 Loading characteristic of Pick IV-1.

Figure 7-34 Failure pattern of Pick IV-2.

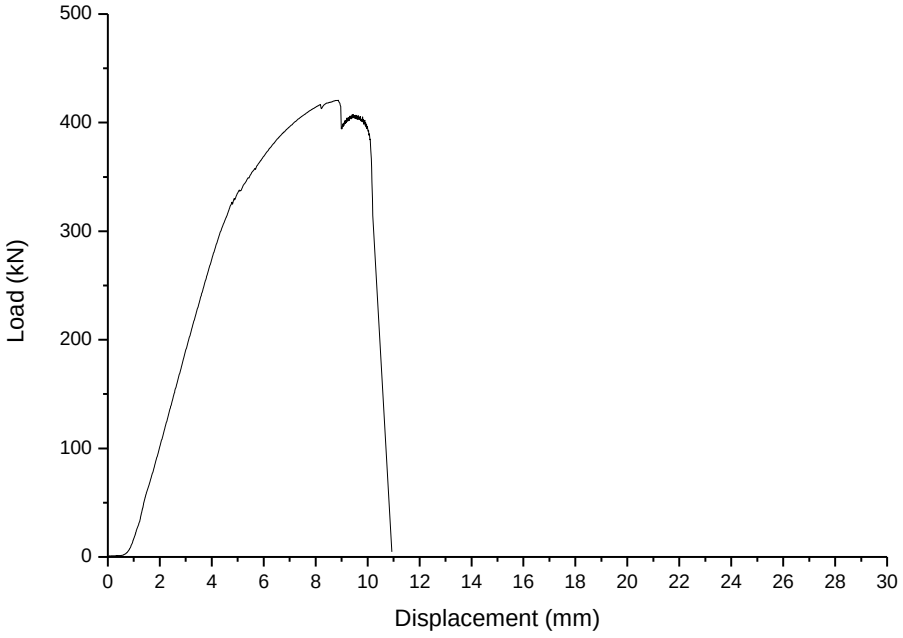

Figure 7-35 Loading characteristic of Pick IV-2.

Figure 7-36 Failure pattern of Pick IV-3.

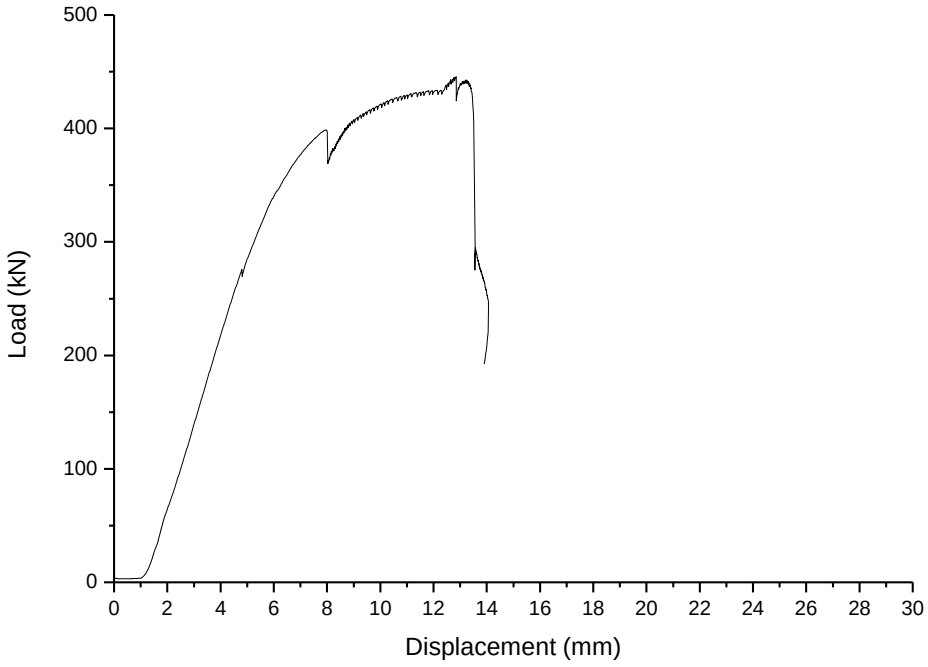

Figure 7-37 Loading characteristic of Pick IV-3.

7.3.5 Pick V testing results

Three Pick V cutting picks all failed at the shank, as shown in Figures 7-38 to 7-43. Their strength values were 436 kN, 436 kN and 414 kN respectively, with the mean value of 429 kN.

Figure 7-38 Failure pattern of Pick V-1.

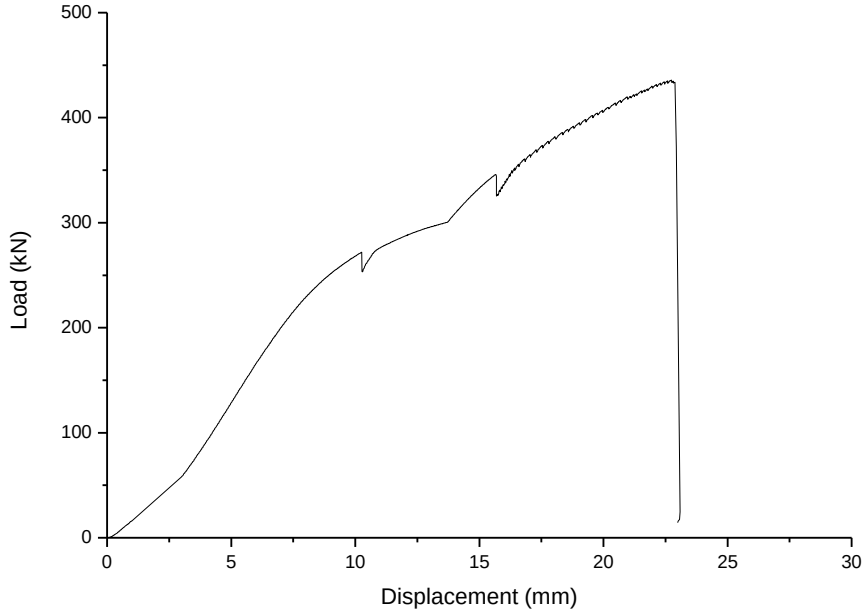

Figure 7-39 Loading characteristic of Pick V-1.

Figure 7-40 Failure pattern of Pick V-2.

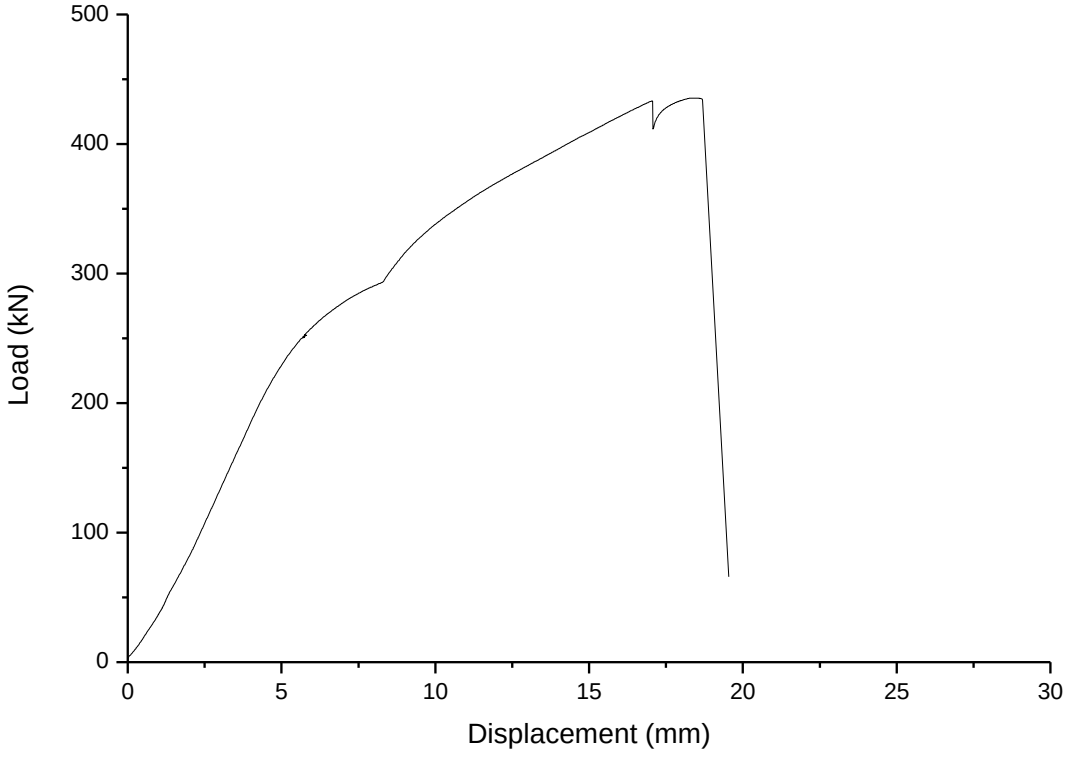

Figure 7-41 Loading characteristic of Pick V-2.

Figure 7-42 Failure pattern of Pick V-3.

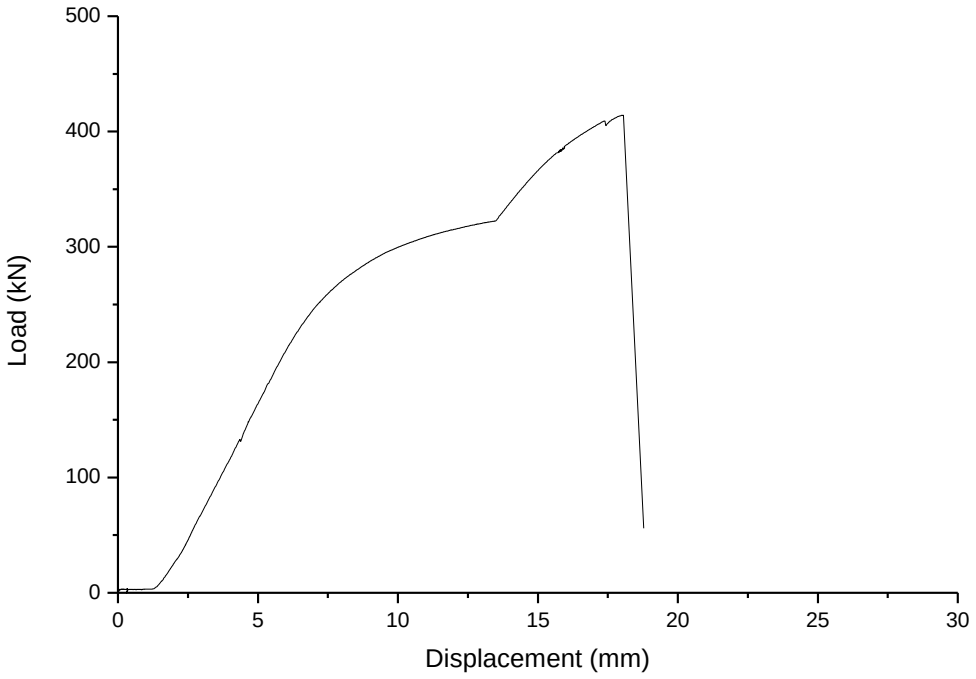

Figure 7-43 Loading characteristic of Pick V-3.

The experimental result related to pick failure patterns is presented in Table 7-3.

Table 7-3 Failure patterns of the tested picks.

Pick	Tip attachment	Tool range (mm)	Tip	Shank	Both
I	Slotted tip	100	3	0	0
II	Laid-on tip	130	0	1	2
III	Slug tip	100	2	1	0
IV	Slotted tip	110	3	0	0
V	Slotted tip	140	0	3	0

7.4 Analysis

7.4.1 Failure pattern

Experimental results show that, the tungsten carbide tip attachment pattern has a great influence on the pick failure pattern, which in turn affects the frictional ignition risk in a gassy workplace. Pick I and pick III have the same tool range length of 100 mm, but the cutting tip of pick I is slotted and pick III's is slug, which is reinforced by extra welding. In the experiment, detipping occurred for all pick I but two-thirds for pick III; i.e. less frictional ignition risk for the latter one. It suggests that welding reinforcement of the tip can reduce the detipping risk to some extent; however, it can hardly control the risk to an acceptable level. For the slotted tip and the laid-on tip, by comparison of failure patterns of pick II and pick V presented in Table 7-3, it can be seen that the slotted tip may have some advantages over the laid-on tip with respect to frictional ignition prevention as detipping occurred on two laid-on tipped specimens, while no slotted pick detipped. Conclusively, the slug tip attachment pattern has the lowest detipping risk, followed by slotted and then laid-on ones.

Another finding is that the tool range length of a pick is one key geometric parameter with respect to detipping prevention. The tungsten carbide attachment method of pick I, IV and V are all slotted but their tool range lengths are different. The experimental result show that, detipping occurs while the tool range lengths are 100 or 110 mm, but pick failure changes to shank failure if its tool range length enlarges to 140 mm. As the tool range length is a flexible parameter for pick design, therefore, it should be optimised to reduce frictional ignition risk.

It is interesting to find that pick failure may occur at the tip and the shank simultaneously (case of pick II). This failure pattern has less frictional ignition risk than detipping, as the shank failure would make the pick body fall off the cutting drum; which prevents the exposed steel body from rubbing. Theoretically, such pick design is the optimum utility of the material. However, from the viewpoint of risk control, failure at the tip should be avoided if the cutting machinery may be operated in a gassy environment.

7.4.2 Mechanical performance

Pick strength is an important mechanical parameter for rock cutting, and is closely related to frictional ignition risk control. Generally, high pick strength is favourable as the pick may cut surrounding hard rocks, or rub with siliceous nodules, lenses or bands within coal seam. The load-displacement curves of all tested specimens are shown in Figure 7-44.

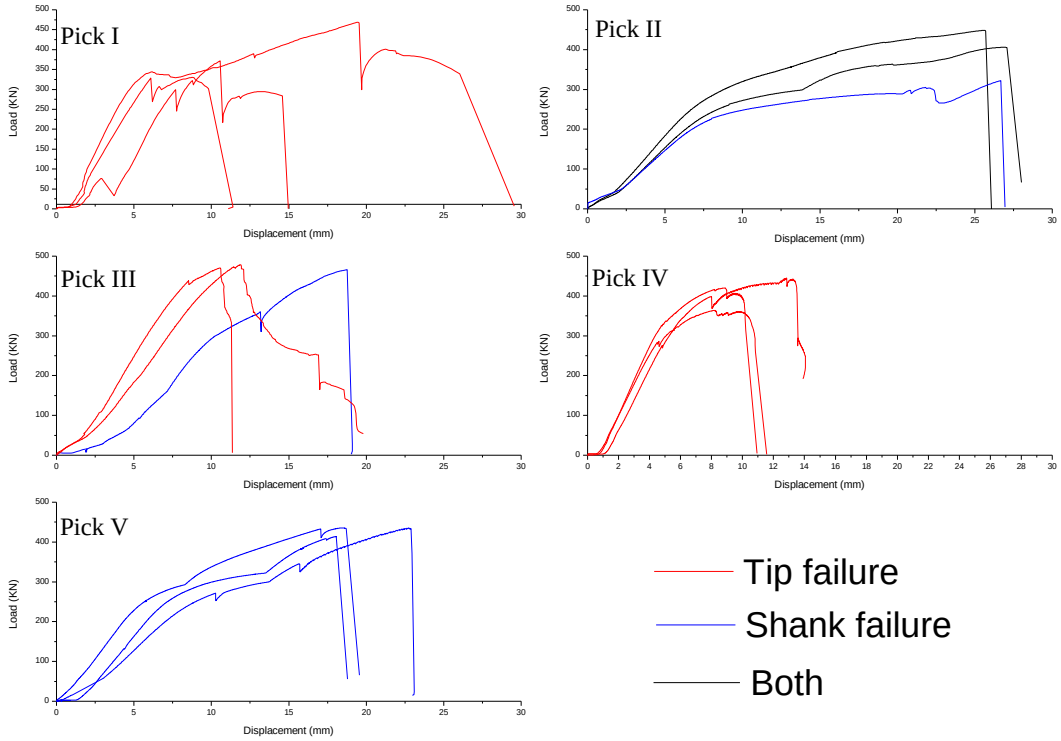

Figure 7-44 Load-displacement characteristics and failure patterns of the tested picks.

The mean values of the peak load of picks I to V are 390, 393, 472, 409 and 429 kN, respectively. The load capacity of pick III (slug tip) is the greatest among all kinds of tip patterns and tool range lengths. It is most likely due to its welding reinforcement of the tip. For different pick failure patterns, the average loading capacities are 419, 415 and 428 kN in the cases of tip failure, shank failure and both tip and shank failure, respectively. It suggests that the pick failure pattern may not be taken into consideration in current pick design as the pick strengths for different failure patterns have no statistical difference.

The displacement of a pick at its peak load is an indicator of its stiffness of performance. Experimental result shows that the average displacements at peak load are 11.4, 21.0 and 26.3mm for detipped, shank failed and both tip and shank failed picks, respectively. It indicates that a detipped pick has high brittleness. Therefore, increasing the pick ductility is supposed to be an effective way to reduce the detipping risk and in turn the frictional ignition risk in pick design.

7.4.3 Resilience analysis

In cutting action, picks might impact on hard rock plies, bands or nodules. Under the given impact energy, high energy absorbing capacity will mitigate load build-up to reduce the chance of pick failure. Pick Resilience (R) is defined as the amount of energy that a pick can absorb before failure. It can be calculated by integrating the load-displacement curve from zero to the displacement at peak load, as shown in Equation (7-1).

$$R = \int_0^{s_p} f\, ds \qquad (7\text{-}1)$$

Where:

R is the pick resilience;

s is the displacement;

s_p is the displacement at peak load;

f is the load.

Experimental results show that the average pick resilience values are 2894, 5222 and 7640 Nm for tip failed, shank failed and both tip and shank failed picks, respectively. It demonstrates that detipped picks have low pick resilience. In addition, picks with low resilience below 3837 Nm all failed at the tip. Therefore, increasing the pick resilience is suggested to be an effective way in pick design to reduce the detipping risk.

7.5 Summary

Five types of cutting picks commonly used in the underground coal mining industry were tested to study the pick geometric parameters' influence on failure pattern. Their tool range lengths were between 100 and 140 mm, with different tip patterns of slotted, slug and laid-on. Experimental results identified three kinds of failure

patterns: at tip (detipping), at shank, and at tip and shank simultaneously. Cutting picks' mechanical performances were also recorded and analysed.

Tip attachment pattern and tool range length demonstrated notable influences on failure pattern. Experimental results indicate that, with the same tool range length, slug tipped picks have the lowest detipping risk, followed by slotted and then laid-on ones. Increasing tool range length can change the failure pattern from detipping to shank failure, in turn reduce the frictional ignition risk; the threshold value to eliminate the chance of detipping is 140 mm for the tested picks.

Detipped picks showed distinctive features of high stiffness and low pick resilience. The load-displacement characteristics demonstrate that detipped picks had the average displacement at peak load of 11.4 mm, while it was 21.0 and 26.3 mm for the other two failure patterns. The average pick resilience for detipped picks was 2894 Nm, while that of the other two failure patterns were 5222 and 7640 Nm.

The findings provide guidelines for cutting pick selection and design to minimize the risk of frictional ignition. For selection among the available ones, pick V was demonstrated to be the most favourable one with no chance of detipping in the tests. For new pick design, slug tip attachment pattern, reasonably large tool range length, high resilience and high ductility are suggested to be adopted to reduce the risk of detipping and frictional ignition.

8 CHAPTER EIGHT – CONCLUSIONS AND RECOMMENDATIONS

Along with increased coal consumption, underground coal mining operations are becoming deeper and progressively more intensified. This brings new challenges to underground coal mine development. A large number of stone roadways have to be developed to cope with the stress and gas problems resulting from mining operations at greater depth. Higher coal drivage rates are required to maintain smooth longwall panel succession.

TBMs are advanced tunnelling machinery that can achieve much higher advance rates than conventional methods, and have been proposed to accommodate the challenges for both stone drivage and coal drivage. As a part of the project feasibility study, proposed TBM application would need guidelines and experience of previous historical cases to assist performance prediction and avoid similar operational problems. Lack of knowledge about the influence of confining pressure on disc cutting hinders the accurate prediction of TBM performance in deep underground coal mines because the roadways are exposed to high ground stresses. In addition, the coal drivage projects face the risk of cutting frictional ignitions.

This thesis presented a detailed study on the application of TBMs in underground coal mines in three parts. The first part is a critical literature review of historical cases. The second one studies disc cutter cutting force prediction models and rock breaking mechanisms, which is closely related to the application in stone drivage. The third part studies the cutting pick selection for coal driving TBMs to prevent cutting frictional ignitions.

8.1 Conclusions from historical cases study

Literature review of historical cases of the application of TBMs in underground coal mines provides valuable lessons and experiences. The majority of the historical cases were successful from the perspective of advancing rate, and some of them were both faster and more economical than conventional methods; although a few turned out to be failures.

From the perspective of excavation rate, all TBMs outperformed the conventional excavation methods in competent geological conditions. In the Donkin-Morien project, the TBM drove four times faster than the drill and blast method in the -20% decline section. In the Selby mine project, TBM's advancing rate was over twice that of roadheader's on both bases of maximum and average. At the long straight section of the Gneisenau mine project, the TBM achieved an advancing rate of over 20 meters per day. In the Monopol mine project, with the roster of 18 hours boring, six hours maintenance per day, five-day week, the maximum advance rate of 570 m per month and average advance rate of 280 m per month were achieved. Bad performance was also experienced ranging from unsatisfactory advancing rate heading to withdrawal of the machine in adverse geological conditions.

From the perspective of excavation cost, most TBM projects had higher cost than their conventional methods. However, in favourable conditions, where tunnels were long and straight in competent ground, TBMs could outperform conventional methods. In the Selby mine project, where two 13.5 km straight tunnels were driven, the total excavation cost of the TBM was just 16.5% higher than that of a roadheader. In the Gneisenau mine project, TBM's overall excavation cost was lower than that of the drill and blast method.

Important lessons from the historical cases were the sensitivity of TBM's performance to geological conditions, machine reliability and the backup system reliability. Most failures of TBM projects, such as the two times withdrawal of the TBM from the face in the Dawdon project were from the severely faulted ground; the poor performance of TBM in the West Cliff project was mainly caused by its main bearing failure and hydraulic faults.

8.2 Conclusions for application of TBMs in stone drivage

For the applications in stone drivage, high advance rate is the most important merit that makes TBMs stand out over conventional tunnelling methods. Prediction of advance rate is an integral part of the feasibility study for TBM projects. The prediction is based on the analysis of cutting forces. Numerous efforts have been

made to develop accurate cutting force predicting models for disc cutters. These models are mainly based on theoretical analysis combined with laboratory test verification. However, an extensive model for all disc cutters and rocks has not been developed.

Evans model does not include disc cutter diameter and cut spacing into calculations. The calculated normal force is smaller than the measured. The compressive failure mechanism proposed in the Roxborough and Phillips model does not take cut spacing into consideration, which makes it hardly be used for the cutterhead layout design.

The most widely accepted model in industry is the Colorado School of Mines (CSM) one. It provides reasonably accurate predictions for V shape disc cutters. However, it is not applicable to CCS disc cutters because the calculated value will be negative infinite according to this model. For CCS disc cutters, no models have been developed to provide reasonably accurate predictions. This might be due to the lack of knowledge on rock breaking mechanism of CCS disc cutters. Although, the shear failure mechanism has facilitated the most accepted model for V shape disc cutters, i.e. the CSM model. However, its modified version for CCS disc cutters prediction is not widely accepted by the industry.

Introduction of the tensile failure mechanism is the distinctive feature for the Sanio model. It raises the debate about the rock failure mode in disc cutting, especially for CCS disc cutters. However, the Sanio model is not applicable to CCS disc cutters. So, a mixed failure mode of shear and tensile failure mechanism would be closer to reality for CCS disc cutters. Without getting a better understanding about the rock cutting mechanisms, it is difficult to establish an accurate prediction model for CCS disc cutters.

Since the introduction of disc cutters, there have been numerous studies to investigate the disc cutting mechanism. Analytical, experimental and numerical approaches were all employed to conduct researches. Studies have revealed that disc

cutting consists of different phases, stress build-up, formation of crushed zone, and initiation and propagation of fractures.

Analytical analysis was employed to predict the stress field and failure zone caused by the applied load. However, the analytical models have to be simplified as linear, isotropic and elastic scenarios, which are discrepant to the complex tool-rock interaction associated with realistic disc cutting. Some important factors were ignored in the analytical studies, such as rock heterogeneity and crushed zone. In addition, the early analytical analysis lacked experimental verification. With the improvement of laboratory testing power, researchers turned to experimental studies.

Experimental studies improved the understanding of disc cutting mechanisms by avoiding the linear, isotropic and elastic simplifications. In addition, they are essential for validating the analytical and numerical studies. Experimental studies have evolved from the perspectives of test scale, applied confinement pressure, and the observation of sub-surface crushed zone and crack development. However, only a few experimental studies take all these factors into consideration as large scale experiment with confinement and sub-surface observation is costly and time consuming.

Numerical study turned out to be a practical, cost effective and time saving approach to improve the knowledge of disc cutting, based on rapid improvement of computing power and not needing physical experimental preparation. It is convenient to trace the crushed zone and crack development, as it can provide a better description of the mechanical behaviours of disc cutting than other methods. In addition, numerical studies can also avoid important factor simplifications, such as rock heterogeneity. However, the numerical study results are questionable without validation by experimental tests.

In spite of all the completed studies, there is still considerable debate about the disc cutting mechanisms. This is partly because of the discrepancies between study simplifications and field realities. To advance the understanding of disc cutting mechanisms, based on the critical analysis of the previous experimental and

numerical studies, a more realistic experimental study was conducted. Confining stresses, penetrations up to 9 mm, and observation of subsurface crushed zone and cracks are taken into consideration. As part of the experimental study, the tested rock physical and mechanical properties were measured, which provided prerequisite parameters for further cutting force analysing.

The laboratory indentation test improved the understanding of the cutting force development and disc cutting mechanisms at the TBM excavation faces, where high stress regimes are present. For the CCS disc cutter, the cutting force disparities among different confining pressures were of marginal extent and irregular with shallow penetration. The disparities increased and became notable with deepening penetration. Positive correlation was found between confinement pressure and the maximum load force with confinement less than 6 MPa. While the thrust load began to flatten or even decrease from some point between 6 and 9 MPa confinement. For the V shape disc cutter, the cutting force disparities among different confining pressures were irregular but generally increased with increasing confinement pressure. While compared with the CCS disc cutter, the confinement pressure's influence on the maximum load was more marginal and irregular.

Disc cutter patterns also imposed significant influence on cutting forces. The thrust load under the same confinement pressure and penetration was always substantially lower for the V shape disc cutter than that of the CCS one. The maximum load for the CCS disc cutter was nearly constantly two times that of the V shape disc cutter under the given experimental set up.

Post-test observation of subsurface crack system development revealed that indentation under different disc cutters induced distinctive crack systems with the same penetration and confinement pressures. CCS disc cutter indentation had denser cracks and the crack orientation was more lateral, which is favourable for rock chipping. V shape disc cutter indentation was less sensitive to confinement pressure, with no notable increase of crack number and crack orientation turning.

The study on crushed zones revealed that they were of wedge shapes under the CCS disc cutter, which overturned the circular shape simplification in theoretical studies. The crushed zones had the same width as cutter thickness. However, the wedge height changed with varying confinement pressure and penetration. Deepening of penetration increased the height of the crushed zones, while the increase of confining pressure decreased that. In addition, the crushed zones' boundaries were delimited by shear failure cracks, and they initiated from shear cracks. For the V shape disc cutter, the crushed zones were of little significance from both shape and size perspectives. However, their enlargement with increasing of penetration and confinement pressure was appreciable.

The findings of confining pressure's influence on cutting forces partly explained the conflicting opinions about ground stresses' influence on disc cutting. The ground stresses could either unfavourably or favourably influence boreability. It depends on the ground stresses magnitude and rock strength. When ground stress is lower than a threshold value, it would unfavourably influence boreability; after surpassing the threshold value, its influence could convert to favourable.

The aforementioned findings provide guidelines for cutter head design, by incorporating the *in situ* stress regime into consideration. More specifically, disc cutter spacing should be decreased to achieve the same penetration in intermediate ground stress regimes to avoid large thrust load, while that can be increased in high stress regimes.

8.3 Conclusions for application of TBMs in coal drivage

Aside from the application of conventional circular TBMs in stone drivage, unconventional rectangular TBMs has also been proposed for application in coal drivage. Being favourable to other coal development approaches, the TBM concept could provide an integrated, continuous full face cutting, bolting and coal clearance system, which would notably increase development rates. In 2014, the first coal driving TBM was launched by the Shenhua mining group.

Cutting frictional ignition is a frequent and fearful hazard for the underground coal mining industry, especially for longwall gateroad development operations, where coal driving TBMs are applied. It has been claiming a lot of miners, like the Upper Big Branch coal mine disaster which killed 29 miners in 2010, in the U.S. The occurrence of cutting frictional ignitions is closely related to cutting picks. It is necessary to identify the incendive cutting picks and prevent their adoption on coal driving TBMs.

Five types of cutting picks commonly used in the underground coal mining industry were tested to study the pick geometric parameters' influence on their failure pattern, which is closely related to cutting pick incendivity. Their tool range lengths range from 100 to 140 mm, with different tip patterns of slotted, slug and laid-on. Experimental results identified three kinds of failure patterns: at tip (detipping), at shank, and at tip and shank simultaneously. Cutting picks' mechanical performances were also recorded and analysed.

Tip attachment pattern and tool range length demonstrated notable influences on failure pattern. Experimental results indicate that, with the same tool range length, slug tipped picks have the lowest detipping risk, followed by slotted and then laid-on ones. Increasing tool range length can change failure patterns from detipping to shank failure, which in turn reduces the frictional ignition risk; the threshold value to eliminate the detipping chance is 140 mm for the tested picks.

Detipped picks showed distinctive features of high stiffness and low pick resilience. The load-displacement characteristics demonstrate that detipped picks had the average displacement at peak load of 11.4 mm, while it was 21.0 and 26.3 mm for the other two failure patterns. The average pick resilience for detipped picks was 2894 Nm, while that of the other two failure patterns were 5222 and 7640 Nm.

The findings provide guidelines for cutting pick selection and design to minimize the risk of frictional ignition. For selection among the available ones, pick V, which has the largest tool range and slotted tip was demonstrated to be the most favourable one with no chance of detipping in the tests. For new pick design, slug tip attachment

pattern, reasonably large tool range length, high resilience and high ductility are suggested to be adopted to reduce the risk of detipping and frictional ignition.

8.4 Recommendations for future research

Further studies are recommended to enhance current TBMs applications in the following field:

- The experimental study in this thesis has confirmed that ground stresses pose a significant influence on cutting force. However, proposing a cutting force prediction model incorporating ground stresses factor is beyond the scope of this study because more efforts including laboratory experiments, field investigation, theoretical analysing, and industrial support are needed to achieve that. It is suggested that such a model can be developed in future research works to provide guidelines for TBM performance prediction and cutter head design in deep tunnels.
- Aside from indentation tests, linear cutting tests and rotary cutting tests provide more realistic actions for disc cutters. It is recommended to conduct further linear cutting tests and rotary cutting tests to improve the findings drawn from the indentation test.
- Field study is the ultimate convincing verification of the new findings and models. Aside from the limited field data in literature review, application of TBMs in underground coal mines with high overburden has been undertaken in the Zhangji colliery, Huainan Mining Group in 2015. It is recommended to gain access to the TBM operational data for verification of the study's findings.

REFERENCES

Akiyama, T. 1970. A theory of the rock-breaking function of the disc cutter. Komatsu Technology. Vol.16, Iss.3, pp.56-61.

Aston, T., Gilby, J. and Yuen, C. 1988. A comparison of rock mass disturbance in TBM and drill and blast drivages at the Donkin Mine, Nova Scotia. International Journal of Mining and Geological Engineering. Vol.6, Iss.2, pp.147-162.

Athorn, M. L. and Snowdon, R. A. 1986. Performance of a TBM and a roadheader in the coal measures. Proceedings of the 27th US Symposium on Rock Mechanics (USRMS), American Rock Mechanics Association. pp.771-774.

Balci, C. 2009. Correlation of rock cutting tests with field performance of a TBM in a highly fractured rock formation: A case study in Kozyatagi-Kadikoy metro tunnel, Turkey. Tunnelling and Underground Space Technology. Vol.24, Iss.4, pp.423-435.

Bell, S. 2012. Commissioner for Mine Safety and Health, Queensland Mines Inspectorate, Annual Performance Reprot 2011-2012. Department of Natural Resources and Mines. Queensland.

Browning, E. J. 1988. Frictional ignitions. Proceedings of the Fourth International Mine Ventilation Congress. Brisbane, Queensland.

Brox, D. 2013. Technical considerations for TBM tunneling for mining projects. Transactions of The Society for Mining, Metallurgy, and Exploration. Vol.334, pp.498-505.

Cigla, M. and Ozdemir, L. 2000. Computer modeling for improved production of mechanical excavators. Society of Mining, Metallurgy and Exploration (SME) Annual Meeting, Salt Lake City, UT.

Cigla, M., Yagiz, S. and Ozdemir, L. 2001. Application of tunnel boring machines in underground mine development. Proceedings of the 17th International Mining Congress and Exhibition of Turkey, 2001. pp.155-164.

Cook, N., Hood, M. and Tsai, F. 1984. Observations of crack growth in hard rock loaded by an indenter. International Journal of Rock Mechanics and Mining Sciences & Geomechanics Abstracts. Vol.21, Iss.2, pp.97-107.

Courtney, W. G. 1990. Frictional ignition with coal mining bits. U.S. Department of The Interior, Bureau of Mines, Washington, D.C..

Dawood, A. D. 2011. Investigation into the potential for dust and gas explosions in underground coal mines with reference to pick tip geometry. The AusIMM bulletin- Journal of the Australian Institute of Mining and Metallurgy.

Department of Mineral Resources, New South Wales 1998. Review of reportable frictional igntions of methane in NSW underground coal mines 1987-1998.

Donnelly, C., Ramage, G. and Donghi, M. 2014. Alternative excavation methods in underground coal mining. Proceedings of 2014 Coal Operators' Conference. Wollongong, Australia. pp.216-223.

Evans, I. 1974. Relative efficiency of picks and discs for cutting rock. Proceedings of 3rd Congress on Advances in Rock Mechanics. pp.1399-1406.

Farmer, I. and Glossop, N. 1983. Design constraints for full-face tunnelling machines in coal mines. International Journal of Mining Engineering. Vol.1, Iss.1, pp.57-70.

Forrest W., Drobig K. N., and Larmour A. S. F. 1983. Selected design and construction aspects of the Selby coalfield project. Proceedings of the Institute of Civil Engineers. Vol.74, Iss.3, pp.365-386.

Forrest W., Drobig K. N., and Larmour A. S. F., Bornemann, E., Hammond, T., Vallis, J., Potter, U., Evans, A., Halfin, A. and Pickford, J. 1985. Selected design and construction aspects of the Selby coalfield project (DISCUSSION). Proceedings of the Institute of Civil Engineers. Vol.78, pp.379-387.

Frenzel, C., K Sling, H. and Thuro, K. 2008. Factors influencing disc cutter wear. Geomechanics and Tunnelling. Vol.1, Iss.1, pp.55-60.

Gibson, G. 2005. Australian roadway development–current practices. Australian Coal Association Research Program: Australia.

Handewith, H. 1983. TBM tunnels in the western hemisphere-an overview. Tunnelling Technology Newsletter. Vol.41**,** pp.1-8.

Hao, F., Liu, M., and Zuo, W. 2014. Coal and gas outburst prevention technology and management system for chinese coal mines: a review. Mine Planning and Equipment Selection - Proceedings of the 22nd MPES Conference, Dresden, Germany. ISBN:9783319026770.

Harding, P. 1981. TBM's stay down the mine. Tunnels Tunnell, Vol.13.

Hoek, E. and Brown, E. T. 1980. Underground excavations in rock. London, Institution of Mining and Metallurgy. ISBN:0900488557.

Howarth, D. and Bridge, E. 1988. Microfracture beneath blunt disc cutters in rock. International Journal of Rock Mechanics and Mining Sciences & Geomechanics Abstracts. Vol.25, Iss.1, pp.35-38.

Hunt, M. 1978. Rapid road construction in a German mine. Tunnels & Tunnelling. Vol.3, pp.13-15.

IHI and coal, 2012. IHI and mine development. [online]. Last accessed 15th Dec. 2015 at: *http://esvc000766.wic060u.server-web.com/ihicoal/mine.html*.

Innaurato, N. and Oreste, P. P. 2000. L'interazione utensile-roccia nelle macchine di scavo per roccia. In: Barla, G.(ed.) VIII ciclo di Conferenze di Meccanica ed Ingegneria delle Rocce. Torino, Dec. 2000, pp.111-158.

Innaurato, N., Oggeri, C., Oreste, P. and Vinai, R. 2007. Experimental and numerical studies on rock breaking with TBM tools under high stress confinement. Rock Mechanics and Rock Engineering. Vol.40, Iss.5, pp.429-451.

Innaurato, N. and Oreste, P. 2011. Theoretical study on the TBM tool-rock interaction. Geotechnical and Geological Engineering.Vol.29, Iss.3, pp.297-305.

Kizil, M. S., McAllister, A. and Pascoe, R. 2011. Simulation of development in longwall coal mines. Proceedings of the 11th Underground Coal Operators' Conference, University of Wollongong. pp.91-98.

Klein, S., Schmoll, M. and Avery, T. 1995. TBM performance at four hard rock tunnels in California. Proceedings of The Rapid Excavation and Tunnelling Conference 1995. Society for Mining, Metallurgy & Exploration. pp.61-76.

Krog, R. B. and Schatzel, S. J. 2009. Frictional ignitions in underground bituminous coal operations 1983-2005. Proceedings of 2007 Society for Mining, Metallurgy & Exploration Inc. (SME) Annual Meeting, Denver, CO.

Lama R. D. and Bodziony J. 1998. Management of outburst in underground coal mines. International Journal of Coal Geology. Vol.35, Iss.1, pp.83-115.

Lawn, B. and Swain, M. 1975. Microfracture beneath point indentations in brittle solids. Journal of materials science. Vol.10, Iss.1, pp.113-122.

Lindqvist, P.-A. 1982. Rock fragmentation by indentation and disc cutting: some theoretical and experimental studies.

Lindqvist, P.-A. 1984. Stress fields and subsurface crack propagation of single and multiple rock indentation and disc cutting. Rock mechanics and rock engineering. Vol.17, Iss.2, pp.97-112.

Lindqvist, P.-A., Lai, H.-H. and Alm, O. 1984. Indentation fracture development in rock continuously observed with a scanning electron microscope. International Journal of Rock Mechanics and Mining Sciences & Geomechanics Abstracts. Vol.21, Iss.4, pp.165-182.

Liu, H., Kou, S., Lindqvist, P.-A. and Tang, C. 2002. Numerical simulation of the rock fragmentation process induced by indenters. International Journal of Rock Mechanics and Mining Sciences. Vol.39, Iss.4, pp.491-505.

Liu, Q., Huang, X. and Shi, K. 2012. Utilization of full face roadway boring machine in coal mines deeper than 1 000 m and the key rock mechanics problems. Journal of China Coal Society. Vol.37, Iss.12.

Liu, Q., Shi, K., and Huang X. 2013. Feasibility of application of TBM in construction of deep coal mine and its key scientific problems. Journal of Mining & Safety Engineering. Vol.30, Iss.5, pp.633-641.

Massey, C. and Stenton, J. 1984. The selby project Britain's greatest coal mine. Interdisciplinary Science Reviews. Vol.9, Iss.1, pp.70-81.

McAteer, J. D., Beall, K., Beck, J. A. J., Mcginley, P. C., Monforton, C., Roberts, D. C., Spence, B. and Weise, S. 2011. Upper Big Branch: The April 5, 2010, explosion: a failure of basic coal mine safety practices. West Virginia Governor's independent investigation panel. Shepherdstown, West Virginia.

McStravick, F. G. 1989. Point attack picks on shearer drums - cutting and environmental aspects. Colliery guardian. Vol.237, Iss.1, pp.7-10.

Misra, A. 1996. Cost effectiveness of various development systems in Australian longwalls. Mining Technology. Vol.78, pp.307-311.

Mo, Z.-Z., Li, H.-B., Zhou, Q.-C., He, E.-G., Zou, F., Zhu, X.-M. and Zhao, Y. 2012. Research on numerical simulation of rock breaking using TBM disc cutters based on UDEC method. Rock and Soil Mechanics. Vol.33, Iss.4, pp.1196-1202.

Nemcik, J. 2013. Rock Mechanics Lecture Notes. University of Wollongong.

NHI, 2014. QMJ4260 full face coal tunnel boring machine. [online]. Last accessed 15th December 2015 at: *http://www.nhi.com.cn/qmj4260quanduanmianmeixianggaoxiaojuejinji/438.html*.

Ofiara, D. 2014. TBM's for Mining Applications.

Ouchterlony, F. 1973. Fracture mechanics applied to rock blasting. Publisher:SveDeFo.

Ozdemir, L., Miller, R. and Wang, F. 1977. Mechanical Tunnel Boring prediction and machine design. Research Applied to National Needs, National Science Foundation, Washington, D.C. 20550.

Palmer, J., Lovat, R. and Marsh, J. 1985. Performance of a 7.6-m diameter full-face tunnel-boring machine designed for a Canadian coal mine. Proceedings of the Fourth International Symposium, Brighton, England. pp.4-8.

Paul, B. and Sikarskie, D. L. 1965. A preliminary theory of static penetration by a rigid wedge into a brittle material. Transactions of the American Institute of Mining, Metallurgical, and Exploration, Inc. Vol.232, pp.372-383.

Peng, Q. 2014. Research on influence mechanism of confining pressure on rock breakage by TBM cutters. Chinese Journal of Rock Mechanics and Engineering. Vol.33, Iss.supplement 1, pp.2743-2749.

Philips, H. R. 1996. Identify methods to reduce the risk of explosions and fires caused by frictional ignition hazards. University of The Witwatersrand.

Philips, H. R. 1997. Establish the current status of research, development and operational experience of wet head cutting drums for the prevention of frictional ignitions. Department of Mining Engineering, University of the Witwatersrand.

Powell, F. and Billinge, K. 1975. The frictional ignition hazard associated with colliery rocks. The Mining Engineer. Vol.134, pp.527-533.

Ramamurthy, T. 2008. Penetration rate of TBM's. World Tunnel Congress 2008 - underground facilities for better environment and safety - India.

Roby, J., Sandell, T., Kocab, J. and Lindbergh, L. 2008. The current state of disc cutter design and development directions. Proceedings of 2008 North American Tunneling Conference, SME. Vol.4, pp.36-45.

Rostami, J. 2013. Study of pressure distribution within the crushed zone in the contact area between rock and disc cutters. International Journal of Rock Mechanics and Mining Sciences. Vol.57, pp.172-186.

Rostami, J. and Ozdemir, L. 1993. A new model for performance prediction of hard rock TBMs. Proceedings of 1993 Rapid Excavation and Tunneling Conference, Boston, Massachusetts. Society for Mining, Metallurgy, and Exploration, Inc. (SME).

Roxborough, F. F. and Phillips, H. R. 1975. Rock excavation by disc cutter. International Journal of Rock Mechanics and Mining Sciences & Geomechanics Abstracts. Vol.12, Iss.12, pp.361-366.

Royal Commission on the Pike River Coal Mine Tragedy Report 2012. Royal commission on the Pike River coal mine tragedy report. Wellington, New Zealand, ISBN: 978-0-477-10378-7.

Sanio, H. 1985. Prediction of the performance of disc cutters in anisotropic rock. International Journal of Rock Mechanics and Mining Sciences & Geomechanics Abstracts. Vol.22, Iss.3, pp.153-161.

Snowdon, R., Ryley, M. and Temporal, J. 1982. A study of disc cutting in selected British rocks. International Journal of Rock Mechanics and Mining Sciences & Geomechanics Abstracts. Vol.19, Iss.3, pp.107-121.

Stack, B. 1982. Handbook of mining and tunnelling machinery. Publisher:Wiley.

Sundin, N. O. and Wänstedt, S. 1994. A boreability model for TBM's. 1st North American Rock Mechanics Symposium. American Rock Mechanics Association.

Tarkoy, P. J. and Marconi, M. 1991. Difficult rock comminution and associated geological conditions. Proceedings of Tunneling. pp.195-207.

Tarkoy, P. J. 1995. Comparing TBMs with drill + blast excavation. Tunnels & Tunnelling International. Vol.27, Iss.10.

Taylor, G. and Watson, T. 2011. Longwall shearer frictional ignition hazard. Significant incident report of Mines Inspectorate, Department of Employement, Economic Development and Innovation, Queensland.

The Robbins company, 2013. The best products for tough jobs – you won't be alone when you buy a Robbins TBM. [online]. Last accessed 15th December 2015 at: *http://www.therobbinscompany.com/en/our-products/tunnel-boring-machines/*.

Trackemas, J. D. and Peng S. 2013. Factors considered for increasing longwall panel width. Coal age. Vol.118, Iss.8, pp.32-42.

Ulusay, R. and Hudson, J. A. 2007. The complete ISRM suggested methods for rock characterization, testing and monitoring: 1974-2006. International Society for Rock Mechanics, Commission on Testing Methods.

Wagner H. and Schumann E. H. R., 1971. The stamp-load bearing strength of rock an experimental and theoretical investigation. Rock mechanics. Vol.3, Iss.4, pp.185-207.

Wang, L., Kang, Y., Cai, Z., Zhang, Q., Zhao, Y., Zhao, H. and Su, P. 2012. The energy method to predict disc cutter wear extent for hard rock TBMs. Tunnelling and Underground Space Technology. Vol.28, pp.183-191.

Ward, C. R., Crouch, A. and Cohen, D. R. 2001. Identification of potential for methane ignition by rock friction in Australian coal mines. International Journal of coal geology. Vol.45, pp.91-103.

Weir International, Inc. 2010. United states longwall mining statistics 1989-2010. Website: http://www.weirintl.com/literature/. Access date: 10th July 2013.

White, S. 1978. The use of a Tunnel Boring Machine on a coal mine decline. Proceedings of the Third Australian Tunnelling Conference, Sydney, Australia. pp.66-70.

Willis, D. 2012. Mechanized Mining: Are TBMs the way into the Future? "Tunnel" website. Iss. 05/2012.

Willis, D. 2013. One machine, two modes. "Tunnels and Tunnelling International" website. Iss. 12/Dec/2013.

Xia, Y., Zhang, K. and Liu, J. 2015. Design optimization of TBM Disc cutters for different for different geological conditions. World Journal of Engineering and Technology. Vol.3, Iss.4.

Xu, G. 2010. Study on match technology for fully mechanized longwall coal mining face. Journal of China Coal Society. Vol. 11.

Zhang, Z. H. 2008. The research on theory and techniques of service life management of TBM disc cutters [D]. Beijing: North China Electric Power University.

Zhao, X., Cai, M. and Cai, M. 2010. Influence of dilation on rock mass displacement around underground excavations—a case study of the Donkin-Morien tunnel in Canada. Chinese Journal of Rock Mechanics and Engineering. Vol.11.